

Aus dem
Comprehensive Pneumology Center (CPC)
Institut für Experimentelle Pneumologie der Ludwig-Maximilians-Universität München
Kommissarische Direktorin: Dr. Antje Brand

Dissecting the role of proteasome activators in lung biology and disease

Dissertation
zum Erwerb des Doktorgrades der Naturwissenschaften
an der Medizinischen Fakultät der
Ludwig-Maximilians-Universität München

vorgelegt von

Vanessa Ninon Welk
aus Frankfurt am Main

2017

**Gedruckt mit Genehmigung der Medizinischen Fakultät
der Ludwig-Maximilians-Universität München**

Betreuerin: Prof. Dr. rer. nat. Silke Meiners

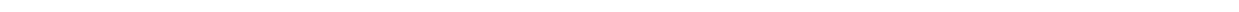
Zweitgutachterin: Prof. Dr. rer. nat. Regina Fluhrer

Dekan: Prof. Dr. med. dent. Reinhard Hickel

Tag der mündlichen Prüfung: 02.03.2018

*"We keep moving forward,
opening up new doors and doing new things,
because we're curious... and curiosity
keeps leading us down new paths."*

Walt Disney



Eidesstattliche Versicherung

Ich, Vanessa Ninon Welk, erkläre hiermit an Eides statt, dass ich die vorliegende Dissertation mit dem Thema

„Dissecting the role of proteasome activators in lung biology and disease“

selbstständig verfasst, mich außer der angegebenen keiner weiteren Hilfsmittel bedient und alle Erkenntnisse, die aus dem Schrifttum ganz oder annähernd übernommen sind, als solche kenntlich gemacht und nach ihrer Herkunft unter Bezeichnung der Fundstelle einzeln nachgewiesen habe.

Ich erkläre des Weiteren, dass die hier vorgelegte Dissertation nicht in gleicher oder in ähnlicher Form bei einer anderen Stelle zur Erlangung eines akademischen Grades eingereicht wurde.

München, 06.03.2018

Ort, Datum

Unterschrift



Table of contents

Eidesstattliche Versicherung	V
Table of contents	VII
Summary	XIII
Zusammenfassung	XV
1 Introduction	1
1.1 The proteasome – a major regulator of cellular proteostasis	1
1.1.1 Proteasomal protein degradation	2
1.1.2 The 20S proteasome core particle	3
1.1.3 20S proteasome inhibitors	5
1.1.4 Regulation of proteasome activity by proteasome activators	7
1.1.5 Regulation of proteasome function according to cellular needs – the building block concept	13
1.2 Idiopathic pulmonary fibrosis	17
1.2.1 Pathological hallmarks of IPF	17
1.2.2 Pathomechanisms of IPF	19
1.2.3 Regulation of proteostasis in fibrotic tissue remodeling	21
2 Aims	23
3 Materials	25
3.1 Antibodies	25
3.1.1 Primary antibodies	25
3.1.2 Secondary Antibodies	26
3.2 Oligonucleotides and vectors	27
3.2.1 Primers for quantitative RT-PCR	27
3.2.2 Primers for genotyping of PA200 ^{-/-} mice	28
3.2.3 Primers for cloning of PA200 construct	28
3.2.4 siRNAs	28
3.2.5 Plasmids	28
3.3 Cell culture	29

3.3.1	Cell lines	29
3.3.2	Primary human lung fibroblasts.....	29
3.3.3	Cell culture media.....	29
3.4	Human donor and IPF lung tissue	30
3.5	Human lung cancer tissue	30
3.6	Drugs and treatments	31
3.7	Enzymes	31
3.8	Kits.....	31
3.9	Markers	31
3.10	Buffer formulations.....	32
3.11	Reagents	33
3.12	Chemicals.....	35
3.13	Consumables	36
3.14	Technical devices and further equipment	36
3.15	Software.....	37
4	Methods.....	39
4.1	Animal experiments	39
4.1.1	Oxalate-induced kidney fibrosis mouse model	39
4.1.2	<i>Kras</i> ^{LA2} mutant lung cancer mouse model.....	39
4.1.3	Bleomycin-induced lung fibrosis of PA200 ^{-/-} mice	39
4.2	Cell culture.....	42
4.2.1	Cultivation of mammalian cell lines	42
4.2.2	Isolation and culture of primary human lung fibroblasts	42
4.2.3	Treatment of cells.....	43
4.2.4	RNA interference.....	43
4.2.5	Transient overexpression of PA200	44
4.2.6	Cell harvest.....	44
4.2.7	MTT assay	45
4.2.8	BrdU Assay	45
4.2.9	Annexin V/ PI staining.....	45
4.3	Protein biochemistry.....	46

4.3.1	Protein extraction from cells and tissue	46
4.3.2	Bicinchoninic acid (BCA) assay	46
4.3.3	SDS-PAGE and Western blot analysis	47
4.3.4	Native gel electrophoresis	48
4.3.5	Proteasome activity assays	49
4.3.6	Labeling of active proteasome complexes with activity-based probes (ABPs)	50
4.3.7	Co-immunoprecipitation	50
4.3.8	Histology	51
4.3.9	Histone extraction	52
4.3.10	Proteomic screen	53
4.4	Nucleic acid biochemistry.....	55
4.4.1	Quantitative real-time RT-PCR.....	55
4.4.2	Transcriptome microarray analysis	56
4.4.3	Preparation of plasmid DNA for transfection.....	57
4.5	Statistics.....	59
5	Validating the specificity of antibodies for analysis of the proteasome activator PA200	61
5.1	Introduction	61
5.2	Results.....	61
5.2.1	Antibody against aa 1620-1634 recognizes 160 kDa protein species not responding to PA200 silencing.....	61
5.2.2	Blocking of the antibody with its immunizing peptide prevents its binding to both the 200 kDa and 160 kDa protein species	63
5.2.3	PA200 ^{-/-} confirms 160 kDa protein species being not related to PA200.....	64
5.3	Discussion	67
5.3.1	Specific antibodies are essential for reliable research	67
5.3.2	The use of unspecific antibodies limits available information on PA200	68
6	Inhibition of proteasome activity induces formation of alternative proteasome complexes.....	71
6.1	Introduction	71
6.2	Results.....	72

6.2.1	Proteasomal activators are recruited to 20S and 26S proteasomes in response to proteasome inhibition.	72
6.2.2	Formation of alternative proteasome complexes is a rapid response to proteasome inhibition.	73
6.2.3	Proteasome inhibition also mediates recruitment of PA28 γ in HeLa cells.	74
6.2.4	Direct interaction of PA28 γ and PA200 with 20S proteasome complexes is enhanced upon proteasome inhibition.	75
6.2.5	Early recruitment of proteasomal activators is not regulated by their transcription.	76
6.2.6	Specific decrease of 26S and 30S proteasome complexes induces recruitment of PA200 but not PA28 γ	78
6.2.7	The extent of active site inhibition defines the dimensions of proteasomal activator recruitment.	81
6.2.8	Recruitment of PA28 γ to purified 20S complexes is not enhanced in response to catalytic proteasome inhibition <i>in vitro</i>	83
6.2.9	Proteasome inhibition induces activator recruitment in native cell extracts	84
6.2.10	Alternative proteasome complexes persist after recovery of proteasome activity.	86
6.2.11	Silencing of PA28 γ decreases ability of cells to cope with proteasome inhibition	87
6.3	Discussion	90
6.3.1	Regulation of the proteasome in response to active site inhibition	90
6.3.2	Potential mechanisms for alternative proteasome complex formation	91
6.3.3	Function of newly formed alternative proteasome complexes in the cell	96
6.3.4	Importance of defining molecular functions of proteasome inhibitors and development of more specific proteasome inhibitors.	97
7	Analyzing the regulation and function of PA200 in hyperproliferative chronic lung disease	99
7.1	Introduction	99
7.2	Results	100
7.2.1	PA200 is upregulated in fibrotic tissue remodeling.	100
7.2.2	The PA200 interactome is regulated according to cellular growth	109
7.2.3	PA200 does not degrade acetylated histones in lung fibroblasts.	116
7.2.4	PA200 regulates growth and survival of primary human lung fibroblasts.	120

7.2.5	PA200 ^{-/-} increases the survival of mice during development of bleomycin-induced fibrosis.....	136
7.2.6	PA200 is strongly induced in lung cancer tissues.....	142
7.3	Discussion.....	145
7.3.1	Induction of PA200 in hyperproliferative tissues is a new aspect of proteasome regulation in diseased tissues.....	145
7.3.2	Characterization of PA200 in the cell.....	149
8	Concluding remarks.....	161
9	References.....	165
	List of abbreviations.....	183
	Acknowledgements.....	187

Summary

Proteostasis is the cellular control mechanism ensuring the maintenance of a functional proteome, which is essential for proper cellular and organismal function. Being the main proteolytic system of the cell, the proteasome is an indispensable component of the cellular proteostasis network. Proteasomes are large protein complexes consisting of different subcomponents. The 20S proteasome catalytic core particle associates with different proteasome activators, including the 19S regulator and the alternative proteasome activators PA28 $\alpha\beta$, PA28 γ , or PA200, which open the 20S proteasome gate to facilitate substrate entry into the proteolytic chamber. Whereas the 19S regulator mediates ubiquitin- and ATP-dependent degradation of the majority of cellular proteins, the alternative proteasome activators function in an ubiquitin- and ATP-independent manner. According to the previously proposed building block concept, the recruitment of these proteasome activators to the 20S catalytic core particle allows for the fast adaption of proteasome function in response to cellular stimuli. Although the alternative proteasome activators have been implicated in the degradation of specific substrates, their function and regulation is largely unknown. Here, the regulation of alternative proteasome activators was investigated in lung biology and disease with the particular focus to provide proof-of-concept evidence for the fast regulation of activators upon cellular stimuli and to investigate the dysregulation and function of PA200 in hyperproliferative lung diseases.

First, the specificity of a commercially available and widely used PA200 antibody targeting amino acids 1620-1634 of the human protein was analyzed using PA200 silencing in cells as well as tissues from PA200^{-/-} mice. The data provided in this thesis revealed that the 160 kDa protein species detected by the antibody is not an isoform of PA200 as stated previously in the literature. Antibodies targeting different epitopes of the activator specifically recognized the 200 kDa PA200 protein and were used for further experiments.

The second study of this thesis analyzed the regulation of alternative proteasome activators in response to proteotoxic stress mediated by inhibition of the proteasome. Here, a rapid recruitment of proteasome activators PA28 γ and PA200 to the 20S proteasome was observed in response to inhibition of the 20S catalytic subunits *via* small molecule inhibitors in primary human lung fibroblasts (pHLF). Investigating the underlying mechanism revealed that the recruitment of PA28 γ and PA200 was independent from their transcriptional

induction at early time points and that the extent of activator recruitment depended on the degree of proteasome inhibition. The rapid assembly of PA28 γ and PA200 with 20S proteasome complexes in response to proteasome inhibition thus provides first evidence for a fast regulation of these activators according to cellular needs supporting the building block concept.

The third study of this thesis analyzed the regulation and function of PA200 in hyperproliferative tissue remodeling. The results demonstrated upregulation of PA200 protein levels not only in tissues of idiopathic pulmonary fibrosis (IPF) patients as well as in experimentally induced fibrosis of the lung and kidney but also in human biopsies from different types of lung cancer. In IPF tissues the induction of PA200 protein levels specifically localized to myofibroblasts and abnormal hyperplastic basal cells of the bronchial epithelium. LC-MS/MS analysis revealed that the PA200 interactome in pHLF strongly adapts according to cellular activation and proliferation involving the interaction of PA200 with ribosomal proteins and heterogeneous nuclear ribonucleoproteins (hnRNPs) in proliferating cells. Transcriptomic and proteomic screens of PA200-silenced pHLF revealed pronounced activation of cellular proliferation and survival, which was confirmed in cell culture experiments. In line with this observation, PA200^{-/-} mice showed an improved survival in response to bleomycin-induced lung injury.

In summary, the results obtained from these studies provide first evidence for the regulation of alternative proteasome activators PA28 γ and PA200 upon different cellular stimuli. This supports the previously stated building block hypothesis suggesting the adaption of proteasome function on the level of activator recruitment to the 20S core particle. In addition, a dysregulation of PA200 in hyperproliferative lung diseases was observed and the activator was discovered to be a novel regulator of fibroblasts activation, proliferation and survival.

Zusammenfassung

Proteostase bezeichnet den zellulären Kontrollmechanismus, welcher die Instandhaltung eines funktionellen Proteoms gewährleistet und damit maßgeblich zur physiologischen Funktion von Zellen oder ganzen Organismen beiträgt. Als eines der wichtigsten proteolytischen Systeme der Zelle ist das Proteasom ein essentieller Bestandteil dieses Proteostase-Netzwerks. Proteasomen sind sehr große Proteinkomplexe, welche aus verschiedenen Subkomponenten bestehen. Der 20S Kernpartikel kann mit verschiedenen Proteasomaktivatoren wie dem 19S Regulator oder den alternativen Proteasomaktivatoren PA28 $\alpha\beta$, PA28 γ , oder PA200 assoziieren, was seine Öffnung induziert und die Aufnahme von Substraten in dessen proteolytische Kammer ermöglicht. Im Gegensatz zum 19S Regulator, der für den Ubiquitin- und ATP-abhängigen Abbau eines Großteils der zellulären Proteine verantwortlich ist, agieren die alternativen Proteasomaktivatoren ATP- und Ubiquitin-unabhängig. Gemäß des kürzlich postulierten „Baustein-Konzepts“ erlaubt die Rekrutierung dieser Proteasomaktivatoren zum 20S Kernpartikel eine schnelle Adaption der Proteasomfunktion an zelluläre Veränderungen. Die genaue Funktion und Regulation der alternativen Proteasomaktivatoren ist größtenteils unbekannt, obwohl angenommen wird, dass sie den Abbau spezifischer Substrate vermitteln. Im Rahmen der vorliegenden Dissertation wurde daher die Regulation alternativer Proteasomaktivatoren in der Lungenphysiologie als auch in Lungenerkrankungen mit dem besonderen Fokus untersucht, einen ersten Nachweis für die vom „Baustein-Konzept“ beschriebene Adaption alternativer Proteasomaktivatoren gemäß zellulärer Stimuli zu erbringen sowie eine potenzielle Dysregulation von PA200 in hyperproliferativen Lungenerkrankungen zu erforschen.

In der ersten Studie wurde die Spezifität eines kommerziell erhältlichen und weitverbreiteten PA200 Antikörpers, welcher gegen die Aminosäuren 1620-1634 des humanen Proteins gerichtet ist, mittels siRNA-vermittelter Herabregulierung der PA200 Expression sowie in Geweben von PA200^{-/-} Mäusen untersucht. Diese Analyse ergab, dass dieser Antikörper eine Proteinspezies von 160 kDa detektiert, welche im Gegensatz zur bisherigen Einschätzung der Literatur keine Isoform von PA200 darstellt, weshalb dieser Antikörper nicht für die spezifische Detektion von PA200 geeignet ist. Da die Spezifität anderer PA200 Antikörper, welche gegen andere Epitope des Proteins gerichtet sind, bestätigt werden konnte, wurden diese in den weiteren Experimenten verwendet.

In der zweiten Studie wurde die Regulierung alternativer Proteasomaktivatoren bei proteotoxischem Stress untersucht, der durch Proteasomhemmung erzeugt wurde. Die Inaktivierung der katalytischen 20S Untereinheiten durch niedermolekulare Inhibitoren verursachte eine schnelle Rekrutierung der Proteasomaktivatoren PA28 γ und PA200 an das 20S Proteasom in primären humanen Lungenfibroblasten (phLF). Die Untersuchung des zugrundeliegenden Mechanismus ergab, dass die Rekrutierung von PA28 γ und PA200 unabhängig von einer transkriptionellen Hochregulation der Aktivatoren induziert wurde und dass die Rekrutierung vom Grad der Proteasominaktivierung abhing. Die rasche Assemblierung von PA28 γ und PA200 mit dem 20S Proteasomkomplex bei Inhibierung des Proteasoms bestätigt somit die schnelle Regulation der Proteasomfunktion gemäß des „Baustein-Konzepts“.

Die dritte Studie dieser Dissertation untersuchte die Regulation und Funktion von PA200 in hyperproliferativen Lungenerkrankungen. Die hierfür durchgeführten Studien zeigten eine Hochregulation von PA200 in fibrotischen Geweben der idiopathischen Lungenfibrose (IPF), experimentell-induzierter Fibrose von Lunge oder Niere sowie verschiedener Arten humaner Lungentumore. Die histologische Analyse von IPF Geweben zeigte insbesondere eine Erhöhung des PA200 Proteingehalts in Myofibroblasten und abnormalen hyperplastischen Basalzellen des Bronchialepitheliums. Mittels LC-MS/MS Analyse konnte eine deutliche Regulation des PA200 Interaktoms gemäß der zellulären Aktivierung und Proliferation festgestellt werden, wobei PA200 in proliferierenden Zellen vor allem mit ribosomalen Proteinen und heterogenen nukleären Ribonucleoproteinen (hnRNP) interagiert. Die Transkriptom- sowie Proteom-Analyse von phLF mit siRNA-vermittelter Herabregulation von PA200 ergab eine deutliche Aktivierung der Proliferation und des Überlebensprogramms der Zellen, was mittels Zellkulturrexperimenten bestätigt werden konnte. Außerdem zeigten PA200^{-/-} Mäuse eine erhöhte Überlebensrate bei einer Bleomycin-induzierten Lungenschädigung im Vergleich zu Wildtyptieren.

Zusammenfassend bestätigen die Ergebnisse dieser Dissertation die Regulation von PA28 γ und PA200 gemäß bestimmter zellulärer Stimuli und erbringen somit eine erste Validierung des „Baustein-Konzepts“ hinsichtlich der alternativen Proteasomaktivatoren. Zudem wurde erstmalig eine Dysregulation von PA200 im Krankheitskontext beobachtet und eine bisher unbekannt Funktion des Aktivators als Regulator der Aktivierung, Proliferation und des Überlebens von Zellen entdeckt.

1 Introduction

1.1 The proteasome – a major regulator of cellular proteostasis

Proteins are large biomolecules that exert most cellular functions and are therefore involved in almost all biological processes. Protein quality control and protein homeostasis, also called proteostasis, control the maintenance of a functional proteome and are essential for the health of cells and organisms (Balch et al., 2008; Hartl et al., 2011; Meiners and Ballweg, 2014). Different environmental, genetic or inflammatory influences can affect cellular proteostasis and lead to cellular and organismal malfunction (Figure 1.1). Dysregulation of proteostasis has been implicated in the pathogenesis of diseases of different organs, including the lung (Balch et al., 2014). Proteostasis controls the life cycle of a protein on several levels: synthesis of a linear amino acid chain by translation of the mRNA sequence through the ribosome, the folding thereof into a native, functional protein by molecular chaperones, and finally its timely controlled degradation by the autophagy pathway or the ubiquitin-proteasome system (UPS) (Hartl et al., 2011). Whereas autophagy mainly involves lysosomal degradation of protein aggregates and whole organelles, up to 80 % and thus the majority of all cellular proteins in mammals are degraded via the proteasome (Rock et al., 1994). For this reason, the proteasome is a major regulator of proteostasis and its function is crucial for cellular function and viability.

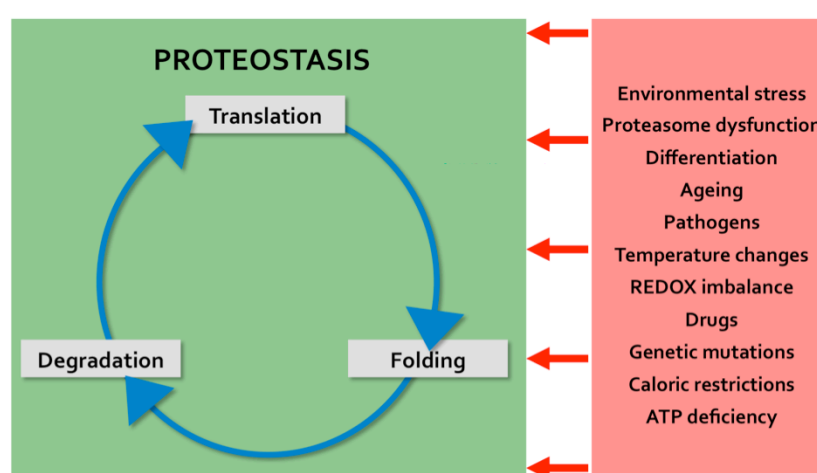


Figure 1.1: Maintenance of proteostasis during the life cycle of proteins. The life cycle of proteins includes the following steps: the translation of the mRNA sequence into a peptide sequence, the modification, localization and folding of the peptide chain into a functional, native structure and finally the controlled degradation of the protein. Proteostasis controls and balances these processes to maintain a functional proteome. Different insults and perturbations (red box) can lead to dysregulation of proteostasis, which can severely affect the cellular and organismal health (adapted from Martinon *et al.* Aksentijevich, Nature Reviews Rheumatology, 2014).

1.1.1 Proteasomal protein degradation

The proteasome is a huge, evolutionarily conserved, multicatalytic protease complex involved in several important cellular functions in addition to protein quality control, which include, amongst others, cell cycle control, apoptosis, inflammation, transcription, signal transduction and major histocompatibility complex (MHC) class I antigen presentation (Finley, 2009). The UPS degrades the majority of cellular proteins, such as short-lived regulatory proteins and damaged soluble proteins, but also long-lived proteins, in an ubiquitin- and ATP-dependent fashion. ATP-dependent proteolysis was first recognized in the late 1970s (Ciechanover et al., 1978; Etlinger and Goldberg, 1977). Later, ubiquitin was noticed as an important recognition motif for proteins targeted for degradation and finally the proteasome was discovered as the actual proteolytic complex (Arrigo et al., 1988; Hershko et al., 1980; Hough et al., 1987). As proteolysis is irreversible and its malfunction can have severe effects on cell viability, ubiquitin-dependent protein degradation is a highly controlled, multistep process (Collins and Goldberg, 2017). Targeting of proteins for degradation requires the covalent attachment of a chain of at least four ubiquitin molecules to lysine 48 (K48) residues (Thrower et al., 2000). This is achieved by ubiquitin activating E1 enzymes, ubiquitin-conjugating E2 enzymes and ubiquitin E3 ligases in a multistep and ATP-dependent enzymatic cascade (Finley, 2009). It involves tagging of the protein with ubiquitin, recognition of the protein substrate by the 26S proteasome via its ubiquitin-tag, its deubiquitination, ATP-dependent unfolding and the translocation into the 20S core particle where it is finally degraded (Figure 1.2) (Finley, 2009; Hershko and Ciechanover, 1998).

In addition, an ubiquitin-independent type of proteasomal degradation was discovered involving proteolysis of unfolded or structurally disordered proteins by the 20S proteasome catalytic core or degradation of specific substrates mediated by alternative proteasome complexes that contain other proteasome activators, such as PA28 γ (Baugh et al., 2009; Ben-Nissan and Sharon, 2014; Eralles and Coffino, 2014).

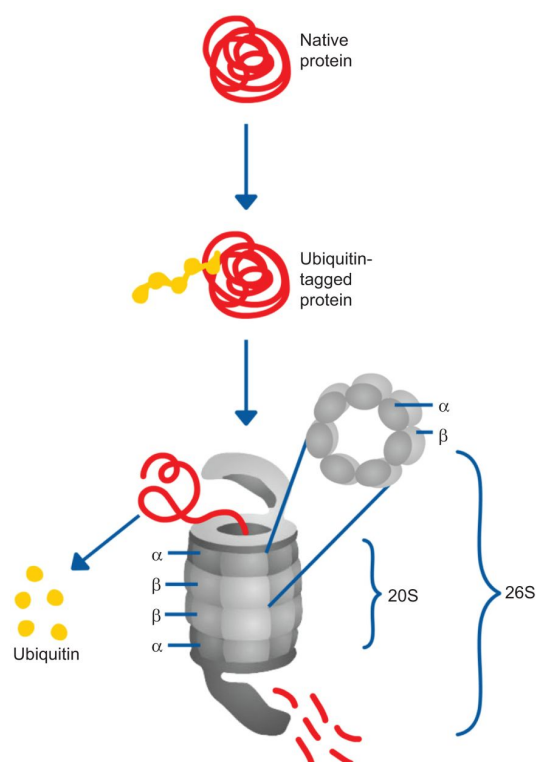


Figure 1.2: The majority of cellular proteins are degraded in an ubiquitin-dependent manner by the 26S proteasome. Proteins targeted for degradation are covalently tagged with a polyubiquitin chain, which allows for their selective recognition via the 19S regulatory particle that is associated with the 20S core complex forming the 26S proteasome. The 19S regulator deubiquitinates and unfolds the substrates and translocates them into the catalytic core of the 20S proteasome core complex, where they are cleaved into small peptides (from Meiners *et Eickelberg*, 2012).

1.1.2 The 20S proteasome core particle

The proteasome consists of the 20S core particle that can associate with different proteasomal activators and therefore exhibits large structural complexity (Meiners *et al.*, 2014). Peptides targeted for degradation enter the 20S core complex through a pore in the center of the outer α -ring, which functions as gate controlling entry of substrates into the particle (Groll *et al.*, 2000). The N-terminal tails of the outer α -ring subunits close the entry pore into the central proteolytic chamber thereby preventing uncontrolled access of substrates due to this closed conformation (Groll *et al.*, 2000). Association of different proteasome activators with binding pockets on the surface of the 20S α -ring induces gate opening and facilitates the entry of peptides into the catalytic cavity for degradation (Stadtmueller and Hill, 2011).

The 20S core particle is a ≈ 700 kDa protein complex composed of 28 subunits. They are symmetrically arranged in four rings of seven α -subunits ($\alpha 1-7$) on the outside flanking two

rings of seven β -subunits (β_1 -7) in the inside forming a barrel-shaped structure (Figure 1.3) (Kish-Trier and Hill, 2013). The proteolytic activity of the proteasome resides within the internal cavity of this barrel-shaped complex and encloses the three different catalytic active sites β_1 , β_2 and β_5 on each β -ring, which exhibit caspase-like (C-L), trypsin-like (T-L) and chymotrypsin-like (CT-L) activities. Here, peptides are cleaved into smaller fragments having a length of 3-20 amino acids (Kisselev et al., 1999). The proteasome belongs to the family of N-terminal nucleophilic hydrolases with all catalytic sites containing a threonine at position 1 (Thr1) mediating peptide cleavage in an autocatalytic process (Brannigan et al., 1995; Groll and Huber, 2003). This involves the nucleophilic attack of its hydroxyl group on the carbonyl carbon atom of the peptide to be cleaved, while its N-terminus serves as a proton acceptor.

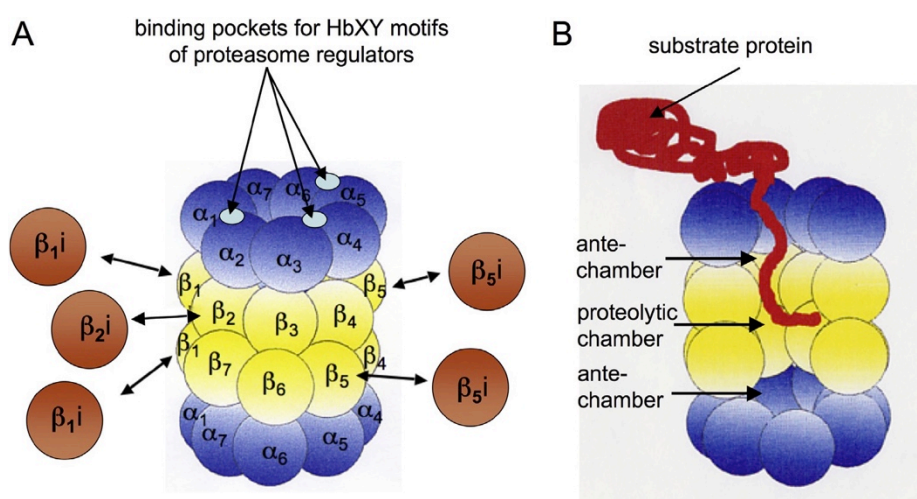


Figure 1.3: Schematic representation of the 20S core particle. A) The 20S proteasome consists of two α -rings and two β -rings in a symmetric α_1 -7 β_1 -7 β_1 -7 α_1 -7 conformation. The catalytic subunits β_1 , β_2 and β_5 of the 20S standard proteasome can be replaced by immunoproteasome subunits β_{1i} , β_{2i} and β_{5i} . The outer α -rings exhibit a closed conformation unless binding of a regulator induces opening of the entry pore. Different proteasomal regulators bind via their HbXY motifs to binding pockets within the α -ring and induce gate opening. B) Substrates enter the 20S core particle through the gate within the center of the α -ring, where they pass the antechamber in order to be finally degraded in the proteolytic chamber (from B. Dahlmann, 2016).

This so-called standard or constitutive proteasome is ubiquitously expressed in all nucleated cells. The immunoproteasome represents another type of 20S proteasome composed of the specialized catalytic subunits β_{1i} (LMP2), β_{2i} (MECL-1) and β_{5i} (LMP7) (Groettrup et al., 2010). Although these subunits are expressed and incorporated into newly assembled proteasomes in immune cells, their expression can also be induced by cytokines like interferon gamma ($\text{IFN}\gamma$), tumor necrosis factor alpha ($\text{TNF}\alpha$) or lipopolysaccharide (LPS) in non-immune cells (Groettrup et al., 2010). In contrast to the standard proteasome,

immunoproteasome subunits have a differential cleavage specificity producing peptides with more hydrophobic residues at their C-terminus (Groettrup et al., 2001). These peptides are preferentially loaded onto MHC I molecules in the endoplasmic reticulum (ER), which are then presented as antigens on the cell surface. Therefore, immunoproteasomes have been discovered to play an important role in shaping the immune response, although it is assumed that this represents only one aspect of their function and others still need to be identified (Dahlmann, 2016). Another specialized $\beta 5t$ catalytic subunit exists in the thymus forming the so-called thymoproteasome, which has been discovered to be essentially involved in the development of CD8⁺ T cells (Murata et al., 2007).

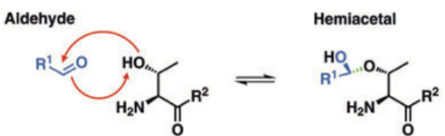
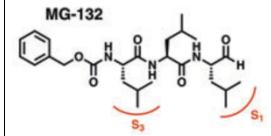
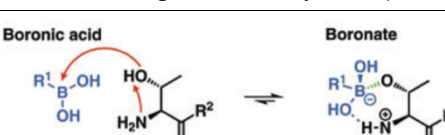
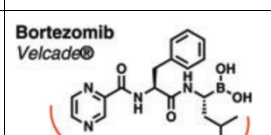
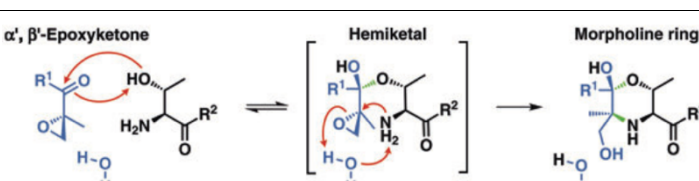
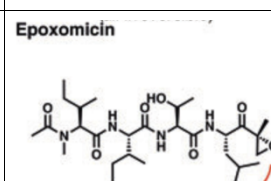
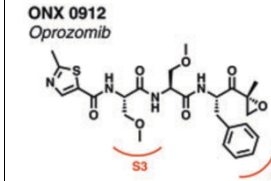
1.1.3 20S proteasome inhibitors

The development of proteasome inhibitors targeting the proteolytic active sites of the 20S proteasome core complex has largely influenced proteasome research and also cancer therapy, as they were shown to efficiently kill tumor cells that are highly dependent on proteasomal protein degradation (Kisselev et al., 2012). In 2003, bortezomib (BZ) (Velcade®) was approved by the United States Food and Drug Administration (FDA) as the first 20S proteasome inhibitor for third-line treatment of relapsed and refractory mantle cell lymphoma and later also as a first-line treatment of newly diagnosed multiple myeloma patients (Kane et al., 2003, 2006, 2007). In 2012, the second-generation inhibitor carfilzomib (Kyrpolis®) was approved for the treatment of multiple myeloma exhibiting reduced side effects compared to the previously approved BZ (Herndon et al., 2013).

In recent years, a variety of small molecule inhibitors have been developed that covalently or non-covalently bind to the catalytic sites of the 20S proteasome with different specificities thereby reversibly or irreversibly inhibiting its protease activities (Dick and Fleming, 2010). Irreversible inhibitor binding induces sustained proteasome inhibition, as recovery of proteasome activity requires *de novo* synthesis of 20S core particles. However, these molecules exhibit a negative pharmacodynamic profile since they also inhibit proteasomes of healthy and non-malignant cells when administered intravenously (Beck et al., 2012; Schmidtke et al., 1996). In contrast, reversible inhibitors were described to have less side- and off-target effects (Beck et al., 2012). Covalent inhibitors of the 20S proteasome proteolytic sites generally consist of two pharmacophores, a peptide scaffold and an

electrophilic anchor, which can be a boronate, α',β' -epoxyketone, aldehyde or β -lactone to only name a few examples (Beck et al., 2012; Kisselev et al., 2012). All proteolytic subunits bind to the inhibitors via a common mechanism involving the nucleophilic addition of their Thr1 hydroxyl group to the inhibitor analogously to the nucleophilic attack of peptides for degradation. Of note, the composition of side chains - but not the reactive group or the peptide backbone - defines the substrate specificity of the inhibitor. Several different classes of proteasome inhibitors are shown in Table 1 focusing on the inhibitors used in this study.

Table 1: Overview of covalent proteasome inhibitor classes, their inhibitory mechanisms and profiles and examples. The table shows a selection of covalent inhibitor classes, which are widely used in research or were applied in this study (adapted from Beck et al., 2012).

Structural class	Inhibitory mechanism and profiles	Examples and their specificities
Peptide aldehydes	<p>Aldehyde</p>  <p>Hemiacetal</p> <ul style="list-style-type: none"> ▪ first inhibitors ▪ rapidly reversible and potent ▪ also inhibiting serine and cysteine proteases 	<p>MG-132</p>  <p>$\beta 5 > \beta 2 > \beta 1$</p>
Peptide boronates	<p>Boronic acid</p>  <p>Boronate</p> <ul style="list-style-type: none"> ▪ more potent than aldehydes ▪ reversible inhibitors but lower dissociation than aldehyde ▪ dose-limiting toxicity by inhibition of serine proteases 	<p>Bortezomib Velcade®</p>  <p>$\beta 5 > \beta 1 > \beta 2$</p>
Peptide α',β' -epoxyketones	<p>α',β'-Epoxyketone</p>  <p>Hemiketal</p> <p>Morpholine ring</p> <ul style="list-style-type: none"> ▪ most specific and potent inhibitors ▪ irreversible ▪ site-specific inhibitors and activity-based probes (ABPs) 	<p>Epoxomicin</p>  <p>$\beta 5 > \beta 2 > \beta 1$</p> <p>ONX 0912 Oprozomib</p>  <p>$\beta 5$-specific</p>

Besides covalent inhibitors, different classes of molecules interacting with the proteasome catalytic subunits in a non-covalently fashion have been generated, such as cyclic peptides or noncyclic peptides (Kisselev et al., 2012). In recent years, several inhibitors of specific catalytic subunits were developed, such as the β 5-specific inhibitor oprozomib (ONX-0912) or the immunoproteasome-specific inhibitor ONX-0914 targeting β 5i, which represents another milestone in proteasome inhibitor discovery (Muchamuel et al., 2009). Although these specific inhibitors have not yet entered the clinic, they are widely used in research in example for monitoring active proteasome complexes with so-called activity-based probes (ABPs) (Verdoes et al., 2010).

1.1.4 Regulation of proteasome activity by proteasome activators

Several proteasome activators have been discovered, including the 19S regulator and the alternative proteasome activators PA28 $\alpha\beta$, PA28 γ , PA200, and PI31, that have different substrate specificities and thereby fine-tune selective protein degradation (Figure 1.4) (Stadtmueller and Hill, 2011). The 19S regulator is an essential component of the UPS, as it forms the so-called 26S proteasome upon binding to the 20S core particle and is therefore essentially involved in ubiquitin-dependent protein degradation. Discovery of alternative proteasome activators, however, has further extended the complexity of proteasome structure and function. Despite exhibiting distinct functionalities, both 19S regulators and the alternative activators PA28 $\alpha\beta$, PA28 γ and PA200 bind to the α -ring of the 20S proteasome and induce opening of its axial pore via similar mechanisms involving their C-terminal regions. Whereas the three 19S regulator ATPase subunits RPT2, RPT3, and RPT5 as well as the alternative proteasome activator PA200 contain so-called HbXY motifs at their C-terminal regions that interact with the binding pockets within the α -ring, the PA28 family of activators binds to the 20S α -subunits *via* a C-terminal internal loop structure also inducing an open gate conformation (Kish-Trier and Hill, 2013).

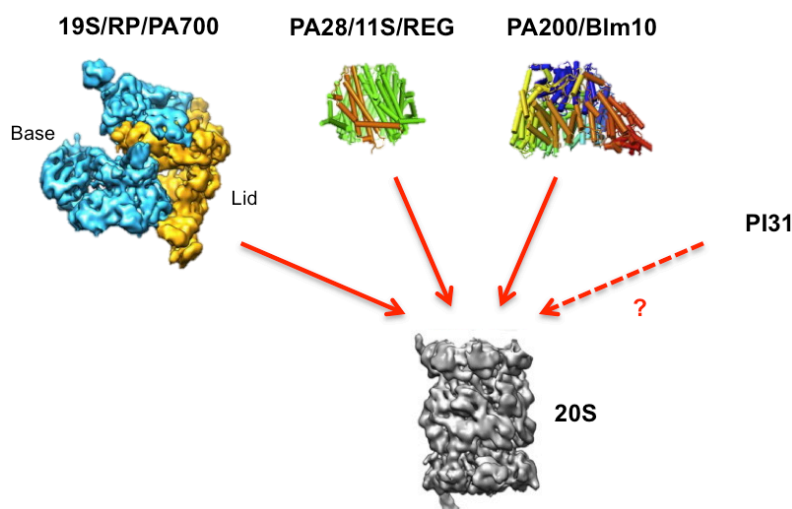


Figure 1.4: Association of proteasome activators with the 20S core particle increases the complexity of the proteasome system. Different proteasome activators can associate with the 20S core particle (shown in grey) and induce opening of its otherwise closed α -ring allowing for the entry of substrates. Whereas the 19S regulator binds to the 20S proteasome in an ATP-dependent manner driving degradation of ubiquitinated proteins, the alternative activators of the PA28 family (also called 11S or REG), including PA28 $\alpha\beta$ and PA28 γ , or PA200/Blm10 do not require ATP for their association with the 20S core complex and subsequent protein degradation. Although they have been implicated to be involved in ubiquitin-independent protein degradation of specific substrates, it still requires further investigation to determine their exact function. PI31 has initially been described as an inhibitor of proteasome activity, but these observations are controversially discussed and its function is not fully understood (adapted from Schmidt *et al.*, 2014).

1.1.4.1 The 19S regulator

The 19S regulator, also called regulatory particle (RP) or PA700, is a large protein complex composed of at least 19 subunits (Lander *et al.*, 2012). Its role in targeting ubiquitinated proteins to the catalytic core of the 20S proteasome for their degradation is well established. Binding of one or two 19S regulators to the 20S proteasome forms 26S or 30S proteasomes respectively, which degrade the majority of cellular proteins. In contrast to the alternative proteasome activators, its function involving substrate binding, deubiquitination, unfolding and translocation as well as the stabilization of the 19S-20S interaction is strongly energy-dependent and requires hydrolysis of ATP (Liu *et al.*, 2006). The 19S regulator is subdivided into two sub-compartments, the so-called “base” binding to the 20S core particle, and the “lid” (Figure 1.4). The base is composed of a ring of six AAA+ ATPase subunits RPT1-RPT6, which are in direct contact with the α -ring of the 20S core particle, and four non-ATPase subunits including RPN1, RPN2, RPN10 and RPN13 that are mainly functioning as ubiquitin receptors recognizing ubiquitinated substrates. The lid consists of nine non-ATPase subunits and is essentially involved in deubiquitination of substrates by the deubiquitinases RPN11, UCH37 and UBP6/USP14 (Lander *et al.*, 2013).

1.1.4.2 The PA28 family of proteasome activators

The PA28 family of alternative proteasome activators, which are also called 11S or REG, comprises two different ring-shaped particles composed of seven 28 kDa subunits each, the heteroheptamer PA28 $\alpha\beta$ and the homoheptamer PA28 γ (Rechsteiner and Hill, 2005). In contrast to the 19S regulator, they are reported to activate the 20S core particle in an ATP-independent manner and mediate ubiquitin-independent degradation of substrates.

PA28 $\alpha\beta$ is localized in the cytoplasm of cells from many organs with the highest expression in immune tissues (Rechsteiner et al., 2000). In this regard, the expression of PA28 α and PA28 β subunits and the formation of PA28 $\alpha\beta$ complexes can be induced by INF γ . Moreover, the activator preferentially associates with the immunoproteasome and *in vitro* characterization of purified complexes indicated that this activator stimulates all active sites of the proteasome (Fabre et al., 2015; Realini et al., 1997). Recently, the crystal structure of this activator complex revealed that it preferentially forms PA28 $\alpha_4\beta_3$ complexes, which are more stable and most strongly stimulate proteasome activity when compared to PA28 α or PA28 β homoheptamers (Huber and Groll, 2017). Several functional studies suggest that PA28 $\alpha\beta$ is involved in MHC I antigen processing (Dick et al., 1996; Groettrup et al., 1996; Preckel et al., 1999).

In contrast, the activator PA28 γ is exclusively found in the nucleus and was reported to stimulate activity of the proteasome *in vitro* with a preference for T-L activities (Realini et al., 1997; Stadtmueller and Hill, 2011). Several studies proposed that PA28 γ mediates the degradation of specific nuclear substrates, such as the cyclin-dependent kinase inhibitors p16, p19 and p21, the steroid receptor co-activator-3 (SRC-3) or the deacetylase SIRT1 (Chen et al., 2007; Dong et al., 2013; Li et al., 2006, 2007a). In line with mediating the degradation of important cell cycle inhibitors, PA28 $\gamma^{-/-}$ mice exhibit growth retardation and mouse embryonic fibroblasts (MEFs) show increased apoptosis when compared to wildtype cells (Murata et al., 1999). An interaction of PA28 γ with apoptotic factors has been reported suggesting an anti-apoptotic function of the activator, which has not been mechanistically understood yet (Rechsteiner and Hill, 2005).

Although structural studies on PA26 - the homologue of PA28 in *Archaea* - revealed that this activator mediates ATP-independent opening of the 20S core particle with its C-terminal residues in a similar manner as the ATP-dependent 19S regulator, it is still unclear how entire

proteins and not only small peptides or unfolded proteins can enter its small pore for degradation (Förster et al., 2005; Stadtmueller and Hill, 2011; Whitby et al., 2000).

1.1.4.3 PI31

PI31 is the currently least understood proteasomal regulator. It was reported to associate with the 20S proteasome via multiple regions and was also detected to interact with 26S proteasomes (Li et al., 2014). Initial *in vitro* studies described PI31 as an inhibitor of proteasome activity, but this has been controversially discussed in recent studies characterizing the regulator in *Drosophila* or mammalian cells (Bader et al., 2011; Li et al., 2014). Recent publications reported that the approximately 31 kDa protein PI31 forms a dimer and interacts with human Fbxo7, a component of the SCF-type E3 ubiquitin ligase, as well as with the E3 ubiquitin ligase Nutcracker in *Drosophila*, but its exact function remains unknown (Bader et al., 2011; Kirk et al., 2008; Li et al., 2014).

1.1.4.4 Proteasome activator 200 (PA200)

The proteasome activator 200 (PA200) was first described by Ustrell *et al.* in 2002 as a 200 kDa, monomeric, nuclear proteasome activator that activates all catalytic sites but mainly stimulates the C-L activity of the 20S proteasome (Ustrell et al., 2002). Moreover, PA200 did not degrade model substrates such as ubiquitinated lysozyme or casein in *in vitro* degradation assays, which led to the conclusion that PA200 does only degrade peptides but not intact proteins in an ATP- and ubiquitin-independent manner. PA200 and its yeast homologue Blm10 bind to 20S proteasomes and were also found in association with 26S proteasomes forming so-called hybrid proteasomes (Blickwedehl et al., 2007; Schmidt et al., 2005; Ustrell et al., 2002).

PA200 is expressed in several eukaryotes including mammals, *Saccharomyces cerevisiae*, *Caenorhabditis elegans* and *Arabidopsis thaliana*, but not in *Arachae* or *Drosophila melanogaster* (Fort et al., 2015; Ustrell et al., 2002). Although it is highly conserved among mammals, the sequence homology of the human PA200 and its yeast homologue Blm10 is very limited with only 17 % amino acid similarity (Ustrell et al., 2002). Despite this generally poor conservation, the sequence similarity is higher at the C-terminal region, which binds to

the 20S core particle and induces its gate opening (Fort et al., 2015; Sadre-Bazzaz et al., 2010).

Structural evidence on the activator is mainly provided by several studies analyzing the yeast analogue Blm10 (Iwanczyk et al., 2006; Sadre-Bazzaz et al., 2010; Schmidt et al., 2005). However, both proteins PA200 and Blm10 are composed of so-called HEAT (Huntingtin elongation factor 3 - PR65/A subunit of PP21- lipid kinase TOR) repeats consisting of two α -helices linked by a short loop and therefore seem to be structurally conserved (Fort et al., 2015; Kajava et al., 2004; Schmidt et al., 2005). The crystal structure of Blm10 indicates that the 32 highly variable HEAT repeats form a solenoid, dome-like structure capping the 20S core particle with a narrow entry pore (Sadre-Bazzaz et al., 2010; Stadtmueller and Hill, 2011). Association of Blm10 with the 20S core particle involves binding of the C-terminal regions of the activator to the 20S subunit α 5 inducing its repositioning, which forms a disordered and not fully opened gate into the core particle. This suggests that rather small, unfolded peptides and but not intact proteins are able to enter the 20S proteasome complex *via* the activator. Cryo-electron microscopy (cryo-EM) analysis of mammalian PA200-20S complexes purified from bovine testis also observed that the activator has an asymmetric and dome-like structure when bound to the 20S complex thus confirming data obtained from yeast (Figure 1.5) (Ortega et al., 2005).

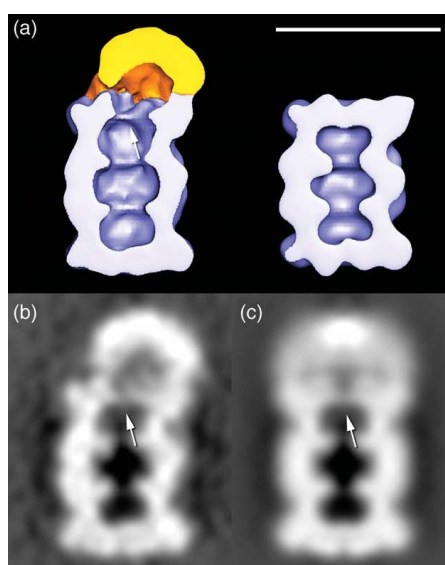


Figure 1.5: Structure of PA200-20S proteasome complexes obtained by cryo-EM analysis. A) Cut-through of an isosurface representation of PA200-20S (left) and 20S proteasomes (right) isolated from bovine testis analyzed by cryo-EM. PA200 is shown in yellow and the 20S catalytic core complex in blue. The arrow indicates the opening of the α -ring upon PA200 binding, whereas the pores of the uncapped 20S are in a closed state. Cryo-EM pictures of B) and C) show a central section (A) and a cylindrical average (B) corresponding to the complex shown in A). The arrow indicates decreased density at the α -ring (from Ortega *et al.*, 2005).

PA200 is in contact with all α -subunits of the 20S except $\alpha 7$, which forms an entry into the core particle. Moreover, the α -ring opens upon binding of PA200 allowing for the entry of substrates into the axial channel of the 20S proteasome.

Despite having a similar structure and associating with the 20S core particle, recent studies provided evidence for a differential function of mammalian PA200 and yeast Blm10 presumably resulting from the limited sequence homology of the protein in both species. Blm10 was suggested to be involved in proteasome maturation and assembly, as well as maintenance of mitochondrial integrity, which was not confirmed for mammalian PA200 (Fehlker et al., 2003; Li et al., 2007b; Marques et al., 2007; Tar et al., 2014). Moreover, Blm10-proteasome complexes were reported to mediate the degradation of Sfp1, a transcription factor driving ribosomal protein gene expression (Lopez et al., 2011). Another study proposed a role for Blm10 in maintaining genomic integrity and preventing DNA damage (Doherty et al., 2012).

In mammals, PA200 is ubiquitously expressed in different organs but it is most abundant in testis (Ustrell et al., 2002). It preferentially binds to standard 20S proteasomes and not to immunoproteasomes, which accords well with the observation that its expression is not inducible by INF γ (Blickwedehl et al., 2007; Fabre et al., 2014). PA200^{-/-} knockout mice are viable and do not exhibit developmental abnormalities except from a decrease in male fertility caused by impaired spermatogenesis. Qian *et al.* claimed that PA200 mediates ubiquitin-independent degradation of acetylated core histones, which is essential in the process of spermatogenesis. Defective histone degradation would therefore explain the phenotype of male infertility of PA200^{-/-} mice (Qian et al., 2013). They also proposed that acetylation of histones allows for the binding of PA200 via its bromodomain-like regions. However, as this study did not use a full deletion of all PA200-coding exons and claimed that Blm10 - despite its low conservation - exerts the same function in yeast, these data have to be considered with caution. Several other studies suggested an involvement of PA200 in DNA repair, as PA200-26S hybrid complexes were reported to accumulate on chromatin upon ionizing radiation and PA200 silencing decreased survival of cells upon the treatment (Blickwedehl et al., 2008; Ustrell et al., 2002). However, PA200-deficient embryonic stem cells did not show an increased sensitivity to DNA damage by radiation or bleomycin treatment, and therefore PA200 does not seem to be essential for DNA damage repair in this cell type (Khor et al., 2006). Later, it was suggested that PA200 maintains glutamine homeostasis by

increasing post-glutamyl activity of the proteasome thus elevating cellular glutamine levels and improving cellular survival in response to ionizing radiation treatment (Blickwedehl et al., 2012). In general, data on PA200 function have to be considered with caution, because unspecific antibodies were used in many studies as described in the results section 5 of this thesis. A recent study reported downregulation of PA200 by miRNA29b, which was suggested to be mediated by binding of the miRNA29b to the 3' untranslated region (UTR) of the *PSME4* gene (Wang et al., 2017). Here, PA200 was claimed to be a positive regulator of proteasome activity, which was not analyzed in more detail.

Taken together, the cellular function of PA200 is rather unclear. Recent publications reviewing the available data proposed that due to its structure PA200 could also exert a protein degradation-independent function by for example serving as a proteasomal adaptor protein recruiting 26S proteasome complexes to certain cellular compartments (Rechsteiner and Hill, 2005; Savulescu and Glickman, 2011; Stadtmueller and Hill, 2011). Besides the illusive functional role of PA200, its regulation and involvement in the pathogenesis of diseases is completely unknown and illustrates the need for further studies to unravel the role of this alternative proteasome activator.

1.1.5 Regulation of proteasome function according to cellular needs – the building block concept

Accurate adjustment of proteasome function is required for timely- and spatially-controlled, selective protein degradation, which is essential for various cellular processes and functions. Being a huge protein complex composed of different sub-components, proteasomes can be regulated on several levels (Livneh et al., 2016). These include the regulation *via* transcription of proteasomal genes, post-translational modifications (PTMs) of proteasomal subunits as well as the association of the 20S core particle with different activators. The quantity of cellular proteasomes can be regulated *via* the induction of proteasome subunit expression in response to certain cellular stimuli, but transcriptional and translational induction of proteasome subunits followed by *de novo* assembly of these huge protein complexes is time consuming and therefore does rather not allow for a fast adaption of proteolysis according to cellular needs (Meiners et al., 2003, 2014; Steffen et al., 2010).

The discovery of so-called intermediate 20S core particles consisting of different catalytic subunits of the standard but also the immunoproteasome as well as of additional alternative proteasome activators binding to the 20S core particle further increases the complexity of proteasome regulation and led to a novel concept on how cells are able to quickly adjust protein degradation (Dahlmann, 2016; Meiners et al., 2014). According to this concept, the cleavage specificity of the proteasome is determined by the catalytic subunits forming different intermediate 20S proteasome particles. The substrate specificity as well as timely- and spatially-controlled turnover of proteins, however, is regulated by proteasome activators associated to the core particle (Meiners et al., 2014). The recruitment of different proteasome activators to one or both sides of the various 20S core proteasomes can give rise to a variety of different proteasome complexes contributing to the complexity of the system (Figure 1.6 A and B).

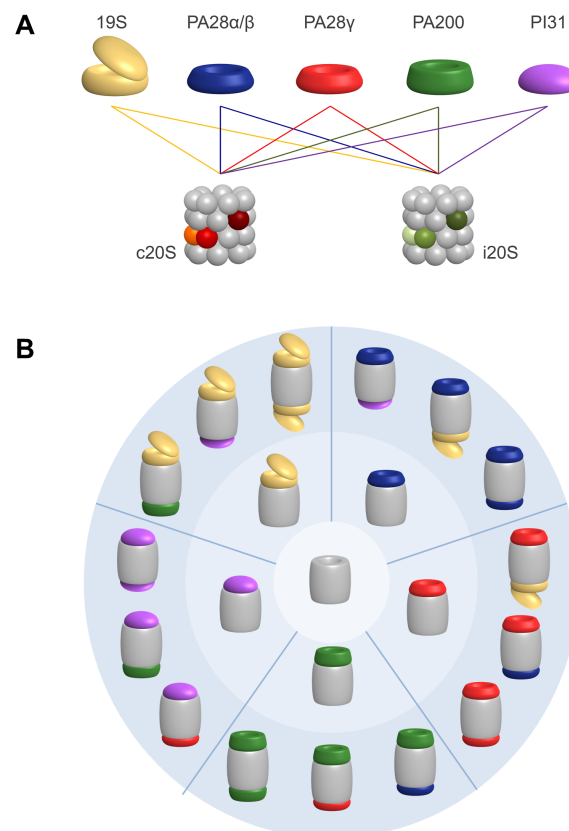


Figure 1.6: Building block concept: association of activators with the 20S core complex facilitates formation of diverse proteasome complexes. A) Proteasome complexes are composed of 20S proteasomes that are either uncapped or associated with one or two proteasome activators. Binding of the different proteasomal activators, including the 19S regulator (yellow), PA28αβ (blue), PA28γ (red) and PA200 (green), or PI31 (purple) to one or both ends of the 20S core particle can - in theory - give rise to many different complexes shown in B). Although not all of the depicted complexes have been identified within the cell yet, it is assumed that the association of activators with the catalytic core particle can allow for timely- and spatially-controlled regulation of proteasomal protein degradation according to cellular needs (adapted from Meiners et al., 2014).

Moreover, it provides a conceptual framework of how proteasome function can be adapted to cellular function: our so-called building-block concept hypothesizes that activators are recruited to the 20S proteasome in a timely- and spatially-controlled manner thus allowing for a fast adaption of proteasome function according to the cellular situation because new proteasomes complexes can be quickly assembled from free pools of their subcomponents. So far, only a very limited amount of studies provided evidence for fast adaption of proteasome complexes to certain cellular events. These mainly assessed the regulated assembly of 26S and 30S proteasomes from 20S cores and 19S regulators via post-translational modifications. Phosphorylation and acetylation of proteasomal subunits as well as the S-glutathiolation of 20S subunit $\alpha 5$ were reported to enhance proteasome activity, whereas glycosylation and oxidative modifications occurring during ageing and at conditions of oxidative stress inhibit proteasome activity (Guo et al., 2017; Livneh et al., 2016; Silva et al., 2012; VerPlank and Goldberg, 2017; Wang et al., 2013; Zhang et al., 2003). One recent study, for example, reported that 26S proteasome assembly and activity is regulated by protein kinase A-mediated phosphorylation of the 19S subunit RPN6 at Ser14 according to cellular cAMP levels (Lokireddy et al., 2015). Moreover, phosphorylation of 19S subunit RPT3 was shown to induce 26S/30S proteasome activity by enhancing substrate translocation during cell cycle progression (Guo et al., 2015). Evidence for the adaptive assembly of alternative proteasome complexes according to cellular needs, however, is currently lacking. Some studies describe an altered assembly of alternative proteasome complexes at conditions of oxidative stress such as the increased formation of PA28 $\alpha\beta$ complexes supporting the concept of adaptive regulation of the proteasome system upon cellular dysfunction (Pickering and Davies, 2013).

The proposed building block concept predicts that proteasome function - especially involving the association of activators to the 20S proteasome - is also adjusted in diseased tissues, when proteostasis is dysregulated (Balch et al., 2014). So far, evidence supporting this concept with regard to alternative proteasome complexes is limited to the observation that PA28 γ expression is induced in several types of cancer cells (Chai et al., 2014; Okamura et al., 2003; Xiong et al., 2014). While dysregulation of overall proteasomal activity has been observed for several diseases, such as in neurodegenerative and cardiovascular disorders and recently also for chronic lung diseases, altered association of proteasome regulators with the 20S catalytic core is a novel concept for cellular homeostasis and disease

pathogenesis (Dahlmann, 2007; Kammerl et al., 2016; Meiners et al., 2014; Schmidt and Finley, 2014; Semren et al., 2015; VerPlank and Goldberg, 2017). Targeting the specific interaction of proteasome activators with the 20S proteasome thus may provide a promising, novel approach to therapeutically interfere with specific subsets of proteasome complexes, which is in contrast to the global inhibition of 20S proteasomes by small molecule inhibitors of the catalytic sites (Gaczynska and Osmulski, 2015).

1.2 Idiopathic pulmonary fibrosis

Idiopathic pulmonary fibrosis (IPF) is a devastating, progressive and chronic interstitial lung disease (ILD) (Fernandez and Eickelberg, 2012a; Wynn, 2011). It is characterized by fibrotic remodeling of the lung architecture, which involves excessive deposition of extracellular matrix leading to loss of lung elasticity, an impairment of gas exchange and finally organ failure. Among all ILDs, which comprise diseases arising in the lung interstitium within the alveolar interspace, IPF occurs most frequently and progresses most aggressively (King et al., 2011). According to a meta-analysis of studies between 1968 and 2012, IPF has a rising incidence of on average 3-9 cases per 100 000 persons in Europe and North America affecting more men than women (Hutchinson et al., 2015). Age is considered as one of the main demographic risk factors, and the median age of patients at diagnosis is 66 years (Martinez et al., 2017; Nalysnyk et al., 2012). Despite its rather low incidence, IPF progresses aggressively and patients have a very poor prognosis with a median survival of 3-5 years after diagnosis (Fernandez and Eickelberg, 2012a). So far, treatment options are limited, which contributes to the low survival of patients. Cigarette smoking as well as exposure to dust from metals or wood have been described as environmental risk factors for developing the disease (Baumgartner et al., 2000). Different comorbidities, such as gastroesophageal reflux, obesity, diabetes mellitus or pulmonary hypertension - to only name a few examples - are discussed to contribute to the disease progression, but require further investigation (King et al., 2011; Raghu and Meyer, 2012). However, as the term "idiopathic" implicates, the etiology of the disease has not been fully understood yet and therefore the understanding of its pathogenesis is - besides the discovery of new biomarkers enabling early diagnosis - of high interest for current and future research (Raghu et al., 2011).

1.2.1 Pathological hallmarks of IPF

IPF displays a very heterogeneous histological pattern with alternating areas of normal tissue, injured and hyperplastic alveolar epithelium in honeycombing areas as well as fibrotic patches (Figure 1.7) (Fernandez and Eickelberg, 2012a; Martinez et al., 2017).

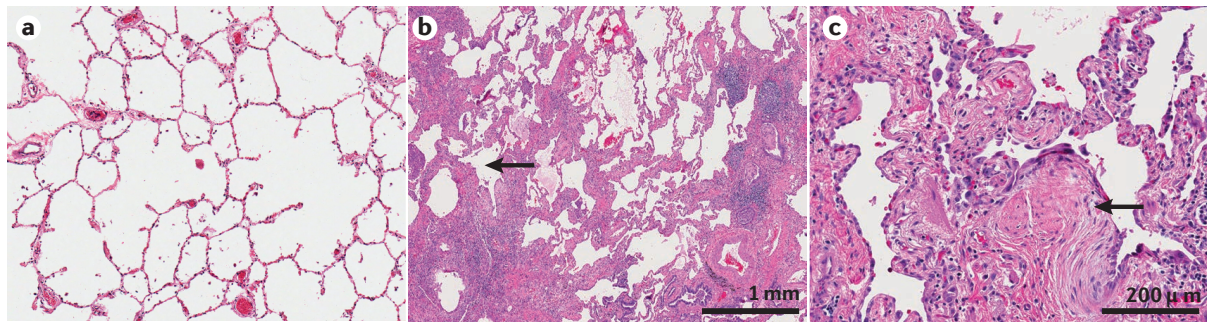


Figure 1.7: IPF tissue is characterized by a heterogeneous but characteristic histological pattern. A) Histological analysis (hematoxylin & eosin (H&E) staining) of a normal lung showing the terminal bronchiole, respiratory bronchiole, alveolar duct and alveoli. B) Low magnification H&E staining of a lung biopsy from an usual interstitial pneumonia (UIP) patient indicating characteristic honeycombing (arrow). UIP with an unknown cause is also termed idiopathic pulmonary fibrosis. C) Higher magnification histological analysis of the same patient as shown in B) indicating the presence of fibroblasts foci (arrow) (from Martinez *et al.*, 2017).

The sub-pleural parenchyma is the mostly affected region of the lung, which often indicates advanced tissue remodeling (Wolters *et al.*, 2014). The disease progresses from the exterior towards the central part of the lobule with sites of chronic injury being rather located in the parenchymal region and areas of active fibrosis being more in the central regions (Figure 1.8).

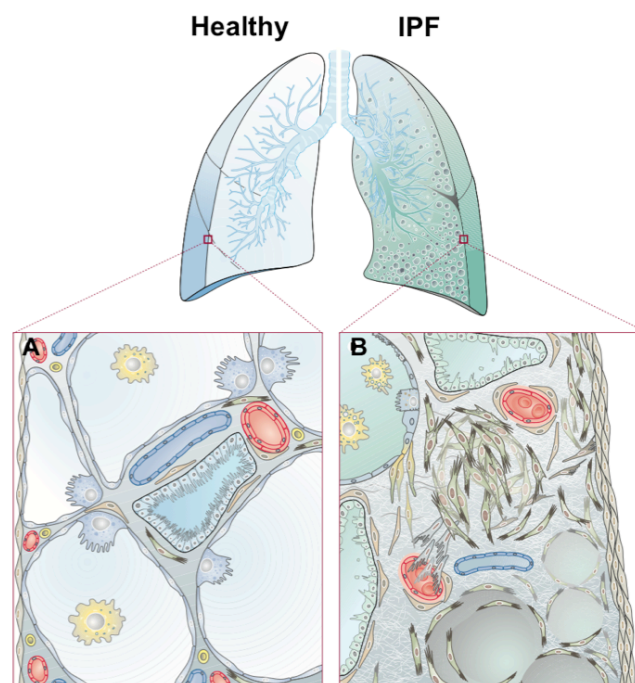


Figure 1.8: Schematic representation of normal lung architecture and IPF lung. Comparison between normal lung architecture (A) and severe fibrotic remodeling (B) in IPF lungs. Remodeling mostly localizes to the subpleural parenchyma in the lower parts of the lung lobes. Pathological hallmarks of IPF include an injured and hyperplastic alveolar epithelium, accumulation of myofibroblasts in so-called fibrotic foci, increased deposition of extracellular matrix and thickening of pleural septa (adapted from Fernandez *et al.* Eickelberg, 2012).

The pathological hallmarks of IPF are septal thickening, areas of airspace enlargement (so-called honeycombs), as well as fibrotic foci, which all contribute to the destruction of the alveolar architecture and reduction of pulmonary elasticity (Figure 1.7 and Figure 1.8) (Fernandez and Eickelberg, 2012a; Wolters et al., 2014). Honeycombs are areas of enlarged airspace containing mucus and inflammatory cells that are surrounded by fibrotic tissue. Fibroblast foci are accumulations of active and proliferating myofibroblasts, which secrete excessive amounts of extracellular matrix. They are often surrounded by hyperplastic pneumocytes or bronchiolar cells and frequently found at the interface of fibrotic and normal lung tissue at sites of epithelial injury. In contrast to scar tissue and honeycombs, fibroblast foci are indicative for areas of progressing fibrosis with ongoing injury and their presence has been associated with poor prognosis of patients (Cavazza et al., 2010).

1.2.2 Pathomechanisms of IPF

The pathogenesis of IPF is considered as an aberrant or dysregulated wound healing response to repetitive microinjuries of the alveolar epithelium, which leads to excessive deposition of extracellular matrix in the lung (Martinez et al., 2017). This results in progressive lung scarring and loss of the defined lung structures and elasticity impairing alveolar gas exchange. The general, physiological wound healing process consists of four steps leading to proper restoration of injured tissues (Figure 1.9) (Wynn, 2011): First, circulating platelets, which are essential components of the coagulation cascade, are activated by inflammatory mediators secreted from damaged epithelium or endothelium and form fibrin clots mediating wound closure. In a second step, these platelets induce recruitment of inflammatory cells, such as neutrophils, lymphocytes, macrophages and eosinophils, to the site of injury by increasing vessel permeability and secreting chemokines. Inflammatory cells in turn secrete transforming growth factor beta 1 (TGF- β 1) and other cytokines that augment the inflammatory response and mediate the activation, proliferation and migration of myofibroblasts. The different sources of myofibroblast are not completely understood yet, but might involve differentiation of resident fibroblasts, invasion of bone marrow fibrocytes or epithelial to mesenchymal transition (EMT) of epithelial cells. In the last step, myofibroblasts induce wound closure due to their contractile function and secrete extracellular matrix (ECM) components, which function as a scaffold for migration of

epithelial and endothelial cells mediating re-epithelialization and reconstitution of the tissue (Martin, 1997; Singer and Clark, 1999). Under normal conditions, the effector cells and ECM components are eliminated upon restoration of the tissue (Rockey et al., 2015).

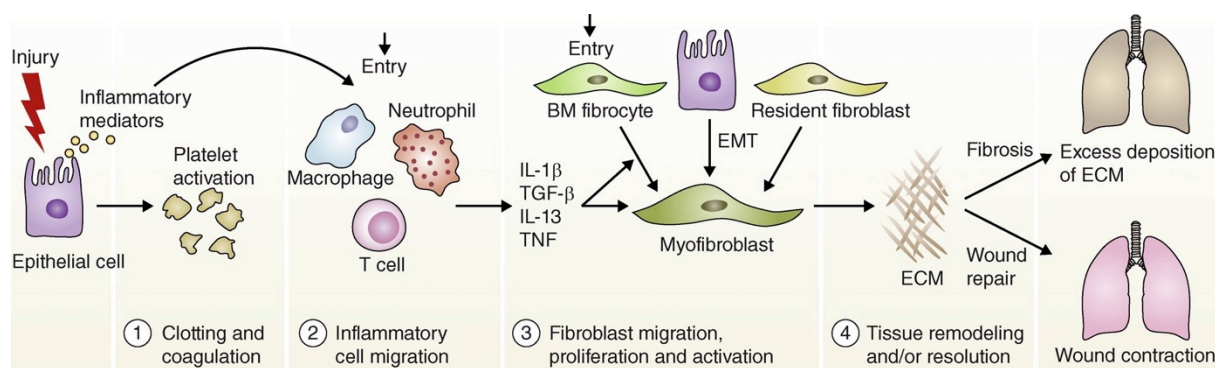


Figure 1.9: Dysregulation of normal wound healing induces fibrotic tissue remodeling of the lung. The scheme indicates the four stages of physiological wound healing: Epithelial cell injury induces secretion of inflammatory mediators and platelet activation, which also mediate wound closure. Inflammatory cells are recruited to the site of injury to prevent the entry of pathogens, to remove dead cells and to secrete pro-fibrotic cytokines, for example TGF- β 1. In the next step, these cytokines activate myofibroblasts from different origins, which then secrete ECM components to facilitate the migration of endothelial and epithelial cells to the sites of tissue repair and induce wound contraction under normal conditions leading to tissue repair. Fibrotic tissue remodeling is regarded as dysregulation of wound healing involving an excessive deposition of ECM and thereby destructing functional lung tissue (from Wynn *et al.*, 2011).

Fibrosis, however, arises when chronic injury or dysregulation of the physiological wound healing process leads to continuous ECM deposition and scar formation destroying the original tissue architecture (Rockey et al., 2015; Wynn, 2011). Research on the pathomechanism of IPF is focused on diverse aspects of the disease and a plethora of different factors have been discussed to contribute to its pathogenesis, but the exact underlying mechanism is not known yet. Fibrotic diseases from different organs often involve persistent inflammation (Thannickal et al., 2004; Wynn, 2011). The role of inflammation in IPF, however, is controversial as fibrotic remodeling was reported to precede without a remarkable inflammatory response, which accords well with the observation that anti-inflammatory therapies exhibit low efficiency (Rafii et al., 2013; Thannickal et al., 2004). The exact role of the innate and adaptive immune system, however, still requires further evaluation (Martinez et al., 2017). Ageing is considered as an important factor in IPF due to the fact that it is an age-related disease and lungs indeed show several molecular hallmarks of ageing (Martinez et al., 2017). Alveolar epithelial type 2 (AEC2) cells, progenitors of alveolar epithelial type 1 (AEC1) cells playing an important role in alveolar epithelial cell regeneration, exhibit different characteristics of ageing, such as genomic instability, cellular

senescence, mitochondrial dysfunction and loss of proteostasis to only name a few examples (Lehmann et al., 2017; Selman and Pardo, 2014). A genetic predisposition for developing IPF has also been discussed recently and several mutations in the lung epithelium have been identified in sporadic or familial IPF, including several genes contributing to telomere maintenance, the gene encoding the AEC2 marker protein surfactant protein C or mutations in the promoter region of the gene encoding mucin 5B (Armanios et al., 2007; Mulugeta et al., 2015; Seibold et al., 2012). Alveolar epithelial cells and myofibroblasts are considered as the main cell types involved in the continuous fibrotic remodeling in IPF (Wynn, 2011). Although the initial paradigm that repetitive epithelial micro-injury contributes to dysregulation of repair processes and fibrosis might be an important factor, the diversity of epithelial cell phenotypes in the diseased tissue including apoptosis, senescence but also hyperplastic proliferation is not understood yet (Martinez et al., 2017). Fibroblast foci are regarded as the active sites of fibrotic remodeling and myofibroblasts were discovered to be essentially involved in the production of ECM components, but the cellular origin of these myofibroblasts as well as how their persistence in the diseased lung is mediated has not been clarified yet. TGF- β 1 is the most extensively studied profibrotic cytokine influencing cellular differentiation, proliferation and apoptosis (Fernandez and Eickelberg, 2012b). Produced by a variety of different cells in the lung, TGF- β 1 induces recruitment of macrophages and fibroblasts, activation of myofibroblasts and secretion of other pro-inflammatory or pro-fibrotic cytokines and is thus considered as an important driver of fibrotic tissue remodeling.

The complex interaction between the described components, such as epithelial and mesenchymal cells as well as the ECM, requires further investigation in order to determine the exact mechanism leading to IPF.

1.2.3 Regulation of proteostasis in fibrotic tissue remodeling

The lung is in direct contact with the environment and constantly exposed to mechanical and environmental stresses, which challenge cellular proteostasis (Balch et al., 2014). Therefore, perturbation of proteostasis has been proposed to contribute to different lung diseases and has also gained more and more attention in IPF research (Balch et al., 2014; Weiss et al., 2010). The risk to develop IPF increases with age, and several studies reported that the ability

to cope with proteotoxic stress also decreases during ageing, suggesting that the proteostasis network could be affected in IPF (Kikis et al., 2010). Indeed, several components of the proteostasis network were observed to be regulated in fibrotic lung remodeling supporting this concept. Enhanced expression of ER stress markers and activation of the unfolded protein response (UPR) was observed in AEC2 cells in lungs of sporadic IPF patients (Korfei et al., 2008). However, the exact underlying mechanism – especially in sporadic IPF – has not been discovered yet, although herpes virus infection was discussed to contribute to enhanced ER stress (Lawson et al., 2008). In addition, several mutations in the *SPC* gene inducing misfolding of the protein in AEC2 that induce ER stress were discovered in cases of familial IPF (Korfei et al., 2016; Lawson et al., 2008; Mulugeta et al., 2015). Insufficient degradation of misfolded or redundant proteins induces proteotoxic stress and leads to an imbalance of protein homeostasis (Mora et al., 2017). Autophagy, one of the two main cellular degradation machineries, was shown to be decreased in IPF tissues (Patel et al., 2012). Moreover, impaired autophagy promoted myofibroblast differentiation and senescence of epithelial cells as well as fibrotic remodeling in mice leading to the assumption that an age-related impairment of autophagy might contribute to fibrosis in patients (Araya et al., 2013; Cabrera et al., 2015; Pardo and Selman, 2016).

The regulation of the proteasome as the major degradation machinery for intracellular proteins was first analyzed by a recent study of our group, which showed that 26S ubiquitin-dependent protein degradation is activated in fibrotic lung tissue (Semren et al., 2015). Here, we observed an induction of proteasome activity in fibrotic lungs of bleomycin-treated mice, which is a common animal model for experimentally induced fibrotic remodeling of the lung. IPF tissues exhibited elevated protein levels of the 19S subunit RPN6, which is rate-limiting for formation of 26S proteasomes (Pathare et al., 2012; Vilchez et al., 2012). RPN6 was mainly upregulated in myofibroblasts of fibroblast foci in IPF lungs, and *in vitro* experiments confirmed that proteasome function is indeed essential for TGF- β 1-induced myofibroblast differentiation. Therefore, regulation of the proteasome represents a further aspect of imbalanced proteostasis in IPF tissues.

2 Aims

The discovery of the different alternative proteasome activators has further extended the complexity of proteasome function. According to the building block concept, the recruitment of proteasome activators to different 20S proteasome core particles allows for fast, timely- and spatially-controlled adaption of proteasomal function according to cellular needs (Meiners et al., 2014). According to this concept, any imbalance of proteostasis in disease will involve adaptive alterations of proteasome function and alternative complex formation. However, the knowledge about the regulation of alternative proteasome activators and their association with the 20S proteasome core complex upon certain cellular stimuli or in the pathogenesis of disease is limited, and PA200 in particular has not been described in a disease context so far. The present study aimed to extend current knowledge on the regulation of proteasomal activators in lung biology and disease. The specific aims were as follows:

1. *Validating the specificity of antibodies for analysis of the proteasome activator PA200*

Preliminary data suggested that the widely used PA200 antibody that targets aa 1620-1634 of the human protein also detects a protein not related to PA200, which has previously been described as an isoform of the activator (Ustrell et al., 2002). In the first part of the thesis, this and other commercially available antibodies were validated for their specificity in detecting mouse or human isoforms of PA200 using PA200 siRNA-mediated silencing and tissues of PA200^{-/-} mice in order to ensure reliable and specific detection of PA200 in subsequent experiments.

2. *Investigating the regulation of alternative proteasome complexes in response to proteotoxic stress induced by proteasome inhibition*

Catalytic proteasome inhibition induces pronounced proteolytic stress and feeds back on the proteasome system by transcriptional upregulation of proteasomal genes (Meiners et al., 2003, 2007). Regulation of alternative proteasome complex formation, however, has not been studied in this system. Thus, the second chapter of this thesis aimed to investigate the regulation of proteasome complexes in response to proteasome inhibition

focusing on the kinetics of activator recruitment and on the underlying mechanism of alternative proteasome complex formation.

3. *Dissecting the regulation of PA200 in hyperproliferative lung diseases and investigating its function in primary human lung fibroblasts*

The third part of this thesis aimed to investigate the regulation of PA200 in hyperproliferative lung diseases including fibrotic tissue remodeling and lung cancer. For this purpose, IPF and lung cancer biopsies but also tissues from experimental murine kidney and lung fibrosis as well as lung cancer were analyzed to provide first evidence for a regulation of PA200 in disease. Moreover, the function of PA200 was investigated in primary human lung fibroblasts (phLF) by analyzing its interactome and characterizing the functional consequence of its silencing *via* transcriptomic and proteomic screens as well as validating suggested functions in cell culture experiments.

In summary, the present study aims to provide new insights into the adaption of the alternative proteasome activators PA28 γ and PA200 in response imbalanced proteostasis or diseases of the lung, thereby supporting the concept of the fine-tuned adjustment of proteasome function according to cellular needs *via* the recruitment of proteasomal activators to the 20S proteasome. Moreover, the detailed characterization of the so far unknown regulation of PA200 in disease as well as its cellular function adds a novel aspect to the pathogenesis of IPF and contributes to a better understanding of the underlying pathomechanism.

3 Materials

3.1 Antibodies

3.1.1 Primary antibodies

Antigen	Product number	Host	Type	Application	Dilution	Provider
Acetyl-Histone H2B (Lys5) (D5H1S)	12799	Rabbit	Monoclonal	WB	1:1000	Cell Signaling, Danvers, USA
Acetyl-Histone H3 (Lys9) (C5B11)	9649	Rabbit	Monoclonal	WB	1:1000	Cell Signaling, Danvers, USA
Acetyl-Histone H4 (Lys8)	2594	Rabbit	Polyclonal	WB	1:1000	Cell Signaling, Danvers, USA
AKT (pan) (C67E7)	4691	Rabbit	Monoclonal	WB	1:1000	Cell Signaling, Danvers, USA
CASP3	9662	Rabbit	Polyclonal	WB	1:2000	Cell Signaling, Danvers, USA
Cleaved CASP3	9661	Rabbit	Polyclonal	WB	1:1000	Cell Signaling, Danvers, USA
COL1A1	600401103	Rabbit	Polyclonal	WB	1:5000	Rockland Immunochemicals, Limerick, USA
Cyclin D1	2978	Rabbit	Monoclonal	WB	1:1000	Cell Signaling, Danvers, USA
Fibronectin	sc-9068	Rabbit	Polyclonal	WB	1:1000	Santa Cruz, Dallas, USA
GAPDH (HRP-linked)	14C10	Rabbit	Monoclonal	WB	1:80 000	Cell Signaling, Danvers, USA
Histone H2B (D2H6)	12364	Rabbit	Monoclonal	WB	1:1000	Cell Signaling, Danvers, USA
Histone H3 (D1H2)	4499	Rabbit	Monoclonal	WB	1:2000	Cell Signaling, Danvers, USA
Histone H4 (D2X4V)	13919	Rabbit	Monoclonal	WB	1:1000	Cell Signaling, Danvers, USA
IgG control	VEC-I-1000	Rabbit	Polyclonal	IP	as IgG control	Biozol Diagnostica, Eching Germany
Mouse IgG1 K isotype control	16-4714-82	Mouse	-	IP	as IgG control	Thermo Fisher Scientific, Waltham, USA
Normal rabbit IgG	2729	Rabbit	Polyclonal	IHC	as IgG control	Cell Signaling, Danvers, USA
p21	MAB88058	Mouse	Monoclonal	WB	1:3000	Merck Millipore, Billerica, USA
PA200 (for human)	NBP1-22236	Rabbit	Polyclonal	WB IP IHC IF	1:2500 3 μ L 1:500 1:500	Novus Biologicals, Littleton, USA
PA200 (for mouse)	NBP2-32575	Rabbit	Polyclonal	WB	1:500	Novus Biologicals, Littleton, USA
PA200	PA1-1961	Rabbit	Polyclonal	WB IHC	1:1000 1:600	Thermo Fisher Scientific, Waltham, USA
PA200	sc-135512	Rabbit	Polyclonal	IHC	1:50	Santa Cruz, Dallas, USA

Antigen	Product number	Host	Type	Appli- cation	Dilution	Provider
PA28 α	ab155091	Rabbit	Monoclonal	WB	1:1000	Abcam, Cambridge, United Kingdom
PA28 γ	sc-136025	Mouse	Monoclonal	WB IF	1:1000 1:300	Santa Cruz, Dallas, USA
PA28 γ	BML-PW8190	Rabbit	Polyclonal	WB IP	1:2000 3 μ L	Enzo Life Science, Lörrach, Germany
PARP (46D11)	9532	Rabbit	Monoclonal	WB	1:2000	Cell Signaling, Danvers, USA
PCNA	18-0110	Mouse	Monoclonal	WB	1:2000	Thermo Fisher Scientific, Waltham, USA
Phospho-AKT (Ser473) (D9E)	4060	Rabbit	Monoclonal	WB	1:1000	Cell Signaling, Danvers, USA
PSMA4	ab119419	Mouse	Monoclonal	WB	1:2000	Abcam, Cambridge, United Kingdom
RPL19	ab58328	Mouse	Monoclonal	WB	1:1000	Abcam, Cambridge, United Kingdom
RPN6	NBP1-46191	Rabbit	Polyclonal	WB	1:2000	Novus Biologicals, Littleton, USA
RPT5	A303-538A	Rabbit	Polyclonal	WB	1:5000	Bethyl Laboratories, Montgomery, USA
THBS1	ab85762	Rabbit	Polyclonal	WB	1:1000	Abcam, Cambridge, United Kingdom
UBIK48	05-1307	Rabbit	Monoclonal	WB	1:1000	Merck Millipore, Billerica, USA
α 1-7 (MCP231)	ab22674	Mouse	Monoclonal	WB	1:1000	Abcam, Cambridge, United Kingdom
α 4	BML-PW8120	Mouse	Monoclonal	WB IP	1:2000 3 μ L	Enzo Life Science, Lörrach, Germany
α 7	2456 S	Rabbit	Polyclonal	WB	1:1000	Cell Signaling, Danvers, USA
α SMA	A5228	Mouse	Monoclonal	WB	1:1000	Sigma Aldrich, St. Louis, USA
β 5	ab90867	Rabbit	Polyclonal	WB	1:1000	Abcam, Cambridge, United Kingdom
β -Actin (HRP-linked)	A3854	Mouse	Monoclonal	WB	1:80 000	Sigma Aldrich, St. Louis, USA

3.1.2 Secondary Antibodies

Antigen	Product number	Host	Appli- cation	Dilution	Provider
Anti-mouse IgG HRP-linked	7076	Horse	WB	1:40 000	Cell Signaling, Danvers, USA
Anti-mouse IgG HRP-linked	7074	Horse	WB	1:40 000	Cell Signaling, Danvers, USA

3.2 Oligonucleotides and vectors

Primers for quantitative real time polymerase chain reaction (RT-PCR), cloning and genotyping were purchased from Eurofins, Luxembourg.

3.2.1 Primers for quantitative RT-PCR

Gene	Species		Sequence 5'-3'
ACTA (α SMA)	human	FW	CGAGATCTCACTGACTACCTCATGA
		REV	AGAGCTACATAACACAGTTTCTCCTGA
ACTB (β -Actin)	human	FW	TCCATCATGAAGTGTGACGT
		REV	GAGCAATGATCTTGATCTCAT
CCND1 (Cyclin D1)	human	FW	CGTGGCCTCTAAGATGAAGG
		REV	CTGGCATTGGGAGAGGAAG
COL1A1	human	FW	CAAGAGGAAGGCCAAGTCGAG
		REV	TTGTCGCAGACGCAGATCC
FN	human	FW	CCGACCAGAAGTTTGGGTTCT
		REV	CAATGCGGTACATGACCCCT
GAPDH	human	FW	TGACCTCAACTACATGGTTTACATG
		REV	TTGATTTGGAGGGATCTCG
HPRT	human	FW	TGAAGGAGATGGGAGGCCA
		REV	AATCCAGCAGGTCAGCAAAGAA
PSMA3	human	FW	AGATGGTGTGTCTTTGGGG
		REV	AACGAGCATCTGCCAACAA
PSMB5	human	FW	TCAGTGATGGTCTGAGCCTG
		REV	CCATGGTGCCTAGCAGGTAT
PSMC3	human	FW	GTGAAGGCCATGGAGGTAGA
		REV	GTTGGATCCCCAAGTTCTCA
PSMD11	human	FW	GCTCAACACCCCAGAAGATGT
		REV	AGCCTGAGCCACGCATTTTA
PSME1	human	FW	CAAGGTGGATGTGTTTCGTG
		REV	TGCTCAAGTTGGCTTCATTG
PSME3	human	FW	TAGCCATGATGGACTGGATGG
		REV	CCTTGGTTCCTTGAAGGCT
PSME4	human	FW	CCAACAGGAAAAGAATGCCGA
		REV	CCAGGGCAGGTTTCTTTGCT
RPL19	human	FW	TGTACCTGAAGGTGAAGGGG
		REV	GCGTGCTTCCTTGGTCTTAG
TGFB1	human	FW	CGACTCGCCAGAGTGGTTAT
		REV	TAGTGAACCCGTTGATGTCCA
Col1a1	mouse	FW	CCAAGAAGACATCCCTGAAGTCA
		REV	TGCACGTCATCGCACACA
Fn	mouse	FW	GTGTAGCACAACCTCCAATTACGAA
		REV	GGAATTTCCGCCTCGAGTCT
Psme4	mouse	FW	CATCCTTCAAATAATGGGCG
		REV	AAGCTTATGGCTTTCAGGCA
Rpl19	mouse	FW	CGGGAATCCAAGAAGATTGA
		REV	TTCAGCTTGTGGATGTGCTC
Tnc	mouse	FW	GCTTCACTGGCAAAGACTGCAA
		REV	CGTAAAGCCCTCATGGCAGATA

3.2.2 Primers for genotyping of PA200^{-/-} mice

Primer	Sequence 5'-3'	T _m [°C]
PA200-wt-as	GTTGTTTGTAGTTGTCAGGCTC	56.0
I15.07	CCACCATCTAGGTTAAAGGT	53.0
I29.02.Xho	CCGCTCGAGGGCAGTACAGTCTTACT	67.0

3.2.3 Primers for cloning of PA200 construct

Primer	Sequence 5'-3'	T _m [°C]
PA200 FW	TATGCTAGCCCGAGGAGATCTGC	69
PA200 REV	ATGGTACCCTATGCATAATAGCATGGTG	69

3.2.4 siRNAs

Silencer® select siRNAs for RNA interference were obtained from Ambion, Thermo Fisher Scientific, Waltham, USA. siRNAs were dissolved in nuclease free water at a stock concentration of 10 µM and stored in aliquots at -20 °C.

siRNA	siRNA ID	Product number	Species
Silencer Select PSME4 siRNA 1	s23262	4392420	Human
Silencer Select PSME4 siRNA 2	s23263	4392420	Human
Silencer Select PSME3 siRNA 1	s19871	4392420	Human
Silencer Select PSME3 siRNA 2	s19873	4392420	Human
Silencer Select PSMD11 siRNA	s11413	4392420	Human
Silencer Select PSME4 siRNA 1	S98099	4390771	Mouse
Silencer Select PSME4 siRNA 2	S98098	4390771	Mouse
Silencer Select Negative Control No.1	-	4390843	Mouse/Human
Silencer Select Negative Control No. 2	-	4390847	Mouse/Human

3.2.5 Plasmids

Vector	Product number	Provider
Myc-DDK N-terminal tagged human PSME4	RC222965	OriGene Technologies, Rockville, USA
pcDNA3.1/Zeo(+)	V79020	Thermo Fisher Scientific, Waltham, USA

3.3 Cell culture

3.3.1 Cell lines

All cell lines were purchased from the American Type Culture Collection (ATCC), Manassas, USA.

Cell line	Origin	Specification
A549	Human adenocarcinoma, alveolar epithelial basal cell	ATCC-Nr. CCL-185
CCL-206	Mouse newborn lung fibroblast	ATCC-Nr. CCL-206

3.3.2 Primary human lung fibroblasts

Primary human lung fibroblasts from different donors were provided by Prof. Dr. Andreas Günther, Universities of Giessen and Marburg Lung Center (UGMLC), Giessen, Germany.

ID	Patient data
406	Female, 50 years, peripheral normal lung tissue, organ donor
409Sp	Male, 51 years, peripheral normal lung tissue, organ donor
411a	Female, 44 years, peripheral normal lung tissue, organ donor
423g	Female, 41 years, peripheral normal lung tissue, organ donor
Gi-151	Female, 60 years, histologically normal areas of lung specimens obtained after resective surgery for benign or malignant tumors
Gi-152	Female, 72 years, histologically normal areas of lung specimens obtained after resective surgery for benign or malignant tumors

3.3.3 Cell culture media

Cell type	Cell culture medium	Product number	Provider
phLF	MCDB 131	P04-80057	PAN-Biotech, Aidenbach,, Germany
	10 % Fetal bovine serum (FBS) Superior	S 0615	Biochrom, Berlin, Germany
	100 U/mL Penicillin/Streptomycin	15140-122	Thermo Fisher Scientific, Waltham, USA
	2 mM L-glutamine	G7513	Sigma-Aldrich, St. Louis, USA
	2 ng/mL Basic-FGF	13256029	Thermo Fisher Scientific, Waltham, USA
	0.5 ng/mL EGF	E9644	Sigma-Aldrich, St. Louis, USA
	5 µg/mL Insulin	12585-O14	Thermo Fisher Scientific, Waltham, USA
A549	DMEM + GlutaMAX	21885025	Thermo Fisher Scientific, Waltham, USA
	10 % FBS Superior	S 0615	Biochrom, Berlin, Germany
	100 U/mL Penicillin/Streptomycin	15140-122	Thermo Fisher Scientific, Waltham, USA
CCL-206	DMEM-F12	31330	Thermo Fisher Scientific, Waltham, USA
	10 % FBS Superior	S 0615	Biochrom, Berlin, Germany
	100 U/mL Penicillin/Streptomycin	15140-122	Thermo Fisher Scientific, Waltham, USA

3.4 Human donor and IPF lung tissue

Lung tissues of donors and IPF patients were provided by Prof. Dr. Andreas Günther, Universities of Giessen and Marburg Lung Center (UGMLC), Gießen, Germany. All samples were approved with ethical consent according to national and international guidelines.

ID	Patient data
198	Male, 61 years, peripheral normal lung tissue, organ donor
2B	Male, 29 years, peripheral normal lung tissue, organ donor
22	Unknown, peripheral normal lung tissue, organ donor
46	Unknown, peripheral normal lung tissue, organ donor
58	Male, 53 years, peripheral normal lung tissue, organ donor
Gi-151	Female, 60 years, histologically normal areas of lung specimens obtained after resective surgery for benign or malignant tumors
200	Male, 42 years, peripheral normal lung tissue, organ donor
406	Female, 50 years, peripheral normal lung tissue, organ donor
409Sp	Male, 51 years, peripheral normal lung tissue, organ donor
411a	Female, 44 years, peripheral normal lung tissue, organ donor
146	Male, 60 years, IPF patient
190	Female, 44 years, IPF patient
207	Male, 47 years, IPF patient
302	Male, 54 years, IPF patient
324	Male, 34 years, IPF patient
325	Female, 51 years, IPF patient
327	Male, 61 years, IPF patient
330	Female, 46 years, IPF patient
331	Male, 57 years, IPF patient
334	Female, 42 years, IPF patient
335	Female, 57 years, IPF patient

3.5 Human lung cancer tissue

Human lung tissue obtained from patients surgically treated for lung cancer was provided by the Asklepios Biobank for Lung Disease, Gauting, Germany. Samples were approved with ethical consent according to national and international guidelines (project number 333-10).

ID	Patient data
ASK89	Female, 72 years old, squamous cell carcinoma
ASK86	Male, 60 years old, squamous cell carcinoma
ASK223	Female, 61 years old, adenocarcinoma
ASK215	Male, 67 years old, adenocarcinoma
ASK211	Male, 76 years old, typical carcinoid
ASK210	Male, 83 years old, adenocarcinoma
ASK204	Male, 67 years old, squamous cell carcinoma
ASK147	Female, 75 years old, adenocarcinoma

3.6 Drugs and treatments

Drug	Solvent	Stock concentration	Provider
Bortezomib	DMSO	2.6 mM	Millenium, Pharmaceuticals, Takeda, Cambridge, USA
Oprozomib	DMSO	10 mM	Onyx Pharmaceuticals, San Francisco, USA
Epoxomicin	DMSO	10 mM	APExBio, Houston, USA
TGF- β 1	4 mM HCl + 1 mg/mL BSA	1000 ng/mL	R&D Systems, Minneapolis, USA
Staurosporine	DMSO	1 mM	Biomol, Hamburg, Germany

3.7 Enzymes

Product	Provider
DNase 2 U/ μ L	Peqlab, Erlangen, Germany
KpnI	New England Biolabs, Ipswich, USA
M-MLV Reverse Transcriptase	Sigma-Aldrich, St. Louis, USA
NheI	New England Biolabs, Ipswich, USA
Phusion Polymerase	Thermo Fisher Scientific, Waltham, USA
Proteinase K	AppliChem, Darmstadt, Germany
Taq Polymerase	Thermo Fisher Scientific, Waltham, USA

3.8 Kits

Product	Provider
NucleoSpin [®] Plasmid purification kit	Macherey-Nagel, Düren, Germany
NucleoBond [®] PC500 plasmid purification kit	Macherey-Nagel, Düren, Germany
NucleoSpin [®] Gel and PCR clean up	Macherey-Nagel, Düren, Germany
Cell Proliferation ELISA, BrdU (colorimetric)	Roche Diagnostics, Mannheim, Germany
LightCycler 480 SYBR Green I Master	Roche Diagnostics, Mannheim, Germany
Pierce BCA Protein Assay Kit	Thermo Fisher Scientific, Waltham, USA
Proteasome-Glo [™] Assay	Promega, Fitchburg, USA
Roti-Quick RNA Extraction Kit	Carl Roth, Karlsruhe, Germany
Vulcano Fast Red Chromogen Kit	Biocare Medical, Concord, Canada
peqGOLD Total RNA-Kit	Peqlab, Erlangen, Germany
Trichrome (Masson) Staining Kit	Sigma-Aldrich, Munich, Germany
WT PLUS Reagent Kit	Affymetrix, Santa Clara, US

3.9 Markers

Product	Provider
Protein Marker IV (10-245 kDa)	AppliChem, Darmstadt, Germany
DNA-ladder 100 bp Plus, peqGOLD	VWR Peqlab, Rednore, USA
DNA-ladder 1 kb Plus, peqGOLD	VWR Peqlab, Rednore, USA

3.10 Buffer formulations

All buffers were prepared with Milli-Q® water.

Buffer	Reagent	Concentration
0.1 M Phosphate buffer pH 8	Na ₂ HPO ₄	93.2 mM
	NaH ₂ PO ₄	6.8 mM
2x Fluorescence proteasome activity assay buffer	Tris pH 8.2	450 mM
	KCl	90 mM
	Magnesium acetate	15 mM
	Magnesium chloride	15 mM
5x Native loading buffer	Tris	250 mM
	Glycerol	50 % (v/v)
	Bromophenol blue	0.01% (w/v)
6x Laemmli buffer	Tris	300 mM
	Glycerol	50 % (v/v)
	SDS	6% (w/v)
	Bromophenol blue	0.01 % (w/v)
	DTT	600 mM
AnnexinV binding buffer	HEPES	10 mM
	NaCl	140 mM
	CaCl ₂	2.5 mM
Citrate buffer pH 6	Citric acid monohydrate	1.8 mM
	Sodium citrate tribasic	8.2 mM
Extraction buffer (histone extraction)	HEPES pH 7.9	10 mM
	KCl	10 mM
	MgCl ₂	1.5 mM
	Sucrose	0.34 M
	Glycerol	10 % (v/v)
High-salt solubilization buffer (histone extraction)	Tris-HCl pH 8.0	50 mM
	NaCl	2.5 M
	IGEPAL	0.05 % (v/v)
Native gel running buffer	Tris	89 mM
	Boric acid	89 mM
	EDTA	2 mM
	MgCl ₂	5 mM
	ATP	2 mM
	DTT	1 mM
No-salt buffer (histone extraction)	EDTA	3 mM
	EGTA	0.2 mM
PBNB buffer	KCl	50 mM
	Tris-HCl pH 8.3	10 mM
	MgCl ₂	2.5 mM
	Gelatin	0.01 % (w/v)
	IGEPAL	0.45 % (v/v)
PBST washing buffer	Tween-20	0.45 % (v/v)
	NaCl	137 mM
	KCl	2.7 mM
	Na ₂ HPO ₄	10 mM
	KH ₂ PO ₄	2 mM
Phosphate buffered saline (PBS) pH 7.4	Tween-20	1 % (v/v)
	NaCl	137 mM
	KCl	2.7 mM
	Na ₂ HPO ₄	10 mM
	K ₂ HPO ₄	2 mM

Buffer	Reagent	Concentration
Proteasome activity overlay assay reaction buffer	Tris pH 7.5	50 mM
	ATP	1 mM
	MgCl ₂	10 mM
	DTT	1 mM
	Suc-LLVY-AMC	0.05 mM
RIPA lysis buffer pH 7.5	Tris/HCl pH 7.5	50 mM
	NaCl	150 mM
	IGEPAL	1 % (v/v)
	Sodium deoxycholate	0.5 % (w/v)
	SDS	0.1 % (w/v)
	cOmplete® protease inhibitor	1x
SDS PAGE running buffer	Tris	25 mM
	Glycin	192 mM
	SDS	0.1 % (w/v)
Solubilization buffer	Na ₂ CO ₃	66 mM
	SDS	2 % (w/v)
	β-mercaptoethanol	1.5 % (v/v)
TAE buffer	Tris	40 mM
	Acetic acid	20 mM
	EDTA	1 mM
Tris buffered saline and Tween (TBST) pH 7.6	Tris pH 7.6	20 mM
	NaCl	135 mM
	Tween-20	0.02 % (v/v)
TSDG buffer pH 7.0	Tris pH 7.0	10 mM
	NaCl	10 mM
	MgCl ₂	1.1 mM
	EDTA	0.1 mM
	DTT	1 mM
	NaN ₃	1 mM
	Glycerol	10 % (v/v)
Western blot transfer buffer	Tris	25 mM
	Glycine	192 mM
	Methanol	10 % (v/v)

3.11 Reagents

Product	Solvent	Stock concentration	Provider
4',6-Diamidin-2-phenylindol (DAPI)	PBS	1 M	Sigma-Aldrich, St. Louis, USA
6x DNA Loading Dye	-	6x	Thermo Fisher Scientific, Waltham, USA
Activity based probe LW124	DMSO	2.5 μM	Prof. Dr. H. Overkleeft, University of Leiden, Netherlands
Activity based probe MV151	DMSO	50 μM	Prof. Dr. H. Overkleeft, University of Leiden, Netherlands
Activity based probe MVB127	DMSO	25 μM	Prof. Dr. H. Overkleeft, University of Leiden, Netherlands
Adenosine triphosphate (ATP)	-	-	Roche Diagnostics, Mannheim, Germany

Product	Solvent	Stock concentration	Provider
Ampicillin	-	100 mg/mL	Bioline, Luckenwalde, Germany
Annexin V-FITC	-	-	BD Biosciences, San Jose, USA
Antibody diluent	-	-	Dako, Hamburg, Germany
Bouin's Solution	-	-	Sigma-Aldrich, St. Louis, USA
Bovine serum albumin (BSA)	-	-	AppliChem, Darmstadt, Germany
Bz-valine-glycine-arginine-aminomethylcoumarine (Bz-Val- Gly-Arg-AMC)	DMSO	2 mM	Bachem, Bubendorf, Switzerland
cOmplete™ protease inhibitor cocktail	H ₂ O	25x	Roche, Basel, Switzerland
Dithiotreitol (DTT)	H ₂ O	1 M	Life Technologies, Carlsbad, USA
Dynabeads™ Protein A	-	-	Thermo Fisher Scientific, Waltham, USA
Dynabeads™ Protein G	-	-	Thermo Fisher Scientific, Waltham, USA
ECL prime Western blotting reagent	-	-	GE Healthcare, Cölbe, Germany
Entellan	-	-	Merck Millipore, Darmstadt, Germany
Eosin G 0.5 %	H ₂ O	-	Carl Roth, Karlsruhe, Germany
First Strand Buffer	-	5x	Life Technologies, Carlsbad, USA
Fluorescent Mounting Medium	-	-	Dako, Hamburg, Germany
Hemalaun	-	-	Carl Roth, Karlsruhe, Germany
Immunizing peptide of PA200 Thermo antibody	-	-	GenScript, Piscataway, USA
Kanamycin	-	10 mg/mL	PAN Biotech, Aidenbach, Germany
LB Agar	-	-	Carl Roth, Karlsruhe, Germany
LB Medium	-	-	Carl Roth, Karlsruhe, Germany
Lipofectamine® LTX with Plus Reagent	-	-	Thermo Fisher Scientific, Waltham, USA
Lipofectamine® RNAiMAX	-	-	Thermo Fisher Scientific, Waltham, USA
Luminata™ Classico Western HRP Substrate	-	-	Merck Millipore, Darmstadt, Germany
Luminata™ Forte Western HRP Substrate	-	-	Merck Millipore, Darmstadt, Germany
MACH 2 Rabbit AP-Polymer	-	-	Biocare, Concord, USA
Normal Goat Serum	-	-	Cell Signaling, Danvers, USA
Nuclease-Free Water	-	-	Ambion, Thermo Fisher Scientific, Waltham, USA
Nucleotide Mix	-	10 mM	Promega, Fitchburg, USA
Opti-MEM Reduced Serum Medium	-	-	Thermo Fisher Scientific, Waltham, USA
Penicillin/Streptomycin	-	-	Thermo Fisher Scientific, Waltham, USA
Propidium iodide	-	-	BD Biosciences, San Jose, USA
Random Hexamers	-	250 µM	Promega, Fitchburg, USA
RNAasin RNase Inhibitor	-	40 U/µL	Promega, Fitchburg, USA
Rodent Block M	-	-	Biocare, Concord, USA

Product	Solvent	Stock concentration	Provider
Roti-Block	-	10x	Carl Roth, Karlsruhe, Germany
Roti-Immunoblock	-	10x	Carl Roth, Karlsruhe, Germany
SOC medium	-	-	Takara, Kusatsu, Japan
Succinyl-leucine-leucine-valine-tyrosine-aminomethylcoumarine (Suc-LLVY-AMC)	DMSO	2 mM	Bachem, Bubendorf, Switzerland
SuperSignal West FEMTO	-	-	Thermo Fisher Scientific, Waltham, USA
SYBR Safe	-	-	Thermo Fisher Scientific, Waltham, USA
Trypsin (0.25 % EDTA)	-	-	Thermo Fisher Scientific, Waltham, USA
Vulcan Fast Red	-	-	Biocare, Concord, USA
Weigert's Iron Hematoxylin solution	-	-	Sigma-Aldrich, St. Louis, USA
Z-norleucine-proline-norleucine-aspartate-aminomethylcoumarine (Z-nLPnLD-AMC)	DMSO	2 mM	Bachem, Bubendorf, Switzerland

3.12 Chemicals

Product	Provider
Boric acid	AppliChem, Darmstadt, Germany
Bromophenol blue	AppliChem, Darmstadt, Germany
Citric acid monohydrate	AppliChem, Darmstadt, Germany
Dithiothreitol (DTT)	Life Technologies, Carlsbad, USA
DMSO	Carl Roth, Karlsruhe, Germany
EDTA	AppliChem, Darmstadt, Germany
EGTA	AppliChem, Darmstadt, Germany
Ethanol	AppliChem, Darmstadt, Germany
Gelatin	Sigma-Aldrich, St. Louis, USA
Glycerol	AppliChem, Darmstadt, Germany
Glycine	AppliChem, Darmstadt, Germany
IGEPAL	Sigma-Aldrich, St. Louis, USA
Isopropanol (p. A.)	AppliChem, Darmstadt, Germany
Magnesium acetate	Sigma-Aldrich, St. Louis, USA
Magnesium chloride	AppliChem, Darmstadt, Germany
Methanol (p. A.)	AppliChem, Darmstadt, Germany
Paraformaldehyde	AppliChem, Darmstadt, Germany
Potassium chloride	AppliChem, Darmstadt, Germany
Potassium phosphate monobasic	AppliChem, Darmstadt, Germany
Sodium azide	AppliChem, Darmstadt, Germany
Sodium chloride	AppliChem, Darmstadt, Germany
Sodium citrate tribasic dihydrate	AppliChem, Darmstadt, Germany
Sodium deoxycholate	AppliChem, Darmstadt, Germany
Sodium phosphate dibasic	AppliChem, Darmstadt, Germany
Sodiumdodecylsulfate (SDS)	AppliChem, Darmstadt, Germany
Sucrose	AppliChem, Darmstadt, Germany
Tris	AppliChem, Darmstadt, Germany
Triton X-100	Life Technologies, Carlsbad, USA
Tween-20	AppliChem, Darmstadt, Germany
Xylene	AppliChem, Darmstadt, Germany
β -Mercaptoethanol	AppliChem, Darmstadt, Germany

3.13 Consumables

Product	Provider
6/24/96 well plates	TPP, Trasadingen, Switzerland
96 well plates, white, for luminescence detection	Berthold Technologies, Bad Wildbad, Germany
Cell culture dishes (6 cm, 10 cm 15 cm)	Nunc, Wiesbaden, Germany
Cell culture flasks (75 cm ² , 175 cm ²)	Nunc, Wiesbaden, Germany
Cryovials 1.5 ml	Greiner Bio-One, Frickenhausen, Germany
D-Tube™ Dialyzer Midi, MWCO 3.5 kDa	Merck Millipore, Darmstadt, Germany
Dismembrator Tubes (Nalgene Cryogenic Tubes)	Thermo Fisher Scientific, Waltham, USA
Falcon tubes (15 mL, 50 mL)	BD Bioscience, Heidelberg, Germany
Glass pasteur pipettes	VWR International, Darmstadt, Germany
Microplate 96-well, PS, flat bottom (for BCA assay)	Greiner Bio-One, Frickenhausen, Germany
NuPAGE Novex 3-8 % Tris-Acetate Gel 1.5 mm (10 & 15 well)	Thermo Fisher Scientific, Waltham, USA
PCR plates, white, 96 well	Biozym Scientific, Hessisch Oldendorf, Germany
Pipet tips	Biozym Scientific, Hessisch Oldendorf, Germany
Protein LoBind tube 1.5 mL	Eppendorf, Hamburg, Germany
PVDF membrane	Bio-Rad, Hercules, USA
SafeSeal reaction tubes (0.5 mL, 1.5 mL, 2.0 mL)	Sarstedt, Nümbrecht, Germany
Sealing foil for qPCR plate	Kisker Biotech, Steinfurt, Germany
Serological pipettes Cellstar 2, 5, 10, 25 and 50 mL	Greiner Bio-One, Frickenhausen, Germany
Sterican cannulas	BD Bioscience, Heidelberg, Germany
Super RX Fuji medical X-ray film	Fujifilm Corporation, Tokyo, Japan
Syringes (10 mL, 20 mL, 50 mL)	Neolab, Heidelberg, Germany
Whatman blotting paper 3 mm	GE Healthcare, Freiburg, Germany

3.14 Technical devices and further equipment

Technical device	Provider
-20 °C freezer MediLine LGex 410	Liebherr, Biberach, Germany
-80 °C freezer	Eppendorf, Hamburg, Germany
-80 °C freezer U570 HEF	New Brunswick, Hamburg, Germany
Analytical scale XS20S Dual Range	Mettler-Toledo, Gießen, Germany
Autoclave DX-45	Systec, Wetztenberg, Germany
Autoclave VX-120	Systec, Wetztenberg, Germany
Cell culture work bench Herasafe KS180	Thermo Fisher Scientific, Waltham, USA
Centrifuge MiniSpin plus	Eppendorf, Hamburg, Germany
Centrifuge Rotina 420R	Hettich, Tuttlingen, Germany
Centrifuge with cooling, Micro220R	Hettich, Tuttlingen, Germany
CO ₂ cell incubator BBD6620	Thermo Fisher Scientific, Waltham, USA
Cytospin 2 centrifuge	Hettich, Tuttlingen, Germany
Dismembrator S	Satorius, Göttingen, Germany
Dry ice container Forma 8600 Series, 8701	Thermo Fisher Scientific, Waltham, USA
DynaMag-2	Thermo Fisher Scientific, Waltham, USA
Electrophoretic Transfer Cell, Mini Protean Tetra Cell	Bio-Rad, Hercules, USA
FACS LSRII	Becton Dickinson, Franklin Lakes, USA
Film developer Curix 60	AGFA, Morsel, Belgium
flexiVent system	SCIREQ, Montreal, Canada
Fluorescent scanner Typhoon TRIO+	Amersham Biosciences, Amersham, UK
Gel imaging system ChemiDoc XRS+	Bio-Rad, Hercules, USA
Hemocytometer	Brand, Wertheim, Germany
Hyrax M55 microtome	Zeiss, Jena, Germany

Technical device	Provider
Ice machine ZBE 110-35	Ziegra, Hannover, Germany
Intell-Mixer RM-2	Schubert & Weiss Omnilab, Munich, Germany
Light Cycler LC480II	Roche Diagnostics, Mannheim, Germany
Liquid nitrogen cell tank BioSafe 420SC	Cryotherm, Kirchen/Sieg, Germany
Liquid nitrogen tank Apollo 200	Cryotherm, Kirchen/Sieg, Germany
Magnetic stirrer KMO 2 basic	IKA, Staufen, Germany
Mastercycler gradient	Eppendorf, Hamburg, Germany
Mastercycler Nexus	Eppendorf, Hamburg, Germany
Microm STP 420D Tissue Processor	Thermo Fisher Scientific, Waltham, USA
Milli-Q® Advantage A10 Ultrapure Water Purification System	Merck Millipore, Darmstadt, Germany
Milli-Q® Integral Water Purification System for Ultrapure Water	Merck Millipore, Darmstadt, Germany
Mini Centrifuge MCF-2360	Schubert & Weiss Omnilab, Munich, Germany
Mirax scanner	Zeiss, Jena, Germany
Multipette stream	Eppendorf, Hamburg, Germany
Nalgene Freezing Container (Mister Frosty)	Omnilab, Munich, Germany
NanoDrop 1000	PeqLab, Erlangen, Germany
pH meter InoLab pH 720	WTW, Weilheim, Germany
Plate centrifuge 5430	Eppendorf, Hamburg, Germany
Plate reader Sunrise	Tecan, Crailsheim, Germany
Plate reader TriStar LB941	Berthold Technologies, Bad Wildbach, Germany
Power Supply Power Pac HC	Bio-Rad, Hercules, USA
Refrigerator Profi Line	Liebherr, Biberach, Germany
Research plus pipettes	Eppendorf, Hamburg, Germany
Roll mixer	VWR International, Darmstadt, Germany
Scale XS400 2S	Mettler-Toledo, Giessen, Germany
Shaker Duomax 1030	Heidolph, Schwabach, Germany
Thermomixer compact	Eppendorf, Hamburg, Germany
Tissue Lyser II	Quiagen, Hilden, Germany
Vacuum pump NO22AN.18 with switch 2410	KNF, Freiburg, Germany
Vortex mixer	IKA, Staufen, Germany
Water bath Aqua Line AL 12	Lauda, Lauda-Königshofen, Germany

3.15 Software

Software	Provider
Adobe Illustrator	Adobe Systems, San Jose, USA
Axio Vision	Zeiss, Jena, Germany
BD FACSDIVA™	Becton Dickinson, Franklin Lakes, USA
GraphPad Prism 5 and 7	GraphPad Software, La Jolla, USA
Image Lab	Bio-Rad, Hercules, USA
ImageJ	National Institutes of Health, Bethesda, USA
LightCycler® 480 SW 1.5	Roche Diagnostics, Mannheim, Germany
Magellan Software	Tecan, Crailsheim, Germany
Microsoft Office Professional Plus 2010	Microsoft, Redmond, USA
Pannoramic Viewer	3DHISTECH, Budapest, Hungary
Tristar MicroWin 2000	Berthold Technologies, Bad Wildbach, Germany

4 Methods

4.1 Animal experiments

4.1.1 Oxalate-induced kidney fibrosis mouse model

Murine fibrotic kidney tissue (frozen and paraffin-embedded) and control tissue was provided by the group of Prof. Dr. Anders (Medizinische Klinik und Poliklinik IV, Klinikum der Universität München, Munich, Germany). Kidney fibrosis was induced by feeding female mice with 50 $\mu\text{mol/g}$ sodium oxalate in a standard diet for 21 days, which causes chronic kidney disease (CKD) (Mulay et al., 2016).

4.1.2 *Kras*^{LA2} mutant lung cancer mouse model

The 129S/Sv-*Kras*^{tm3Tyj/J} (*Kras*^{LA2}) mutant mouse strain was obtained from the Jackson Laboratory. Mice were crossbred with FVB-NCrl wildtype females (Charles River Laboratories) for more than seven generations. *Kras*^{LA2} mice exhibit a genetically induced duplication of exon 1 in the *Kras* gene. Both of these exon 1 copies contain an activating glycine to aspartic acid mutation at codon 12 (G12D). *In vivo* recombination causes an active, oncogenic G12D allele in heterozygous animals, while homozygous mice already die during embryogenesis, as *Kras* is an essential gene. *Kras*^{LA2} mice are characterized by random and spontaneous development of lung tumors over time and thus represent a close-to-human lung cancer animal model (Johnson et al., 2001).

4.1.3 Bleomycin-induced lung fibrosis of PA200^{-/-} mice

4.1.3.1 PA200^{-/-} knockout mice

Frozen sperm of PA200^{-/-} mice was obtained from the laboratory of Barry Sleckman (Department of Pathology and Immunology, Washington University School of Medicine, St. Louis, USA). This mouse model involves deletion of the 45 coding exons of PA200 spanning 108 kb by a Cre-loxP site-specific recombination system (Khor et al., 2006). The PA200^{-/-} strain was generated by *in vitro* fertilization of C57BL/6 N mice and embryo transfer in the Research Unit of Comparative Medicine of the Helmholtz Zentrum München – Deutsches Forschungszentrum für Gesundheit und Umwelt (HMGU). Afterwards animals were kept in

the facilities of the Small Animal Platform (SMAP) of the Comprehensive Pneumology Center (HMGU) at constant temperature and humidity with a 12 hours light cycle and food and water *ad libitum*.

4.1.3.2 Genotyping of PA200^{-/-} mice

Ear punches were lysed in 200 μ L PBND buffer + 1 μ L proteinase K (AppliChem) at 56 °C shaking at 1250 rpm overnight. Samples were centrifuged for 1 min at 13 000 rpm. The supernatant was mixed with a PCR master mix (Table 2) and PCR was performed using a temperature-time profile as shown in Table 3.

Table 2: Composition of PCR master mix for genotyping of PA200^{-/-} mice.

Component	Final concentration	Amount
10x PCR Rxn buffer (Thermo Fisher Scientific)	1x	2.5 μ L
10 mM dNTP Mix (Promega)	200 μ M	0.5 μ L
50 mM magnesium chloride (Thermo Fisher Scientific)	2 mM	1 μ L
Primer PA200-wt-as 5 μ M	0.25 μ M	1.25 μ L
Primer I15.07 5 μ M	0.25 μ M	1.25 μ L
Primer I29.02.Xho 5 μ M	0.25 μ M	1.25 μ L
5U/mL Taq polymerase (Thermo Fisher Scientific)	0.025 U/mL	0.125 μ L
Template		2 μ L
H ₂ O	ad 25 μ L	15.125 μ L

Table 3: Temperature and time profile of PCR for PA200^{-/-} genotyping.

Repeats	Temperature [°C]	Time [min:sec]
1x	94	03:00
30x	95	00:30
	60	00:45
	72	01:30
1x	72	10:00
1x	4	ever

The PCR product was mixed with 6x DNA loading dye (Thermo Fisher Scientific) and analyzed by gel electrophoresis using a 1.5 % agarose gel containing SYBR Safe (Thermo Fisher Scientific) for 30 min at 90 V and visualized under UV light with the ChemiDoc XRS+ system (Bio-Rad). A band of 381 bp indicates the wildtype allele, whereas successful deletion of the allele results in band of 500 bp. Presence of bands with both sizes indicates a heterozygous genotype.

4.1.3.3 Experimental bleomycin-induced lung fibrosis

All animal experiments were approved by the local government for the administrative region of Upper Bavaria and conducted according to the guidelines of the approval (animal approval file number: 55.2-1-54-2532-114-2016). Two independent animal experiments were performed for this study using age- and sex-matched PA200^{-/-} and littermate wildtype mice at an age of 8-9 weeks and 12 weeks. Animal experiments were conducted by Dr. Ilona E. Kammerl, postdoctoral scientist at the CPC, and David Kutschke, technician at the Institute for Lung Biology and Disease (ILBD) both at the HMGU. Specific-pathogen-free mice were narcotized by intraperitoneal administration of 500 µg medetomidin, 5 mg midazolam and 50 µg fentanyl (MMF) per kg body weight. Mice were instilled with 50 µL bleomycin dissolved in PBS (2 U/kg body weight) or PBS as control. Narcosis was antagonized by subcutaneous administration of 2.5 mg atipamezole, 500 µg flumazenil and 1.2 mg naloxone per kg body weight. Mice were monitored daily until the end of the experiments at day 14. They were narcotized with MMF (as reported previously) as well as 100 mg ketamin per kg body weight and lung function measurement using the flexiVent system (SCIREQ) was conducted by Dr. Isis E. Fernandez, postdoctoral scientist at the CPC (HMGU). Mice were sacrificed by exsanguination and bronchoalveolar lavage (BAL) was obtained and processed as described in section 4.1.3.4. Lungs were perfused by injection of PBS into the heart and the right lung was snap frozen in liquid nitrogen for subsequent protein and mRNA analysis. For histological analysis the left lung was infused with 4 % (w/v) PFA prior to withdrawal and then fixed in 4 % (w/v) PFA for 24 h at 4 °C prior to embedding in paraffin using the tissue processor Microm STP 420D (Thermo Fisher Scientific).

4.1.3.4 Bronchoalveolar lavage

Bronchoalveolar lavage (BAL) was obtained by rinsing the lungs three times with 500 µL PBS containing cOmplete® protease inhibitor cocktail (Roche). The obtained BAL fluid was centrifuged for 10 min at 1400 rpm, the BAL supernatant was snap frozen in liquid nitrogen for further analysis and the cell pellet was resuspended in 500 µL PBS + cOmplete® protease inhibitor. The total cell count was determined using a hemocytometer (Neubauer counting chamber) and 30 000 BAL cells were transferred onto glass slides by centrifugation at 400 rpm for 6 min using a Cytospin 2 centrifuge (Hettich). BAL cells were dried at RT

overnight and May-Grünwald Giemsa staining was performed. Cells on glass slides were stained for 10 min in May-Grünwald staining solution (Merck) and rinsed in tap water for 2 min. Then slides were stained for 15 min in Giemsa staining solution (Merck) diluted 1:20 with tap water directly before usage. After rinsing in tap water for 2 min and drying at RT, BAL cells were mounted on glass slides with Entellan mounting medium (Merck). Slides were imaged using a Mirax scanning system (Zeiss). At least 200 cells per sample were analyzed regarding their morphology to determine the number of different immune cells in the BAL fluid, including macrophages, lymphocytes and neutrophils.

4.2 Cell culture

4.2.1 Cultivation of mammalian cell lines

Human adenocarcinoma A549 cells and murine lung CCL-206 fibroblasts obtained from ATCC (American Type Culture Collection, Manassas, USA) were cultured as monolayers in 75 cm² or 175 cm² cell culture flasks (Thermo Fisher Scientific) at 37 °C in a humidified atmosphere of 5 % CO₂. A549 were cultivated in DMEM + GlutaMax and CCL-206 in DMEM F12 supplemented with 10 % (v/v) fetal bovine serum (FBS) (Biochrome) and 100 U/mL penicillin/streptomycin (Gibco, Thermo Fisher Scientific). They were passaged twice a week at a ratio according to their growth rate.

4.2.2 Isolation and culture of primary human lung fibroblasts

Primary human lung fibroblasts (phLF) were provided by Prof. Dr. Andreas Günther (Universities of Giessen and Marburg Lung Center (UGMLC)) and isolated as previously described (Jordana et al., 1987, 1988). phLF from organ donors were cultivated in MCDB medium supplemented with 10 % (v/v) FBS (Biochrome), 100 U/mL penicillin/streptomycin (Gibco, Thermo Fisher Scientific), 2 mM L-glutamine (Thermo Fisher Scientific), 5 µg/mL insulin (Thermo Fisher Scientific), 2 ng/mL basic-FGF (Thermo Fisher Scientific) and 0.5 ng/mL human EGF (Sigma-Aldrich). phLF were grown until 90 % confluence and splitted twice a week. For this purpose, cells were washed with PBS, incubated for 2-3 min with Trypsin-EDTA (0.25 %) (Sigma) at 37 °C, re-suspended in cell culture medium and plated onto new cell culture dishes. All experiments were performed with phLF from passage 3 to 5. For

cryopreservation, pHLF were frozen in 1 mL freezing medium consisting of culture medium supplemented with 10 % DMSO at -80 °C using a freezing container (Nalgene). For long-term storage cells were transferred into a liquid nitrogen tank.

4.2.3 Treatment of cells

Prior to treatment with proteasome inhibitors or TGF- β 1, pHLF were synchronized in medium supplemented with 1 % FBS for 24 h. Medium was replaced and proteasome inhibitors bortezomib (Millennium, Takeda), oprozomib (Onyx Pharmaceuticals), epoxomicin (APExBIO) and TGF- β 1 (R&D Systems) or respective controls were added to the cell culture medium for indicated times. For induction of apoptosis, staurosporine or DMSO as control were directly added to the cell culture medium without prior synchronization of cells.

4.2.4 RNA interference

Silencing experiments were performed by reverse transfection of siRNAs against two different regions of *PSMD11* (final concentration 2 nM), *PSME3*, *PSME4* (final concentration of 10 nM) or two control siRNAs at the same concentration (Ambion, Life Technologies). For this purpose a transfection mix was prepared for control and knockdown samples as indicated in Table 4. siRNAs and Opti-MEM (Gibco, Life Technologies) were mixed and incubated for 5 min at RT, the RNAiMax was added and the total mixture was incubated for another 20 min at RT.

Table 4: Composition of silencing master mixes

Reagents	Per well in 6-well plate (total volume 2.5 mL)	Per 10 cm dish (total volume 6 mL)
Opti-MEM	500 μ L	1000 μ L
siRNA 1 + 2	1.25 + 1.25 μ L	3 + 3 μ L
RNAiMax	5 μ L	10 μ L

In the meantime, pHLF were washed with PBS, trypsinized and collected in MCDB medium supplemented with 1 % or 10 % FBS without penicillin/streptomycin. After adjusting cell density, 2 mL of cell suspension (= 100 000 cells) were plated per well of a 6-well plate and 5 mL cell suspension (= 500 000 cells) per 10 cm dish. Subsequently, the silencing

transfection mix was carefully dispersed drop wise on the cells. After 16-24 h medium was replaced with standard cultivation medium or starvation medium containing 1 % FBS.

4.2.5 Transient overexpression of PA200

Overexpression of PA200 was performed by forward transfection of an expression vector using the Lipofectamine LTX reagent (Thermo Fisher Scientific). Cells were plated one day prior to transfection and cultured until 80 % confluence. For transfection, transfection mix A and B were prepared in microcentrifuge tubes as indicated in Table 5 below.

Table 5: Composition of transfection mixes A and B (per well in a 6-well plate).

Transfection mix A		Transfection mix B	
Opti-MEM	100 μ L	Opti-MEM	100 μ L
DNA	1 μ g	Lipofectamine LTX	4 μ L
Plus Reagent (3 mg/mL)	2.5 μ L		

Both transfection mixes were incubated at room temperature for 5 min followed by addition of transfection mix B to transfection mix A and incubation for 5 min. Meanwhile, each well of cells to be transfected was washed with 1.5 mL culture medium without penicillin/streptomycin. 200 μ L transfection mix were dispersed drop-wise on the cells. After incubation for 4 h at 37 °C the transfection mix was removed and cells were cultured in normal pHLF culture medium.

4.2.6 Cell harvest

For harvest, cells were washed with PBS and either scraped in PBS or harvested by detaching with trypsin and collecting in cell culture medium. After collecting cells, they were pelleted by centrifugation for 5 min at 5000 rpm and 4 °C. Cells detached with trypsin were washed once with PBS. Cell pellets were stored at -80 °C until further use. For extraction of mRNA, cells were directly scraped in 500 μ L RotiQuick 1 solution (Carl Roth) and stored at -20 °C until continuing the RNA extraction.

4.2.7 MTT assay

Cellular metabolic activity was determined by measuring the reduction of MTT (3-(4,5-dimethylthiazol-2-yl)-2,5-diphenyltetrazolium bromide) to purple colored, insoluble formazan by NAD(P)H-dependent cellular oxidoreductases (Mosmann, 1983). Cells were cultured in 24- or 96-well-plates. 100 μ L (or 20 μ L for 96 well-plates) of 5 mg/mL thiazolyl blue tetrazolium bromide (Sigma) in PBS were added per well and incubated for 1 h at 37 °C. Wells containing only medium but no cells served as blanks. Medium was aspirated and the formazan crystals were dissolved in 500 μ L (100 μ L for 96-well-plate) isopropanol + 0.1 % Triton X-100 (AppliChem). Absorbance was measured at 570 nM with a Sunrise™ plate reader (TECAN).

4.2.8 BrdU Assay

Cellular proliferation was assessed using a colorimetric immunoassay quantifying BrdU incorporation into newly synthesized DNA according to the manufacturer's protocol (Roche). For transient silencing of PA200 pHLF were mixed with transfection reagent and 4000 cells were plated per well in 96-well-plates in triplicates. 72 h after transfection, pHLF were labeled with 10 μ M BrdU in cell culture medium for 2 h at 37 °C. Subsequently, cells were fixed and denatured by addition of the FixDenat solution. After incubation with the BrdU-POD antibody (diluted 1:100 in antibody dilution solution) for 90 min at RT, cells were washed and the substrate solution was added to start a colorimetric reaction. Absorbance at 370 nM was measured after 15 min using the Sunrise™ plate reader (TECAN).

4.2.9 Annexin V/ PI staining

Cellular apoptosis or necrosis was assessed in pHLF upon PA200 silencing in response to staurosporine treatment using Annexin V/propidium iodide (PI) staining and flow cytometry analysis. 72 h after PA200 silencing (as described in section 4.2.4) pHLF were treated for 3 h with 1 μ M staurosporine or DMSO as a control. After harvesting cells by detaching with trypsin, they were counted, washed with PBS and suspended in 1x Annexin V binding buffer at a concentration of 1 000 000 cells/mL. 100 μ L cell suspension were transferred to FACS tubes and stained with 5 μ L Annexin V-FITC and 10 μ L PI (BD Biosciences) for 15 min at RT in

the dark. Samples were diluted with 400 μ L 1x Annexin V binding buffer prior to FACS analysis using a Becton Dickinson LSRII and data evaluation using the BD FACSDIVA™ software (BD Biosciences).

4.3 Protein biochemistry

4.3.1 Protein extraction from cells and tissue

4.3.1.1 Native protein extracts

For evaluation of intact and active proteasome complexes cells and tissues were lysed under non-denaturing conditions. Prior to lysis, tissue was homogenized twice for 30 s at 3000 rpm using a Mikro-Dismembrator S (Sartorius). Cell pellets or homogenized tissues were resuspended in TSDG buffer containing 1x cOmplete™ protease inhibitor cocktail (Roche) and lysed by 7 cycles of freezing in liquid nitrogen and thawing in water at RT. Afterwards lysates were centrifuged for 20 min at 15 000 rpm and 4 °C. Supernatant was transferred into new tubes and either directly subjected to determination protein of concentration by BCA assay or stored at -80 °C until further use.

4.3.1.2 Denatured protein extracts

To generate protein lysates under denaturing conditions, tissue was homogenized as described in the previous section. Cell pellets or homogenized tissues were suspended in RIPA buffer containing 1x cOmplete™ protease inhibitor cocktail (Roche) and - if investigation of protein phosphorylation was desired - 1x PhosphoStop phosphatase inhibitor (Roche). After lysis on ice for 20 min, samples were centrifuged for 20 min at 15 000 rpm and 4 °C in order to remove cell debris, supernatant was transferred to new tubes and either directly subjected to determination of protein concentration or stored at -20 °C until further use.

4.3.2 Bicinchoninic acid (BCA) assay

Total protein concentration of RIPA and TSDG lysates from cells and tissues was measured via bicinchoninic acid assay (BCA assay). A bovine serum albumin (BSA) calibration curve with

a concentration range from 0 to 2 $\mu\text{g}/\mu\text{L}$ in PBS served as standard to determine protein concentrations. 20 μL BSA standard, 20 μL protein lysate or pure lysis buffer diluted 1:10 in PBS were mixed with 200 μL BCA reagent according to the manufacturer's protocol (Thermo Fisher Scientific). After incubation at 37 °C for 30 min, absorbance was measured at 562 nm using a Sunrise™ plate reader (TECAN) for subsequent calculation of protein concentrations.

4.3.3 SDS-PAGE and Western blot analysis

4.3.3.1 Sample preparation

10 to 15 μg protein were used per sample for Western blotting. Protein extracts were diluted to an equal volume with Milli-Q® water and mixed with 6x Laemmli sample buffer and heated to 95 °C for 10 min in order to denature the proteins.

4.3.3.2 SDS gel electrophoresis

For electrophoretic separation of proteins, protein samples were loaded onto 7.5 %, 10 %, 12 % or 15 % SDS polyacrylamide gels depending on the protein to be detected. Gels were prepared by mixing components listed in Table 6 and pouring into the casting equipment (Bio-Rad). Subsequently after pouring the resolving gel a layer of isopropanol was added in order to form a proper interface. This layer was removed after full polymerization of the gel by washing with MilliQ® water and then the stacking gel was casted.

Table 6: Composition of 1.5 mm 7.5 %, 10 %, 12 % and 15 % SDS polyacrylamide gels.

Component	SDS resolving gels				SDS stacking gel
	7.5 % Volume (mL/gel)	10 % Volume (mL/gel)	12 % Volume (mL/gel)	15 % Volume (mL/gel)	3.6 % Volume (mL/gel)
4x Resolving buffer	2.0	2.0	2.0	2.0	---
4x Stacking buffer	---	---	---	---	1.0
H ₂ O	4.0	3.3	2.8	2.0	2.52
30 % Acrylamide	2.0	2.7	3.2	4.0	0.48
TEMED	0.012	0.012	0.012	0.012	0.012
10 % APS	0.1	0.1	0.1	0.1	0.050

Protein samples and a Protein Marker V (VWR) were loaded onto SDS gels. Electrophoresis was performed in Bio-Rad gel running chambers at a voltage of 100 V, which was increased to 130 V when samples reached the resolving gel.

4.3.3.3 Immunoblotting

After electrophoresis proteins were transferred to a polyvinylidene fluoride (PVDF) membrane (Bio-Rad) via immunoblotting using the tank method. The membrane was activated in pure methanol and immunoblotting was performed at a constant current of 250 mA for 90 min (or 200 mA for subsequent analysis of histones).

Unspecific binding sites of the PVDF membrane were blocked with Roti®-Block solution (Carl Roth) for one hour. The membrane was incubated with primary antibody diluted in Roti-Block solution either overnight at 4 °C or for one hour at RT. The membrane was washed three times with PBST for 10 min and incubated with horseradish peroxidase-conjugated secondary antibody diluted 1:40 000 in PBST for 60 min at RT on a shaker. After washing three times with PBST for approximately 30 min the proteins were detected using ECL (GE Healthcare) or Luminata™ Classico or Forte reagent (Merck Millipore) according to manufacturer's instructions. Membranes were either exposed to X-ray films for different time spans and developed using a film developing machine (AGFA) or the signal was detected with the Chemidoc XRS+ system (Bio-Rad).

4.3.4 Native gel electrophoresis

The different intact and active proteasome complexes were analyzed by native gel electrophoresis of native protein extracts using the XCell SureLock® Mini-Cell system (Thermo Fisher Scientific). 15-20 µg protein of native TSDG extracts from cells or tissues were mixed with native loading buffer and loaded on gradient NuPAGE™ 3-8 % tris-acetate protein gels (Thermo Fisher Scientific). Electrophoresis was performed with native gel running buffer for 4 h at 150 V and 4 °C. Afterwards, native gels were incubated for 30 min at 37 °C in native gel activity assay buffer containing 50 µM Suc-LLVY-AMC (Bachem), a fluorogenic, synthetic peptide substrate for chymotrypsin-like active sites of 20S proteasome complexes. Active proteasome complexes were detected using the ChemiDoc XRS+ system (Bio-Rad) at an excitation wavelength of 380 nm and emission wavelength of 460 nm. Prior to immunoblotting, the native gels were incubated in solubilization buffer for 15 min at RT to denature proteins and to transfer them more efficiently onto PVDF membranes. Immunoblotting of native gels was performed under standard conditions with a constant current of 250 mA for 90 min on ice. Membranes were blocked with Roti®-Block (Carl Roth),

incubated with primary and secondary antibodies and developed as described in section 4.3.3.3.

4.3.5 Proteasome activity assays

4.3.5.1 Proteasome activity assay with fluorescent substrates

Proteasome activity of all three catalytic sites was measured using fluorogenic substrates specific for the chymotrypsin-like (Suc-LLVY-AMC), caspase-like (Z-Leu-Leu-Glu-AMC) and trypsin-like activities (Bz-Val-Gly-Arg-AMC) (Bachem). 2 µg protein of native TSDG protein extracts per replicate were applied for analysis of the chymotrypsin-like activity and 7 µg protein for caspase- and trypsin-like activities, respectively. Protein extracts were diluted with TSDG buffer to a total volume of 20 µL, subjected to a black flat bottom 96-well plate (Greiner bio-one) and 200 µL of assay buffer were added containing the respective substrate at a concentration of 200 µM. Samples were always analyzed in triplicates and TSDG buffer served as a blank. Fluorescence intensity was measured at an excitation wavelength of 353 nm and emission wavelength of 460 nm for 90 min at 37 °C using a TriStar LB 941 plate reader (Berthold Technologies). Proteasome activity of different active sites was calculated with fluorescence intensities detected after 60 min of measurement.

4.3.5.2 Proteasome activity assay using luminescent substrates

Chymotrypsin- and caspase-like activities were also measured with the Proteasome-Glo™ Assay kit according to the manufacturer's protocol (Promega). This kit cannot be used for measuring trypsin-like activities due to unspecific cleavage of this substrate by other proteases (Wilkins et al., 2014). 1 µg protein of native TSDG extracts from cells and tissues was diluted to an equal volume with TSDG buffer. Then the lysates were adjusted to a total volume of 20 µL with Milli-Q® water. They were mixed with 20 µL reaction buffer provided by the kit in a white flat bottom 96-well plate. Cleavage of the substrates Suc-LLVY-aminoluciferin by CT-L and Z-nLPnLD-aminoluciferin by C-L active sites releases aminoluciferin, which is then transformed into a luminescent signal. Luminescence was measured using a TriStar LB 941 plate reader (Berthold Technologies) every two minutes for 30 min and values reaching the plateau of the signal were used for quantification.

4.3.6 Labeling of active proteasome complexes with activity-based probes (ABPs)

Labeling of proteasomes with activity-based probes (ABPs) was performed as another approach to detect proteolytically active proteasome complexes in cell or tissue extracts. The ABPs consist of an inhibitor, which is fluorescently labeled, and bind to different active sites of proteasome complexes (MV151 binding to all active sites of the proteasome, MVB127 to $\beta 5/\beta 5i$ and LW124 to $\beta 1/\beta 1i$) (Verdoes et al., 2006). 10 μg protein of native TSDG extracts from cells or tissues were incubated with 0.5 μM MV151, 1 μM MVB127 or 0.25 μM LW124 diluted with Milli-Q® water to a final volume of 30 μL for 60 min at 37 °C and 600 rpm in the dark. Afterwards samples were either mixed with 6x Laemmli buffer for further analysis via SDS-PAGE or 5x native loading buffer for analysis of active proteasome complexes via native gel analysis. 5 μg of protein were applied for SDS-PAGE and native gel electrophoresis performed under conditions described in sections 4.3.3.2 and 4.3.4. Labeled, active proteasome subunits were detected with a Typhoon TRIO+ fluorescence scanner (GE Healthcare) in the Cy3/TAMRA channel at 450 PTM and with a resolution of 50 microns. The obtained signal was quantified using ImageJ software. After imaging, gels were stained with Page Blue staining solution (Thermo Fisher Scientific) to confirm equal loading.

4.3.7 Co-immunoprecipitation

For immunoprecipitation (IP) of 20S proteasome subunit $\alpha 4$ or PA200 cells were lysed in TSDG buffer under native conditions as described in section 4.3.1.1 to preserve physiological protein-protein interactions. Immunoprecipitation was performed using magnetic Dynabeads coated with Protein G for co-IP with antibodies raised in mouse or with Protein A for co-IP using antibodies raised in rabbit (Thermo Fisher Scientific). 30 μL of Dynabeads were transferred to protein LoBind tubes (Eppendorf) and washed twice with 100 μL phosphate buffer pH 7.4. They were resuspended in 50 μL phosphate buffer pH 7.4 and subsequently incubated with 3 μL of the antibody directed against the target antigen for 15 min at 1250 rpm and RT. Afterwards, beads were washed twice with 100 μL TSDG buffer + 0.2 % IGEPAL. Protein lysate (50-100 μg protein for IP of $\alpha 4$ and 200 μg protein for IP of PA200) and TSDG buffer containing 0.2 % IGEPAL were added to a total volume of 250 μL . After incubating samples in an overhead shaker for 2 h at 4 °C, 25 μL per sample of the total

mixture as well as supernatant only were transferred to new tubes as input and supernatant controls, respectively. Beads were washed three times with 400 μ L TSDG buffer supplemented with 0.2 % IGEPAL and co-immunoprecipitated proteins were eluted in 25 μ L 1x Laemmli buffer for 10 min at 95 °C. Eluted proteins were further analyzed by Western blotting or sent to the Research Unit Protein Science (HMGU) for mass spectrometry analysis.

4.3.8 Histology

Paraffin embedded mouse and human tissues were cut in 3 μ m thick sections using the Hyrax M55 microtome (Zeiss).

4.3.8.1 Immunohistochemistry of PA200

Tissue sections were incubated for one hour at 60 °C in order to melt paraffin, deparaffinized by incubating two times in xylene for 5 min and rehydrated in a descending alcohol series (100 %, 90 %, 80 % and 70 % (v/v)) for 1 min. To block endogenous protease activity and to permeabilize sections for nuclear staining they were incubated in a methanol/hydrogen peroxide (80 %/1.8 % (v/v)) solution for 20 min. Tissue sections were rinsed in Milli-Q® water and heat-induced antigen retrieval was performed in citrate buffer pH 6 using a decloaking chamber (Biocare Medical). After washing with TBST unspecific binding sites were blocked for 30 min with Rodent Block M (Biocare Medical). The slides were washed again in TBST and incubated with PA200 antibody diluted in Antibody Diluent (DAKO) for 1 h at RT. After extensive washing in TBST sections were incubated with MACH 2 Rabbit AP-Polymer (Biocare Medical) for 30 min at RT. Sections were rinsed again in TBST and incubated in Vulcan Fast Red AP substrate solution (Biocare Medical) for 10 min. Tissue sections were washed in TBST and MilliQ® water and hematoxylin counterstaining (Carl Roth) was performed to visualize nuclei. After repeated washing in TBST, sections were dehydrated in ethanol and xylene and mounted using Entellan mounting medium (Merck Millipore). Slides were imaged using the MIRAX scanning system (Zeiss).

4.3.8.2 Hematoxylin & Eosin staining

Sections were deparaffinized and rehydrated as described in section 4.3.8.1. Tissue was stained in Hemalaun (Carl Roth) for 6 min and rinsed with tap water for 15 min. Afterwards sections were incubated in 0.5 % Eosin G solution containing 1 drop 100 % acetic acid per 100 mL (Carl Roth) for 10 min. After rinsing in tap water for 5 min slides were dehydrated for 5 min in 80 % (v/v) ethanol and for 2x 2 min in 100 % (v/v) ethanol followed by incubation in xylene for 2x 5 min. Finally, tissue sections were mounted using Entellan (Merck Millipore) and imaged with the MIRAX scanning system (Zeiss).

4.3.8.3 Masson's trichrome staining

Masson's trichrome staining was performed using the Trichrome Stain (Masson) Kit (Sigma-Aldrich) according to manufacturer's instructions. Tissue sections were deparaffinized and rehydrated as described earlier in section 4.3.8.1. Slides were incubated in Bouin's solution (Sigma-Aldrich) at RT overnight. After washing in tap water for 15 min, slides were stained with Weigert's Iron Hematoxylin solution (Sigma-Aldrich) for 5 min and rinsed with tap water for 5 min. After washing in Milli-Q® water, slides were stained with Biebrich Scarlet-Acid Fuchsin solution for 5 min. After rinsing in Milli-Q® water sections were incubated in Phosphotungstic/Phosphomolybdic Acid Solution followed by subsequent staining in Aniline Blue Solution for 5 min. Slides were washed with 1 % acetic acid for 2 min and dehydrated through alcohol, cleared in xylene and finally mounted with Entellan mounting medium (Merck Millipore). After drying overnight, tissue sections were imaged with the Mirax scanning system (Zeiss).

4.3.9 Histone extraction

Histones were extracted by high-salt extraction according to a previously published protocol (Shechter et al., 2007). pHLF transfected with control or PA200 siRNAs were cultured in 15 cm dishes for 72 h as the protocol requires a lot of cells to obtain enough protein. The extraction procedure was performed on ice or 4 °C to minimize activity of enzymes and proteases. Cells were lysed in 200 µL extraction buffer containing 0.2 % IGEPAL and cComplete™ protease inhibitor cocktail (Roche) for 10 min on ice. After centrifugation of cell lysates for 5 min at

6500 x *g* supernatant (= cytosolic fraction) was transferred to a new tube. The remaining pellet (= the nuclei) was washed with extraction buffer without detergent. After complete removal of supernatant nuclei were resuspended in 200 μ L no-salt buffer and lysed by repetitive vortexing for 1 min followed by incubation on a rotator for 30 min at 4 °C. Lysates were again centrifuged for 5 min at 6500 x *g* and supernatant (= nucleoplasm) was kept for further analysis. The chromatin pellet was then re-suspended in high-salt solubilization buffer by vortexing for 2 min and incubated on a rotator for 30 min at 4 °C. DNA and nuclear debris were spun down for 10 min at 16 000 x *g*. The supernatant was transferred to D-Tube™ Dialyzer Midi MWCO 3.5 kDa tubes (Merck Millipore) and dialyzed in 1 L 10 mM TRIS-Cl pH 8.0 for 1 h under slow stirring. After 1 h the dialysis buffer was replaced with fresh 10 mM TRIS-Cl pH 8.0 and incubated for another hour. Protein concentration of different fractions was determined by BCA assay (as described in section 4.3.2). 10 μ g protein of cytosolic fraction and 2 μ g protein of the nucleoplasm and chromatin fraction were further analyzed by immunoblotting.

4.3.10 Proteomic screen

Proteomic analysis by LC-MS/MS as described in the following section was performed by Dr. J. Merl-Pham, Research Unit Protein Science (HMGU).

4.3.10.1 Sample preparation for proteomics

10 μ g protein of whole cell RIPA lysate or IP eluates were subjected to tryptic digest applying a modified FASP procedure (Grosche et al., 2016; Wiśniewski et al., 2009). After protein reduction and alkylation using DTT and iodoacetamide, samples were denatured in UA buffer (8 M urea in 0.1 M Tris/HCl pH 8.5), centrifuged on a 30 kDa cut-off filter device (PALL or Sartorius) and washed twice with UA buffer and twice with 50 mM ammoniumbicarbonate (ABC). Proteins were proteolysed for 2 h at room temperature using 1 μ g Lys-C (Wako) and subsequently for 16 h at 37 °C using 2 μ g trypsin (Promega). Peptides were collected by centrifugation and acidified with 0.5 % trifluoroacetic acid (TFA).

4.3.10.2 Mass spectrometric measurements

LC-MS/MS analysis was performed on a LTQ Orbitrap XL (Thermo Scientific) or on a Q-Exactive HF mass spectrometer (Thermo Scientific) each online coupled to a nano-RSLC (Ultimate 3000 RSLC; Dionex). The analysis on the LTQ Orbitrap XL was performed as described before (Hauck et al., 2010; Merl et al., 2012). For subsequent analysis on the Q-Exactive HF, tryptic peptides were accumulated on a nano trap column (300 μm inner diameter \times 5 mm, packed with Acclaim PepMap100 C18, 5 μm , 100 \AA ; LC Packings) and then separated by reversed phase chromatography (customized ACQUITY UPLC M-Class HSS T3 Column, 1.8 μm , 75 μm X 250 mm; Waters) in a 80 min non-linear gradient from 3 to 40 % acetonitrile (ACN) in 0.1 % formic acid (FA) at a flow rate of 250 nL/min. Eluted peptides were analyzed by the Q-Exactive HF mass spectrometer equipped with a nano-flex ionization source. Full scan MS spectra (from m/z 300 to 1500) and MS/MS fragment spectra were acquired in the Orbitrap with a resolution of 60 000 or 15 000 respectively, with maximum injection times of 50 ms each. The up to ten most intense ions were selected for HCD fragmentation depending on signal intensity (TOP10 method). Target peptides already selected for MS/MS were dynamically excluded for 30 s.

4.3.10.3 Label-free analysis using Progenesis LC-MS

The acquired spectra per project were loaded to the Progenesis QI software (version 3.0, Nonlinear) for label free quantification and analyzed as previously described (Hauck et al., 2010; Merl et al., 2012), except all features were exported as Mascot generic file (mgf) and used for peptide identification with Mascot (version 2.4) in the Ensembl Human protein database (release 83, 83462 sequences, 31286148 residues). Search parameters used were: 10 ppm peptide mass tolerance and 0.02 Da or 0.6 Da fragment mass tolerance, one missed cleavage allowed, carbamidomethylation was set as fixed modification, methionine oxidation and asparagine or glutamine deamidation were allowed as variable modifications. A Mascot-integrated decoy database search calculated an average false discovery of <1 %. The Mascot Percolator algorithm was used for the discrimination between correct and incorrect spectrum identifications (Brosch et al., 2009). Peptides with a minimum percolator score of 13 were re-imported into the Progenesis QI software and the abundances of the three most abundant peptides allocated to each individual protein were summed up (TOP3). Statistics

was based on the ANOVA calculated by the Progenesis QI software, on arcsinh() transformed normalized protein abundances (Grosche et al., 2016), followed by FDR-correction, resulting in given q-values.

4.3.10.4 Stoichiometry calculations

For calculation of protein stoichiometries the abundances of the three most abundant peptides per protein were summed up and referenced to the bait protein PSME4 (TOP3 method, (Fabre et al., 2014)).

4.4 Nucleic acid biochemistry

4.4.1 Quantitative real-time RT-PCR

4.4.1.1 RNA isolation of cells

Total RNA of cells was isolated by phenol-chloroform extraction using the Roti®-Quick Kit (Carl Roth). Cells were lysed in 500 μ L Roti®-Quick 1 solution. After thoroughly mixing with 625 μ L Roti®-Quick 2 solution, samples were incubated for 10 min on ice and centrifuged for 15 min at 10 000 rpm and 4 °C in order to allow phase separation. The upper aqueous phase was transferred to a new tube and 500 μ L Roti®-Quick 3 solution was added. Samples were either incubated at -80 °C for 40 min or at -20 °C overnight. RNA was sedimented by centrifugation for 20 min at 13 000 rpm and 4 °C. Supernatant was removed and RNA pellets were washed twice with 70 % (v/v) ethanol. After drying on ice, the RNA pellet was dissolved in 30 μ L nuclease-free water (Ambion, Thermo Fisher Scientific) and concentration was measured at a wavelength of 260 nm with the NanoDrop 1000 (Thermo Fisher Scientific).

4.4.1.2 Reverse transcription of mRNA

For reverse transcription, 0.5 to 1 μ g RNA were diluted to 9.5 μ L with nuclease-free water and mixed with 2 μ L of 250 μ M Random Hexamers (Thermo Fisher Scientific). After incubation for 10 min at 70 °C samples were placed on ice. 8.5 μ L of a reverse transcription master mix was added (final concentrations: 1x First Strand Buffer, 10 mM DTT, 0.5 mM dNTPs, 1 U/ μ L RNasin RNase Inhibitor, 10 U/ μ L M-MLV transcriptase). Reverse transcription was performed with annealing for 5 min at 25 °C and elongation for 60 min at 37 °C using a

Mastercycler Nexus (Eppendorf). cDNA was digested with 1 U DNase at 37 °C for 15 min followed by heat inactivation at 75 °C for 10 min and diluted 1:5 with nuclease-free water (Ambion, Thermo Fisher Scientific).

4.4.1.3 Quantitative real-time RT-PCR

Quantitative real-time RT-PCR was performed using a SYBR Green LC480 system (Roche). A mix of 2.5 µL cDNA and 5 µL LC480 SYBR Green I Master mix (Roche) was subjected per well in a 96-well plate format. 2.5 µL forward and reverse primer dilution was added resulting in a final concentration of 0.5 µM. Samples were always measured in duplicates and plates were centrifuged for 2 min at 1000 rpm prior to starting measurement using the standard program of the Light Cycler 480II (Roche). Gene expression of the different samples was normalized to housekeeping genes ribosomal protein L 19 (*RPL19*) and hypoxanthine-guanine phosphoribosyltransferase (*HPRT*). Relative gene expression was determined using the $\Delta\Delta C_T$ method. The specificity of primers was controlled by measurement of a melting curve.

4.4.2 Transcriptome microarray analysis

Total RNA was isolated as explained in section 4.4.1.1. Microarray analysis as described in this section was performed by Dr. Martin Irmeler, Institute of Experimental Genetics (HMGU). RNA quality was assessed using the Agilent 2100 Bioanalyzer and RNA of high quality (RIN > 7) was further used for microarray analysis. 300 ng total RNA was amplified using the WT PLUS Reagent Kit (Affymetrix). Amplified cDNA was hybridized on Human Clariom S arrays (Affymetrix). Staining and scanning was performed according to the Affymetrix expression protocol.

Expression console (v.1.4.1.46, Affymetrix) was used for quality control and to obtain annotated normalized RMA gene-level data (Gene Level - SST-RMA). Statistical analyses were performed by utilizing the statistical programming environment R (R Development Core Team Ref1). Gene-wise testing for differential expression was done employing the limma t-test and Benjamini-Hochberg multiple testing correction (FDR < 10 %). For probe sets with identical values across all samples only one probe set was kept in the final gene sets. To reduce background, gene sets were filtered for average expression >30 (arbitrary

units) in at least one experimental group. Pathway analyses were generated through the use of QIAGEN's Ingenuity Pathway Analysis (IPA®, QIAGEN, www.qiagen.com/ingenuity) using Fisher's Exact Test p-values.

4.4.3 Preparation of plasmid DNA for transfection

4.4.3.1 Transformation of DH5 α

For transformation of Z-competent™ DH5 α , bacteria were thawed on ice, 2 μ L plasmid were added to the bacteria and gently mixed. After 10 min incubation on ice DH5 α were plated on agar dishes containing the respective antibiotic (50 μ g/mL ampicillin or 25 μ g/mL kanamycine). Bacteria transformed with a plasmid containing a kanamycine resistance gene were incubated with 200 μ L SOC medium (Takara) for 1 h at 200 rpm and 37 °C prior to plating on agar dishes.

4.4.3.2 Cloning of PA200 into a pcDNA3.1 vector

For overexpression experiments, PA200 cDNA was cloned into a pcDNA3.1 (+) vector. A fragment comprising the cDNA of PA200 was amplified from a commercial PA200 construct with a C-terminal Myc-DKK tag (Origene) by polymerase chain reaction (PCR) using a master mix and time-temperature profile as indicated in

Table 7 and Table 8.

Table 7: Composition of PCR master mix (per reaction).

Component	Final concentration	Quantity
5x HF/GC buffer	1x	10 μ L
10 mM dNTPs	200 μ M	1 μ L
Primer forward 10 μ M	0.5 μ M	2.5 μ L
Primer reverse 10 μ M	0.5 μ M	2.5 μ L
10 ng/ μ L DNA template	0.2 ng/ μ L	1 μ L
Phusion Polymerase	1 U/50 μ L	0.5 μ L
H ₂ O	Ad 50 μ L	32.5 μ L

Table 8: Temperature and time profile of PCR for PA200 amplification.

Repeats	Temperature [°C]	Time [min]
1x	98	03:00
8x	98	00:10
	53	00:30
	72	03:00
35x	98	00:10
	69 (gradient 3°C)	00:30
	72	03:00
1x	72	10:00
1x	4	ever

The obtained PCR fragment was purified by agarose gel electrophoresis and gel extraction using a NucleoSpin® Extraction Kit (Macherey-Nagel).

The purified PCR product and the pcDNA3.1 (+) vector were digested with KpnI and NheI enzymes (NEB) in buffer provided by the manufacturer at 37 °C for 1 h. After purification of digested vector and PA200 fragments by agarose gel extraction, ligation of the fragment and vector was performed using the Quick Ligation Kit (NEB) according to the manufacturer's protocol. 50 ng of vector and a threefold excess of the insert were incubated in reaction buffer for 5 min at RT. The ligation product was transformed into Z-competent™ DH5α and spread onto LB-agar plates containing 50 µg/mL ampicillin (Bioline). Selected colonies were inoculated in LB medium containing 50 µg/mL ampicillin and plasmid DNA was extracted from bacteria using a NucleoSpin® Plasmid mini kit (Macherey-Nagel). Potential positive clones were selected by restriction analysis and the construct was sequenced (GATC Biotech AG).

4.4.3.3 Preparation of plasmid DNA

For generation of plasmid DNA used for transfection of cells, transformed DH5α were inoculated with LB medium containing the respective antibiotic at 200 rpm and 37 °C overnight. DNA was isolated using the NucleoBond PC 500 kit (Macherey-Nagel) according to the manufacturer's protocol. DNA was then dissolved in nuclease-free water (Ambion, Life Technologies), concentration was measured at 260 nm using a NanoDrop 1000 (Thermo Scientific) and the plasmids were diluted to a concentration of 1 µg/µL for further applications.

4.5 Statistics

Generated data were statistically analyzed as indicated in the figure legends. Cell culture experiments performed with pHLF from different organ donors examined for protein and mRNA expression as well as proteasome activity were analyzed by one sample t-test. One-way ANOVA and Bonferroni's multiple comparison test was used to statistically evaluate apoptosis assays. Nonparametric Mann-Whitney U test was applied for statistical analysis of protein and mRNA expression of human and mouse tissues. Results obtained from examination of BAL cells, lung function and mRNA levels in bleomycin-induced lung fibrosis of wildtype and PA200^{-/-} mice were statistically analyzed with Kruskal Wallis test and Dunn's multiple comparison test.

Statistic tests and graphic illustration of the data was conducted using the GraphPad Prism software (version 5.00 and 7.00). P-values < 0.05 were considered statistically significant (*p < 0.05, **p < 0.01, ***p < 0.001). Data represent mean +/- SEM.

5 Validating the specificity of antibodies for analysis of the proteasome activator PA200

5.1 Introduction

A major requirement to generate reliable data on protein function is the use of specific antibodies. Although PA200 has already been first described by Ustrell *et al.* in 2002, only a limited number of studies on the function of this proteasomal activator has been published in recent years. While some of those studies did not use antibodies for detection of the activator, the most frequently commercially available antibody was first described by Ustrell *et al.* and targets an epitope comprising amino acids (aa) 1620-1634 of the human protein (Ustrell *et al.*, 2002). However, this immunoglobulin also recognizes a protein species at 160 kDa, which is alleged to be an isoform of the activator (Ustrell *et al.*, 2002). Therefore, initial experiments of this study aimed to test the specificity of antibodies targeting different epitopes of PA200, which are listed in Table 9

Table 9: PA200 antibodies indicating epitopes, product numbers and publications they were used for.

Epitope	Antibody product number	Publications
aa 1620-1634 of the human protein	PA1-1691 (Thermo Fisher Scientific)	Ustrell 2002, Blickwedehl 2007, 2008, 2012
	ab5620 (Abcam)	Pickering 2013
aa 1-50 of the human protein	NBP1-22236 (Novus Biologicals)	Welk 2016
aa 1019-1109	NBP2-32575 (Novus Biologicals)	-
unknown (near C-terminus of human protein)	sc-135512 (Santa Cruz)	George 2013

5.2 Results

5.2.1 Antibody against aa 1620-1634 recognizes 160 kDa protein species not responding to PA200 silencing

First, silencing of PA200 was applied to test the specificity of two antibodies for human PA200, namely PA1-1961 (Thermo Fisher Scientific) directed against aa 1620-1634 and NBP1-22236 (Novus Biologicals) recognizing aa 1-50 of the human protein, which are not present in the mouse homologue. Primary human lung fibroblasts (phLF) were transfected with control or PA200 siRNAs and harvested after 24, 48 and 72 h. Immunoblotting with antibodies PA1-1961 and NBP1-22236 revealed a differential band pattern (Figure 5.1). The

widely used PA1-1961 recognized a predominant band at 160 kDa and a faint band of approximately 250 kDa both not responding to siRNA-mediated knockdown as well as a faint protein species of 200 kDa disappearing upon PA200 silencing. In contrast, NBP1-22236 recognized only one 200 kDa protein species, which was decreasing over time in response to transfection of pHLF with PA200 siRNAs, implying a much more specific detection of the activator. This accorded well with a strong decrease in full-length PA200 mRNA levels upon silencing of the activator under the same conditions (shown in Figure 7.25 of section 7.2.4.4).

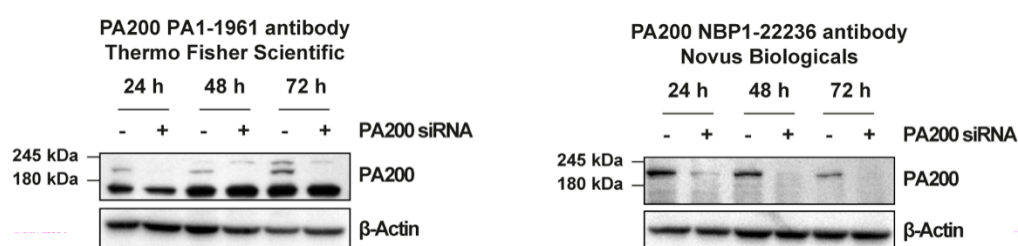


Figure 5.1: PA200 antibodies against the human protein vary in their specificity. RIPA extracts of primary human lung fibroblasts with transient silencing of PA200 for 24, 48 and 72 h were analyzed using immunoblotting with the antibody PA1-1961 from Thermo Fisher Scientific (left) and NBP1-22236 from Novus Biologicals (right) for detection of PA200.

Specificity of antibodies for murine PA200 was tested using CCL-206 murine lung fibroblasts, which were transfected with control or PA200 siRNAs for 24, 48, 72 and 96 h. Immunoblotting with antibody PA1-1961 resulted in a similar band pattern as previously observed in human samples (Figure 5.2 A). The very abundant protein species at 160 kDa did not respond to the silencing, whereas a very faint band at approximately 200 kDa disappeared upon knockdown of PA200. Antibody NBP2-32575 (Novus Biologicals) suitable for detection of the murine protein recognized a single band of approximately 200 kDa, which decreased over time upon knockdown and started to recover after 96 h. Moreover, efficient silencing of the activator was confirmed using an additional method measuring mRNA levels after 24, 48 and 72 h of silencing in CCL-206 (Figure 5.2 B). Here, qPCR revealed a strong decrease of mRNA expression after 24 and 48 h, which slightly started to recover 72 h after transfection. Concluding, the widely used antibody PA1-1961 targeting aa 1620-1640 recognizes a prominent band at 160 kDa in cells of human and mouse origin which does not respond to PA200 silencing. In contrast, antibodies NBP1-22236 and NBP2-32575 targeting other regions of the protein specifically detect the 200 kDa protein species of human and mouse PA200 by immunoblotting.

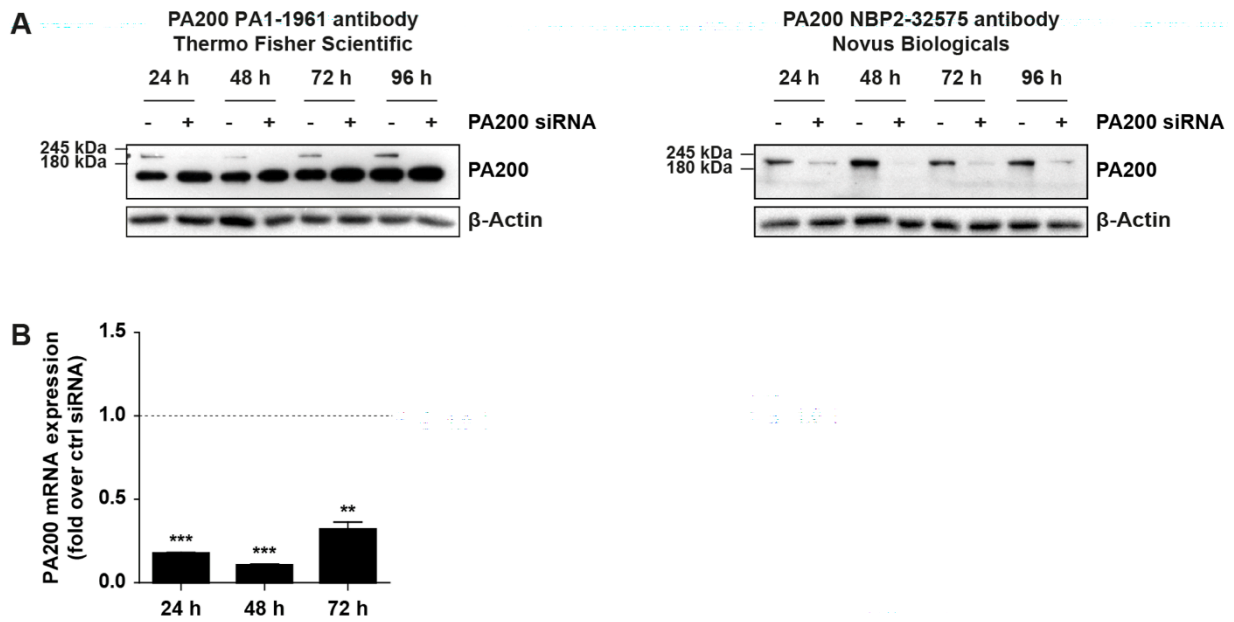


Figure 5.2: PA200 antibody PA1-1961 recognizes additional protein species not responding to PA200 silencing in murine CCL-206. (A) Transient silencing of PA200 for 24, 48, 72 and 96 h in murine CCL206 cells was analyzed using immunoblotting with the antibody PA1-1961 (Thermo Fisher Scientific, left figure) and NBP2-32575 from (Novus Biologicals, right figure) for detection of PA200. (B) PA200 mRNA expression of samples used in (A) were determined by qPCR. *RPL19* served as housekeeping gene. Bars show mRNA level normalized to time-matched controls (one-sample t-test, $n = 3$). Experiments were performed by T. Meul, master student at the CPC 2016.

5.2.2 Blocking of the antibody with its immunizing peptide prevents its binding to both the 200 kDa and 160 kDa protein species

To investigate whether the antibody PA1-1961 recognizes the 160 kDa protein species *via* its antigen binding site, blocking experiments were performed with the 15 aa immunizing peptide used for generation of the antibody comprising aa 1620-1640 of the human PA200 protein. The antibody was diluted 1:1000 in blocking reagent and incubated with 0 to 6 $\mu\text{g}/\text{mL}$ peptide over night at 4 °C. Western blots of the same CCL-206 lysate were then developed using the antibody blocked with increasing amounts of peptide. The signal for both bands at 160 and 200 kDa was already blocked with a peptide concentration of 0.25 $\mu\text{g}/\text{mL}$ (Figure 5.3 A). Remaining bands were also not blocked at higher concentrations and thus resulted from binding of other antibody regions to cellular proteins.

In a second approach, the ability of the immunizing peptide to prevent binding of the antibody to its target sequence was also tested by immunohistochemistry (IHC). Diluted antibody PA1-1961 was incubated with the immunizing peptide at a final concentration of 4 $\mu\text{g}/\text{mL}$ overnight prior to staining of lung tumor sections from *Kras*^{LA2} mutant mice. No

signal was obtained using antibody with blocked recognition site, whereas antibody without blocking peptide led to a strong staining of tumor regions (Figure 5.3 B).

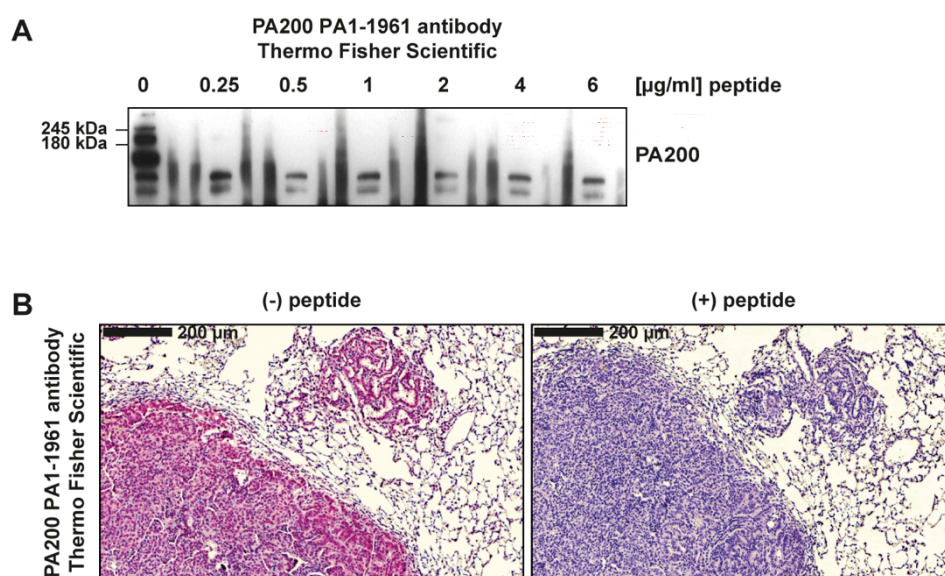


Figure 5.3: The immunizing peptide of PA200 antibody PA1-1961 efficiently blocks binding of the antibody to 200 kDa PA200 and the unknown 160 kDa protein species. (A) PA200 antibody PA1-1961 (Thermo Fisher Scientific) diluted 1:1000 in blocking solution was incubated overnight with its blocking peptide at indicated concentrations. Immunoblotting of a CCL-206 lysate was then stained with the blocked PA200 antibody. (B) *Kras*^{LA2} mouse lung tumor was stained with the PA200 antibody PA1-1961 pre-incubated with the blocking peptide (4 µg/mL) overnight or antibody without blocking peptide (pink). Nuclei (blue) were counterstained with hematoxylin. Experiments were performed by T. Meul, master student at the CPC 2016.

5.2.3 PA200^{-/-} confirms 160 kDa protein species being not related to PA200

Testis and lung tissue of PA200^{-/-} mice was used to investigate whether the additional 160 kDa protein species is an actual isoform of PA200 as stated by previous publications (Blickwedehl et al., 2007; Ustrell et al., 2002). Testis and lung RIPA extracts of PA200^{-/-} and wildtype mice were analyzed with antibodies PA1-1961 and NBP2-32575 by immunoblotting. Of note, antibody PA1-1961 caused a pronounced signal at 160 kDa in testis and lung tissues of wildtype as well as in PA200^{-/-} animals, whereas the 200 kDa species was only observed in the wildtype (Figure 5.4 A). Therefore, the 160 kDa protein species detected with this antibody is not related to PA200 as the knockout mice harbor a full deletion of all PA200 coding exons and do not express an isoform of the activator. In contrast, NBP2-32575 recognized a single band of 200 kDa in wildtype tissues, which was not present in PA200^{-/-}. Therefore, this antibody is well suited for specific immunodetection of PA200 in murine samples.

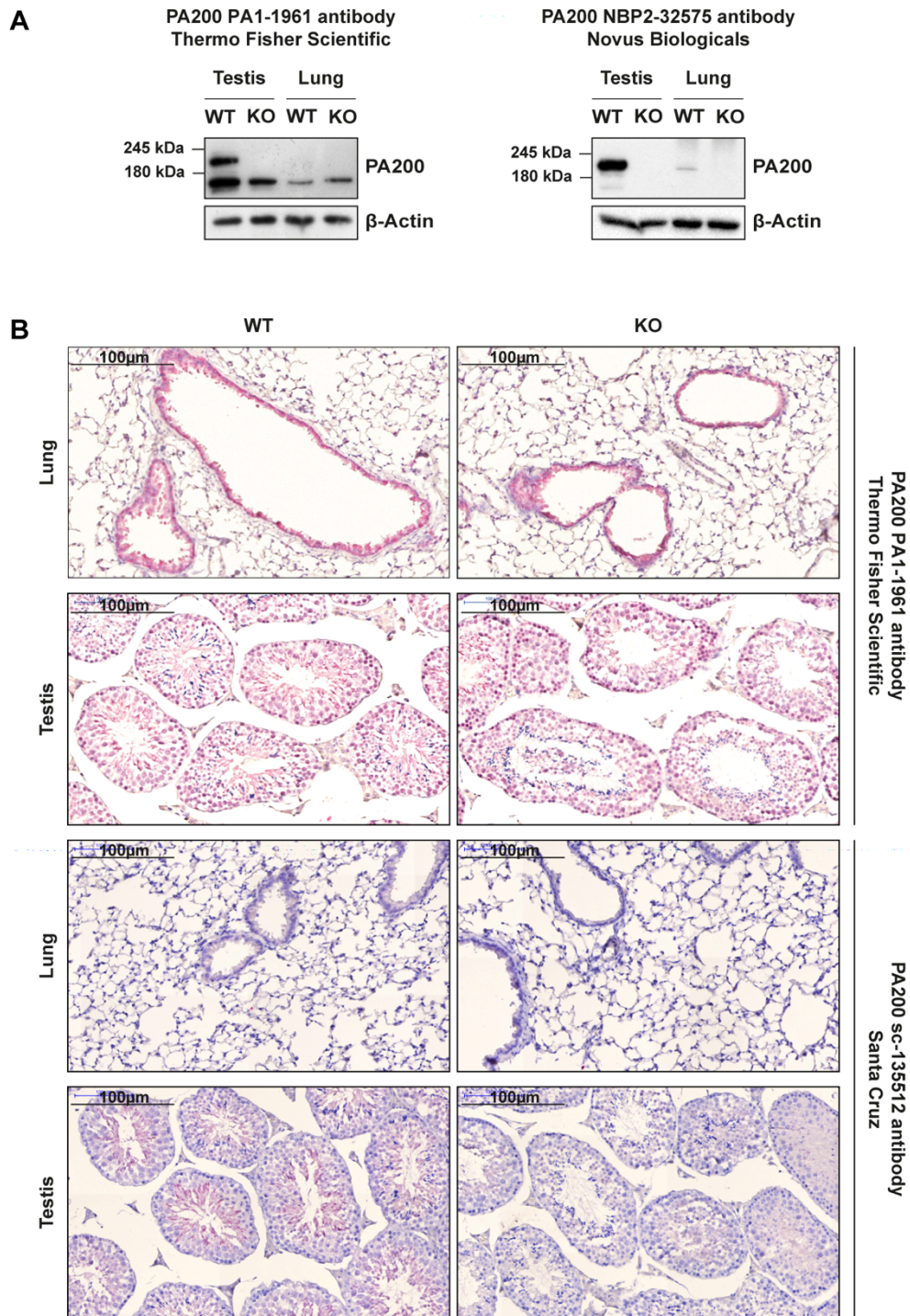


Figure 5.4: PA200 knockout reveals binding of PA1-1961 antibody to protein not related to PA200.

(A) PA200 protein expression in RIPA lysates of testis and lung tissue from wildtype (WT) and PA200^{-/-} (KO) mice was examined with antibodies PA1-1961 (Thermo Fisher Scientific, left figure) and NBP2-32575 (Novus Biologicals, right figure). (B) The antibody specificity was evaluated by immunohistochemical analysis of lung and testis sections from wildtype (WT) and PA200^{-/-} (KO) mice using antibodies PA1-1961 (Thermo Fisher Scientific) and sc-135512 (Santa Cruz). Experiments were performed in collaboration with T. Meul, master student at the CPC 2016.

Specificity of different PA200 antibodies was also analyzed by immunohistochemistry of lung and testis tissues from wildtype and PA200^{-/-} mice. As antibody NBP2-32575 is not suitable

for IHC, sc-135512 (Santa Cruz) was tested for this purpose. PA1-1961 caused a very strong staining of wildtype lung and testis tissue sections although expression of PA200 is generally lower in the lung as compared to testis (Ustrell et al., 2002) (Figure 5.4 B). Moreover, the signal was also present in PA200^{-/-} testis and lung tissue sections confirming unspecific binding. In contrast, sc-135512 specifically stained cells of wildtype testis tissue, whereas no signal was obtained in the PA200^{-/-}. Lung tissue sections exhibited no pronounced staining compared to testis, which accords well with a generally lower expression of the protein in the lung.

Concluding, these findings illustrate the importance of thorough validation of antibody specificity. Using PA200 silencing and knockout approaches these experiments showed that PA1-1961, which is directed against an epitope comprising aa 1620-1634 of the activator and has been most frequently used in recent publications, is not suitable for specific detection of PA200 as it recognizes an additional 160 kDa protein species that is not related to PA200. Antibodies from Novus Biologicals and Santa Cruz directed against other epitopes were proven to be specific for detection of PA200. These validated antibodies were used for all subsequent experiments of this study as indicated in Table 10.

Table 10: Antibodies validated for specific recognition of PA200 and their application in this study.
(WB: Western blotting; IP: immunoprecipitation; IHC: immunohistochemistry)

Antibody	Application	Validated by
NBP1-22236	WB and IP of human samples	Transient PA200 silencing
NBP2-32575	WB of mouse samples	WB of PA200 ^{-/-} and wildtype tissue
sc-135512	IHC of human and mouse tissue	IHC of PA200 ^{-/-} and wildtype tissue

5.3 Discussion

Initial experiments of this study analyzing the specificity of several PA200 antibodies revealed that antibodies directed against aa 1620-1634 of the human protein detect a 160 kDa species which is not related to PA200. As these antibodies were used in most of the published studies, these observations on PA200 need to be considered with caution.

5.3.1 Specific antibodies are essential for reliable research

Antibodies are very important tools for basic and clinical research as well as clinical diagnostics as they are frequently used for detection of proteins. They require an absolute certainty regarding specificity and selectivity for recognition of their antigen; otherwise inconsistent and wrong data are generated leading to misinterpretation of data influencing future directions of research or even treatment of patients. However, a large proportion of commercially available antibodies fail to specifically detect their target protein. When Berglund *et al.* for example tested the specificity of 5436 commercially available antibodies by Western blotting and IHC for the Human Protein Atlas in 2008, they discovered that only approximately 50 % of them were suitable for the tested applications (Berglund *et al.*, 2008). According to the FDA, validation is defined as “the process of demonstrating, through the use of specific laboratory investigations, that the performance characteristics of an analytical method are suitable for its intended analytical use” (Bordeaux *et al.*, 2010). Therefore, validation of antibody specificity is an essential prerequisite for their analytical use to obtain reliable results. However, the use of antibodies not suitable for experimental use because of cross-reactivity, variability of among different batches or wrong applications is a major cause for the increasing lack of data reproducibility in research as recently discussed in an editorial by the Nature journal editor Monya Baker (Baker, 2015). Although non-specific antibodies are a widely discussed pitfall in research and despite the fact that the “International Working Group for Antibody Validation” recently provided a guideline for proper antibody validation, a general policy - especially for commercially available antibodies - does not exist (Bordeaux *et al.*, 2010; Bradbury and Plückthun, 2015; Uhlen *et al.*, 2016).

5.3.2 The use of unspecific antibodies limits available information on PA200

In the present study, analysis of antibody specificity revealed that a frequently used antibody targeting aa 1620-1634 of human PA200 does also recognize proteins not related to PA200. Using this antibody for Western blotting and IHC, a prominent signal was observed upon PA200 silencing in murine and human cells as well as in murine PA200^{-/-} tissues. For this reason, this antibody has to be considered as not specific for the detection of PA200 and thus cannot be applied in further experiments. Specific recognition of PA200 by immunoblotting was achieved using antibodies from Novus Biologicals targeted against aa 1-50 of the human protein or directed against a 93 aa epitope in the middle region of the PA200 mouse homologue. Consequently, antibodies targeting a larger epitope might prevent unspecific recognition of proteins because the probability for detection of a similar epitope in a given sample is lower.

PA200 antibodies targeting aa 1620-1634 are commercially available from different companies and have been used in several recent studies. They were first generated by Ustrell *et al.* by immunizing rabbits with three synthetic fragments of human PA200 (Ustrell *et al.*, 2002). All three antibodies recognized a 160 kDa protein species by Western blotting, which was claimed to be an isoform of PA200. However, in this early study the antibody specificity was not further validated by silencing or knockout of the gene. When using this antibody for immunofluorescence staining, PA200 was described to localize in the nucleus and to form nuclear foci upon radiation (Ustrell *et al.*, 2002). Both findings are not reliable, because stainings do not allow for discrimination between the unspecific 160 kDa and the PA200 200 kDa protein species.

The same antibody was also used in a study investigating the regulation of alternative proteasome activators in response to oxidative stress (Pickering and Davies, 2013). Here, the authors claimed that the 200 kDa, but not the 160 kDa and 60 kDa protein species, was increased in response to H₂O₂ treatment. Their further analysis involved immunofluorescence stainings to show formation of nuclear foci by PA200 in response to hydrogen peroxide treatment as well as co-immunoprecipitation of PA200. Again, these results are not reliable as an unspecific antibody was used for analysis.

Blickwedehl *et al.* generated an antibody by immunization with two synthetic peptides with one of these peptides also comprising aa 1620-1634 of human PA200 with some additional

amino acids at the N- and C-terminal regions (Blickwedehl et al., 2007, 2008, 2012). They also observed several protein species claiming they are isoforms of PA200, but only the 200 kDa species was found to be associated with the 20S proteasome. With regard to the results of the present study these other two protein species are most probably not related to PA200. Whereas the first study of Blickwedehl and colleagues in 2007 clearly labeled different protein species detected by Western blotting, this was not the case in the following publications. Although PA200 silencing was used in some of the experiments, they did not discriminate between the different recognized protein bands and whether they are affected by silencing. Therefore, the conclusion drawn from these experiments are also questionable due to the lack of antibody specificity for detection of PA200.

Other publications in recent years did not clearly indicate the source or the recognition site of the applied PA200 antibodies (Jagannathan et al., 2015; Qian et al., 2013; Wang et al., 2017). Their findings involving regulation of PA200 by miR29b as well as the discovery of acetylated histones as first substrates of PA200 should thus to be considered with caution. Especially the study by Qian *et al.* has major deficits regarding the specificity of applied PA200 antisera and quality of obtained results in general. Here, PA200 immunoblots clearly indicate several protein species suggesting that a non-specific antibody targeting aa 1620-1634 was used in these experiments (Qian et al., 2013). Moreover, a signal for the activator was obtained by staining of PA200^{-/-} mouse embryonic fibroblasts with PA200 antisera. Therefore, the results of this study are highly questionable due to the lack of antibody specificity and the use of a PA200 gene knockout, which comprised only a deletion of exon 25-26 out of 45 coding exons.

Concluding, antibody validation experiments performed in this study indicate the absolute necessity for proper evaluation of antibody specificity. Evaluating all studies published on PA200 so far revealed that non-specific immunoglobulins targeting aa 1620-1634 were frequently used and therefore further limit the available information on PA200 and its function. Here in this study, antibody NBP1-22236 recognizing aa 1-50 only present in human PA200 was validated for Western blotting and IHC of human samples, whereas NBP2-32575 was proven specific for detection of the mouse homologue by Western blotting. Antibody sc-135512 targeting an unknown C-terminal region of the activator was shown to be suitable for IHC of human and mouse tissues.

6 Inhibition of proteasome activity induces formation of alternative proteasome complexes

Parts of this chapter were recently published as the following:

Vanessa Welk, Olivier Coux, Vera Kleene, Claire Abeza, Dietrich Trümbach, Oliver Eickelberg and Silke Meiners (2016). Inhibition of Proteasome Activity Induces Formation of Alternative Proteasome Complexes. *The Journal of Biological Chemistry* 291, 13147-13159.

6.1 Introduction

Proteasomes are huge protein complexes built of many different subunits. The constitutive 20S proteasome core complex consists of 28 protein subunits with a total molecular weight of approximately 750 kDa (Groll et al., 1997; Tanahashi et al., 1993). However, additional binding of an activator, such as the 19S regulator and PA28 $\alpha\beta$, PA28 γ or PA200 activators, is required to induce opening of the outer α -ring thereby facilitating the entry and degradation of proteins (Groll et al., 2000; Stadtmueller and Hill, 2011). These proteasomal activators are huge protein complexes within the cell as well. The standard 19S regulator is composed of 19 subunits with a total molecular weight of 700 kDa (Rechsteiner and Hill, 2005; Sharon et al., 2006; Stadtmueller and Hill, 2011). Alternative proteasome activators, such as the heteroheptamer PA28 $\alpha\beta$ and homoheptamer PA28 γ with a total molecular weight of approximately 210 kDa each and the 200 kDa monomer PA200, are also very large in size (Stadtmueller and Hill, 2011). According to the proposed "building block concept", the recruitment of proteasomal activators to the 20S core complex allows for fast adaption of protein turnover *via* this huge proteolytic complex (Meiners et al., 2014). This would allow cells to quickly respond to different stimuli. In contrast to several studies analyzing the phosphorylation of 19S subunits as a mechanism for fast adaption of 26S proteasome function, the assembly of alternative proteasome complexes composed of alternative activators, such as PA28 $\alpha\beta$, PA28 γ and PA200 that bind to 20S and 26S complexes, however, has not been systematically evaluated so far (Guo et al., 2017; VerPlank and Goldberg, 2017). Only rapid recruitment of PA28 $\alpha\beta$ to the 20S proteasome upon catalytic proteasome inhibition was observed in reticulocyte lysates *in vitro* (Shibatani et al., 2006). As proteasome

inhibition has been shown previously to involve autoregulatory feedback adaptation of proteasome function in the cell, it was reasoned that this may also be a good system to study rapid assembly of alternative proteasome complexes to obtain first evidence for a prompt and fine-tuned regulation of alternative proteasome complexes according to certain cellular stimuli (Meiners et al., 2003).

6.2 Results

6.2.1 Proteasomal activators are recruited to 20S and 26S proteasomes in response to proteasome inhibition.

To investigate the regulation of alternative proteasome complexes in response to catalytic inhibition of the proteasome, primary human lung fibroblasts (pHLF) were treated with a low dose of proteasome inhibitor bortezomib (BZ) for 24 h and the composition of proteasome complexes was analyzed *via* native gel electrophoresis (Figure 6.1).

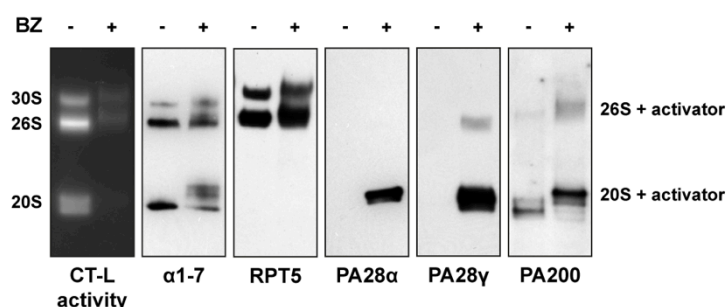


Figure 6.1: Proteasome inhibition induces formation of alternative proteasome complexes. pHLF treated with 10 nM bortezomib (BZ) for 24 h were analyzed by native gel electrophoresis. Activity of the different complexes and their efficient inhibition in response to inhibitor treatment was visualized by an overlay assay using a fluorogenic substrate specific for CT-L activity. Immunoblotting was performed for 20S subunits α 1-7, 19S subunit RPT5 and proteasomal activators PA28 α , PA28 γ and PA200. The figure shows representative results from experiments performed with pHLF from three different organ donors.

An in-gel activity assay using a substrate specific for the chymotrypsin-like (CT-L) activity confirmed effective inhibition of 26S/30S proteasome complexes and an almost complete inhibition of 20S proteasomes. Immunoblotting for 20S subunits α 1-7 and the 19S subunit RPT5 unambiguously identified the distinct 20S and 26S/30S complexes. Moreover, BZ treatment induced the formation of different 20S proteasome-containing sub-complexes of bigger size suggesting recruitment of proteasomal activators to 20S proteasomes. Indeed,

recruitment of alternative proteasome activators PA28 α , PA28 γ and PA200 to mainly the 20S complexes in response to BZ treatment was confirmed by immunoblotting of the native gels.

6.2.2 Formation of alternative proteasome complexes is a rapid response to proteasome inhibition.

According to recent literature the function of proteasome activator PA28 $\alpha\beta$ is mainly associated with the immunoproteasome (Fabre et al., 2015; Groettrup et al., 1996). Therefore, this study focused on the activators PA28 γ and PA200 for further experiments as they are described to preferentially bind to the standard 20S proteasome (Fabre et al., 2015). A time course experiment using BZ treatment of phLF for 2, 6, 16 and 24 h was performed and analysis of proteasome complexes via native gel electrophoresis was applied to further investigate the kinetics of the formation of alternative proteasome complexes. Interestingly, recruitment of PA28 γ and PA200 was already observed after 2 h of proteasome inhibitor treatment and showed the strongest effect after 16 h (Figure 6.2).

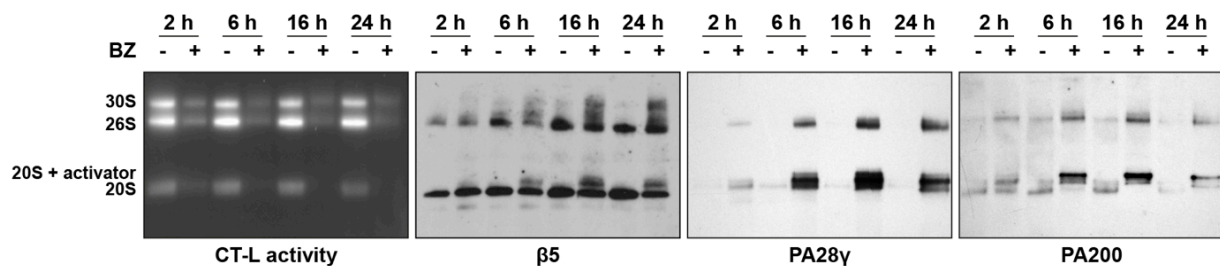


Figure 6.2: Recruitment PA28 γ and PA200 occur rapidly after proteasome inhibition. Recruitment of PA28 γ and PA200 was analyzed in phLF in response to BZ treatment for 2, 6, 16 and 24 h by native gel electrophoresis with overlay assay indicating CT-L activity of resolved complexes and subsequent immunoblotting for the activators PA28 γ and PA200. A representative result from experiments performed with phLF from three different organ donors is shown.

Measurement of proteasome inhibition via a native gel overlay assay using a substrate specific for CT-L active sites as well as via fluorogenic substrates specific for CT-L, C-L and T-L activities confirmed efficient inhibition of CT-L active sites already after 2 h BZ treatment when recruitment of PA28 γ and PA200 was observed (Figure 6.3). The C-L active sites were only partially inhibited and T-L active sites of the proteasome were not affected by the inhibitor treatment, which is in line with the results of previous studies analyzing the specificity of BZ (Dick and Fleming, 2010).

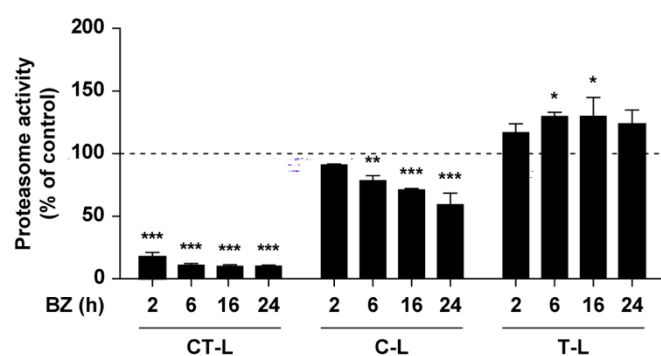


Figure 6.3: Bortezomib treatment efficiently inhibits CT-L proteasome activity in pHLF. Proteasome activity was measured in the same native protein lysates analyzed in Figure 6.2 using fluorogenic substrates specific for CT-L, C-L and T-L active sites. Bar diagram indicates proteasome activity as percentage compared to the time matching control measured in pHLF from three different donors (one-way analysis of variance, Bonferroni's multiple comparison test, $n = 3$).

Proteins ubiquitinated at lysine 48 (K48) already accumulated after 6 h of BZ treatment and increased up to a fivefold induction after 24 h proving efficient inhibition of proteasomal protein degradation (Figure 6.4).

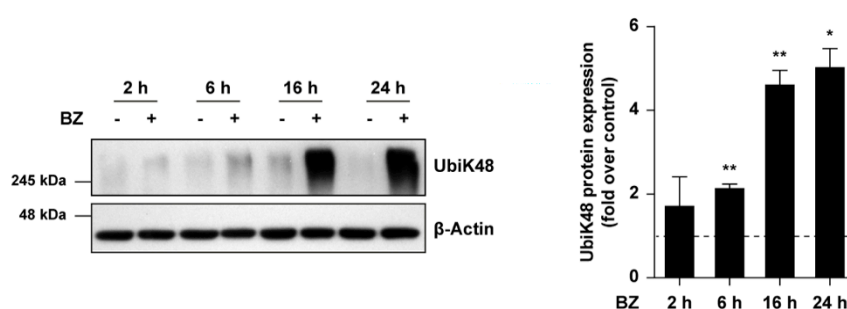


Figure 6.4: Proteins ubiquitinated at lysine 48 accumulate in response to BZ treatment. pHLF were treated with 10 nM BZ for 2, 6, 16 and 24 h and RIPA lysates were analyzed for accumulation of protein polyubiquitinated at lysine 48 (UbiK48) by Western blotting. Bar diagram shows quantification of obtained signals relative to housekeeper β -Actin and normalized to the time-matched control. Experiments were performed in pHLF from three different organ donors (one sample t-test, $n = 3$).

Therefore, these results provide the first evidence for a fast recruitment of proteasome activators in response to certain stimuli in intact cells, which suggest rapid adaptation of proteasome function to cellular needs.

6.2.3 Proteasome inhibition also mediates recruitment of PA28 γ in HeLa cells.

The formation of PA28 γ -alternative proteasome complexes was validated in another cell type in the laboratory of Dr. Olivier Coux (CRBM-CRNS, Montpellier, France). HeLa cells were

treated with 10 nM BZ for 24 h and proteasome complexes were analyzed using gel filtration and immunoblotting (Figure 6.5).

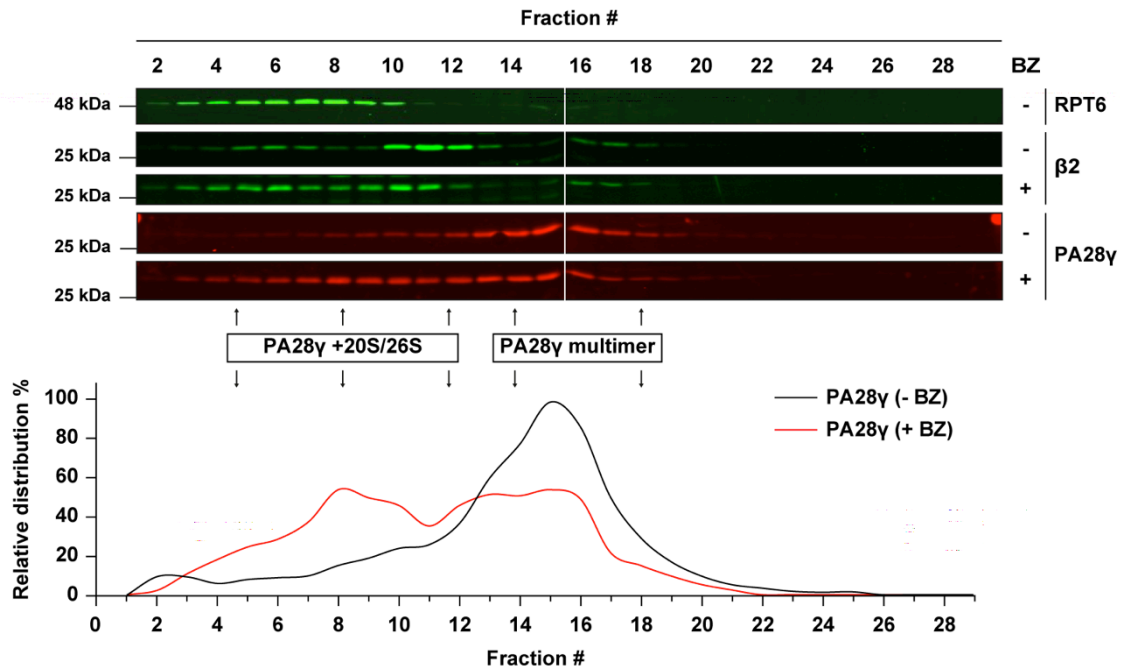


Figure 6.5: Recruitment of PA28 γ upon proteasome inhibition in HeLa cells. Proteasome complexes of HeLa cells treated with 10 nM BZ for 24 h were analyzed by gel filtration. Immunoblotting was performed for 20S subunit β 2, 19S regulatory particle subunit Rpt6 for detection of the 26S and 30S proteasomes and activator PA28 γ to analyze its recruitment. The diagram indicates the relative distribution of PA28 γ in different fractions obtained from control and BZ treated cells. The experiment was performed by Claire Abeza in the laboratory of Dr. Olivier Coux, CRBM-CRNS, Montpellier, France.

Of note, Western blotting for PA28 γ revealed that this activator exists mainly in a free non-proteasome bound form in untreated cells. In response to inhibition of 20S proteasome catalytic activity the activator was recruited to 20S and 26S proteasome complexes as previously observed in pHLF. Therefore, the formation of alternative proteasome complexes does not depend on the cell type but can be considered as a general cellular event upon proteasome inhibition.

6.2.4 Direct interaction of PA28 γ and PA200 with 20S proteasome complexes is enhanced upon proteasome inhibition.

Increased recruitment of PA28 γ and PA200 to the catalytic core complex was validated with a second method using co-immunoprecipitation (co-IP) of the 20S proteasome and its interacting activators as well as other proteins. IP of the 20S subunit α 4 was performed in

pHLF 6 h after BZ treatment in native protein lysates preserving intact proteasome complexes. Immunoblotting confirmed successful enrichment of 20S proteasomes detected with an antibody against 20S subunits $\alpha 4$. Of note, an increased amount of PA28 γ and PA200 interacted with 20S subunit $\alpha 4$ upon inhibitor treatment compared to control treated cells (Figure 6.6).

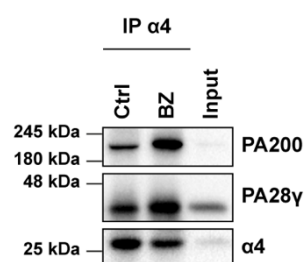


Figure 6.6: Catalytic proteasome inhibition enhances the interaction of the 20S core particle with PA28 γ and PA200. Co-immunoprecipitation of 20S subunit $\alpha 4$ was performed in native lysates of pHLF treated with 10n M BZ for 6 h. Immunoblotting was performed for 20S subunit $\alpha 4$, PA28 γ and PA200. 10% of total lysate used for co-IP was loaded as an input control.

Therefore, the formation of alternative proteasome complexes in response to catalytic inhibition of the 20S complex was confirmed using two different approaches, namely native gel analysis and co-IP.

6.2.5 Early recruitment of proteasomal activators is not regulated by their transcription.

In a next approach, the transcriptional regulation of the activators in response to proteasome inhibition was investigated as a potential mechanism for their enhanced recruitment. pHLF were treated with BZ for 2, 6, 16, and 24 h and protein levels were analyzed via Western blotting (Figure 6.7). Induction of PA28 γ and PA200 protein levels was only observed after 16 and 24 h of treatment, whereas recruitment of activators to the 20S complex already had been observed much earlier after 2 h of treatment with BZ.

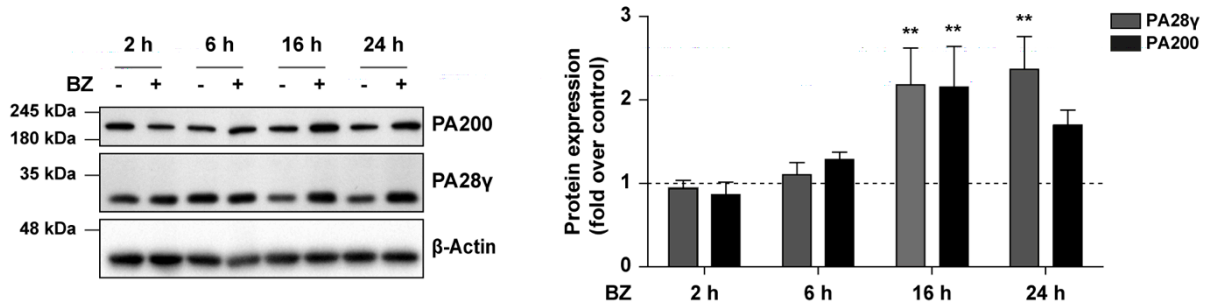


Figure 6.7: Inhibition of proteasome activity induces PA28γ and PA200 protein expression after 16 and 24 h. Protein expression of PA28γ and PA200 was analyzed by Western blotting in pHLF treated with 10 nM BZ for indicated times. Bar diagram indicates the quantification of obtained signals relative to housekeeper β-Actin and normalized to the time-matched control. Experiments were performed in cells from three different organ donors (one sample t-test, $n = 3$).

Analysis of mRNA levels by RT-qPCR indicated a significant increase for PA200, whereas transcription of PA28γ was not upregulated (Figure 6.8). Of note, induction of PA200 mRNA was observed after 16 h and therefore much delayed when compared to recruitment of activators.

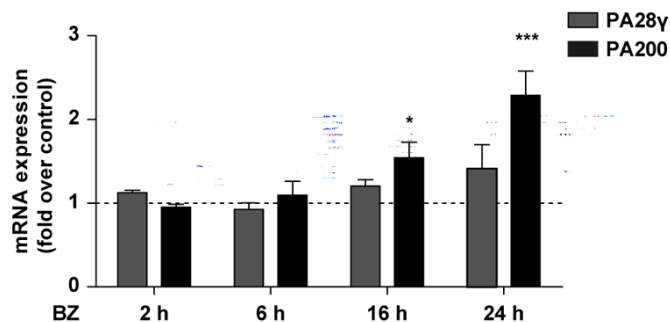


Figure 6.8: BZ treatment only induces PA200 mRNA expression at later time points. PA28γ and PA200 mRNA levels were analyzed by qPCR in pHLF treated with 10 nM BZ for indicated times. RPL19 served as a housekeeping gene. Bar diagram indicates mRNA expression of pHLF treated with 10 nM BZ for indicated times relative to time matching controls. Experiment was performed in cells from three different organ donors (one sample t-test, $n = 3$).

Recent studies already indicated a transcriptional induction of proteasomal genes in response to long-term proteasome inhibition. They identified nuclear factor erythroid-derived 2-related factor 1 (NRF-1) as transcription factor mediating increased expression of proteasomal subunits in response to proteasome inhibitor treatment (Radhakrishnan et al., 2010; Sha and Goldberg, 2014; Steffen et al., 2010). Therefore, an *in silico* promoter analysis using the Genomatix software was performed for this study by Dr. Dietrich Trümbach (Institute of Developmental Genetics, Helmholtz Zentrum München, Germany) to analyze whether the human promoter regions of the *PSME3* and *PSME4* gene

contain potential NRF-1 transcription factor binding sites (TFBSs). Analysis of the *PSME3* promoter revealed only one potential TFBSs approximately 1100 kb upstream from the transcription start site (TSS), which was found to be conserved only among human, chimp and rhesus monkey (Figure 6.9). In contrast, two TFBSs were identified in very close proximity to the TSS in the human *PSME4* promoter. One of these TFBSs was highly conserved among a variety of different species, such as human, chimp, rhesus monkey, mouse, rat and frog. For these reasons this TFBS has a much higher probability for being a functional NRF-1 binding site within the *PSME4* promoter region.

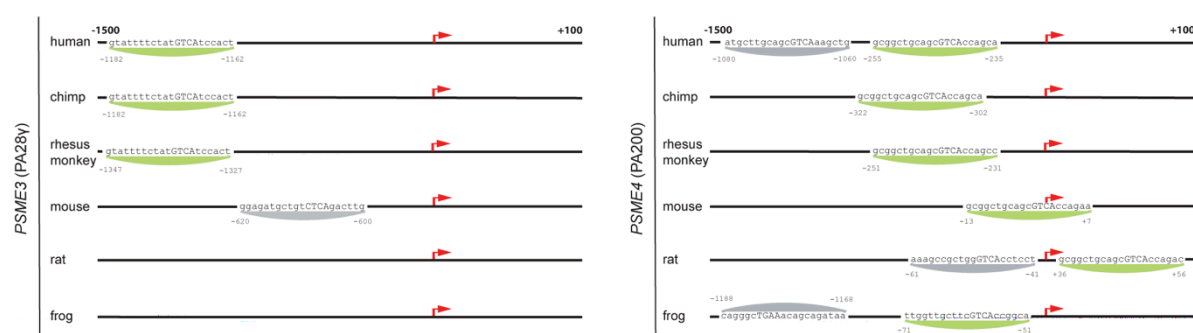


Figure 6.9: Analysis of *PSME3* and *PSME4* promoter for potential NRF-1 transcription factor binding sites. Promoter regions of human *PSME3* (encoding PA28 γ) and *PSME4* (encoding PA200) genes were analyzed for potential NRF-1 transcription factor binding sites (TFBSs) in different species. Red arrows indicate the transcription start site. Green arrows illustrate potential TFBSs of NRF-1 conserved among different species; grey arrows indicate non-conserved potential TFBSs. Analysis was performed by Dr. Dietrich Trümbach, Institute of Developmental Genetics, Helmholtz Zentrum München, Germany.

Concluding, the identification of a potential NRF-1 TFBSs within the *PSME4* promoter as well as the induction of PA200 mRNA levels in response to BZ treatment point towards a transcriptional regulation via NRF-1 in response to inhibitor treatment after 16 to 24 h, whereas PA28 γ protein levels are rather regulated by stabilization of the protein than by induction of its transcription. Of note, recruitment of proteasomal activators at early time points is not regulated via an increase in their expression.

6.2.6 Specific decrease of 26S and 30S proteasome complexes induces recruitment of PA200 but not PA28 γ .

Small molecule proteasome inhibitors, such as BZ, interfere with the catalytic activity of the 20S core complex by binding to its active sites and thereby blocking the cleavage of peptides. Therefore, this type of proteasome inhibition interferes with all different types of

complexes including uncapped 20S proteasomes, 26S and 30S proteasomes as well as alternative proteasome complexes. To further clarify the trigger for alternative proteasome complex formation it was analyzed whether proteasomal activators are also recruited upon specific inhibition of ubiquitin-dependent protein degradation by 26S and 30S proteasomes. The 19S regulator subunit RPN6 functions as a clamp stabilizing the interaction between the 20S core particle and the remaining 19S regulatory particle and is thereby essential for 26S and 30S proteasome assembly functioning as a rate-limiting subunit in this process (Pathare et al., 2012; Santamaria et al., 2003; Semren et al., 2015; Vilchez et al., 2012). For this reason, transient silencing of 19S regulator subunit RPN6 was applied for this study to interfere with the assembly of 26S and 30S in pHLF and thus to specifically inhibit ubiquitin-dependent protein degradation via these complexes. Western blot analysis of protein lysates 72 h after transfection with siRNAs indicated efficient reduction of RPN6 protein levels as well as accumulation of proteins ubiquitinated at lysine 48 (K48) implying inhibition of ubiquitin-dependent protein degradation (Figure 6.10). Moreover, protein analysis revealed induction of PA200 protein levels in these cells, whereas PA28 γ protein expression was not regulated.

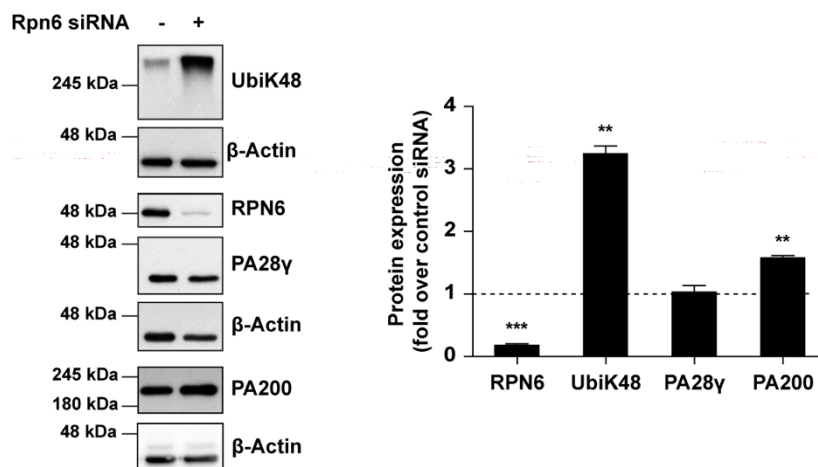


Figure 6.10: RPN6 silencing efficiently inhibits 26S and 30S ubiquitin-mediated protein degradation and induces expression of PA200. Analysis of K48-ubiquitinated proteins (UbiK48), expression levels of RPN6 and proteasomal activators PA28 γ and PA200 by Western blotting in RIPA lysates of pHLF treated with siRNAs against RPN6 or control siRNAs for 72 h. Bar diagram indicates quantification of protein levels of three independent experiments normalized to housekeeper β -Actin and to the respective scrambled siRNA-transfected control (one sample t-test, $n = 3$).

According to these observations, RPN6 silencing for 72 h also strongly upregulated PA200 on the mRNA level while PA28 γ mRNA levels remained unchanged (Figure 6.11).

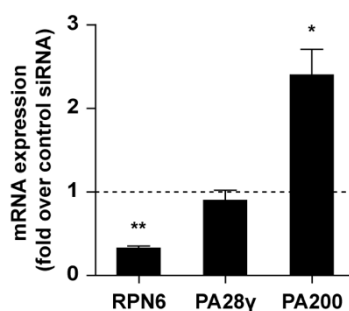


Figure 6.11: Inhibition of 26S and 30S proteasomes strongly induces PA200 mRNA level. mRNA expression of RPN6, PA28 γ and PA200 genes was analyzed in pHLF in response to silencing of RPN6 for 72 h via qPCR. RPL19 served as a housekeeping gene and bars indicate expression levels normalized to control siRNA transfected cells. Experiment was performed in pHLF from three different organ donors (one sample t-test, $n = 3$).

Analysis of proteasome complexes via native gel analysis confirmed effective interference with 26S and 30S assembly by RPN6 silencing (Figure 6.12). An in-gel activity assay using a fluorogenic substrate specific for chymotrypsin-like active sites indicated a strong decrease in 26S and 30S activity. Immunoblotting of the native gel for 19S subunit RPT5 and 20S subunits α 1-7 confirmed loss of 30S and prominent reduction of 26S proteasomes. This was accompanied by the formation of an additional proteasome subset between 26S and 20S complexes presumably representing 20S complexes assembled with only parts of the 19S regulator. Of note, silencing of RPN6 also increased the formation of an additional alternative 20S complex, which suggested recruitment of alternative proteasome activators to the core complex. Indeed, immunoblotting for PA200 confirmed its recruitment to 20S proteasomes whereas PA28 γ containing alternative proteasome complexes – in line with results of expression analysis – were not increased.

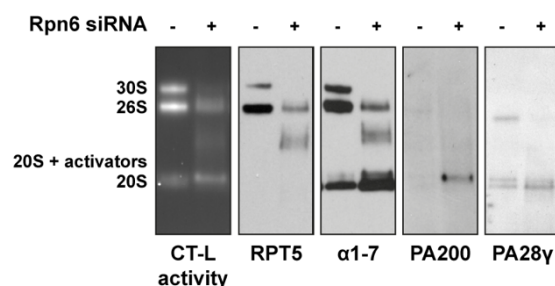


Figure 6.12: Silencing of RPN6 induces recruitment of PA200 to the 20S complex. Native protein lysates of control or Rpn6 siRNA-transfected cells were analyzed by native gel electrophoresis. Proteasome activity was visualized by an overlay assay using a fluorogenic substrate specific for CT-L active sites. Immunoblotting was performed for 19S subunit RPT5, 20S subunits α 1-7 and proteasomal activators PA28 γ and PA200. Figure indicates representative results for experiments performed in pHLF from three different donors.

Concluding from these observations, recruitment of PA200, but not PA28 γ , is sensitive to specific interference with ubiquitin-dependent 26S and 30S protein degradation. This

enhanced formation of PA200-containing alternative proteasomes also involves its transcriptional upregulation as observed for BZ treatment after 16 to 24 h. As induction of mRNA and protein levels was not observed for PA28 γ , it is tempting to speculate that enhanced expression of PA200 is mediated by transcription factor NRF-1, as conserved TFBSs in proximity of the transcription start site were only identified in the *PSME4* and not in the *PSME3* promoter region.

6.2.7 The extent of active site inhibition defines the dimensions of proteasomal activator recruitment.

To investigate the correlation of proteasome inhibition and the formation of alternative proteasome complexes cells were treated with increasing concentrations of proteasome inhibitor BZ. Treatment of pHLF with BZ at 1, 10, 50, and 100 nM for 6 h indicated a dose-dependent reduction of proteasome activity (Figure 6.13 A).

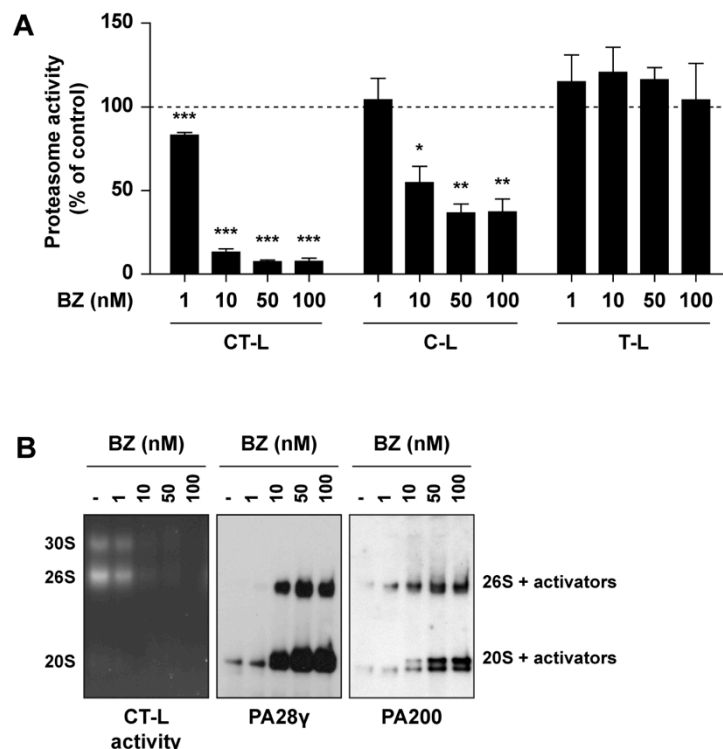


Figure 6.13: BZ treatment induces dose-dependent formation of alternative proteasome complexes. Native lysates of pHLF treated with indicated concentrations of BZ for 6 h were analyzed for (A) chymotrypsin-like (CT-L), caspase-like (C-L) and trypsin-like (T-L) proteasome activity and (B) alternative proteasome complex formation by native gel electrophoresis and immunoblotting for PA28 γ and PA200. Bar diagram indicates the percentage of proteasome activity compared to control (one sample t-test, $n = 3$). Representative results of experiments performed in pHLF from three different donors are shown in (B).

Here, the CT-L activity of the proteasome exhibited the strongest reduction to 10 % remaining activity compared to control at the highest applied BZ concentration, whereas the caspase-like (C-L) activity decreased to approximately 40 % and the trypsin-like (T-L) activity was not affected. This inhibitory profile of BZ treatment accords with recent literature and the data shown in Figure 6.3 (Dick and Fleming, 2010). Native gel analysis confirmed that dose-dependent reduction of CT-L activity caused dose-dependent recruitment of PA28 γ and PA200 to the 20S and 26S proteasome (Figure 6.13 B).

In a following approach it was investigated whether interference with only CT-L active sites is sufficient to induce activator recruitment. pHLF were treated with increasing concentrations of CT-L active site specific proteasome inhibitor oprozomib (10, 50, and 100 nM) for 6 h (Dick and Fleming, 2010). Measurement of proteasome activity by fluorescent substrates confirmed a dose-dependent reduction of CT-L activity, whereas this inhibitor did not affect the other catalytic sites (Figure 6.14 A). Analysis of proteasome complexes by native gel analysis and subsequent immunoblotting for PA28 γ and PA200 indicated a dose-dependent formation of alternative proteasome complexes (Figure 6.14 B). Therefore, inhibition of subunit $\beta 5$ representing the CT-L activity is sufficient to induce the recruitment of activators to 20S and 26S proteasomes.

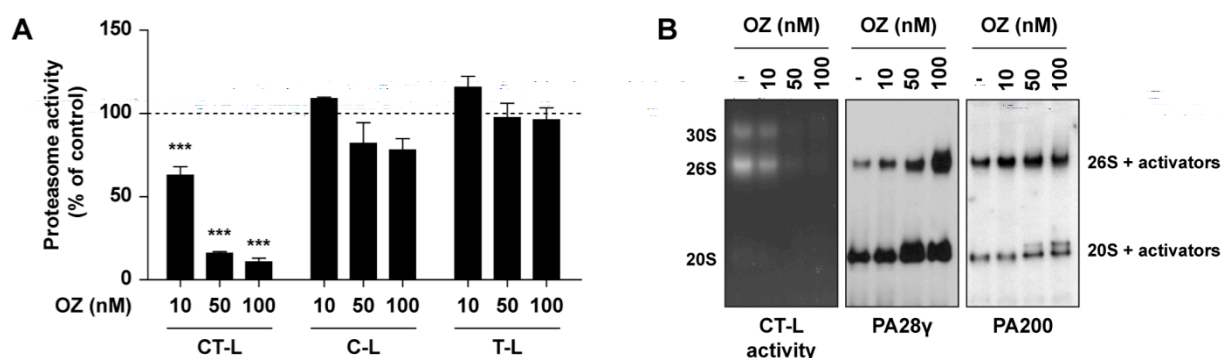


Figure 6.14: Specific inhibition of CT-L active sites is sufficient to induce formation of alternative proteasome complexes. pHLF treated with 10, 50 and 100 nM oprozomib (OZ) for 6 h were analyzed for (A) chymotrypsin-like (CT-L), caspase-like (C-L) and trypsin-like (T-L) proteasome activity and (B) recruitment of proteasomal activators PA28 γ and PA200 by native gel electrophoresis, substrate overlay and subsequent immunoblotting. Bar diagram indicates the percentage of proteasome activity compared to the control (one sample t-test, $n = 3$). Representative results of experiments performed in pHLF from three different donors are shown in (B).

The extent of activator recruitment in response to efficient inhibition of all three catalytic activities of the proteasome in pHLF was analyzed by treatment with 20 μ M epoxomicin for 4.5 h. Analysis of proteasome activity confirmed an almost complete reduction of all three

catalytic activities (Figure 6.15 A). Moreover, under this condition very pronounced recruitment of PA28 γ and PA200 to the 20S core complex was detected when compared to the effect of treatments used so far in this study (Figure 6.15 B).

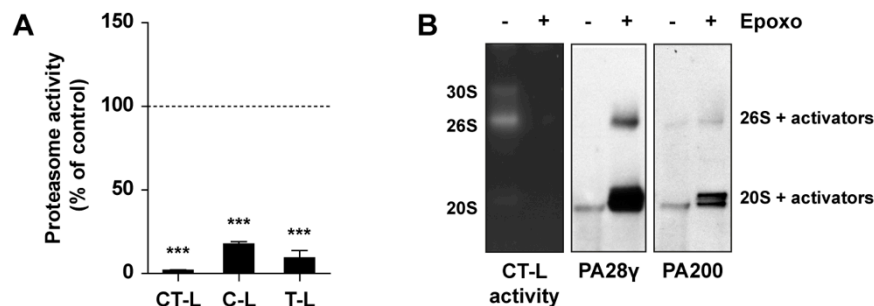


Figure 6.15: Inhibition of all three catalytic active sites of the proteasome induces the most pronounced recruitment of proteasomal activators. (A) pHLF were treated with 20 μ M epoxomicin for 4.5 h and efficient inhibition of all three active sites was confirmed by proteasome activity assay. Bar diagram indicates the percentage of proteasome activity compared to DMSO treated cells (one sample t-test, $n = 3$). (B) Recruitment of PA28 γ and PA200 was analyzed by native gel electrophoresis and immunoblotting. Here, a representative result for three experiments performed in pHLF from different donors is shown.

Hence, these observations suggest that recruitment of PA28 γ and PA200 is titrated according to the extent of proteasome inhibition and that inhibition of the CT-L activity is sufficient to induce the formation of alternative proteasome complexes.

6.2.8 Recruitment of PA28 γ to purified 20S complexes is not enhanced in response to catalytic proteasome inhibition *in vitro*

Several recent publications also suggested that binding of peptide ligands to the active sites induces an allosteric conformational change and opening of the 20S proteasome α -ring (Arciniega et al., 2014; Osmulski et al., 2009; Ruschak and Kay, 2012). Using an *in vitro* approach, Kleijnen *et al.* provided evidence for a stabilization of the weak interaction between 20S and 19S regulator by binding of an inhibitor to the active sites using an *in vitro* approach. This data suggests that occupancy of these catalytic centers signals to the bound regulator via an allosteric mechanism (Kleijnen et al., 2007). To investigate a possible regulation of activator recruitment to the 20S complex via allosteric signaling to the 20S proteasome α -ring, the recruitment of recombinant PA28 γ to purified 20S proteasomes was analyzed in response to proteasome inhibition by our collaboration partner Dr. Olivier Coux, CRBM-CNRS UMR 5237, Montpellier, France. *In vitro* experiments were only performed with

activator PA28 γ , as recombinant human PA200 is not commercially available and its expression failed due to its high molecular weight of 200 kDa (data not shown and personal communication of Dr. A. Geerlof, Protein Expression and Purification Facility, HMGU). 1 μ g purified 20S proteasomes treated with 25 μ M epoxomicin or DMSO as a control were incubated with 2 μ g recombinant expressed PA28 γ for 5 min at 37 °C. Subsequently, the formation of alternative proteasome complexes was examined via native gel electrophoresis (Figure 6.16).

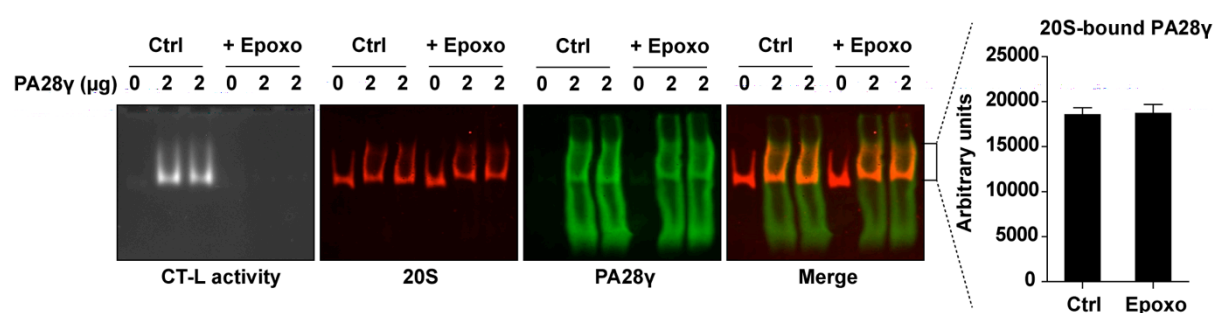


Figure 6.16: Recruitment of PA28 γ to 20S is not enhanced by proteasome inhibition *in vitro*. 1 μ g of purified 20S pre-treated with 25 μ M epoxomicin were incubated with 2 μ g recombinant PA28 γ . The activity of obtained complexes and recruitment of PA28 γ was investigated by native gel electrophoresis, in-gel CT-L overlay assay and immunoblotting. Bar diagram indicates densitometric analysis of immunoblots (data provided by Dr. Olivier Coux, CRBM-CRNS, Montpellier, France).

An in-gel overlay assay using a fluorescent substrate specific for CT-L activity confirmed strong activation of proteasome activity upon addition of PA28 γ implying the formation of active complexes by binding of the activator to the core complex. Pre-treatment with proteasome inhibitor epoxomicin led to an efficient inhibition of 20S activities. Immunoblotting for the 20S proteasome and PA28 γ confirmed formation of PA28 γ -20S proteasome complexes. However, the recruitment of PA28 γ to the 20S core complex was not enhanced in response to occupancy of the catalytic sites by epoxomicin in this experimental setup.

6.2.9 Proteasome inhibition induces activator recruitment in native cell extracts

To analyze whether activator recruitment requires other cellular components or intact cells, the formation of alternative proteasome complexes was determined upon proteasome inhibitor treatment of native cell extracts. Native TSDG extracts of pHLF were incubated with

20 μM epoxomicin inhibiting all three proteasomal catalytic sites for 1 h at 37 $^{\circ}\text{C}$ and 600 rpm. In-gel overlay with a substrate specific for CT-L activity indicated efficient interference with proteasomal activity upon treatment (Figure 6.17 A). Of note, Western blotting of native gels showed increased association of PA28 γ and PA200 with 20S and 26S complexes in extracts treated with epoxomicin.

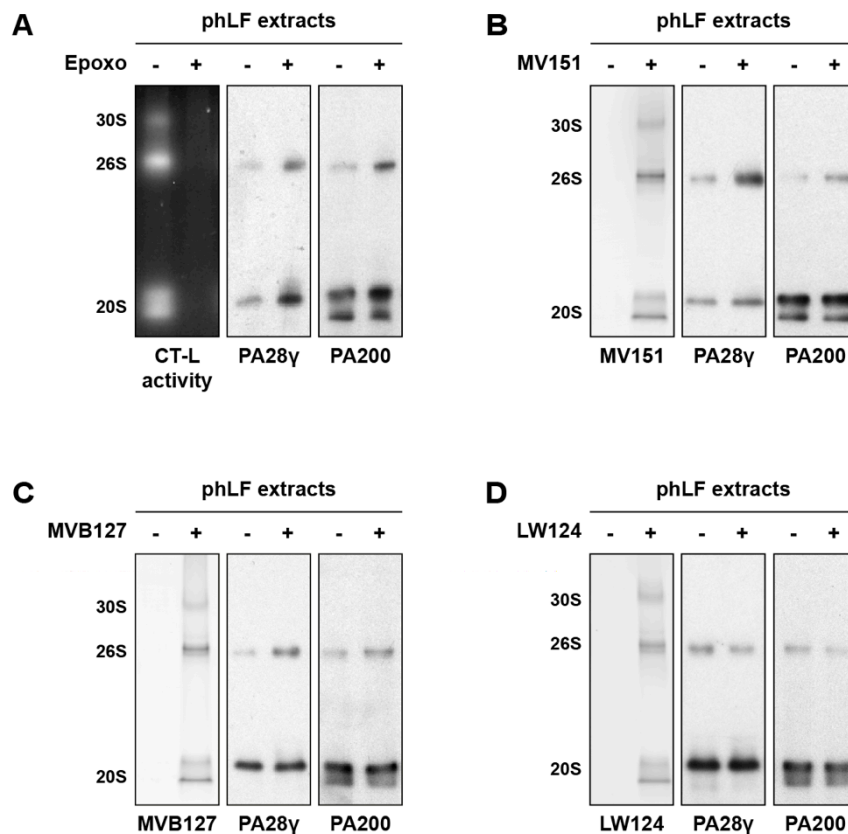


Figure 6.17: Treatment of native phLF extracts with epoxomicin or activity based probes (ABPs) MV151 and MVB127 but not LW124 induces formation of alternative proteasome complexes. Native TSDG extracts of phLF were treated with (A) 20 μM epoxomicin, (B) 0.5 μM ABP MV151, (C) 1 μM ABP MVB127 or (D) 0.25 μM LW124 for 1 h at 37 $^{\circ}\text{C}$ and 600 rpm. Alternative proteasome complexes were then analyzed by native gel electrophoresis and immunoblotting for PA28 γ and PA200. (A) Proteasomal activity in response to proteasome inhibition by epoxomicin was determined by in-gel overlay with a substrate specific for chymotrypsin-like (CT-L) activity. Efficient labeling of proteasome complexes with ABPs MV151, MVB127 and LW124 was confirmed by imaging of fluorescence. Figures indicate representative results for experiments performed with extracts from phLF of four different donors.

ABPs are fluorescently labeled proteasome inhibitors with different specificities for the three active sites, which are widely used for experimental detection of active proteasome complexes (Li et al., 2013; Verdoes et al., 2006). To determine whether these ABPs also induce formation of alternative proteasome complexes, native TSDG extracts of phLF were treated for 1 h at 37 $^{\circ}\text{C}$ and 600 rpm with 0.5 μM MV151 recognizing all three catalytic sites

of the proteasome, 1 μ M MVB127 specifically inhibiting β 5/ β 5i active sites and LW124 binding to β 1/ β 1i sites according to the standard protocol for ABP labeling of proteasomes in cell lysates. Efficient labeling with ABPs was confirmed by imaging of fluorescently tagged proteasomes in native gels (Figure 6.17 B, C and D). Indeed, treatment of cell extracts with both ABPs MV151 and MVB127 induced recruitment of PA28 γ and PA200 mainly to 26S but also 20S proteasomes (Figure 6.17 B and C). In contrast, labeling of pHLF extracts with MV124 inhibiting β 1/ β 1i active sites did not induce recruitment of both activators (Figure 6.17 D). This suggests that inhibition of β 5/ β 5i active sites is necessary for recruitment of proteasomal activators, as proteasome inhibitor oprozomib targeting β 5/ β 5i was sufficient to induce dose-dependent formation of alternative proteasome complexes in intact cells (shown in Figure 6.14)

In conclusion, these experiments showed that formation of alternative proteasome complexes upon proteasome inhibition does not require an intact cellular environment. Moreover, labeling of active proteasomes with ABPs widely used for activity profiling targeting β 5/ β 5i or all three catalytic subunits also induces formation of alternative proteasome complexes thereby changing original cellular proteasome populations.

6.2.10 Alternative proteasome complexes persist after recovery of proteasome activity

In a further approach the potential persistence of alternative proteasome complexes after recovery of proteasome activity was analyzed to obtain insights into the functional role of their recruitment. After treatment of pHLFs with 10 nM BZ for 6 h to induce activator recruitment, cells were allowed to recover proteasome activity in fresh cell culture medium for 24 h. Measurement of proteasome activity for all catalytic sites confirmed inhibition of CT-L and C-L activities after 6 h of treatment (Figure 6.18 A). After incubation in fresh medium, CT-L activity recovered and C-L and T-L activities increased compared to untreated cells harvested at the same time. Native gel electrophoresis and subsequent analysis of proteasome activity using an in-gel overlay assay confirmed recovery of CT-L activity in 26S and 30S complexes (Figure 6.18 B). Moreover, immunoblotting for 20S proteasome subunits α 1-7 indicated formation of 20S containing alternative proteasome complexes running slightly slower than non-capped 20S proteasomes that persisted after recovery of

proteasome activity for 24 h. The amount of 30S proteasomes increased after the recovery phase, which accorded well with the increase in total proteasome activity after recovery. Immunoblotting for PA28 γ and PA200 revealed that alternative proteasome complexes persisted after recovery of proteasome activity. Therefore, recruitment of proteasomal activators could be important for the cell to cope with proteotoxic stress, as these complexes are proteolytically active.

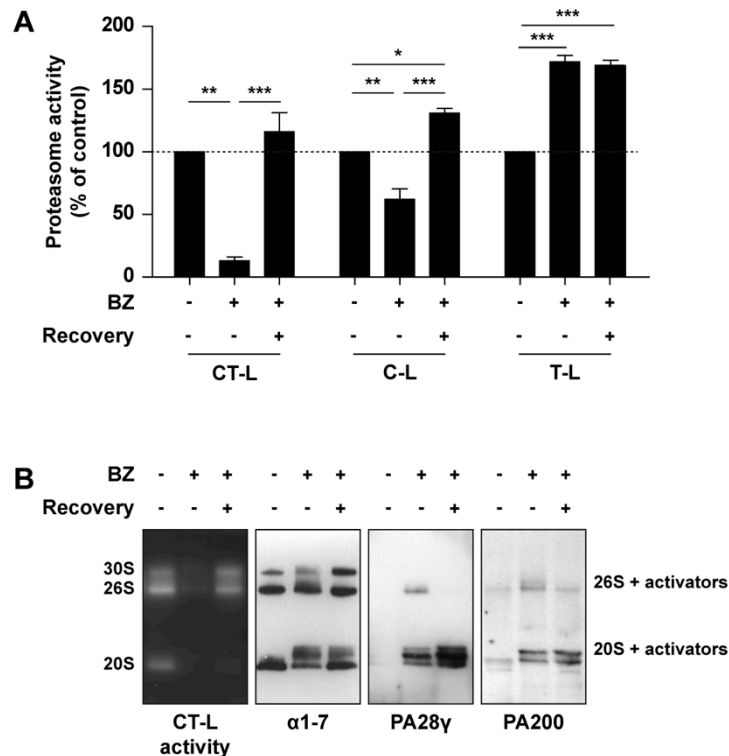


Figure 6.18: Alternative proteasome complexes persist after recovery of proteasome activity. phLF were treated with 10 nM BZ for 6 h and directly harvested or allowed to recover from proteasome inhibition in fresh medium for 24 h. (A) Proteasome activity and (B) proteasome composition using native gel electrophoresis and immunoblotting were analyzed. Bar diagram (A) indicates the percentage of proteasome activity compared to control cells (one sample t-test, $n = 3$). A representative result of experiments performed in phLF of three different organ donors is shown in (B).

6.2.11 Silencing of PA28 γ decreases ability of cells to cope with proteasome inhibition

The ability of cells to cope with proteasome inhibition upon loss of activator expression was investigated by transient silencing of PA28 γ . Here, the effect of interference with alternative proteasomes formation was investigated with regard to cell survival and growth. After silencing of PA28 γ for 48 h phLF were treated with 10 nM BZ for 6 h and allowed to recover in fresh medium for 24 h. Analysis of metabolic activity indicated a reduction in response to

BZ treatment in a similar extent as silencing of PA28 γ (Figure 6.19 A). Of note, reduced levels of PA28 γ in combination with proteasome inhibition further decreased metabolic activity of pHLF. Total cell count, determined as a measure for cellular proliferation, was significantly reduced by BZ treatment (Figure 6.19 B). This corresponds well to the generally accepted notion that inhibition of the proteasome induces cell cycle arrest as many of its regulators, such as the cyclin-dependent kinases (CDKs) are not further degraded thereby blocking cell cycle progression (Hershko, 1997). Although silencing of PA28 γ did not show a significant effect on total cell count, silencing together with BZ treatment significantly decreased cellular proliferation in comparison to BZ treatment alone. Western blot analysis of the same cells confirmed efficient silencing of PA28 γ and also indicated a significant increase in CCND1 and cell cycle inhibitor p21 protein levels validating decreased proliferation and cell cycle arrest under the applied conditions using a second approach (Figure 6.19 C).

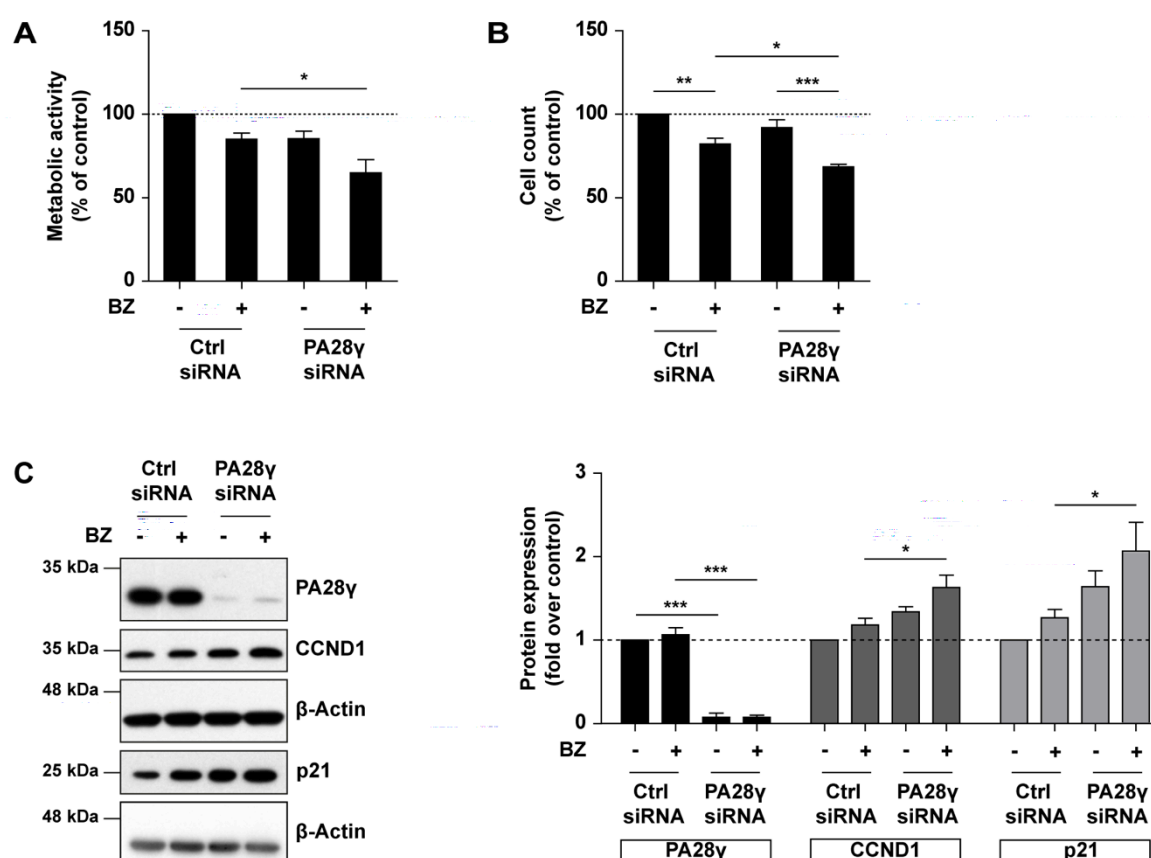


Figure 6.19: PA28 γ -deficiency decreases cell growth in response to proteasome inhibition. After 48 h of transient silencing of PA28 γ pHLF were treated with 10 nM BZ for 6 h and cells were allowed to recover proteasome activity in fresh medium for 24 h. (A) Metabolic activity, (B) cell count and (C) expression of PA28 γ , CCND1 and p21 by Western blotting (C) were analysed. Bar diagrams of (A) and (B) indicate the percentage compared to controls (one-way analysis of variance, Bonferroni's multiple comparison test, $n = 3$). Densitometric analysis of Western blots (C) indicates the fold change of protein levels compared to controls and normalized to housekeeping protein β -Actin (one-way analysis of variance, Bonferroni's multiple comparison test, $n = 3$).

Concluding, these data suggest that formation of PA28 γ -containing alternative proteasome complexes indeed allows cells to better cope with proteotoxic stress as induced by catalytic proteasome inhibition.

6.3 Discussion

Until now, only a very limited amount of studies have provided evidence for a fast adaption of proteasomal function according to cellular needs (Guo et al., 2015; Lokireddy et al., 2015). Here, the effect of inhibition of proteasome function on regulation of alternative proteasome activators was investigated to provide first evidence for a fast adaption of proteasome complexes in intact mammalian cells. This study demonstrated a so far unknown and rapid regulation of proteasome complexes in response to inhibition of the catalytic active sites by small molecule proteasome inhibitors in different cell types. Treatment of cells with inhibitors at different doses and with different specificities for the active sites of the 20S core complex indicated that the formation of alternative proteasomes correlated with the extent of proteasome inhibition and was most pronounced when all three catalytic sites were inactivated. Of note, specific inhibition of 26S and 30S protein degradation caused recruitment of PA200, but not PA28 γ , to the 20S complex, which was accompanied by transcriptional induction of the activator. Alternative proteasome complexes persisted when the active sites regained their activity, which suggests that they are involved in the cellular response to stress. In this regard, cells with PA28 γ silencing showed a decreased ability to cope with proteotoxic stress involving a defect in cellular growth and proliferation.

6.3.1 Regulation of the proteasome in response to active site inhibition

In 2003, small molecule proteasomal inhibitors began to enter the clinic when bortezomib (Velcade) was the first proteasome inhibitor approved by the FDA for the treatment of multiple myeloma (Kane et al., 2003). In the same year our group analyzed the effects of inhibition of proteasomal activity on 26S and 30S proteasomes themselves (Meiners et al., 2003). This study discovered that inhibition of proteasome activity by small molecule inhibitors induced gene transcription and protein levels of 26S subunits as an auto-regulatory feedback loop to compensate its impaired function. Moreover, increased expression of proteasomal subunits accorded with augmented *de novo* assembly of proteasome complexes. Of note, in the aforementioned study treatment of cells for 6-8 h was sufficient to stimulate proteasomal gene expression and biogenesis of new proteasome particles. Despite these drastic effects on the 26S and 30S standard proteasome, the regulation of alternative proteasome complexes has not been investigated in mammalian

cells so far. Book and colleagues observed an induction of PA200 protein level and increased association with purified proteasome in response to proteasome inhibitor treatment for 30 h in *Arabidopsis* (Book et al., 2010). Another study reported recruitment of PA28 $\alpha\beta$ in response to proteasome inhibition in reticulocyte lysates *in vitro* (Shibatani et al., 2006). Hence, the present study identifies a so far unrecognized, remarkably strong and rapid recruitment of alternative proteasome activators to the 20S and 26S proteasomes in primary human cells *in vivo*. Concluding, catalytic inhibitors of the proteasome not only augment the formation of 26S and 30S proteasomes but also stimulate concerted induction of alternative proteasome complexes.

6.3.2 Potential mechanisms for alternative proteasome complex formation

The exact mechanism of alternative proteasome complex formation is still unknown and requires further investigation, although recruitment of PA28 γ and PA200 was studied in detail in response to different ways of proteasome inactivation in this study. However, different possibilities exist which are discussed in the following section.

6.3.2.1 A non-proteasome bound reservoir of activators serves as a pool for rapid formation of alternative proteasomes.

An initial recruitment of PA28 γ and PA200 was already observed after 2 h of proteasome inhibitor treatment. Of note, induction of PA28 γ and PA200 protein levels was only observed after 16 h, much later after the onset of alternative proteasome complex formation. Therefore, early formation of alternative proteasome complexes is transcriptionally independent and results from association of free, non-proteasome bound activators to the standard core complex. Indeed, gel filtration experiments as well as native gel analysis showed that PA28 γ exists mainly in a free form in untreated cells, presumably forming heptamers. Therefore, it can be rapidly recruited to the 20S proteasome upon certain stimuli (Figure 6.5). For PA200, detection of a non-proteasome-bound fraction by native gel electrophoresis remains difficult, because the signal for PA200 is much lower compared to PA28 γ . The reason for this might be a lower affinity of the antibody to its antigen or/and a generally lower expression of the activator. Ustrell *et al.* investigated the expression of PA200 in homogenates from several murine organs, including liver, spleen, brain, heart, kidney, lung

and testis, and observed that the protein was substantially lower expressed in the lung as compared to testis and other organs (Ustrell et al., 2002). Native gel electrophoresis of primary human lung fibroblasts followed by cutting the gel in 10 fragments and analysis by mass spectrometry revealed that PA200 was mainly associated with the 20S proteasome and detected in a lower amount in a free, non-proteasome bound form (data not shown, experiment performed by V. Welk and Dr. O. Vosyka). For this reason - and as its expression levels are not altered as an initial response to proteasome inhibition - this activator presumably also exists in a free form allowing fast recruitment.

6.3.2.2 Rapid formation of alternative proteasome complexes is potentially triggered by an allosteric conformational change of the 20S core complex.

In this study the degree of proteasome inhibition directly correlated with the quantity of newly formed alternative proteasome complexes. Moreover, Shibatani and colleagues observed recruitment of PA28 $\alpha\beta$ upon inhibitor treatment of reticulocyte lysates *in vitro* in the absence of a living cellular environment (Shibatani et al., 2006). These observations suggest that rapid recruitment of alternative proteasome activators might be caused by an allosteric conformational shift of the 20S core particle in response to inhibitor binding. Structural conformational changes of the 20S core particle have been analyzed by several studies in response to substrate or inhibitor binding. An early study by Osmulski and Gaczynska published in 2000 gave first evidence for allosteric regulation of 20S proteasome conformation when they showed by atomic force microscopy that 20S proteasome core complexes of fission yeast exist in an open or a closed conformation and that substrate binding to the catalytic sites promotes the open gate conformation (Osmulski and Gaczynska, 2000). In a follow-up study, the authors provided evidence that a tetrahedral transition state of the active sites induces an allosteric conformational shift in the α -ring inducing its gate opening in *S. cerevisiae* (Osmulski et al., 2009). Structural changes were also observed in the β 5 subunits of yeast and mouse 20S proteasomes upon ligand binding using principal component analysis of the 20S crystal structures (Arciniega et al., 2014). NMR spectroscopy identified an allosteric mechanism that induces conformational changes to the PA28 activator-binding site upon active site modifications in *T. acidophilum* (Ruschak and Kay, 2012). Allosteric conformational changes have also been investigated in the context of

proteasome inhibitors. Kleijnen *et al.* suggested that in the absence of ATP the very fragile interaction of 20S and 19S regulator is stabilized by binding of proteasome inhibitors to the catalytic sites of the 20S proteasome. Indeed, they demonstrated that reactive groups of the inhibitors mediate the stabilization effect and that this effect is dose-dependent (Kleijnen *et al.*, 2007). The first analysis of inhibitor binding on the structure of the human 26S holoenzyme revealed that binding of the inhibitor oprozomib to the catalytic site induces far distance allosteric structural changes up to the ubiquitin receptor RPN10, which are presumably transferred via 19S subunit RPN5 (Haselbach *et al.*, 2017). The effect of an inhibitor-induced conformational change of the 20S proteasome on association with alternative regulators, however, had not been investigated so far. The recruitment of recombinantly expressed PA28 γ to purified 20S proteasome in response to catalytic inactivation of active sites was analyzed using an *in vitro* reconstitution assay. Of note, the results of this experiment did not indicate an increased formation of PA28 γ -bound 20S proteasomes in response to efficient inhibition of proteasome activity by epoxomicin. A very efficient recruitment of PA28 γ was observed with and without inhibitor treatment. However, *in vitro* reconstitution assays are challenging and the observed result may be an artifact resulting from assay limitations. The binding of proteasomal activators to purified 20S proteasomes *in vitro* is a very fast process (personal communication Dr. Olivier Coux). The experimental setup, however, is very limited regarding fast detection of proteasome complexes as it involves time-consuming native gel electrophoresis, which does not allow for analysis within a few seconds after addition of the activator to the 20S core complex. Hence, in an artificial *in vitro* setting, the recruitment may proceed fast and complete impeding the quantitative detection of activator recruitment. Therefore, to draw a final conclusion whether an allosteric conformational change is the underlying trigger for fast formation of alternative proteasome complexes, another method allowing for a faster detection of changes in activator recruitment has to be applied.

Formation of alternative proteasome complexes was also observed in inhibitor-treated protein extracts implying that this process does not require an intact living cell. However, other proteins present in the native extract could still be involved in recruitment of proteasome activators. Interestingly, PA200 was also recruited to 20S proteasomes in response to RPN6 silencing, when catalytic sites were active and not inactivated by inhibitors. Therefore, another so far unknown alternative mechanism of recruitment is also conceivable

and requires further investigation. Of note, analysis of ABP-labeled pHLF extracts indicated that detection of active proteasome complexes with ABPs should be applied with caution, as the labeling procedure induces a shift in alternative proteasomes.

6.3.2.3 Late recruitment of alternative proteasome activators accords with increased protein levels of PA28 γ and PA200.

In this study an enhanced protein expression of PA28 γ and PA200 was observed after 16 h of BZ treatment in time course experiments. These observations suggest that recruitment of alternative proteasome activators at later time points is regulated via increased protein levels. Of note, an induction on mRNA level was only identified for PA200, but not for PA28 γ mRNA expression, suggesting that the increase of PA28 γ protein levels is rather regulated via protein stabilization than via induction of gene transcription. The regulation of proteasomal gene expression in response to proteasome inhibition has been extensively investigated in recent years: When Mitsiades and colleagues examined molecular pathways and the mechanism behind the pro-apoptotic effect of proteasome inhibitor bortezomib (PS-341) in multiple myeloma cells using an oligonucleotide microarray analysis, they observed upregulation of genes of the ubiquitin proteasome system in response to bortezomib treatment (Mitsiades et al., 2002). The previous study of our group provided evidence for transcriptional induction of 26S subunits in response to proteasome inhibitor treatment in non-cancer cells (Meiners et al., 2003). In 2010, nuclear erythroid-derived 2-related factor 1 (NRF1) was discovered as the underlying transcription factor mediating proteasomal gene expression by binding to antioxidant response elements (AREs) of the proteasomal promoter regions in response to inhibition of proteasomal activity (Radhakrishnan et al., 2010). In the same year, Steffen *et al.* confirmed these findings and showed that the ER membrane-resident TCF11, the long isoform of NRF1 which is normally degraded via the ER-associated protein degradation, translocates into the nucleus in response to proteasome inhibition where it induces gene transcription (Steffen et al., 2010). Interestingly, another study also reported a transcriptional induction of PA200 but not PA28 γ in response to 10 nM BZ treatment for 16 h in SHSY-5Y cells (Sha and Goldberg, 2014). Therefore, the results of the present study validate previous findings and in addition identify highly conserved NRF1 binding sites in the promoter region of the *PSME4* gene, which are

not present in the *PSME3* promoter region. Concluding, formation of alternative proteasome complexes in response to long time proteasome inactivation accords with induction of PA28 γ and PA200 protein levels presumably supporting further recruitment and replenishing pools of non-proteasome bound activators.

6.3.2.4 Regulation of PA200 in response to 26S/30S silencing

Silencing of 19S subunit RPN6 was applied to specifically interfere with 26S and 30S proteasomal protein degradation. Here, specific formation of only PA200-alternative proteasome complexes was observed. Delayed recruitment of the activator also accorded with induction of PA200 mRNA and protein levels, whereas PA28 γ was not regulated. Therefore, these results provide first evidence for a differential regulation of both activators. So far, the effect of 26S/30S inhibition on the regulation of proteasomal gene expression and complex formation has only been investigated by a very early study by Wojcik *et al.* using a screen of RNA interference against 20S and 19S subunits in *Drosophila* (Wójcik and DeMartino, 2002). Here, silencing of 19S subunits and subsequent reduction of 26S and 30S complexes induced concerted upregulation of 26S proteasomal genes and increased presence of 20S complexes, but the regulation of alternative proteasome activators was not investigated. An upregulation of 26S proteasomal subunits was also confirmed in the present study (data not shown). An increase in PA200 protein levels has been observed so far in a mutant of 19S regulator subunit Rpn12 in *Arabidopsis* (Book et al., 2010). Therefore, the regulation of PA200 in response to a specific decrease of 26S and 30S proteasomes in mammalian cells is an until now unrecognized and exciting finding, as this activator is described to mediate ubiquitin-independent protein degradation. However, this notion is based on early discoveries that it does not stimulate degradation of a ubiquitin-[¹²⁵I]lysozyme conjugate and a study claiming that it might mediate the degradation of acetylated core histones (Qian et al., 2013; Ustrell et al., 2002).

Several studies observed a protective function of 19S reduction in response to proteasome inhibitor treatment (Acosta-Alvear et al., 2015; Tsvetkov et al., 2015; Wójcik and DeMartino, 2002). Moreover, decreased expression of 19S subunits correlated with resistance against proteasome inhibitor treatment in various cancer cell lines and tumors and was associated with a lower progression-free survival in multiple myeloma patients, implying a medical

relevance of this so far inexplicable observation (Tsvetkov et al., 2017). Of note, none of these studies analyzed the regulation and possible involvement of PA28 γ and PA200 in this context. It is tempting to speculate that these activators might also play a role under these conditions.

6.3.3 Function of newly formed alternative proteasome complexes in the cell

The function of rapidly formed alternative proteasome complexes in response to proteasome inhibition is not yet understood. These complexes are presumably – at least partially – inhibited when proteasome activators are recruited. Although alternative activators were still present when pHLFs regained proteasome activity, native gel electrophoresis indicated that alternative proteasome complexes consisting of 20S and PA28 γ or PA200 did not fully recover CT-L activity (Figure 6.18). So far it is unclear why these complexes are still inhibited. Nevertheless, it is tempting to speculate that recruitment of alternative proteasomal activators contributes to the cellular stress response and helps cells to better cope with proteotoxic stress. The observation that cells were able to better cope with proteasome inhibitor treatment when they were able to express PA28 γ supports this assumption (Figure 6.19). Moreover, proteasome inhibition at nontoxic dose was shown to induce a protective response in endothelial cells by induction of enzymes of the antioxidant defense system, whereas toxic doses of proteasome inhibitors did not induce this effect (Meiners et al., 2006). This protective effect of low dose proteasome inhibition was confirmed in another study characterizing endothelial cells using proteomic and transcriptomic analysis suggesting that adaptive responses of alternative proteasome complex assembly contribute to protective stress responses (Bieler et al., 2009).

PA28 γ and PA200 are described to mediate the degradation of certain substrates, which already have been identified for PA28 γ including cyclin-dependent kinase inhibitors p16, p19 and p21 amongst others (Chen et al., 2007; Li et al., 2007a). Until now, however, acetylated histones are the only specific substrates described for PA200 (Qian et al., 2013). It has been suggested that PA200 contributes to degradation of peptides, unstructured or damaged proteins as its binding to the 20S core particle induces opening of the α -ring (Ortega et al., 2005; Savulescu and Glickman, 2011; Ustrell et al., 2002). Of note, a recent publication claimed a role for alternative proteasome activators in the cellular response to oxidative

stress (Pickering and Davies, 2013). Here, the authors suggested an increased formation of alternative proteasome complexes in response to hydrogen peroxide treatment and argued that PA28 γ has the ability to degrade oxidized proteins, which was not observed for PA200. All these observations raise the interesting possibility that proteasomal activators are recruited to the proteasome core complex in response to proteasome inhibition to facilitate degradation of certain substrates allowing the cell for better recovery from proteotoxic stress.

6.3.4 Importance of defining molecular functions of proteasome inhibitors and development of more specific proteasome inhibitors

Although inhibition of proteasomal active sites by small molecule inhibitors is a non-physiological situation in the cell, it is of major importance to understand the cellular response to these inhibitors as they are an effective treatment for myeloma. The proteasome inhibitors bortezomib (Velcade) and carfilzomib (Krypolis) are widely used in the clinic for FDA-approved treatment of multiple myeloma (Herndon et al., 2013; Kane et al., 2006).

For this reason, it is of major importance to understand the molecular mechanisms and functions of these drugs *in vivo* to identify potential side and off-target effects. Beside the relevance for clinical use of proteasome inhibitors the induction of alternative proteasome complexes also represents an exciting tool for proteasome research, because cellular proteasome levels are generally very tightly regulated as changes in their amount have a major impact on cellular function (Ciechanover and Schwartz, 1998). However, the concerted formation of different alternative proteasome complexes in response to the inhibition of 20S active centers suggests that development of inhibitors interfering with the association of distinct proteasomal activators with the 20S core complex could represent a more specific means to inhibit proteasomal protein degradation and increase the knowledge on proteasome function.

In contrast, the specific decrease of 26S and 30S proteasome complexes is a physiologically relevant setting. Recent studies reported that impaired 26S and 30S function occurs during ageing, neurodegeneration, COPD and oxidative stress (Kammerl et al., 2016; Livnat-Levanon et al., 2014; Myeku et al., 2015; Tonoki et al., 2009; Vernace et al., 2007). The regulation of

alternative proteasome activators upon those conditions has not been analyzed so far but is of major interest for future studies.

7 Analyzing the regulation and function of PA200 in hyperproliferative chronic lung disease

7.1 Introduction

The discovery of alternative proteasome activators and the existence of various complexes built of 20S core particles associated with different activators suggest that proteasomal protein degradation is a highly fine-tuned process. As discussed in the previous chapter, the knowledge about the cellular function of these different complexes in the lung and also other organs but also in disease is very limited and still requires detailed investigation. However, our data on rapid formation of alternative proteasomes in response to induction of proteotoxic stress *via* inhibition of proteasomal activity support the building block concept, which involves regulation of proteasome function according to cellular needs by activator recruitment to 20S core complexes rather than by induced transcription and *de novo* synthesis (Welk et al., 2016). It is tempting to speculate that these alternative proteasome complexes are also regulated in diseased tissues, when proteostasis and cellular function are also imbalanced (Hartl et al., 2011). Therefore, analysis of their regulation in different diseases can improve the understanding of their general cellular functions. PA28 γ , for example, was discovered to be induced in cancers of different organs, which has been linked to its cellular function in mediating the degradation of the oncogenic proteins such as SRC-3 (Chai et al., 2014; Li et al., 2006; Okamura et al., 2003).

Beside very limited knowledge about the cellular function of PA200, regulation of this proteasome activator in diseased tissues as well as its involvement in the respective pathogenesis has not been described so far. For this reason, the following chapter aims to investigate the regulation of PA200 in lung diseases and to use the acquired knowledge for further elucidating the cellular function of PA200.

7.2 Results

7.2.1 PA200 is upregulated in fibrotic tissue remodeling

In a recent study, we observed that 26S proteasome activity is activated in the fibrotic lung. Moreover, proteasome activity is required for differentiation of fibroblasts into myofibroblasts, a major pathogenic driver of fibrosis (Semren et al., 2015). As information about the function of PA200 and its regulation in disease is very limited, the first approach of this study aimed to characterize its regulation in fibrotic tissue remodeling to better understand the function of the proteasome in this disease.

7.2.1.1 PA200 expression is enhanced in idiopathic pulmonary fibrosis

PA200 protein expression was first analyzed in RIPA extracts of IPF and donor tissues, which had been kindly provided by Prof. Dr. A. Günther, Universities of Giessen & Marburg Lung Center (UGMLC), Giessen, Germany. Western blotting indicated a significant induction of PA200 protein levels in fibrotic tissues compared to donor tissues (Figure 7.1). Increased expression of α -smooth muscle actin (α SMA), a marker for myofibroblasts accumulating in the lung during disease progression, confirmed fibrotic tissue remodeling in these samples.

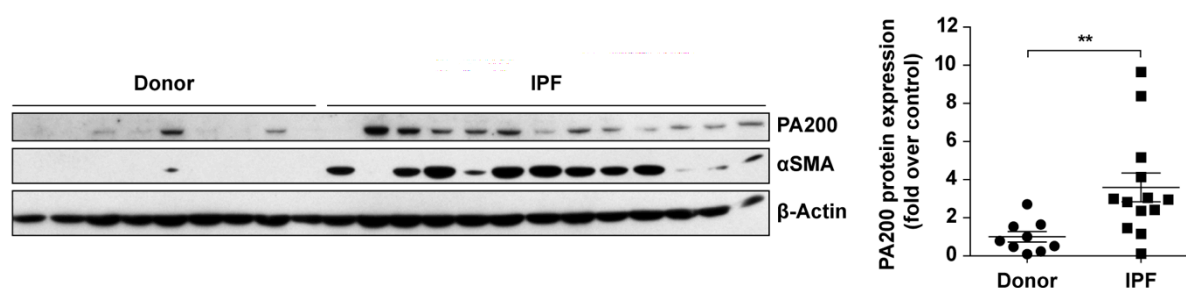


Figure 7.1: PA200 protein levels are elevated in lung homogenates of IPF patients. Protein expression of PA200 and myofibroblast marker α SMA was examined in RIPA lysates of lung homogenates from donors and IPF patients by Western blotting. Diagram shows densitometric analysis of the signal obtained for PA200 normalized to the mean signal of donors (Mann-Whitney U test, donor tissues $n = 9$, IPF tissues $n = 13$).

Interestingly, qPCR of the same tissues analyzed for protein expression did not indicate a significant increase of PA200 mRNA levels in IPF tissues. This suggests that protein levels are rather induced by stabilization of the protein than by increased transcription of the activator (Figure 7.2).

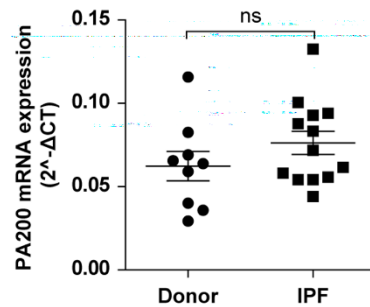


Figure 7.2: PA200 mRNA expression is not significantly induced in IPF tissues. PA200 mRNA expression was determined by qPCR in donor and IPF tissue analyzed for protein expression in Figure 7.1. Diagram indicates mRNA expression as $2^{-\Delta CT}$. *RPL19* served as a housekeeping gene (Mann-Whitney U test, donor tissues $n = 9$ and IPF tissues $n = 13$).

7.2.1.2 PA200 expression is increased in murine bleomycin-induced lung fibrosis

Bleomycin-induced lung fibrosis is a widely applied mouse model for experimental investigation of fibrotic tissue remodeling in the lung. Instillation of bleomycin to the lungs causes inflammation resulting in development of fibrosis after 14 days, which resolves after 56 days. To validate PA200 regulation in fibrotic tissues, its expression was analyzed in total lung homogenates of wildtype mice 14 days after instillation of PBS or bleomycin (3 U/kg body weight) by Western blotting. Development of fibrosis in these animals was confirmed by lung function measurement showing a significant decrease in compliance of mice 14 days after instillation of bleomycin as recently published (Semren et al., 2015). Analysis of PA200 protein expression by Western blotting demonstrated a significant increase in fibrotic lungs when compared to PBS-instilled lungs (Figure 7.3 A). PA200 mRNA expression was not regulated upon fibrotic tissue remodeling as also observed in human IPF tissues (Figure 7.3 B).

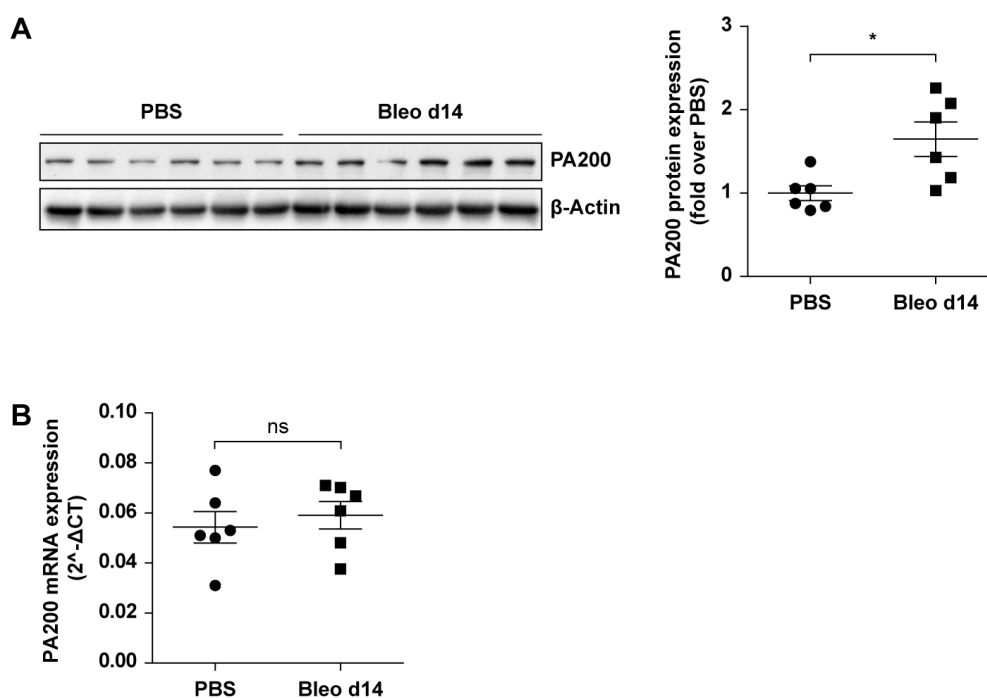


Figure 7.3: PA200 protein expression is induced in fibrotic lungs of bleomycin-instilled mice. (A) Lung homogenates of wildtype mice 14 days after instillation of bleomycin (3 U/kg body weight) or PBS as control were analyzed for PA200 protein expression by Western blotting. Diagram shows densitometric analysis of the signal obtained for PA200 normalized to the mean signal of PBS-instilled mice. (B) PA200 mRNA expression of the same lungs analyzed in (A) was determined by qPCR. Diagram shows expression as $2^{-\Delta\Delta CT}$. *RPL19* served as a housekeeping gene (Mann-Whitney U test, $n = 6$ per group).

7.2.1.3 PA200 is upregulated in murine oxalate-induced kidney fibrosis

A further approach of this study aimed to investigate whether regulation of PA200 is a general feature of fibrotic tissue remodeling in different organs or if this is restricted to the lungs. For this purpose, regulation of PA200 was assessed in a mouse model for oxalate-induced kidney fibrosis provided by Prof. Dr. Anders, Medizinische Klinik und Poliklinik IV, Klinikum der Universität München, Munich, Germany. Induction of fibrotic remodeling in kidneys of mice fed with 50 $\mu\text{mol/g}$ sodium oxalate in a standard diet for 21 days was confirmed by histological analysis using Masson's trichrome staining for collagen deposition and hematoxylin & eosin staining (Figure 7.4 A). Moreover, expression of myofibroblast marker αSMA was also significantly increased in RIPA extracts of oxalate-induced kidney fibrosis compared to non-fibrotic kidneys (Figure 7.4 B). Here, Western blot analysis also indicated a significant induction of PA200 protein levels in fibrotic kidneys. This was accompanied by increased proteasome activity determined by native gel electrophoresis of proteasome complexes in native extracts and subsequent detection of proteasome activity using in-gel overlay of a CT-L activity specific substrate (Figure 7.4 C). Of note,

immunoblotting of the native gel revealed increased association of PA200 with 20S and 26S proteasomes in fibrotic kidneys. Concluding, upregulation of PA200 protein levels is not only restricted to fibrotic remodeling of the lung but is also observed in experimental fibrosis of kidneys suggesting that induction of PA200 expression and its association with the proteasome is a general event of fibrotic tissue remodeling in different organs.

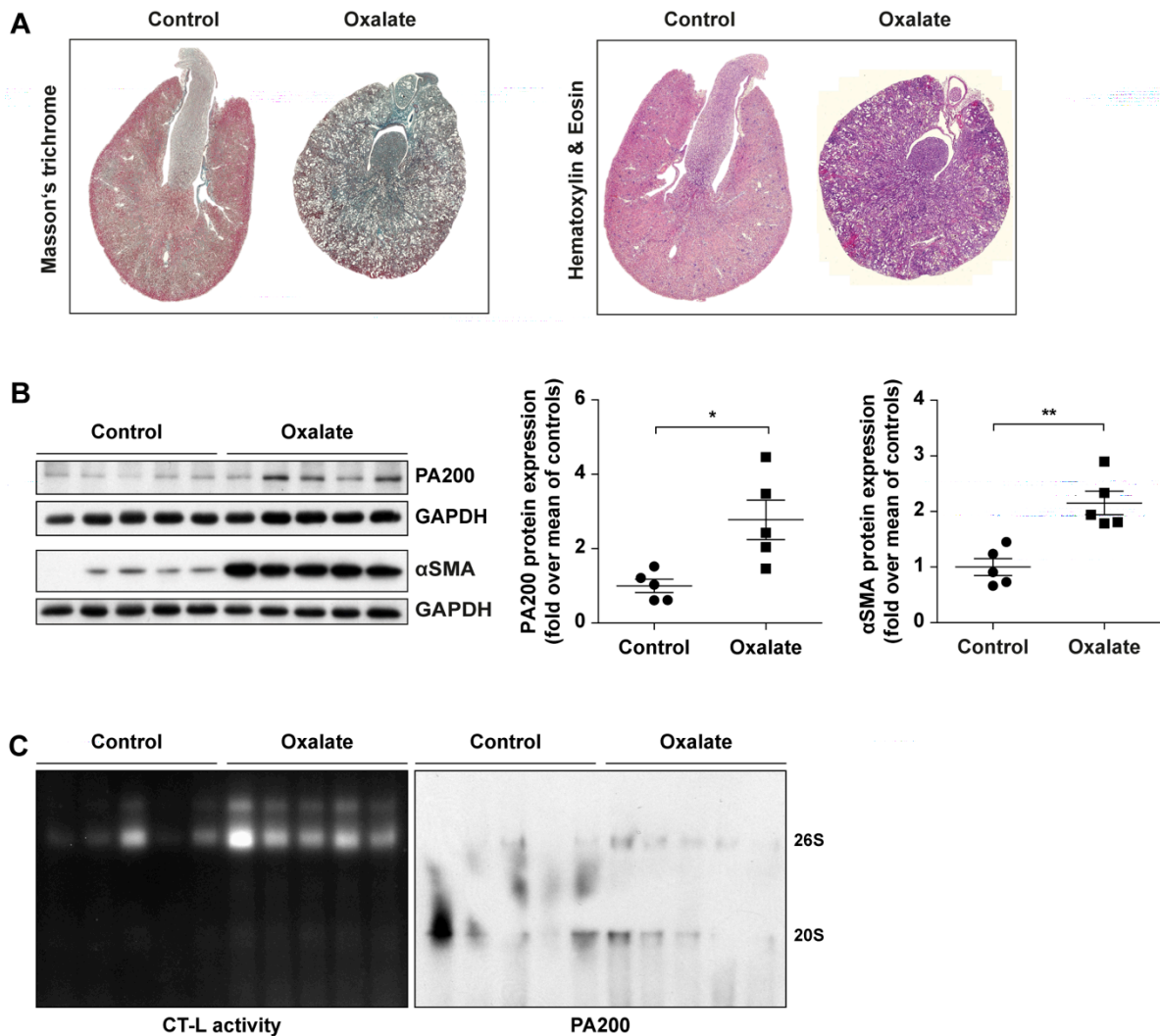


Figure 7.4: PA200 alternative proteasome levels are enhanced in fibrotic kidneys. Mice were fed with 50 $\mu\text{mol/g}$ sodium oxalate in a standard diet for 21 days to induce chronic kidney disease. (A) Tissue sections of control- and oxalate-treated mice were stained with Masson's trichrome (cytoplasm = red, collagen = green, nuclei = dark brown) and hematoxylin & eosin (cytoplasm = pink, nuclei = blue). (B) Expression of myofibroblast marker αSMA and PA200 was analyzed in total kidney RIPA extracts of oxalate- treated and control animals by Western blotting. Diagrams indicate densitometric quantification of the obtained signals normalized to the mean of controls (Mann-Whitney test, $n = 5$ per group). (C) Chymotrypsin-like (CT-L) activity of native extracts from fibrotic and control kidneys was determined by native gel electrophoresis and in-gel overlay assay. PA200 alternative proteasome complexes were detected by subsequent immunoblotting ($n = 5$ per group). Experiments were performed by T. Meul, master student at the CPC 2016.

7.2.1.4 Myofibroblasts and bronchial basal cells are expressing PA200 in IPF lungs

Cell types expressing PA200 in donor and IPF lungs were identified by IHC. A generally very low signal for the activator was obtained in healthy donor lungs (Figure 7.5). Non-fibrotic donor lungs exhibited only very faint expression of the activator in α SMA-positive smooth muscle cells surrounding vessels and keratin 5 (KRT5)-expressing basal cells. In contrast, PA200 expression was strongly induced in tissue sections of fibrotic lungs. Here, PA200 was highly expressed in α SMA-expressing myofibroblasts of fibroblast foci and KRT5-positive abnormal bronchial basal cells.

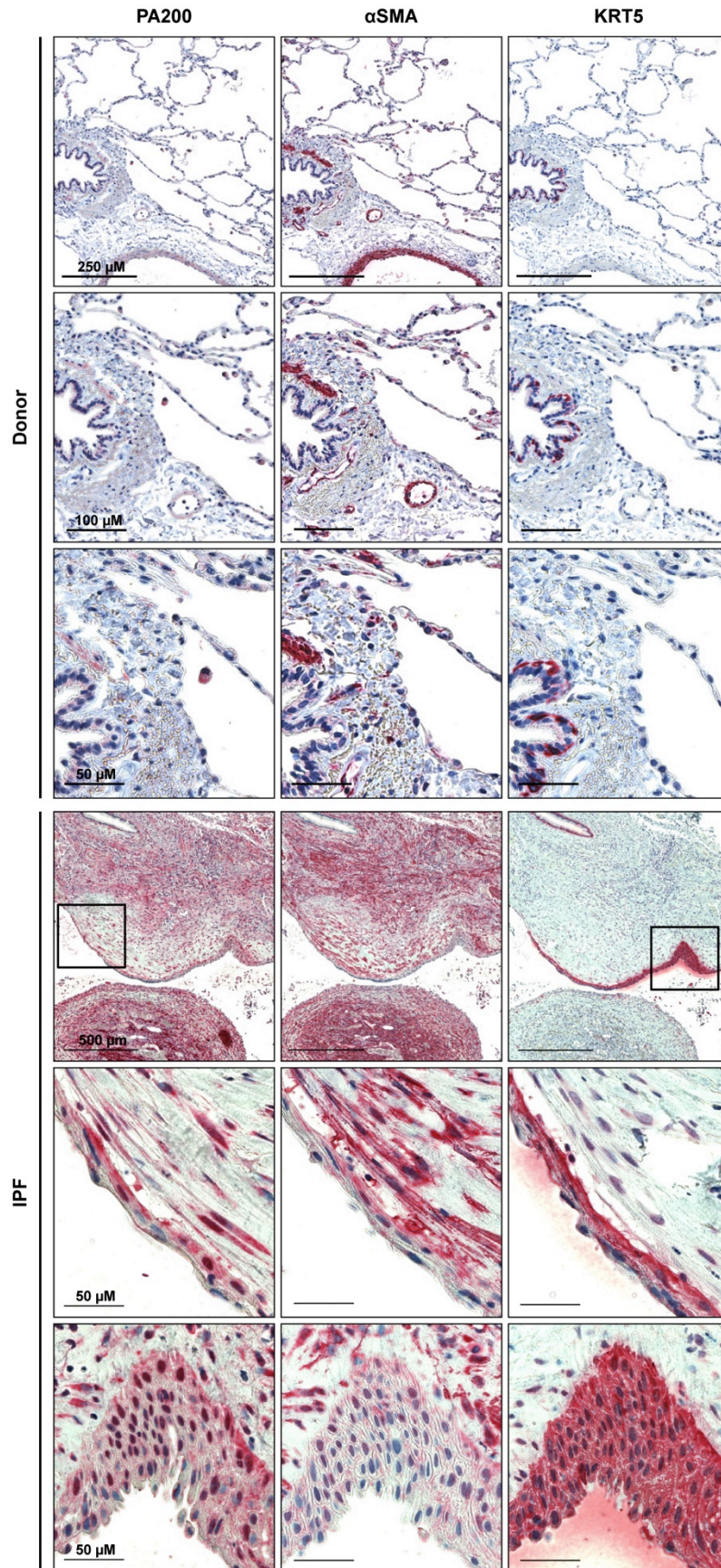


Figure 7.5: PA200 expression is induced in myofibroblasts and abnormal bronchial basal cells of IPF lungs. Immunohistochemistry of PA200, α SMA (myofibroblast marker) and KRT5 (basal cell marker) was performed in sequential lung donor and IPF tissue sections. Data was provided by Dr. M. Korfei, UGMLC Gießen.

7.2.1.5 PA200 expression decreases upon human bronchial epithelial cell differentiation

As PA200 was specifically detected in basal cells of donors and especially in IPF tissues, expression of PA200 was assessed in basal cell differentiation using *in vitro* differentiation of primary human bronchial epithelial cells (phBECs) isolated from donor tissues as previously described (Schamberger et al., 2015). phBECs at day 0 and day 28 of differentiation were kindly provided by Dr. A. Schamberger, postdoctoral scientist at the CPC (HMGU). phBECs showed a significant two-fold decrease in PA200 protein and mRNA levels upon differentiation (Figure 7.6 A and B). To determine whether downregulation of the activator occurs in the early or late phase of the differentiation process, PA200 expression was also assessed in phBECs after 7, 14, 21 and 28 days. Here, only a slight and non-significant decrease of PA200 protein and mRNA levels was observed (Figure 7.6 C and D).

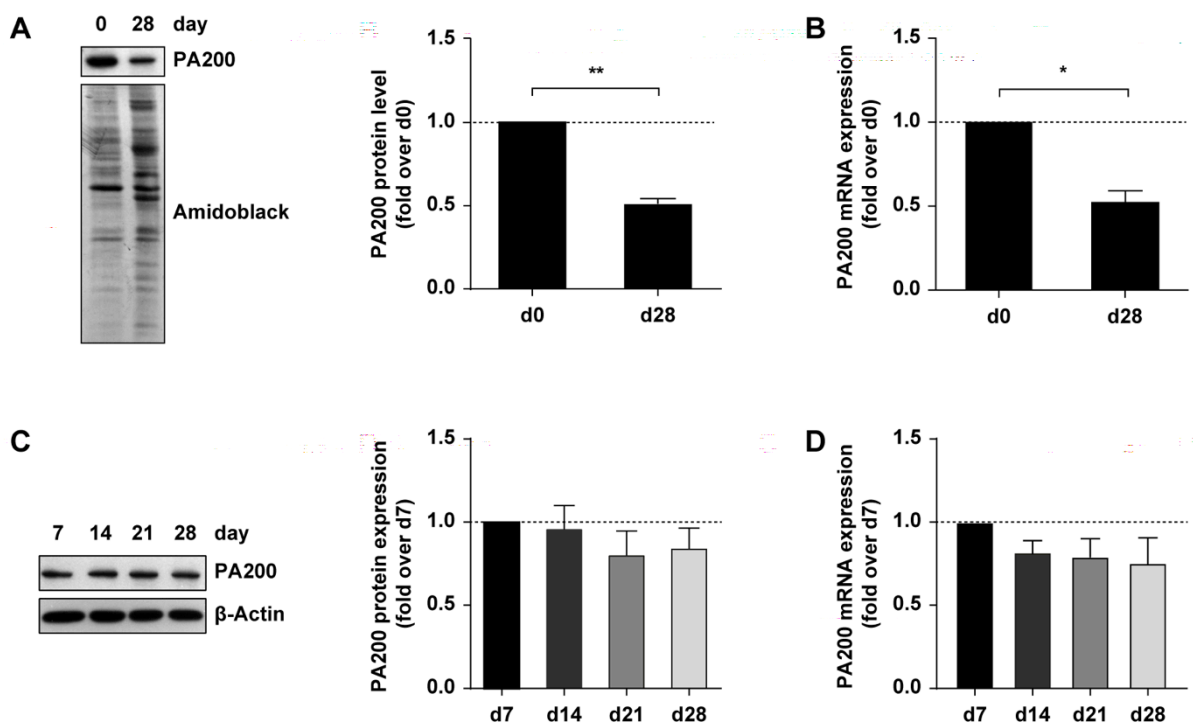


Figure 7.6: Expression of PA200 decreases during differentiation of primary human bronchial epithelial cells. (A) PA200 protein and (B) mRNA levels of primary human bronchial epithelial cells were examined by Western blotting and qPCR at day 0 (d0) and day 28 (d28) of differentiation. Bar diagrams indicate PA200 levels normalized to d0. Amidoblack served as a loading control for Western blotting and *RPL19* as housekeeping gene for qPCR (one-sample t-test, $n = 3$). (C) PA200 protein and (D) mRNA expression was also assessed after 7, 14, 21 and 28 days. Bar diagrams indicate expression levels normalized to day 7 (one-sample t-test, $n = 3$).

Hence, these findings suggest a decrease in activator expression already between day 0 and day 7 of differentiation which accords well with increased expression of PA200 in basal cells as shown in the IHC analysis (Figure 7.5).

7.2.1.6 PA200 is upregulated in TGF- β 1-induced myofibroblast differentiation

PA200 was abundantly expressed myofibroblasts of fibrotic foci in human IPF lungs. Therefore, its regulation upon TGF- β 1-mediated differentiation of primary human lung fibroblasts (phLF) into myofibroblasts was investigated in a further approach. phLF were synchronized in starvation medium for 24 h followed by treatment with 5 ng/mL TGF- β 1 for 48 h. Expression of myofibroblast markers collagen1 α 1 (COL1A1), fibronectin (FN) and α -smooth muscle actin (α SMA) was significantly induced (Figure 7.7 A).

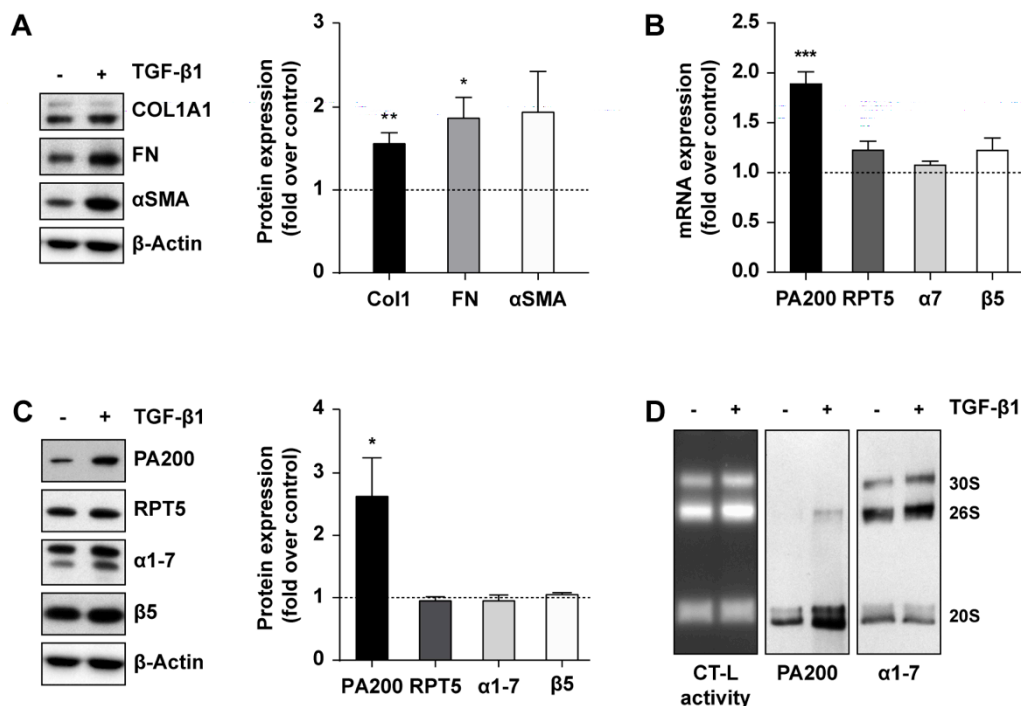


Figure 7.7: PA200 expression and its association with the proteasome are enhanced upon myofibroblast differentiation. phLF cultured in 1% FBS were treated with 5 ng/mL TGF- β 1 for 48 h. (A) Expression of myofibroblast markers collagen1 α 1 (COL1A1), fibronectin (FN) and α -smooth muscle actin (α SMA) was examined by Western blotting. Bar diagram indicates densitometric analysis of signals normalized to controls (one-sample t-test, $n = 6$). (B) mRNA expression of PA200, 19S regulator subunit RPT5, 20S subunit α 7 and β 5 was analyzed by qPCR. Bar diagram indicates mRNA expression as fold over control cells. *RPL19* served as housekeeping gene (one-sample t-test, $n = 6$). (C) Protein expression of PA200 and proteasomal subunits was determined by immunoblotting of the same cell extracts used in (A). Bar diagram indicates densitometric analysis of obtained signals normalized to controls (one-sample t-test, $n = 6$). (D) PA200 alternative proteasome complexes were detected by native gel analysis and immunoblotting for PA200 and 20S subunits α 1-7. Proteasome activity was determined using overlay with a substrate specific for the chymotrypsin-like (CT-L) activity. Figure indicates representative results for experiments performed in phLF from three different organ donors.

Analysis of mRNA and protein expression of PA200, the 19S regulator subunit RPT5 and the 20S proteasome subunits $\alpha 7$ and $\beta 5$ revealed that only PA200 was significantly induced in response to TGF- $\beta 1$ treatment whereas the other proteasomal subunits were not regulated (Figure 7.7 B and C). Of note, the association of PA200 with 20S and 26S proteasome complexes was also enhanced in TGF- $\beta 1$ -treated pHLF compared to controls (Figure 7.7 D). Therefore, TGF- $\beta 1$ -mediated differentiation of pHLF induced PA200 expression and its association to the proteasome forming proteolytically active complexes. These data clearly indicate a functional role for newly formed PA200 alternative proteasomes in myofibroblasts.

7.2.2 The PA200 interactome is regulated according to cellular growth

In order to further dissect the functional role of PA200-containing proteasome complexes in TGF- β 1-mediated differentiation of pHLF, the interactome of PA200 upon different cellular conditions was investigated using an unbiased LC-MS/MS-based approach.

7.2.2.1 Optimized immunoprecipitation protocol enables efficient pulldown of PA200

For analysis of the interactome, an efficient immunoprecipitation (IP) protocol for PA200 had to be established initially. This involved testing of different amounts of PA200 antibody for efficient pulldown of PA200 in native pHLF lysates preserving protein-protein interactions. PA200 protein levels were examined in eluates of control and PA200 IPs by Western blotting. 10 % of each input and supernatant was also analyzed by immunoblotting to control for efficient pulldown of the activator in cell extracts. The activator was strongly enriched by all tested conditions as compared to the input (Figure 7.8). However, immunoblotting of input and supernatant of different IPs indicated that 1 μ g antibody was not sufficient to completely extract the total amount of PA200 in the lysate, as there was still some activator remaining in the supernatant. For this reason, 3 μ g antibody were used for the following experiments to ensure efficient immunoprecipitation of total amount of PA200 present in the cell extract.

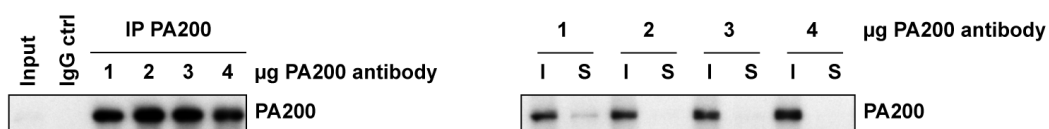


Figure 7.8: Optimized immunoprecipitation protocol indicates efficient pulldown of the activator. Immunoprecipitation of PA200 in a native TSDG lysate of primary human lung fibroblasts using increasing amounts of antibody was assessed for enrichment of PA200 by immunoblotting. Pulldown using an IgG control antibody of the same species served as control. 10 % of the total lysate (= input or I) and supernatant (S) were used to control for efficient immunoprecipitation of PA200 (right figure).

7.2.2.2 PA200 binds with a higher stoichiometry to 20S than to 26S proteasomes

First, the interactome analysis of PA200 was applied to better characterize the interaction of PA200 with the proteasome and to validate the applied protocol for sufficient detection of interacting proteins in pHLF. Pulldown of PA200 in pHLF cultured under standard conditions

in 10 % FBS was analyzed by LC-MS/MS and the interaction stoichiometry of PA200 with different proteasomal subunits was calculated with the obtained data set (Figure 7.9). α - and β -subunits PSMA1-7 and PSMB1-7 of the standard 20S proteasome interacted with PA200 in an interaction stoichiometry of approximately 1 indicating a prominent interaction of PA200 with the 20S catalytic core. Interestingly, the interaction ratio with immunoproteasome subunits PSMB8 (LMP7) and PSMB10 (MECL-1) was only 0.14 and 0.05, respectively. Immunoproteasome subunit PSMB9 (LMP2) was not detected by LC-MS/MS in pHLF. PA200 interacted with subunits of the 19S regulator at an average ratio of 0.25 implying the presence of PA200-26S hybrid proteasomes in pHLF. These data indicate that the association of PA200 with the standard 20S core particle is more frequent than association with 26S proteasomes. Interestingly, PA200 was also found to interact at very low stoichiometry with other alternative proteasome activators presumably by forming doubly capped alternative 20S complexes, such as PA200-20S-PA28 α/β (PSME1 and 2) or PA200-20S-PA28 γ (PSME3) complexes.

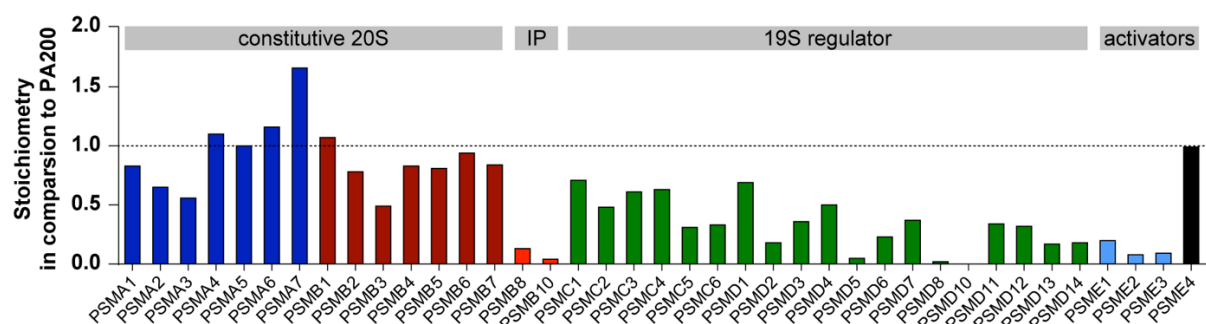


Figure 7.9: PA200 binds with higher stoichiometry to the 20S proteasome than to the 26S proteasome. Interaction of PA200 with subunits of the proteasome was investigated by LC-MS/MS analysis of PA200 co-immunoprecipitation in native lysates of pHLF cultured in 10 % FBS. Bar diagram indicates the interaction stoichiometry of PA200 with subunits of the standard 20S core complex, the immunoproteasome (IP), the 19S regulator or other alternative proteasomal activators. LC-MS/MS analysis was performed by Dr. J. Merl-Pham, Research Unit Protein Science of the HMGU.

In conclusion, with detection of all proteasomal subunits except from PSMB9 the applied co-IP protocol and LC-MS/MS analysis proved to be suitable for uncovering of PA200-interacting proteins. Analysis of interaction stoichiometry indicated that PA200 mainly interacts with 20S complexes but also forms hybrid proteasomes with 26S complexes. Here, the activator preferentially binds to standard 20S proteasomes and not to immunoproteasomes, which are generally low expressed in non-immune cells. Moreover, these data indicate that there is almost no free PA200 in pHLF in the presence of serum.

7.2.2.3 The interactome of PA200 adapts to cellular growth conditions

Next, the PA200 interactome was analyzed upon stimulation of pHLF with TGF- β 1. Pulldown of PA200 was performed in pHLF either cultured in 1 % FBS medium with or without 5 ng/mL TGF- β 1 for 48 h (as applied for experiments in section 7.2.1.6.) or under standard conditions in 10 % FBS. Co-immunoprecipitated proteins were identified by LC-MS/MS and enrichment of proteins was calculated as the fold change compared to IP with IgG control antibody. Proteomic analyses revealed that the PA200 interactome was also strongly depending on cellular growth conditions (Figure 7.10). In cells cultured under starvation conditions in 1 % FBS the number of co-immunoprecipitated proteins was very low (44 proteins identified by at least two peptides with $fc \geq 2$ and $p < 0.05$). Here, identified proteins were mainly proteasomal subunits. Treating cells with TGF- β 1 increased the number of interacting proteins (158 proteins identified by at least two peptides with $fc \geq 2$ and $p < 0.05$). Although a variety of functionally different proteins co-immunoprecipitated with the activator, many proteasomal and ribosomal subunits as well as heterogeneous nuclear ribonucleoproteins (hnRNPs) were observed among the interacting proteins.

In contrast to detection of only few interacting proteins in 1 % FBS, much more proteins were identified by co-IP of PA200 under standard growth conditions in 10 % FBS (218 proteins identified by at least two peptides with $fc \geq 2$ and $p < 0.05$). Here, the interactome was similar to co-IP in 1 % FBS with TGF- β 1 comprising proteasomal and ribosomal proteins as well as hnRNPs.

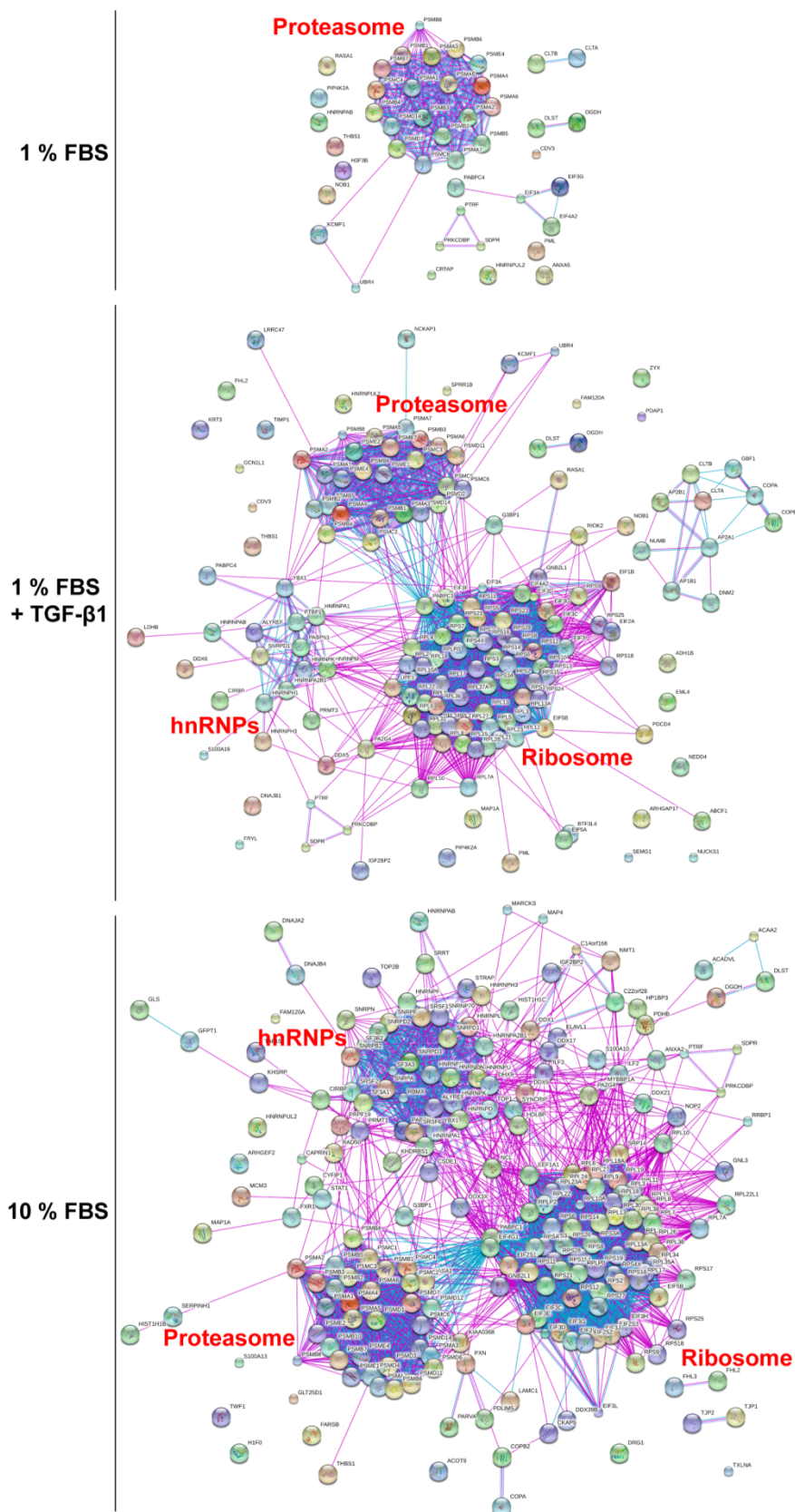


Figure 7.10: The PA200 interactome is regulated according to cellular growth and differentiation conditions. Interactome was examined by immunoprecipitation of PA200 in native pHLF extracts cultured in 10 % FBS, 1 % FBS or 1 % FBS + 5 ng/mL TGF- β 1 for 48 h and LC-MS/MS analysis. Figure indicates identified interacting proteins (enrichment $f_c \geq 2$ compared to IP with IgG control, $p < 0.05$) analyzed for experimentally based physical and functional protein-protein interaction networks using the STRING database. LC-MS/MS analysis was performed by Dr. J. Merl-Pham, Research Unit Protein Science, HMGU.

The so far unknown interaction between PA200 and thrombospondin-1 (THBS1) and ribosomal protein L19 (RPL19) identified by the LC-MS/MS screen was confirmed by IP of PA200 in native extracts of phLF and subsequent Western blotting. THBS1 and RPL19 were highly enriched in the IP of PA200 (Figure 7.11 A). Moreover, analysis of IP input and supernatant indicated that most RPL19 and THBS1 present in the native cell extract interacted with PA200, because almost no protein was detected in the supernatant after pulldown of PA200. However, both proteins THBS1 and RPL19 also interacted with the 20S proteasome as observed by co-IP of 20S subunit $\alpha 3$ (Figure 7.11 B). Therefore, it cannot be established with certainty whether PA200 interacts directly with these proteins or if they indirectly interact via the 20S proteasome.

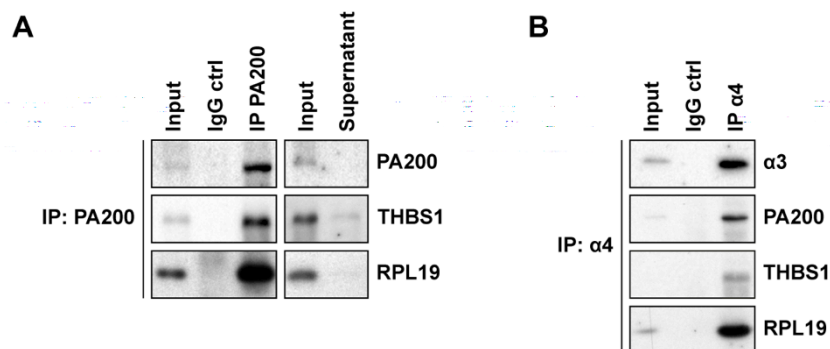


Figure 7.11: Thrombospondin-1 (THBS1) and ribosomal protein L19 (RPL19) interact with PA200 and the 20S proteasome. Immunoprecipitation (IP) of PA200 was performed in native primary human lung fibroblast (phLF) extracts cultured in 10 % FBS and co-IP of THBS1 and RPL19 was investigated by immunoblotting. 10 % of total protein lysate (= input) and supernatant was loaded as controls. Figure indicates representative results of co-IPs performed in phLF from three different organ donors.

To analyze whether THBS1 directly interacts with PA200, co-IP of 20S subunit $\alpha 3$ was performed in native extracts of phLF upon silencing of PA200 for 24, 48 and 72 h. Western blotting confirmed efficient pulldown and showed that THBS1 still interacts with the 20S proteasome when PA200 protein levels were efficiently decreased after 48 and 72 h (Figure 7.12 A and B). These observations indicate that THBS1 interacts with PA200 via the 20S proteasome.

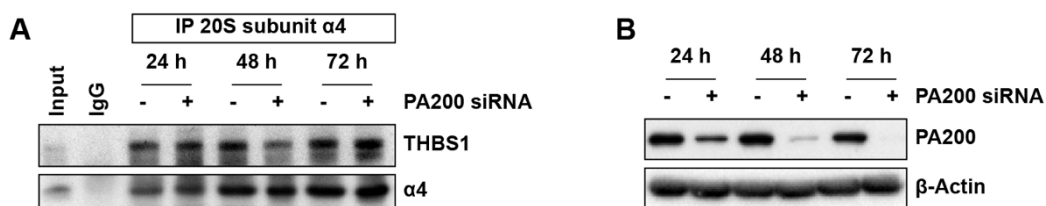


Figure 7.12: Thrombospondin-1 (THBS1) directly interacts with the 20S proteasome. (A) Co-immunoprecipitation (co-IP) of 20S proteasome subunit $\alpha 3$ in native cells extracts of pHLF after 24, 48 and 72 h of transient PA200 silencing cultured in 10 % FBS was analyzed for THBS1 and $\alpha 3$ protein levels by Western blotting. 10 % of the total protein lysate subjected to co-IP were loaded as an input control. IP with IgG served as a control for specific pulldown of proteins. (B) Protein extracts used in (A) were analyzed for expression of PA200 by Western blotting.

As noted above, the PA200 interactome strongly depended on cellular culture conditions with enrichment of interacting proteins at conditions of either 10 % FBS or 1 % FBS with TGF- $\beta 1$, while only few interacting proteins were detected when pHLF were cultured in 1 % FBS. This suggests that the interactome of PA200 is regulated according to cellular growth conditions. Indeed, analysis of PA200 regulation in pHLF cultured under starvation versus growth conditions revealed an increase of PA200 protein levels upon 72 (Figure 7.13 A). This observation accorded well with induced expression of proliferation markers cyclin D1 (CCND1) and proliferating cell nuclear antigen (PCNA) after 72 h. Moreover, association of PA200 with 20S and 26S proteasomes was also enhanced after 72 h when compared to starvation conditions (Figure 7.13 B). Hence, not only PA200 protein levels but also the association of PA200 with the proteasome were induced in pHLF cultured in 10 % FBS, implying an increased formation of PA200-containing alternative proteasome complexes according to cell growth.

In summary, LC-MS/MS analysis of PA200 interacting proteins revealed that the interactome of PA200 is changing according to cellular stimuli. These findings also accord well with the observation that PA200 expression and its association with the proteasome were regulated according to cellular growth conditions. Moreover, it suggests that not only PA200 expression but also its function is adjusted according to cellular growth and differentiation. As PA200 strongly interacts with the 20S core particle, the identified interacting proteins could also be associated with the activator *via* the 20S proteasome. These data, however, indicate that PA200-20S proteasome complexes are localized with certain cellular components of the cytosolic or nuclear compartment that are enriched in hnRNPs and/or ribosomal proteins.

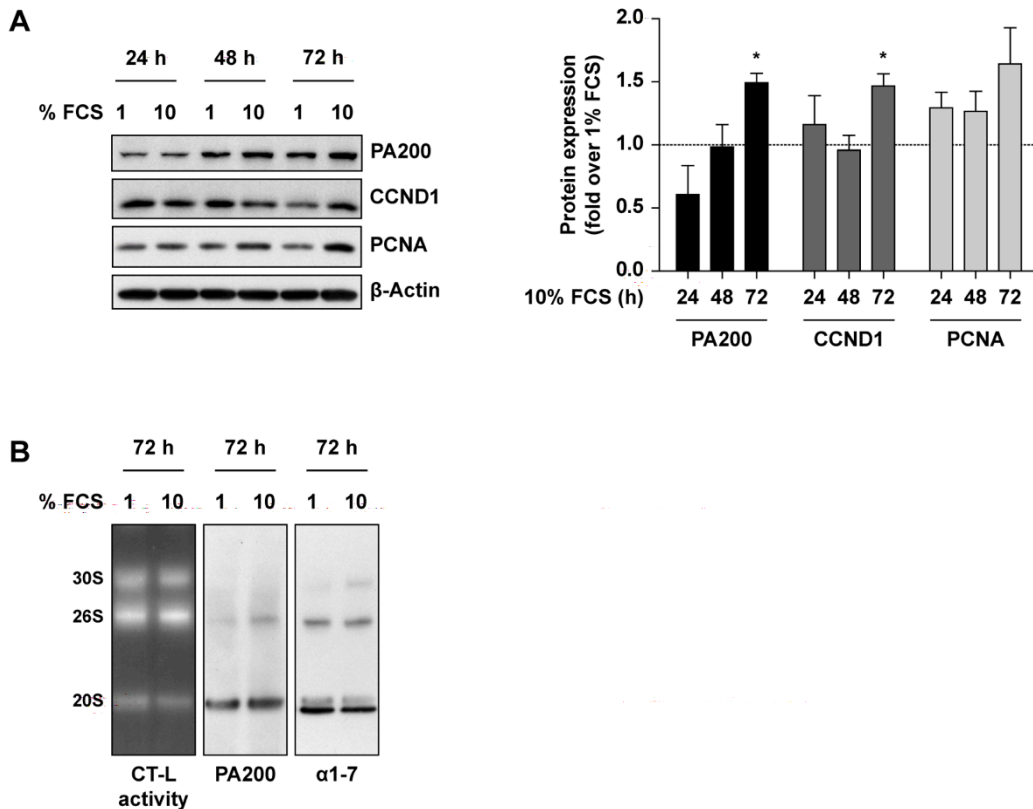


Figure 7.13 PA200 alternative proteasomes are enhanced in pHLF cultured with 10 % FBS. (A) Primary human lung fibroblasts (pHLF) were cultured in medium with 1 % or 10 % FBS for 24, 48 or 72 h and protein expression of PA200, cyclin D1 (CCND1) and PCNA was investigated by Western blotting of native TSDG lysates. Bar diagram indicates densitometric analysis of Western blots normalized to β -Actin and to 1 % FBS treated cells (one-sample t-test, $n = 3$). (B) Proteasome complexes were analyzed by native gel electrophoresis of the same native lysates of pHLF cultured for 72 h used in (A). Proteasome activity was determined by an in-gel overlay with a fluorogenic substrate specific for the chymotrypsin-like (CT-L) activity and the gel was immunoblotted for PA200 and 20S subunits α 1-7. Figure indicates representative results for experiments performed in pHLF from three different donors.

7.2.3 PA200 does not degrade acetylated histones in lung fibroblasts

Qian *et al.* recently proposed that PA200 mediates ubiquitin-independent degradation of acetylated core histones during spermatogenesis (Qian *et al.*, 2013). As histones are essential for chromatin organization and their levels need to be tightly regulated to ensure proper transcription and cell growth, we speculated that the regulation of PA200 during cell growth may fine tune degradation of histones in response to cellular growth stimuli.

7.2.3.1 PA200 silencing decreases amount of free histones

DNA-bound histones strongly interact with the DNA and their isolation requires either acidic or high salt extraction (Shechter *et al.*, 2007). Less stringent lysis conditions are sufficient for isolation of free histones not incorporated into DNA. Potential degradation of free acetylated histones was investigated in RIPA extracts of pHLF upon PA200 silencing for 72 h by Western blotting for total and acetylated histones. Surprisingly, protein levels of total and acetylated histones H2B, H3 and H4 were strongly decreased in response to silencing of the activator contradicting a potential degradation *via* PA200 (Figure 7.14).

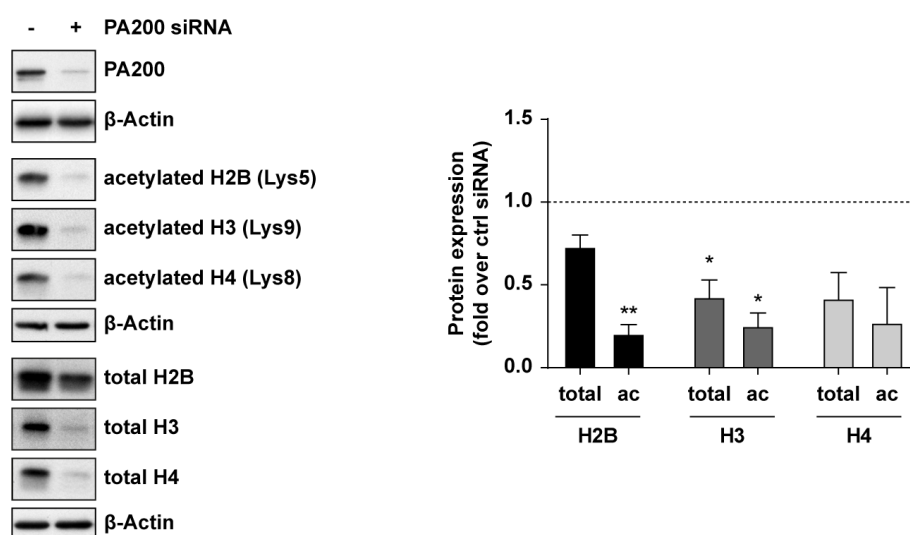


Figure 7.14: Non-DNA bound acetylated and total histones decrease in response to PA200 silencing. Non-DNA bound acetylated and total histones were analyzed by Western blotting of RIPA lysates from primary human lung fibroblasts transfected with control or PA200 siRNA for 72 h. Bar diagram shows densitometric analysis of signals obtained for acetylated and total histones normalized to β -Actin and to respective controls (one-sample t-test, $n = 3$).

Indeed, free total and acetylated histones H3 and H4 did also not accumulate at earlier time points after 24, 48, and 72 h of PA200 silencing but rather decreased over time (Figure 7.15).

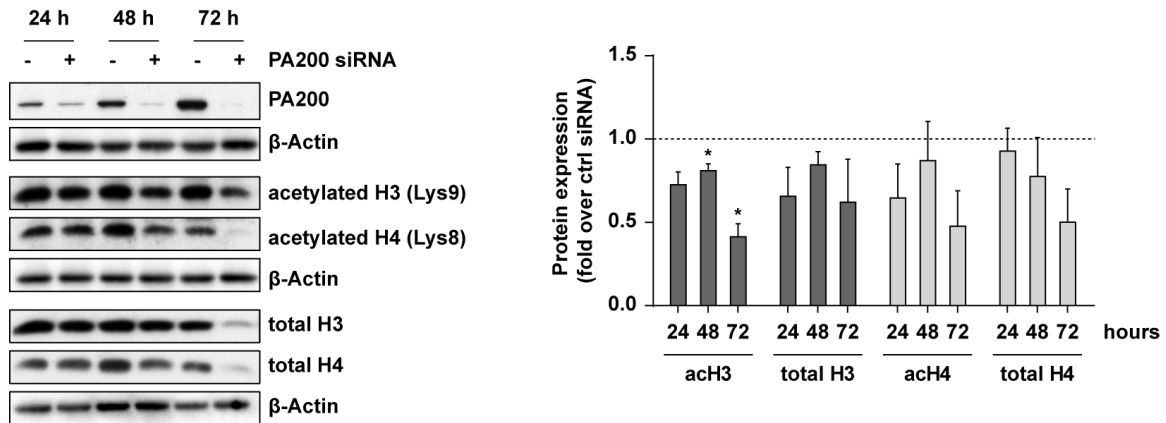


Figure 7.15: Timecourse of PA200 silencing also indicates decrease of histones at earlier time points. Levels of acetylated and total histones H3 and H4 were examined in primary human lung fibroblasts upon silencing of PA200 for 24, 48 and 72 h by immunoblotting of RIPA lysates. Bar diagram shows quantification of Western blots with normalization of the obtained signal to β -Actin and to the time-matched control (one-sample t-test, $n = 3$).

7.2.3.2 Overexpression of PA200 increases levels of free histones

In a further approach the regulation of free total and acetylated histones was investigated upon overexpression of PA200. pHLF were transiently transfected with a full length PA200 cDNA construct and association of the activator with 20S and 26S proteasomes was analyzed by native gel electrophoresis and subsequent immunoblotting for the activator and 20S subunit $\alpha 4$ (Figure 7.16). Indeed, overexpression of the activator resulted in increased recruitment of PA200 to 20S and 26S proteasomes implying the formation of functional PA200-containing alternative proteasome complexes.

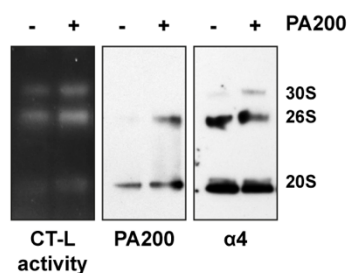


Figure 7.16: PA200 proteasome complexes are formed upon overexpression of the activator. Primary human lung fibroblasts (pHLF) were transiently transfected with a PA200 expression vector or empty vector as a control for 24 h. Native lysates were analyzed for proteasome activity and formation of PA200-containing proteasome complexes by native gel electrophoresis, in-gel overlay with a fluorogenic substrate specific for chymotrypsin-like (CT-L) activity and subsequent immunoblotting for PA200 and 20S proteasome subunit $\alpha 4$. Figure shows representative result of experiments performed with pHLF of three different donors.

Although transfection of pHLF with PA200 only resulted in an approximately threefold induction of its protein level, a significant increase in free total and acetylated histones H3 and H4 was observed (Figure 7.17).

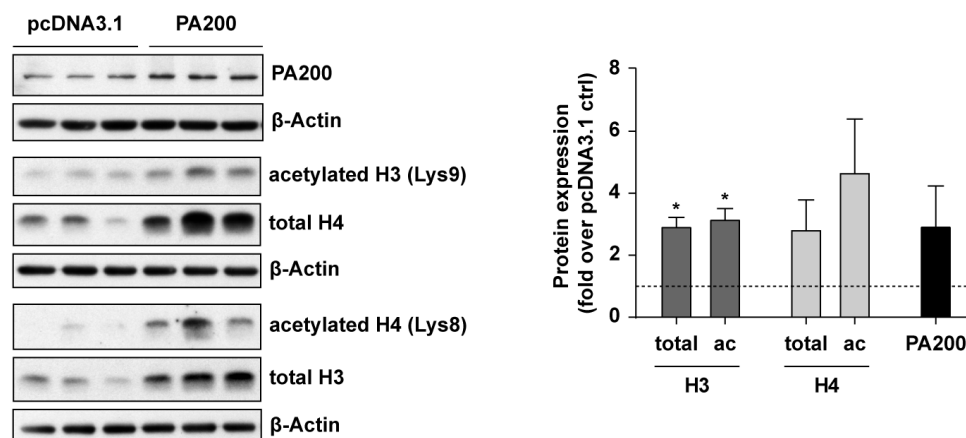


Figure 7.17: Non-DNA bound acetylated and total histones accumulate upon overexpression of PA200. RIPA lysates of primary human lung fibroblasts transfected with PA200 expression vector or pcDNA3.1 empty vector were analyzed for PA200 expression and protein levels of acetylated and total histones H3 and H4 by Western blotting. Bar diagram indicates quantification of immunoblots normalized to β -Actin and to empty vector-transfected controls. Transfection was performed in three technical replicates of pHLF from three different donors (one-sample t-test, $n = 3$).

7.2.3.3 Chromatin-bound histones are not regulated by PA200 silencing

A high salt chromatin extraction protocol was applied for extraction of DNA-bound histones in order to investigate whether PA200 regulates levels of these histones (Shechter et al., 2007). Western blot analysis of cytosolic, nucleoplasmic and DNA-bound acetylated and total H2B, H3 and H4 revealed that the majority of histones was bound to DNA, whereas only a minor amount existed in a free form (Figure 7.18).

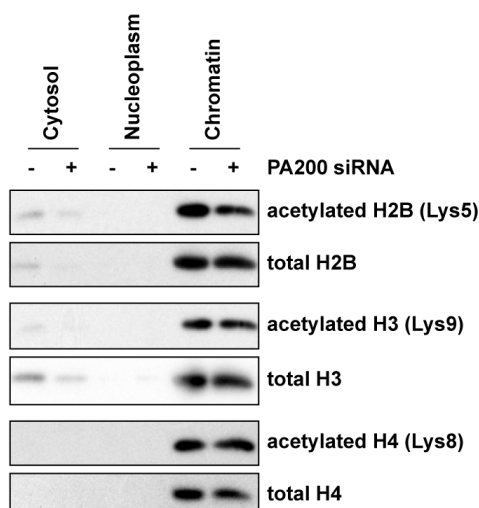


Figure 7.18: DNA-bound histones are not altered in response to PA200 silencing. Histones were extracted from primary human lung fibroblasts (pHLF) with silencing of PA200 for 72 h. 20 μ g protein of cytosolic fraction and 2 μ g protein of nucleoplasm and chromatin fraction were analyzed for levels of acetylated and total histones by Western blotting. Figure shows representative results of extractions with pHLF of three different donors.

Of note, levels of DNA-bound acetylated and total histones were not decreased but rather slightly increased upon PA200 silencing. In contrast, free total and acetylated histones of the cytosolic fraction decreased upon PA200 knockdown when compared to control siRNA transfection. Therefore, these findings accord well with previous experiments analyzing non DNA-bound histones in RIPA extracts.

In summary, these results suggest that acetylated and total histones are not degraded via PA200 in primary human fibroblasts of the lung. Non DNA-bound histones were significantly downregulated upon loss of the activator, whereas overexpression significantly induced histone levels. Therefore, levels of free histones are presumably not targeted for proteasomal degradation via PA200 in pHLF cells but may rather be adjusted as part of the cellular response to altered levels of PA200 in the cell

7.2.4 PA200 regulates growth and survival of primary human lung fibroblasts

Analysis so far has revealed an increased formation of PA200-proteasome complexes and regulation of the PA200 interactome in response to growth and differentiation stimuli. Next, the functional consequence of PA200 silencing in pHLF was analyzed in an unbiased approach using microarray and proteomic screens in order to further elucidate the cellular function of PA200. Results were validated in cell culture experiments.

7.2.4.1 PA200 silencing regulates genes with distinct molecular functions

To investigate the regulation of cellular functions by PA200, siRNA-mediated transient silencing of the activator was performed for 72 h and regulation of gene expression was determined by microarray analysis provided by Dr. M. Irmeler, Institute of Experimental Genetics, HMGU. Knockdown of PA200 efficiently reduced its mRNA levels (fold change = 0.12 and p-value = 4.4×10^{-9} over siRNA-transfected controls; data not shown). Genes that were regulated with a fold change >1.5 and FDR <10 % compared to control siRNA-transfected pHLF were further analyzed for activation or inhibition of specific molecular functions by Ingenuity Pathway Analysis (1162 genes). Here, several molecular functions were predicted to be induced (z-score >2) or inactivated (z-score <2) (Figure 7.19): cell spreading, cell survival, growth of lesions, formation of cellular protrusions, microtubule dynamics as well as organization cytoplasm and cytoskeleton were predicted to be activated in PA200-deficient pHLF. In contrast, formation of cytoskeleton and actin filaments as well as organismal death, morbidity or mortality were predicted to be inhibited. The general picture that emerges is that silencing of PA200 induces regulation of genes with distinct molecular functions involving enhanced cell growth and survival.

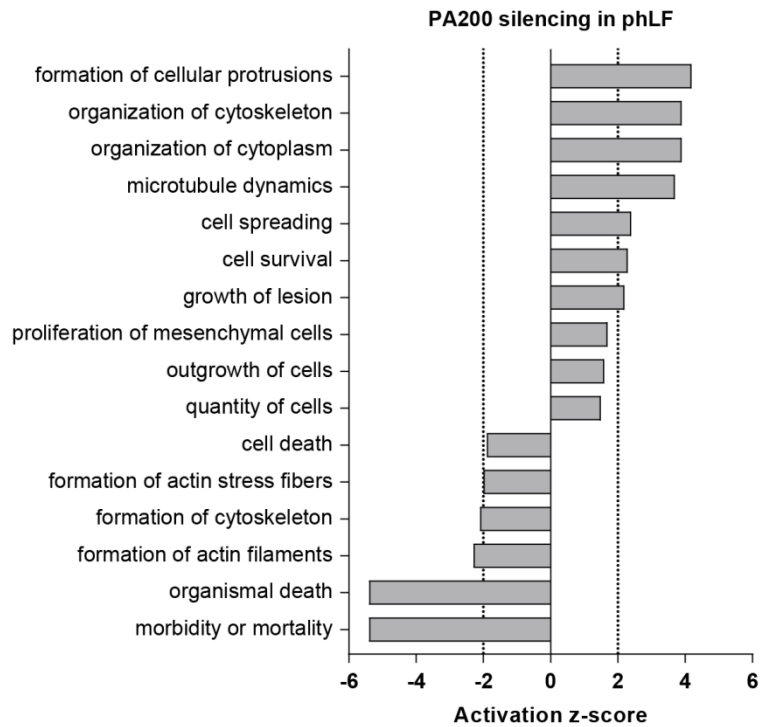


Figure 7.19: Transcriptomic analysis of PA200 silencing in primary human lung fibroblasts (pHLF) indicates regulation of genes with distinct molecular functions. Transient siRNA-mediated silencing of PA200 for pHLF was examined for gene regulation by microarray analysis. Regulated genes ($fc > 1.5$, FDR 10 %) were analyzed for molecular functions by Ingenuity Pathway Analysis. Diagram indicates regulated molecular functions with respective activation z-scores (z-score < 2 = inactivation, z-score > 2 = activation). Microarray analysis was performed by Dr. M. Imler, Institute of Experimental Genetics, HMGU.

7.2.4.2 Proteomic screen confirms regulation of proteins involved in cellular growth and survival upon PA200 silencing

Regulation of cellular function in response to silencing of PA200 was also investigated on protein level using LC-MS/MS. pHLF of two different donors were transfected with control or PA200 siRNA in four technical replicates per condition. In total, the proteomic screen identified 4640 proteins. Although PA200 was not among detected proteins, presumably resulting from its low expression in lung cells, Western blot analysis of samples subjected to LC-MS/MS analysis showed very efficient reduction of PA200 protein levels upon knockdown (Figure 7.20 A). Among all identified proteins several proteins were found up- and down-regulated more than two-fold with a q-value < 0.05 (Figure 7.20 B). Proteins involved in cell death and apoptosis, such as caspase-3 (CASP3) and FAS receptor, were significantly decreased upon silencing of the activator. In contrast, expression of proteins contributing to cell growth, such as IGFBP5, was significantly induced.

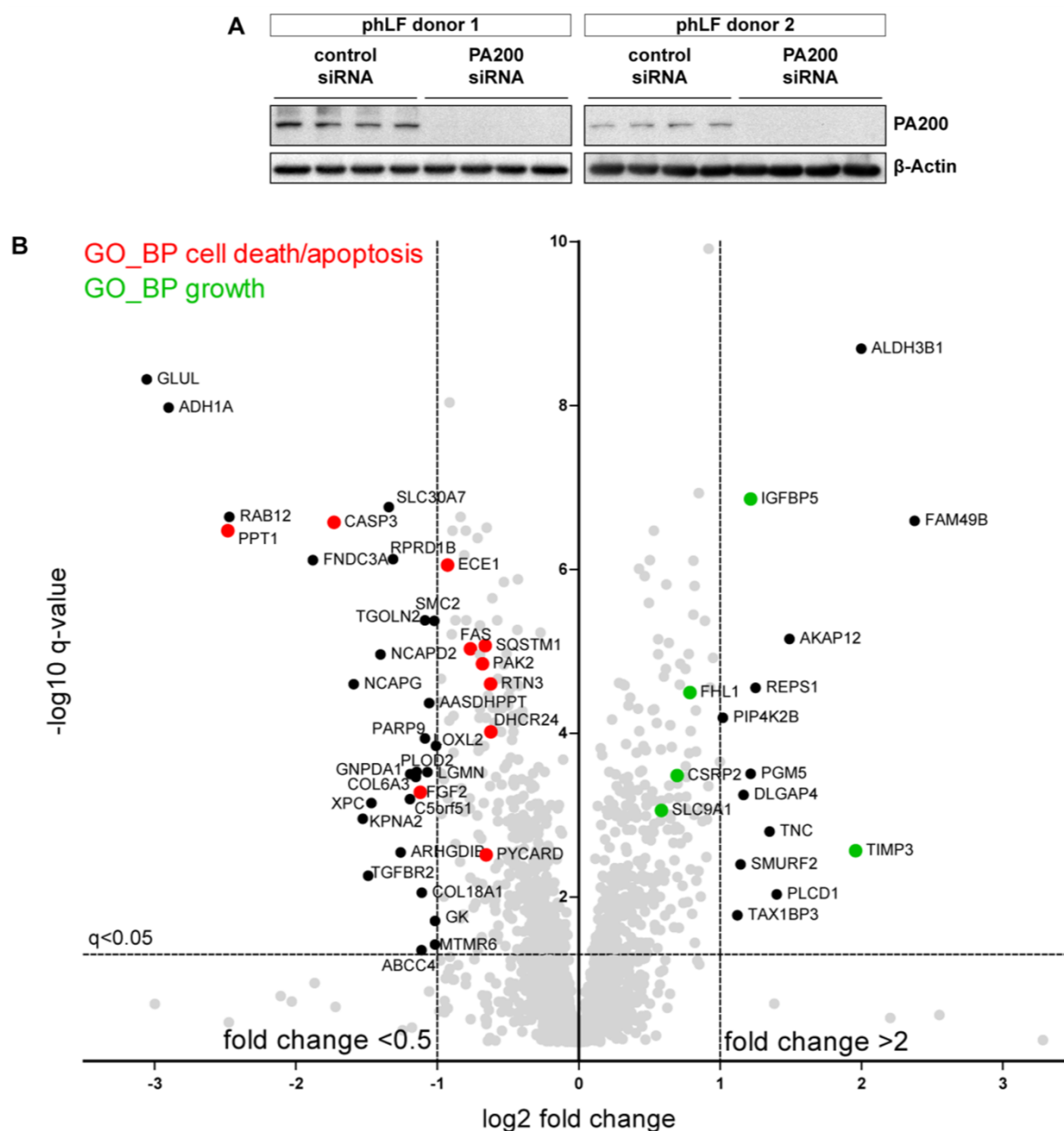


Figure 7.20: Proteomic screen identifies regulation of proteins involved in growth as well as cell death and apoptosis upon silencing of PA200 in primary human lung fibroblasts (phLF). RIPA lysates of phLF with transient silencing of PA200 for 72 h were analyzed by LC-MS/MS. Silencing was performed in cells of two different donors with four technical replicates per condition. (A) Efficient knockdown of PA200 in these samples was confirmed by Western blotting. (B) Diagram indicates proteins identified by LC-MS/MS phLF from two different donors (grey symbols, 4640 proteins). Proteins regulated with $fc \geq 2$ with q -value < 0.05 and identified by ≥ 2 peptides are shown in black. Proteins of the gene ontology biological process cell death/apoptosis are highlighted in red and proteins involved in growth are indicated in green. Gene ontology analysis was performed using the “Database for Annotation, Visualization and Integrated Discovery” (DAVID) Version 6.8. LC-MS/MS analysis was provided by Dr. J. Merl-Pham, Research Unit Protein Science, HMGU.

546 proteins regulated with a fold change ≥ 1.2 and q -value < 0.05 identified by two peptides were subjected to Ingenuity Pathway Analysis to determine their molecular functions.

Processes related to cell death and survival as well as cell growth were significantly enriched, which accords well with the transcriptomic data (Figure 7.21).

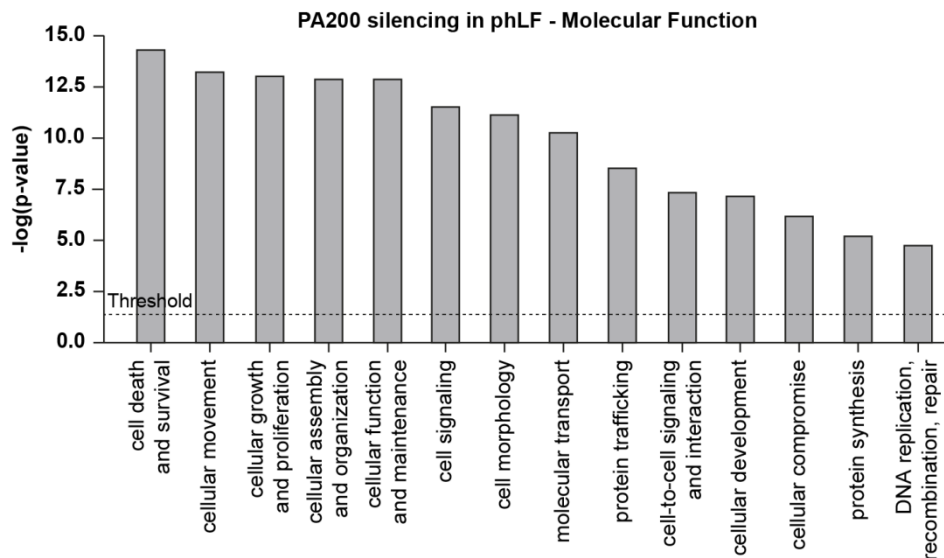


Figure 7.21: Proteomic analysis of primary human fibroblasts (pHLF) upon transient silencing of PA200 indicates regulation of proteins with distinct molecular functions. Proteins regulated by $f_c \geq 1.2$ and $q < 0.05$, (identified by 2 peptides) upon siRNA-mediated silencing of PA200 for 72 h in pHLF identified by LC-MS/MS were analyzed for molecular functions by Ingenuity Pathway Analysis. Bar diagram indicates p-value of significantly regulated molecular functions.

According to the potential function of PA200 in promoting the degradation of specific substrates, a differential regulation of PA200 specific substrates is expected on mRNA *versus* protein level upon PA200 silencing. Therefore, the mRNA and protein levels of genes identified in both the transcriptomic and the proteomic screens were compared. For most of these genes mRNA and protein expression was altered to a similar extent as indicated by plotting of most data points on the bisecting line between both axes (Figure 7.22). The graph discriminates genes that are only significantly regulated only on mRNA level in black, significant regulation only on protein level in blue and significant alteration of both mRNA and protein levels in red. With regard to the potential function of PA200 as a proteasome activator targeting specific substrates for degradation, genes that are strongly increased only on the protein level are of particular interest, as silencing of the activator should induce the accumulation of a given substrate. However, genes that were only significantly altered on protein level showed an up- and downregulation in a similar extent with most upregulated proteins being induced less than 1.5-fold. This comparative approach did thus not clearly identify putative substrates for PA200-specific protein degradation.

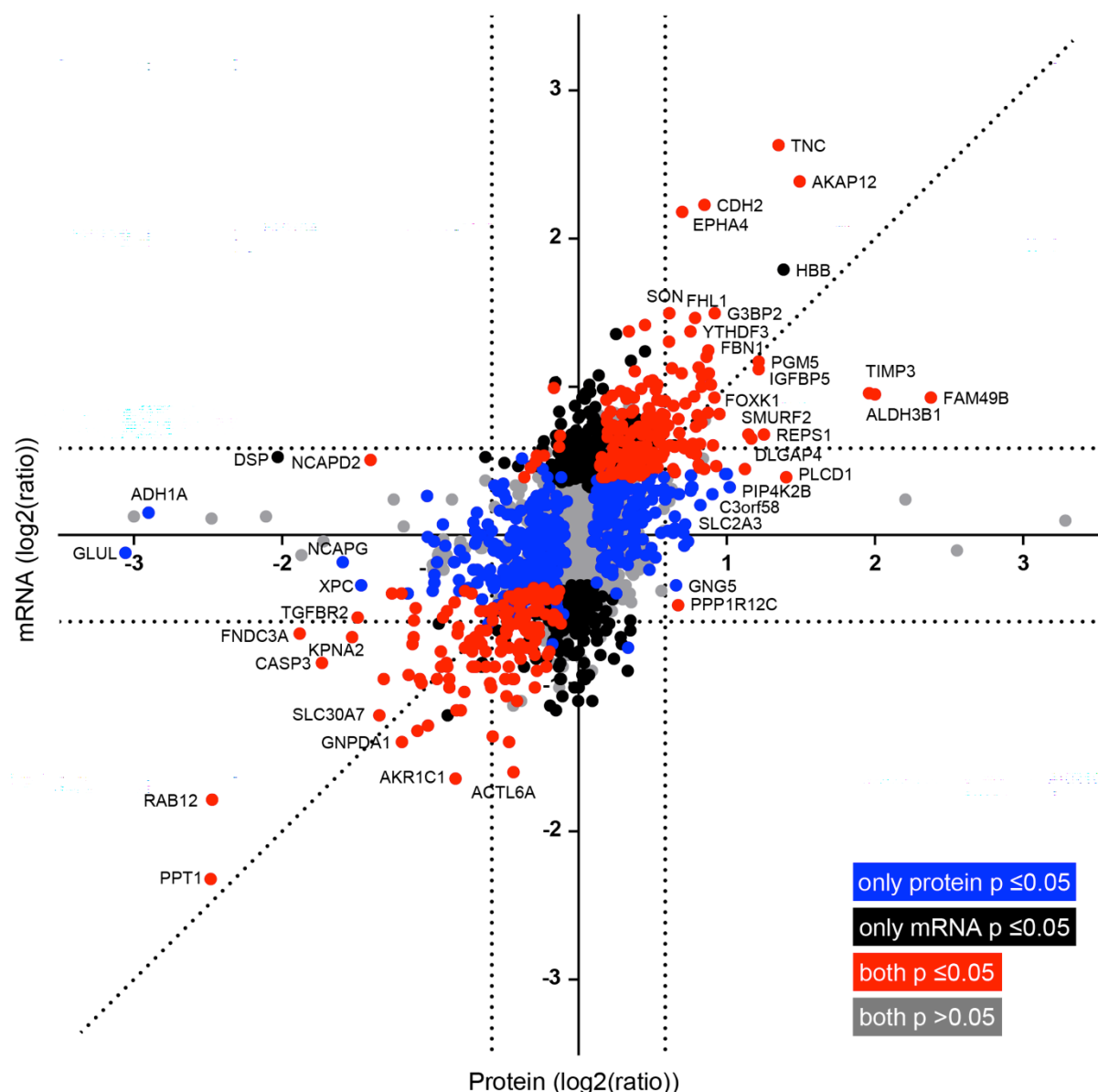


Figure 7.22: Most genes are co-regulated on mRNA and protein levels in response to PA200 silencing. Genes that were identified in both the transcriptomic and the proteomic screen were analyzed for their regulation on mRNA and protein levels in phLF upon siRNA-mediated silencing of PA200 for 72 h (2760 genes). The axes indicate the ratio of the expression in PA200-silenced versus control cells on mRNA and protein level. Genes regulated similarly on mRNA and protein levels are plotted on the diagonal line. Scatter plot shows genes not significantly regulated on protein and mRNA levels in grey and genes only significantly regulated on protein level in blue ($n=443$), on mRNA level in black ($n=377$) and on both protein and mRNA level in red ($n=318$). Horizontal and vertical dashed lines indicate 1.5-fold regulation of mRNA or protein expression.

Concluding, PA200 silencing regulated genes with distinct molecular functions on both mRNA and protein levels, which suggests that regulation of protein expression is rather caused by the cellular effect PA200 silencing than by accumulation of potential substrates of the activator.

7.2.4.3 PA200 silencing activates AKT signaling

The AKT pathway is a key signal transduction pathway for regulation of cellular growth and survival via a plethora of cellular targets (Manning and Toker, 2017). Ingenuity Pathway Analysis of regulated genes and proteins in PA200-silenced pHLF indicated an activation of cell growth and survival as well as inactivation of cellular apoptosis. Hence, a potential activation of AKT signaling via phosphorylation of protein kinase AKT at serine 473 (pAKT (Ser473)) was analyzed in these cells to obtain further insights into the regulation of this central cellular signaling pathway upon PA200 silencing. Protein levels of AKT and pAKT (Ser473) were determined by Western blotting of pHLF in response to silencing of PA200 for 72 h. Here, total AKT levels were not altered upon silencing of the activator, whereas phosphorylation of the protein kinase was significantly increased in PA200-deficient pHLF as compared to controls (Figure 7.23). Therefore, the increased ratio of phosphorylated to total AKT indicates activation of AKT signaling.

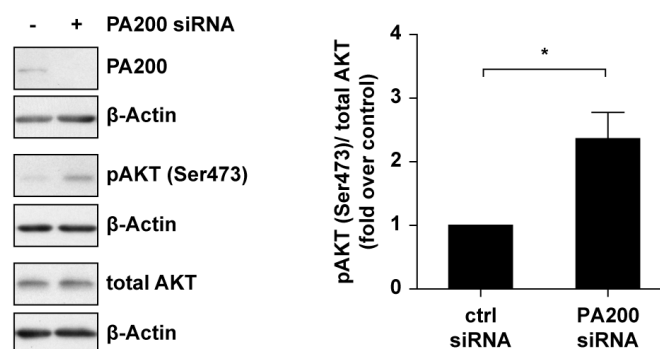


Figure 7.23: PA200 silencing activates AKT signaling. Regulation of AKT signaling in pHLF upon knockdown of PA200 for 72 h was investigated by Western blotting using antibodies directed against PA200, total AKT and AKT phosphorylated at serine 473 (pAKT (Ser473)). Bar diagram indicates densitometric analysis of signals obtained for pAKT (Ser473) normalized to total AKT and control siRNA-transfected cells (one-sample t-test, $n = 3$).

7.2.4.4 PA200 silencing induces proliferation of primary human lung fibroblasts

As microarray and proteomic screens suggested an induction of cellular growth upon PA200 silencing in pHLF, proliferation of these cells was assessed by different approaches. Microscopic evaluation of pHLF after 24, 48 and 72 h of transfection with PA200 siRNA indicated a notable increase in number of cells after 48 h compared to control siRNA-transfected cells (Figure 7.24 A).

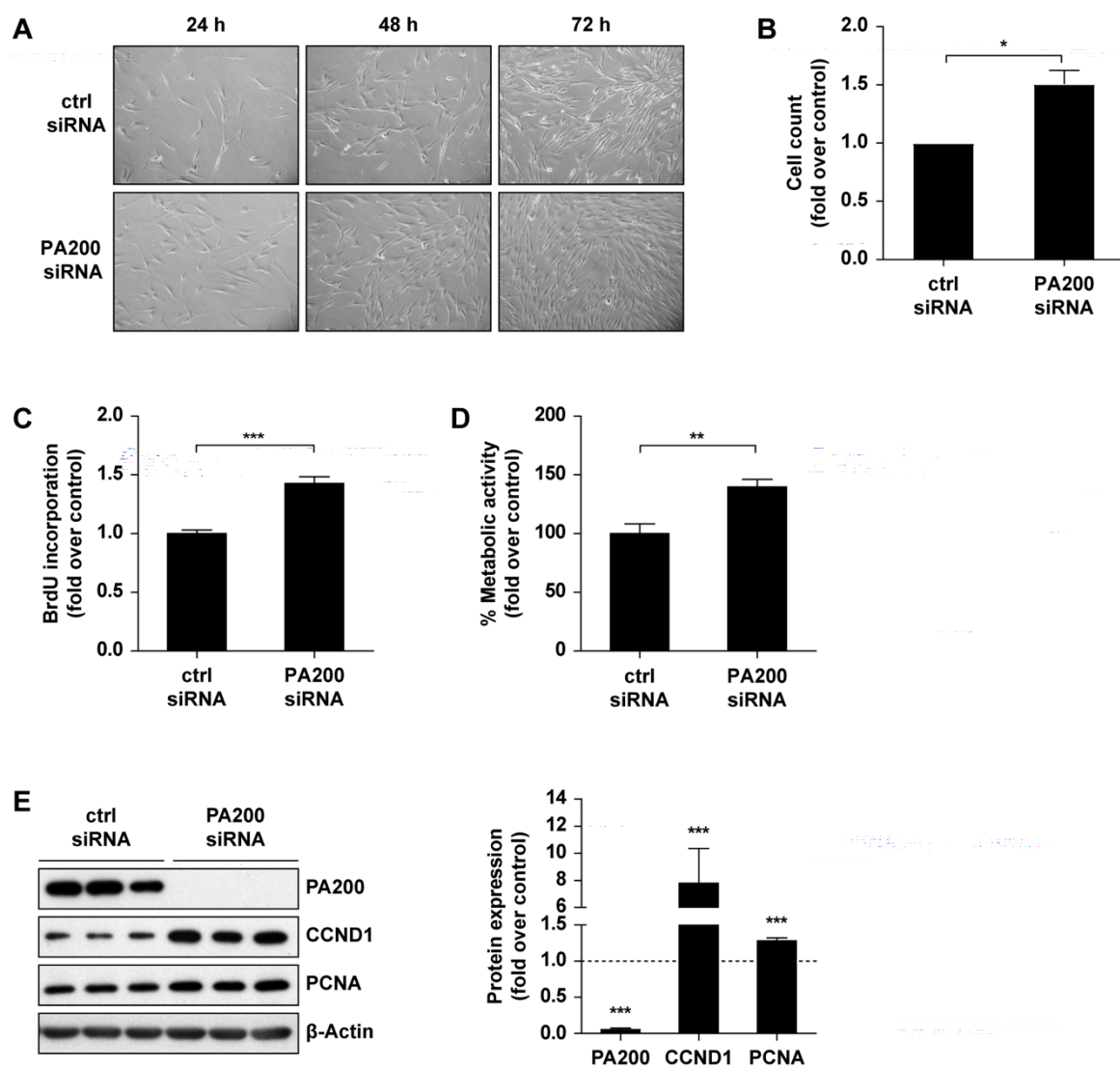


Figure 7.24: siRNA-mediated silencing of PA200 induces proliferation of primary human lung fibroblasts (phLF). (A) phLF were transfected with siRNA against PA200 or control siRNA. Figure indicates representative pictures of cells after 24, 48 and 72 h. (B) phLF were counted 72 h after PA200 silencing. Bar diagram shows cell count normalized to control siRNA-transfected cells of the same patient (one-sample t-test, $n = 3$). (C) Proliferation of phLF was analyzed 72 h after silencing of PA200 by BrdU assay. Bar diagram indicates BrdU incorporation normalized to the mean of control siRNA-transfected cells (Mann-Whitney U test, $n = 4$). (D) Metabolic activity of phLF was measured 72 h after silencing of PA200 by MTT assay. Bar diagram indicates % metabolic activity normalized to the mean of control siRNA-transfected cells (Mann-Whitney U test, $n = 4$). (E) Expression of PA200 and proliferation markers cyclin D1 (CCND1) and PCNA in phLF upon PA200 silencing for 72 h was investigated by Western blotting. Representative immunoblots of experiments performed with three technical replicates per condition in phLF from four different donors are shown. Bar diagram indicates densitometric analysis of PA200 silencing normalized to control siRNA-transfected cells (one sample t-test, $n = 4$).

Moreover, analysis of the cell count in PA200-deficient phLF after 72 h of transfection showed a significant 1.5-fold increase in cell number compared to controls, which accorded well with 1.5-fold induction of BrdU incorporation as a measure for cellular proliferation (Figure 7.24 B and C). Moreover, cellular metabolic activity determined by MTT assay was also significantly enhanced after 72 h of PA200 silencing (Figure 7.24 D). Western blot

analysis confirmed efficient silencing of PA200, as protein levels were strongly decreased after 72 h of knockdown (Figure 7.24 E). In addition, the expression of two markers for cellular proliferation, cyclin D1 (CCND1) required for G1/S cell cycle progression and proliferating cell nuclear antigen (PCNA) involved in DNA replication, was also significantly increased upon knockdown of the activator.

A time course of PA200 silencing in pHLF revealed a significant and strong decrease in PA200 mRNA expression after 24 h persisting up to 72 h after transfection (Figure 7.25 A). CCND1 mRNA expression increased over time and was significantly induced after 48 h with a further increase up to 72 h of PA200 silencing (Figure 7.25 B). This finding thus accords well with microscopic analysis of transfected pHLF over time shown in Figure 7.24. Moreover, qPCR analysis also revealed enhanced TGF- β 1 mRNA expression after 48 h of transfection and induction of α SMA mRNA levels over time, which points towards an activation of pHLF upon silencing of PA200 (Figure 7.25 C and D).

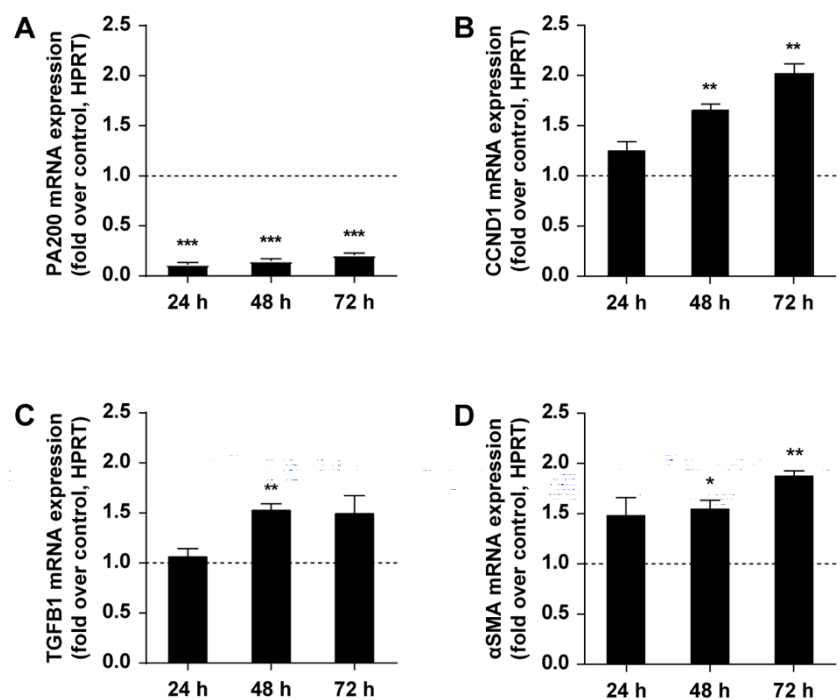


Figure 7.25: Timecourse of PA200 silencing indicates enhanced mRNA expression of proliferation and myofibroblast markers in primary human lung fibroblasts (pHLF). mRNA expression of (A) PA200, (B) cyclin D1 (CCND1), (C) TGF- β 1 (TGFB1) and (D) myofibroblast marker α SMA was measured in pHLF transfected with PA200 or control siRNA for 24, 48 and 72 h. *HPRT* served as housekeeping gene and bars indicate mRNA level normalized to control siRNA transfected cells (one-sample t-test, $n = 3$).

7.2.4.5 Proteasome activity is induced in response to PA200 silencing

As PA200 has been originally described as a proteasome activator that stimulates caspase-like proteasome activity *in vitro* and as it is strongly associated with the 20S proteasome, we assessed whether silencing of PA200 would alter proteasome activities or composition (Blickwedehl et al., 2008; Ustrell et al., 2002).

Proteasome complexes and their activities were analyzed by native gel electrophoresis in native extracts of pHLF transfected with control and PA200 siRNA for 72 h. In-gel overlay with a substrate specific for CT-L activity indicated a significant induction of 20S as well as 26S and 30S activities (Figure 7.26 A). This accorded well with increased presence of 20S, 26S, and 30S complexes shown by immunoblotting of native gels for 20S subunits α 1-7. Regulation of active proteasome complexes was also analyzed by a second approach using labeling of active proteasomes with the activity-based probe (ABP) MV151, which is a fluorescently labeled inhibitor that binds to all catalytic sites of the 20S core particle. Here, native gel electrophoresis and subsequent fluorescent imaging of labeled proteasomes confirmed an increased amount of 26S and 30S complexes upon silencing of PA200 (Figure 7.26 B). The total amount of active proteasomes was also significantly induced as determined by activity based profiling using SDS-PAGE (Figure 7.26 C). These findings demonstrate that silencing of PA200 does not contribute to impairment in proteasome activity but rather results in an activation of overall proteasome activity which is most probably due to enhanced cell growth and survival.

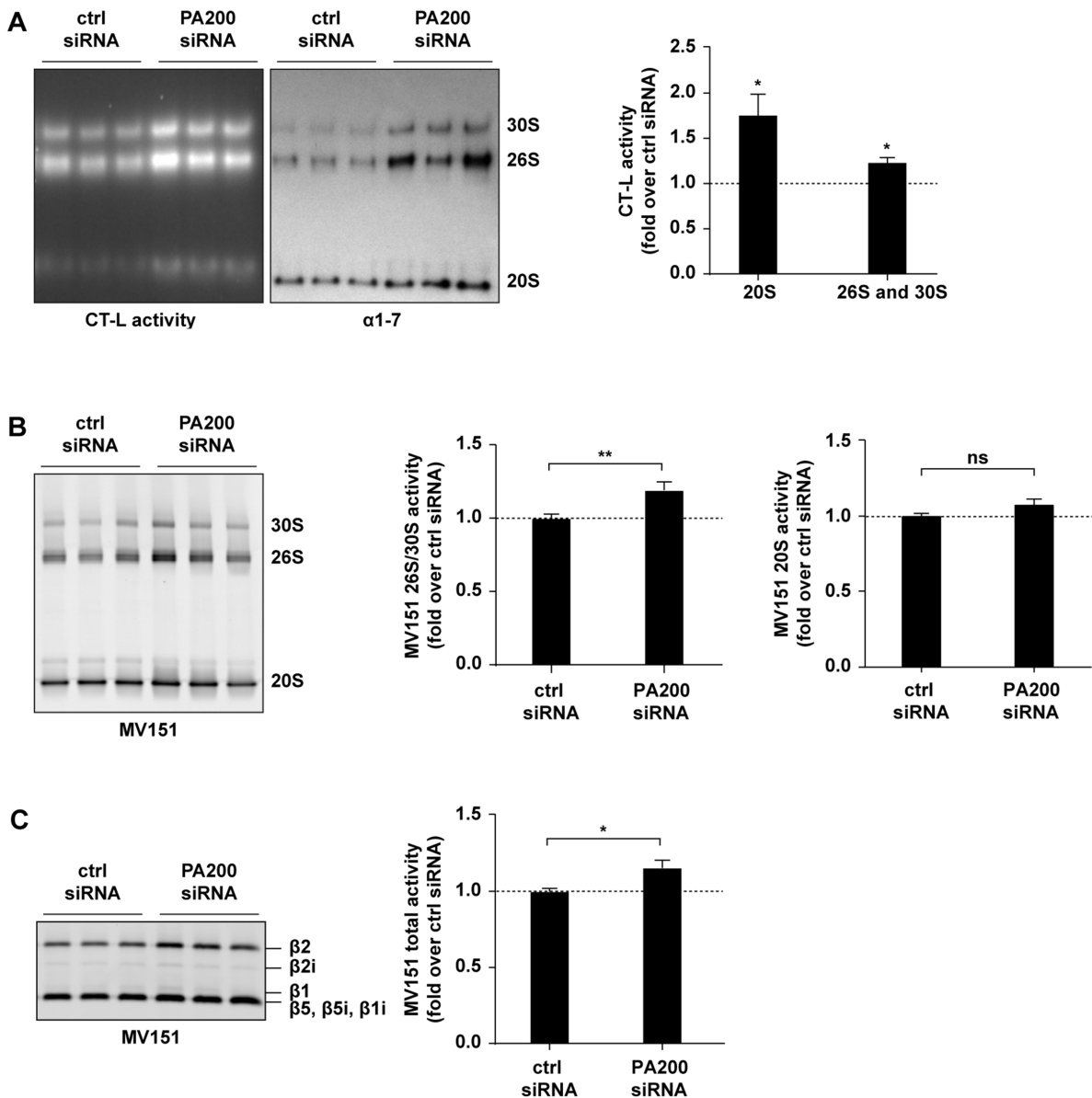


Figure 7.26: Activity and quantity of proteasome complexes are increased in primary human lung fibroblasts (pHLF) in response to PA200 silencing. PA200 silencing was performed in three technical replicates per condition in pHLF for 72 h. (A) Activity of 20S, 26S and 30S proteasomes was determined by native gel electrophoresis and in-gel overlay with a fluorogenic substrate specific for chymotrypsin-like (CT-L) activity. Immunoblotting with an anti- α 1-7 antibody indicates the amount of 20S, 26S and 30S proteasomes. Figure shows representative results of pHLF from one donor. Bar diagram indicates densitometric analysis of 20S and 26S/30S proteasome complexes normalized to control siRNA-transfected cells (one-sample t-test, $n = 4$). (B) Active proteasome complexes in the same lysates used in (A) labeled with fluorescent ABP MV151 were analyzed by native gel electrophoresis. (C) Total amount of active proteasomes was determined by SDS-PAGE of MV151-labeled proteasome subunits. Bar diagrams of (B) and (C) indicate densitometric analysis of obtained signals normalized to the mean of control siRNA transfected pHLF (Mann-Whitney U test, $n = 4$).

Western blot analysis of cell extracts analyzed for proteasome activity and composition in Figure 7.26 confirmed efficient knockdown of PA200 (Figure 7.27 A). Moreover, protein expression of 19S subunit RPN6 of was significantly upregulated upon PA200 silencing, whereas lysine 48 polyubiquitinated proteins, 19S regulator subunit RPT5 and 20S catalytic

subunit $\beta 5$ were not altered. PA200 mRNA expression was also significantly decreased by silencing of the activator (Figure 7.27 B). Proteasomal subunits including 20S subunits $\alpha 7$, 19S regulator subunit RPT5 as well as PA28 γ were not regulated on mRNA level, whereas the 20S catalytic subunit $\beta 5$ was significantly decreased. mRNA expression of RPN6 was slightly – although not significantly – induced according well with its induction on protein level. Concluding, PA200 silencing does not only induce proliferation but also significantly enhances formation of active proteasome complexes in pHLF. Moreover, this accords well with induced expression of 19S subunit RPN6 on protein level, which was previously described as rate limiting subunit for formation of 26S and 30S proteasomes (Santamaria et al., 2003; Semren et al., 2015; Vilchez et al., 2012).

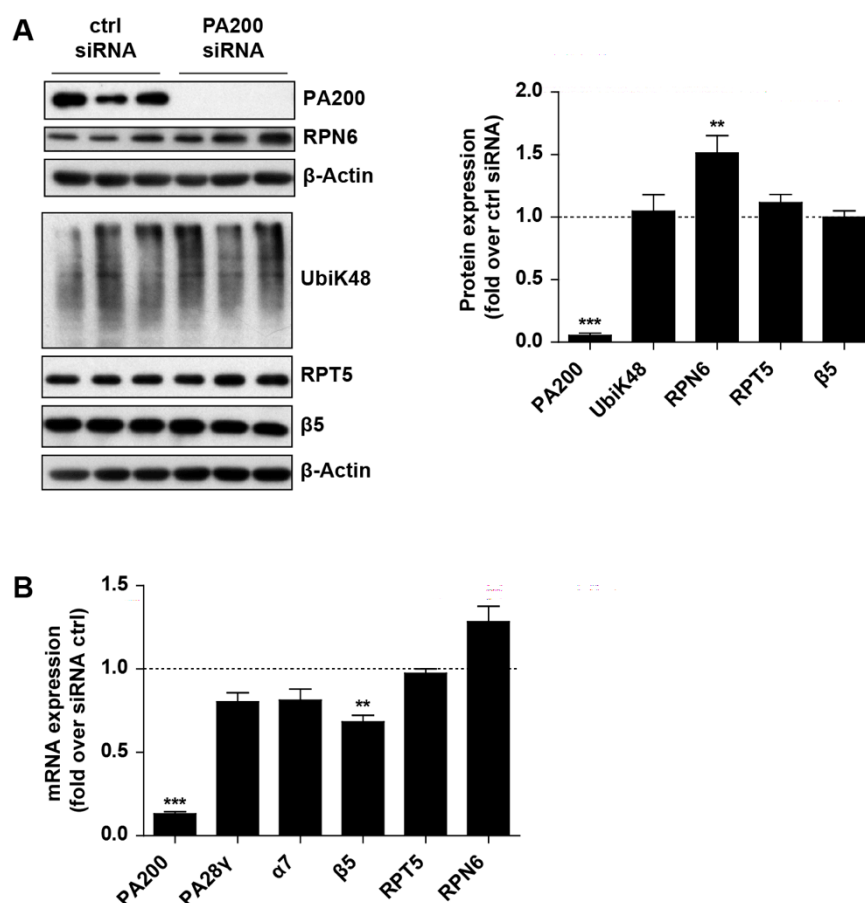


Figure 7.27: Increased RPN6 expression accords well with enhanced proteasome activity upon PA200 silencing in primary human lung fibroblasts (pHLF). (A) Native extracts of pHLF analyzed in Figure 7.26 were analyzed for accumulation of proteins ubiquitinated at lysine 48 (UbiK48) and expression of PA200, 19S subunits RPN6 and RPT5 and 20S catalytic subunit $\beta 5$ by Western blotting. Bar diagram indicates densitometric analysis of obtained signals normalized to control siRNA-transfected pHLF (one-sample t-test, $n = 4$). (B) mRNA expression of PA200, PA28 γ , 20S subunits $\alpha 7$ and $\beta 5$ as well as 19S subunits RPT5 and RPN6 were measured in pHLF analyzed in Figure 7.26. Bar diagram shows mRNA expression normalized to control siRNA-treated cells using RPL19 as housekeeping gene (one-sample t-test, $n = 4$).

7.2.4.6 PA200 silencing decreases activation of apoptotic signaling

Microarray and proteomic screening of PA200-deficient pHLF versus controls suggested – besides induction of cellular growth – downregulation of components of the apoptotic signaling cascade. Therefore, regulation of cellular apoptosis by PA200 was investigated in more detail. Downregulation of caspase-3 (CASP3) protein expression as observed in the proteomic screen (Figure 7.20) was validated by Western blot analysis of protein extracts of PA200-silenced pHLF (Figure 7.28). Here, PA200-deficient pHLF of two different donors exhibited distinctly reduced levels of CASP3 thereby confirming results of the proteomic screen. Downregulation of caspase-3 on the protein level was accompanied by a reduction of its mRNA levels as confirmed by our transcriptomic data set (Figure 7.22).

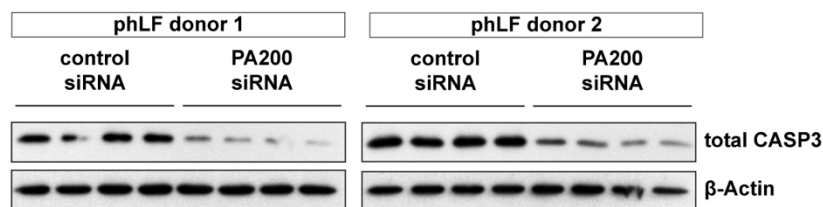


Figure 7.28: Protein levels of total caspase-3 are decreased upon PA200 silencing. Protein levels of total caspase-3 (CASP3) were examined 72 h after silencing of PA200 by Western blotting of the same cell extracts that were used for LC-MS/MS analysis.

CASP3 expression was also evaluated at earlier time points using timecourse of PA200 silencing in pHLF for 24, 48, and 72 h. Western blot analysis confirmed a significant decrease in PA200 protein levels over time (Figure 7.29). Moreover, a delayed downregulation of CASP3 was observed over time indicating the strongest effect after 72 h.

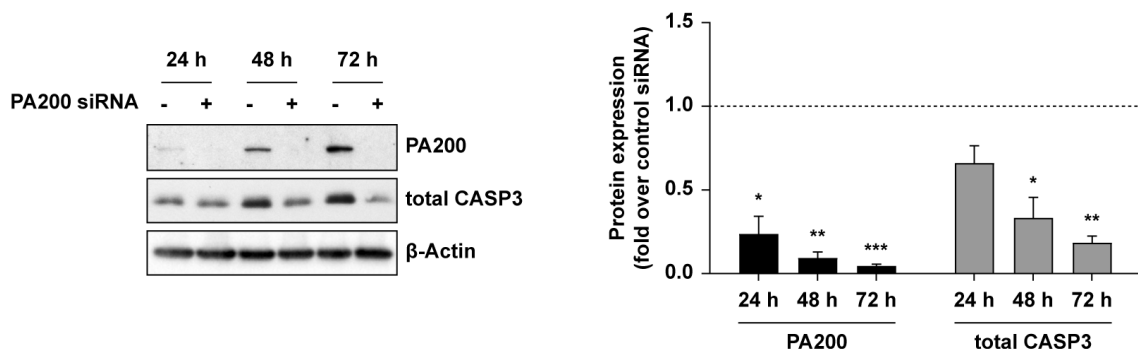


Figure 7.29: Decrease of total caspase-3 protein levels follows siRNA-mediated downregulation of PA200. PA200 silencing for 24, 48 and 72 h in primary human lung fibroblasts was analyzed for protein expression of PA200 and total caspase-3 (CASP3) by immunoblotting. Bar diagram indicates densitometric analysis of obtained signals normalized to β -Actin and time-matched controls (one-sample t-test, $n = 3$).

The functional consequence of CASP3 downregulation in PA200-deficient pHLF was analyzed by assessing activation of the apoptotic cascade by staurosporine treatment in control and PA200 siRNA-transfected pHLF. After silencing of PA200 for 72 h, pHLF were treated for 3 h with 1 μ M staurosporine (STS) for induction of apoptosis or DMSO as a control. Cleavage of CASP3 and its substrate poly (ADP-ribose) polymerase (PARP) – both hallmarks of apoptotic cell death – were analyzed by Western blotting (Figure 7.30 A). Silencing of PA200 again caused a specific reduction of total CASP3 protein level, which was, however, not observed for PARP (Figure 7.30 B). STS treatment led to distinct cleavage of CASP3 and PARP in control siRNA-transfected cells, which was much less abundant in PA200-deficient pHLF. Quantification of Western blots confirmed a significantly increased ratio of cleaved to total CASP3 and PARP in PA200-expressing when compared to PA200-silenced pHLF (Figure 7.30 C).

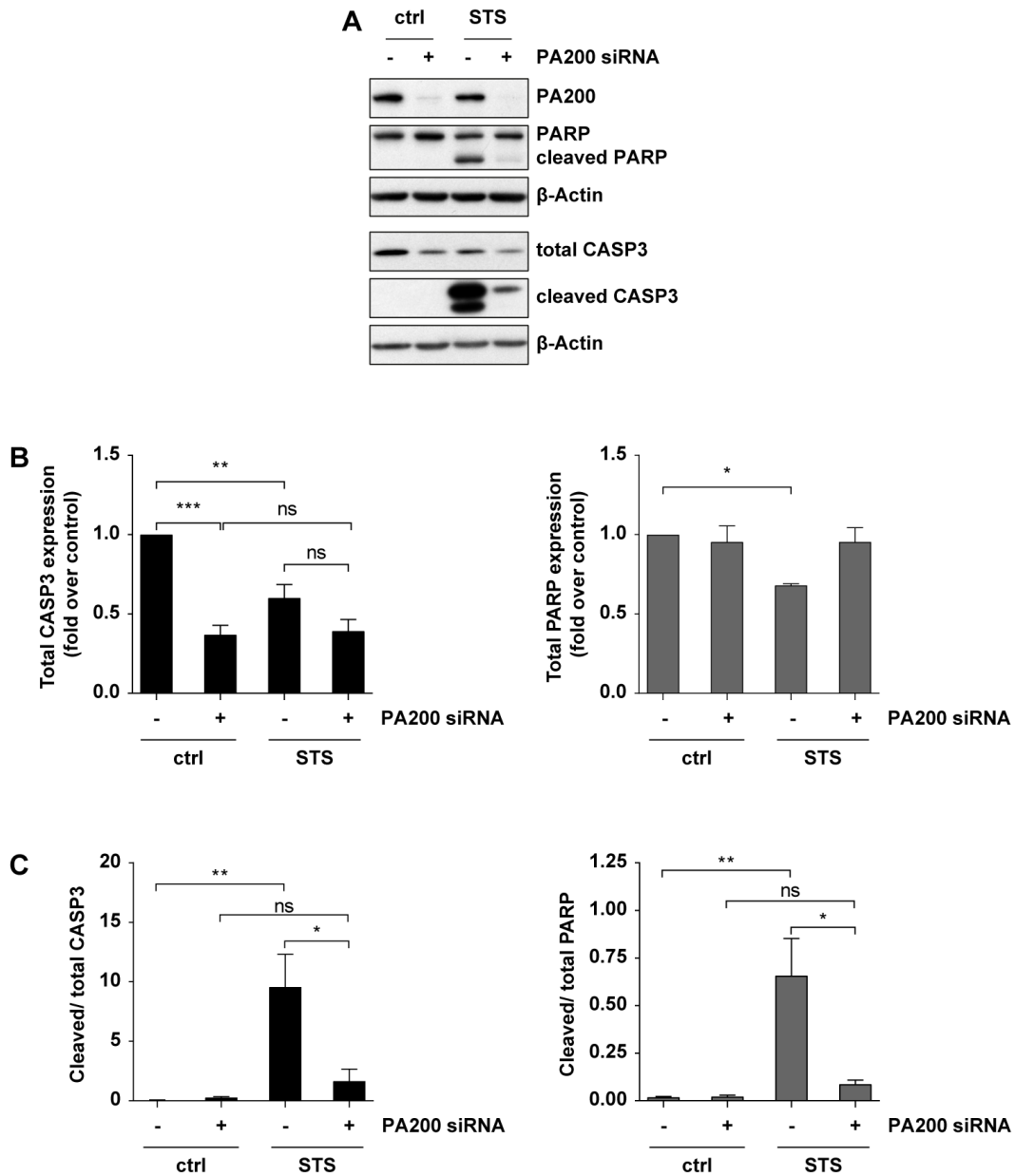


Figure 7.30: Silencing of PA200 impairs cleavage of caspase-3 and PARP in response to apoptosis induction by staurosporine treatment. Primary human lung fibroblasts transfected with control or PA200 siRNA for 72 h were treated with 1 μ M staurosporine (STS) or DMSO as control for 3 h to induce apoptosis. (A) Levels of total and cleaved caspase-3 (CASP3) as well as total and cleaved PARP were examined by western blotting. Figure indicates representative results of experiments performed with cells of four different donors. (B) Bar diagrams indicate quantification of signals obtained for total CASP3 and PARP normalized to controls (one-way ANOVA and Bonferroni's multiple comparisons test, $n = 4$). (C) Ratios of cleaved to total levels of CASP3 and PARP were determined by densitometric analysis of immunoblots (one-way ANOVA and Bonferroni's multiple comparisons test, $n = 4$).

Induction of apoptosis was also assessed using AnnexinV/PI staining as a second approach. AnnexinV (AV) recognizes phosphatidylserine, which is translocated from the inner side of the plasma membrane to the outside during early apoptosis of cells. In contrast, propidium iodide (PI), a fluorescent DNA intercalating agent, cannot penetrate intact plasma

membranes and therefore specifically stains necrotic cells. Thus, this method allows for distinguishing between living AV⁻/PI⁻, early apoptotic AV⁺/PI⁻, late apoptotic AV⁺/PI⁺ and necrotic AV⁺/PI⁺ cells. pHLF transfected with control or PA200 siRNA were treated with STS as described for Figure 7.30. Representative dot plots of FACS analysis with pHLF of one donor are shown in Figure 7.31 A.

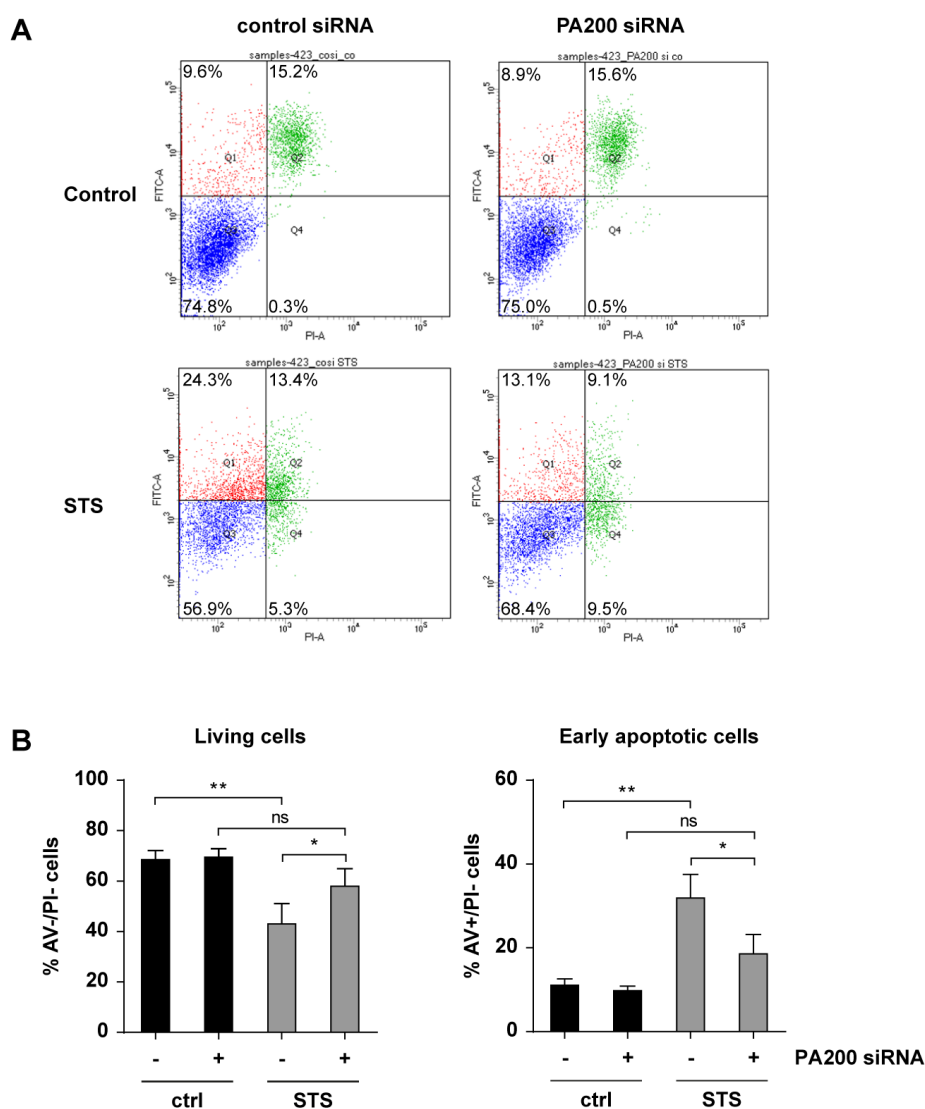


Figure 7.31: FACS analysis demonstrates attenuation of staurosporine-induced apoptotic cell death in PA200-silenced primary human lung fibroblasts (pHLF). pHLF were treated as described in Figure 7.30. (A) Apoptosis was monitored by AnnexinV /PI staining and FACS analysis. Dot plots show AnnexinV FITC versus PI signal of DMSO-treated controls and staurosporine-treated (STS) pHLF upon transfection with control or PA200 siRNAs. 10 000 cells were analyzed per condition. Figure indicates representative results for experiments performed in pHLF of three different donors. (B) Bar diagrams indicate amount of living and early apoptotic cells as the percentage of total cells assessed by FACS analysis (one-way ANOVA and Bonferroni's multiple comparisons test, $n = 3$)

Quantification of living, early apoptotic, late apoptotic and necrotic cells indicated no basal difference between control and PA200-deficient cells. STS treatment strongly decreased the percentage of living cells in control siRNA-transfected pHLF. Induction of apoptotic cell death was clearly attenuated in PA200-deficient pHLF (Figure 7.31 B). Corresponding to these results, STS treatment significantly increased the percentage of early apoptotic AV⁺/PI⁻ cells in control compared to PA200 siRNA-transfected pHLF (Figure 7.31 C). The number of late apoptotic and necrotic cells was not altered by all applied treatments (quantification of late apoptotic and necrotic cells not shown).

In conclusion, Western blot analysis confirmed results of the proteomic screen showing downregulation of total CASP3 protein expression by PA200 silencing. Two distinct approaches reveal that loss of PA200 function results in the decreased ability of pHLF to undergo apoptosis. Moreover, the enhanced survival and growth of PA200-deficient cells corresponds very well to the enrichment of growth-associated genes and concomitant downregulation of pro-apoptotic genes as identified in the unbiased transcriptomic and proteomic screens (Figure 7.19 and Figure 7.21).

7.2.5 PA200^{-/-} increases the survival of mice during development of bleomycin-induced fibrosis

The fundamental effect of PA200 deficiency on survival and growth of primary lung fibroblasts as well as its specific elevation in fibrotic tissue remodeling prompted us to investigate the contribution of PA200 to the development of pulmonary fibrosis. An experimental mouse model of bleomycin-induced lung fibrosis was used to investigate fibrotic remodeling in wildtype and PA200^{-/-} mice. This involved analysis of the survival in mice instilled with bleomycin (2 U/kg), lung function, infiltration of immune cells into the bronchoalveolar lavage fluid, fibrotic marker expression, and fibrotic remodeling by histology.

7.2.5.1 PA200^{-/-} mice better cope with bleomycin challenge of the lung

Although no difference was observed in the fibrotic remodeling of lungs from wildtype and PA200^{-/-} mice, knockout mice were able to cope much better with the treatment. Survival of animals after instillation of bleomycin was assessed for 14 days. Animals were monitored daily and sacrificed upon weight loss of >15%. As indicated in Figure 7.32, PA200^{-/-} mice exhibited a significantly increased survival upon intratracheal instillation of bleomycin when compared to wildtype mice.

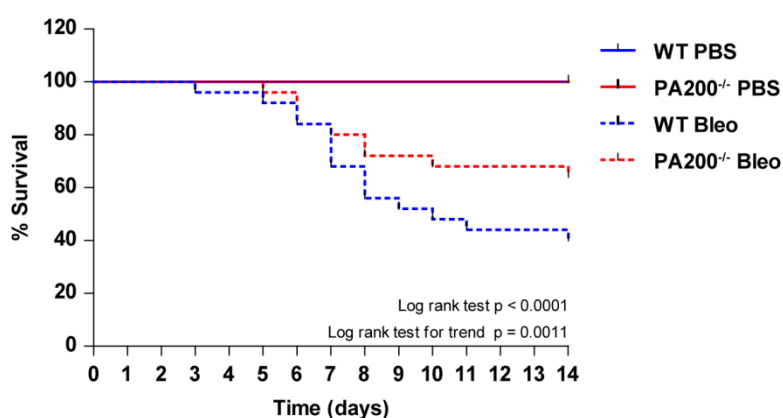


Figure 7.32: Survival of PA200^{-/-} mice is improved compared to wildtype animals in response to bleomycin challenge of the lung. PA200^{-/-} and wildtype (WT) mice were instilled with 2 U/kg body weight bleomycin (Bleo) or PBS and the survival of animals was monitored over 14 days. Animals with a weight loss >15% were sacrificed. Curve indicates the survival of animals as percentage of total animals per group (Log rank test and log rank test for trend, WT PBS $n = 18$, PA200^{-/-} PBS $n = 14$, WT Bleo $n = 25$, PA200^{-/-} Bleo $n = 25$; combined results of two independent experiments).

7.2.5.2 Bleomycin-instilled PA200^{-/-} and wildtype mice have a similar decline in lung function

Lung function of mice was measured 14 days after bleomycin instillation using the flexiVent system that assesses resistance, elastance and compliance of lungs. Although the resistance of the airways to airflow significantly increased in bleomycin-treated wildtype and PA200^{-/-} compared to the respective PBS-treated controls, no difference was observed between bleomycin-instilled knockout and wildtype animals (Figure 7.33 A). The elastance of the lung, which is defined as the change in pressure required for induction of a unit volume change, was also significantly elevated in lungs of bleomycin-instilled wildtype and PA200^{-/-} mice and no significant difference was observed between those two groups (Figure 7.33 B). The lung compliance, the ability of the lung to expand defined as volume change per unit pressure change, significantly declined in bleomycin-treated animals both with PA200^{-/-} and wildtype background (Figure 7.33 C and D).

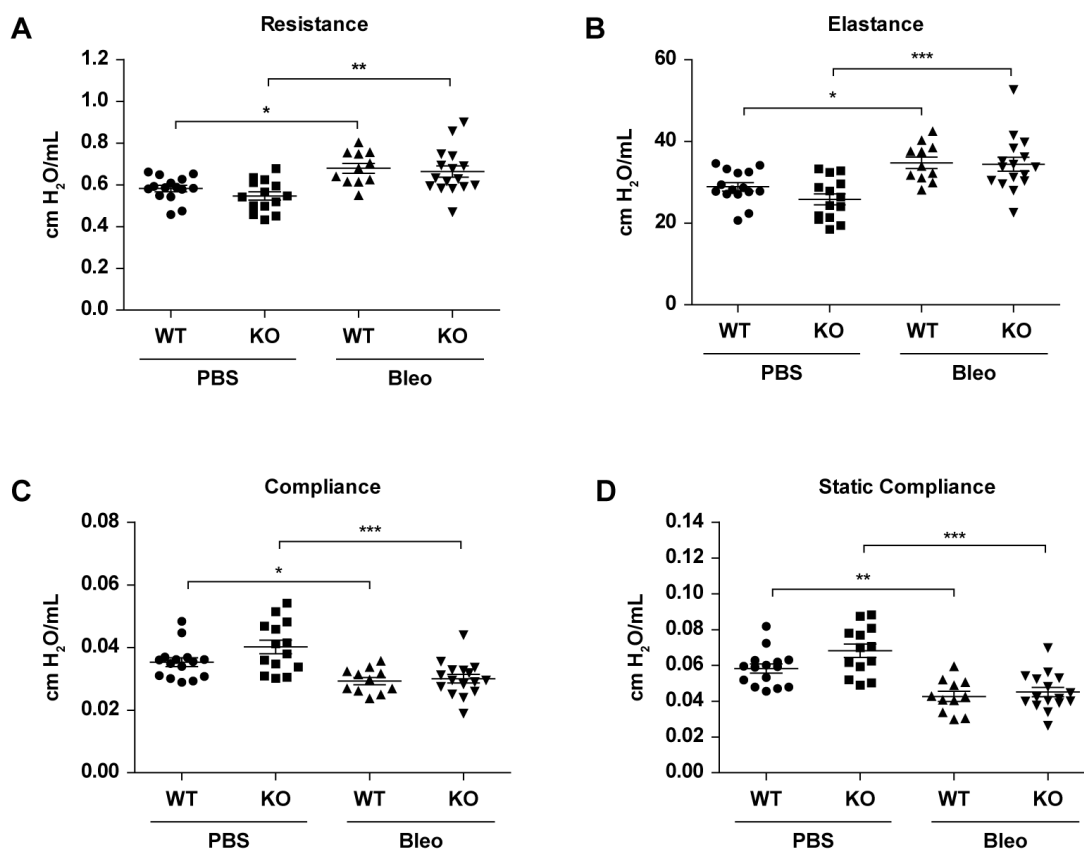


Figure 7.33: Lung function decline is similar in bleomycin-instilled PA200^{-/-} and wildtype mice. Lung function of animals was analyzed 14 days after bleomycin or PBS instillation (Kruskal-Wallis test and Dunn's multiple comparisons test, $n = 11-16$ per group; combined results from two independent experiments). Lung function measurement was performed by Dr. I. E. Fernandez, Postdoc at the CPC 2017.

7.2.5.3 Bleomycin-instilled PA200^{-/-} and wildtype mice have similar pattern of immune cells in the bronchoalveolar lavage

Immune cells within the bronchioalveolar lavage (BAL) were determined as another read out for fibrotic remodeling of the lungs. BAL cells were stained with May-Grünwald Giemsa and the percentage of different immune cells was assessed according to morphological characteristics (Figure 7.34 A). In PBS-instilled wildtype and PA200^{-/-} animals approximately 95 % of BAL cells were macrophages, which were significantly decreased in lungs of bleomycin-instilled mice (Figure 7.34 B). The percentage of lymphocytes was significantly increased in bleomycin-instilled wildtype and PA200^{-/-} mice compared to PBS controls. Here, BAL of PA200^{-/-} mice contained only a slightly higher but not significant percentage of lymphocytes when compared to wildtype animals (Figure 7.34 C). Approximately 1 % neutrophils were detected in both, PBS-instilled PA200^{-/-} and wildtype mice. Their amount was increased to approximately 3 % by bleomycin instillation with again no difference between the two genetic backgrounds.

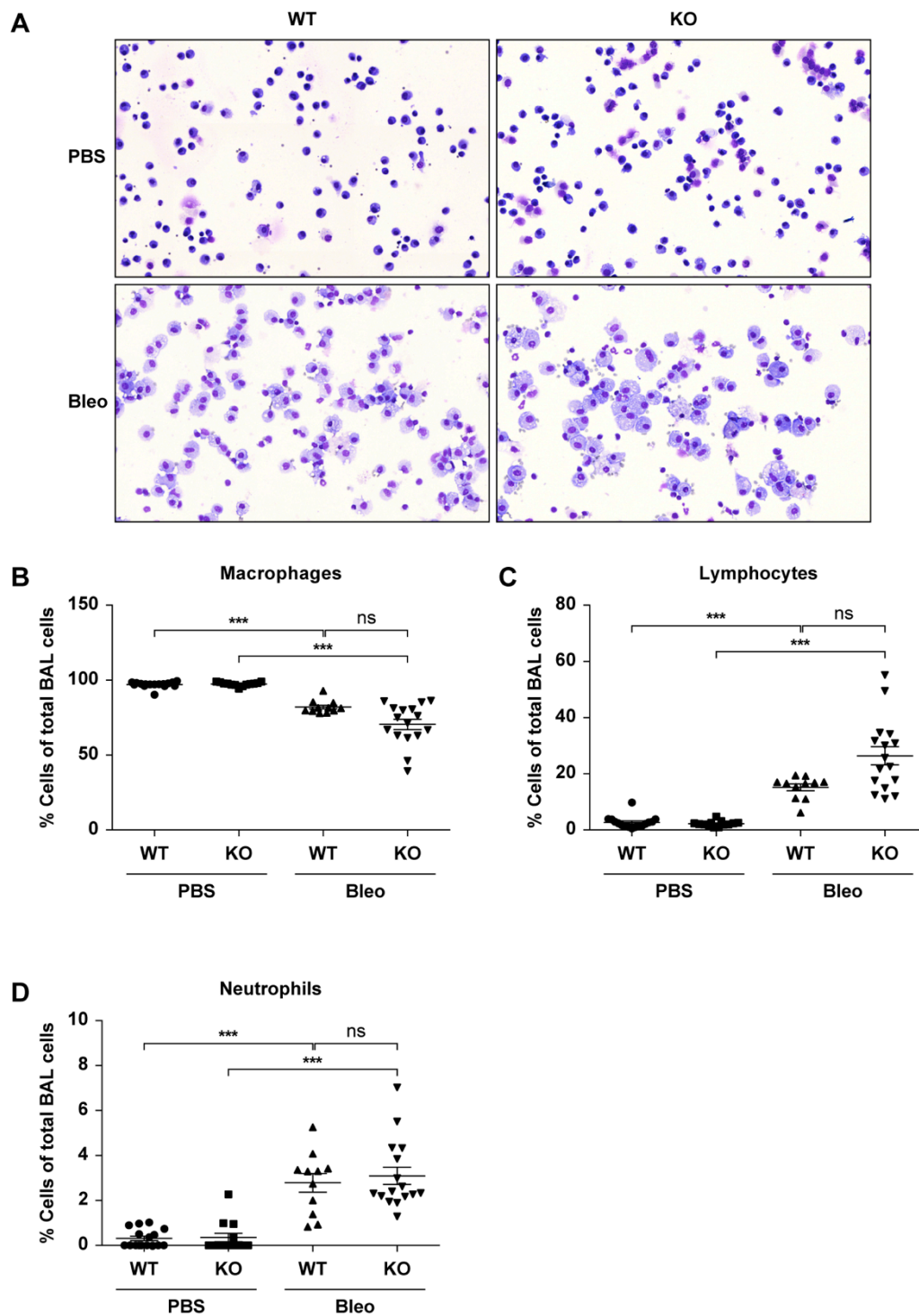


Figure 7.34: Immune cells of the BAL are similar in bleomycin-instilled in wildtype and PA200^{-/-} mice. (A) Immune cells in the bronchoalveolar lavage fluid of PBS- and bleomycin-instilled (Bleo) wildtype and PA200^{-/-} (KO) mice were examined by May-Grünwald Giemsa staining. Figure shows representative stainings. Number of (B) macrophages, (C) lymphocytes and (D) neutrophils was determined according to morphological characteristics assessing at least 200 cells per animal (Kruskal-Wallis test and Dunn's multiple comparisons test, $n = 11-16$ per group; combined results from two independent experiments).

7.2.5.4 Bleomycin-treated PA200^{-/-} and wildtype mice exhibit similar induction of fibrotic markers

Expression of markers for fibrotic tissue remodeling was analyzed by qPCR of lung homogenates. Here, fibronectin (FN), collagen1 α 1 (Col1A1) and tenascin C (TNC) mRNA levels were significantly induced in bleomycin-instilled wildtype and PA200^{-/-} mice (Figure 7.35 A-C). However, no difference in the induction of fibrotic marker expression was observed between PA200^{-/-} and wildtype animals.

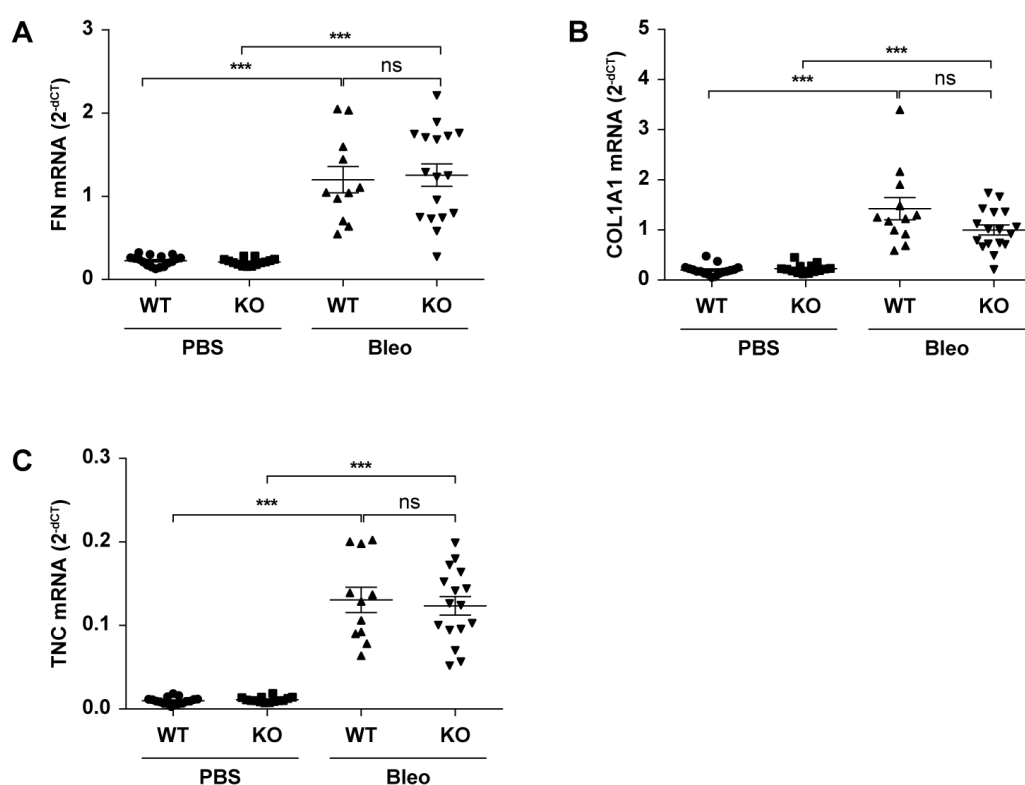


Figure 7.35: mRNA expression of fibrotic markers is equally induced in PA200^{-/-} and wildtype mice in response to bleomycin challenge. mRNA expression of fibrotic markers (A) fibronectin (FN), (B) collagen1 α 1 (COL1A1) and (C) tenascin C (TNC) was analyzed by qPCR in lungs of wildtype and PA200^{-/-} (KO) 14 days after bleomycin or PBS instillation. Diagrams indicate mRNA levels as 2^{-dCT}, *Rpl19* served as housekeeping gene (Kruskal-Wallis test and Dunn's multiple comparisons test, $n = 12-17$ per group; combined results from two independent experiments). qPCR was performed by C. Lukas, technician at the CPC 2017.

7.2.5.5 Histological analysis reveals similar induction of fibrotic remodeling in bleomycin-instilled PA200^{-/-} and wildtype mice

Histological analysis using hematoxylin & eosin staining of lungs from bleomycin-treated mice at day 14 was used as a second approach to assess fibrotic tissue remodeling. This analysis confirmed that PBS-instilled PA200^{-/-} mice exhibit normal lung architecture without

an apparent lung phenotype (Figure 7.36). Histology showed a similar development of fibrosis in wildtype and PA200^{-/-} mice in response to bleomycin instillation as indicated by the dark blue patches of dense cells in the lungs of bleomycin-treated wildtype and PA200^{-/-} mice (Figure 7.36).

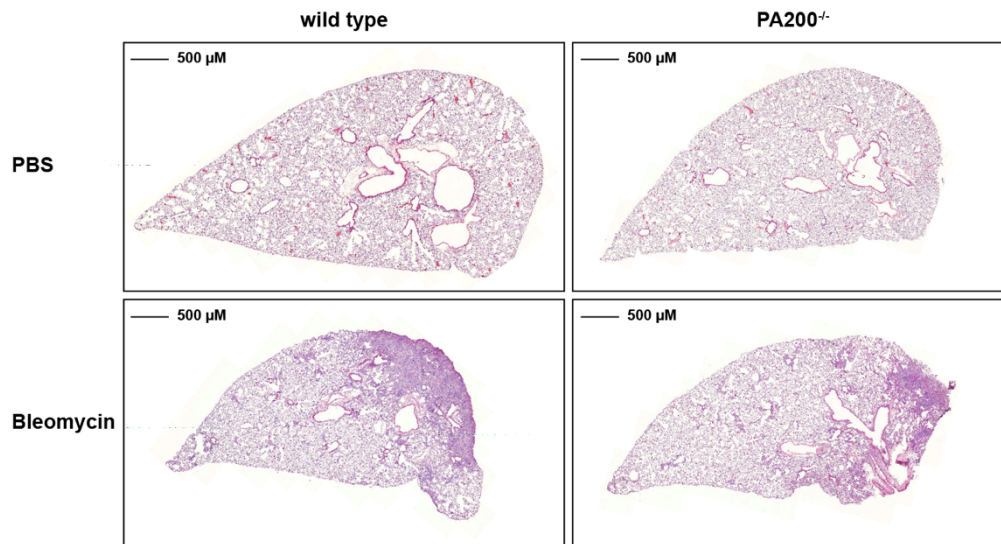


Figure 7.36: Histological analysis reveals similar induction of fibrotic remodeling in lungs of bleomycin-instilled PA200^{-/-} and wildtype mice. Paraffin-embedded tissue sections of PA200^{-/-} and wildtype mice at day 14 after instillation with bleomycin (2 U/kg) or PBS were stained with hematoxylin & eosin (H&E). Figure shows representative histology from two independent animal experiments.

In summary, PA200 deficiency allowed mice to better cope with intratracheal bleomycin challenge but did not protect from fibrotic tissue remodeling in surviving animals. As fibrotic tissue remodeling starts only after initial inflammation after day 7 of bleomycin treatment, deficiency of PA200 potentially protects alveolar cells from initial injury but has no effect on the subsequent fibrotic wound healing response.

7.2.6 PA200 is strongly induced in lung cancer tissues

Previous experiments of this study revealed an increased expression of PA200 upon fibrotic tissue remodeling and a role for PA200 in the regulation of cell growth, apoptosis, and survival. As proliferative signaling and resistance to cell death are also considered as hallmarks of cancer, it was speculated that PA200 might also be regulated in lung cancer (Hanahan and Weinberg, 2011).

7.2.6.1 Homogenates of human lung cancer biopsies show increased expression of PA200

For expression analysis of PA200 non-tumorous and tumor tissues of patients suffering from different types of lung cancers were collected in collaboration with the Asklepios Klinik in Gauting, Germany. Western blot analysis of RIPA extracts of these biopsies indicated a strong upregulation of PA200 protein levels in all tumor tissues compared to non-tumor lung samples of the same patient (Figure 7.37).

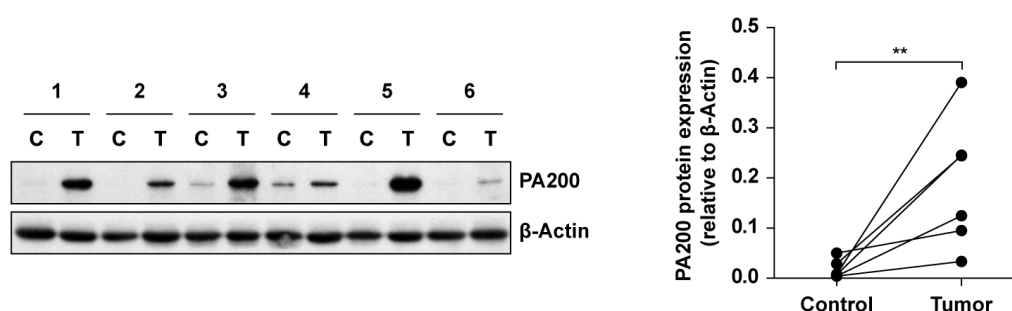


Figure 7.37: PA200 protein levels are significantly elevated in lung tumor tissue. PA200 protein expression was determined in homogenates of non-tumor (C) and tumor (T) tissue from six lung cancer patients by Western blotting. Diagram indicates densitometric analysis of signals obtained for control and tumor tissue relative to β -Actin level (Mann-Whitney U test, $n = 6$).

Of note, PA200 mRNA expression was not significantly induced in these biopsies (Figure 7.38). Therefore, these findings suggest an induction of PA200 protein levels rather due to protein stabilization than increased RNA expression.

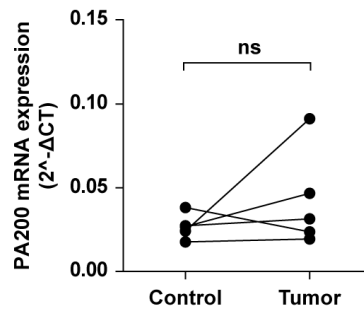


Figure 7.38: PA200 mRNA level are not significantly upregulated in lung tumor tissues. PA200 mRNA levels of tumor and non-tumor control tissue of lung cancer biopsies from five different patients, which were analyzed for protein expression in Figure 7.37, were assessed by qPCR. *RPL19* served as housekeeping gene (Mann-Whitney U test, $n = 5$). qPCR was performed by C. Lukas, technician at the CPC.

7.2.6.2 Lung tumors of *Kras*^{LA2} mutant mice confirm increased expression of PA200

Immunohistochemistry analysis of PA200 was applied to further validate upregulation of the activator in different types of lung cancer. Lung tissue sections of *Kras*^{LA2} mutant mice, which spontaneously develop tumors in the lung, showed induction of PA200 in the cytoplasm and nucleus of tumor cells compared to healthy lungs of wildtype mice (Figure 7.39). Moreover, non-tumorous tissue surrounding tumor areas in lungs of *Kras*^{LA2} mutant mice did not indicate staining for PA200, which corresponds well with very low expression observed in human non-tumorous tissues by Western blot analysis.

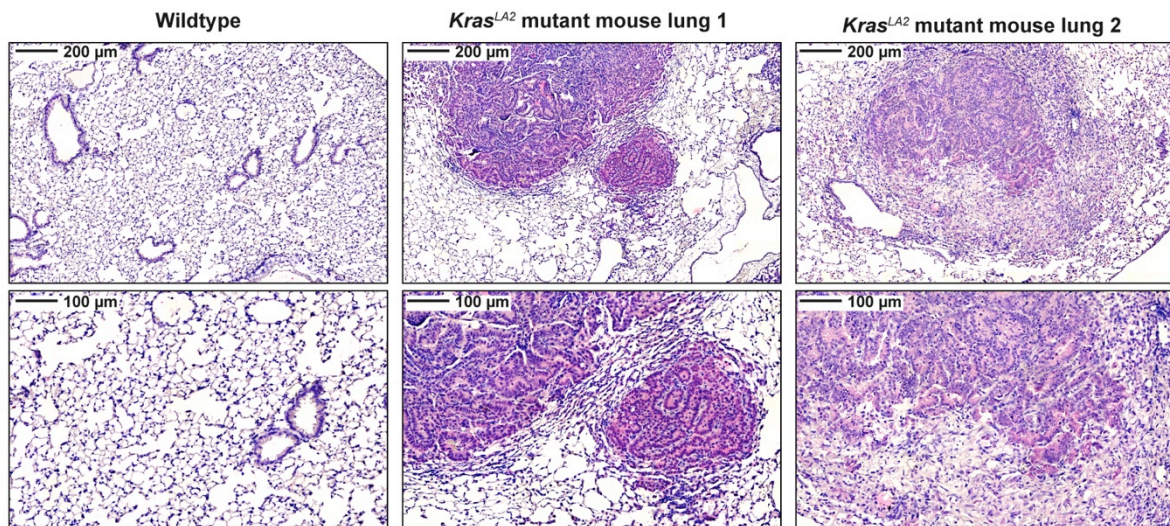


Figure 7.39: PA200 expression is elevated in lung tumors of *Kras*^{LA2} mutant mice. Expression of PA200 (pink) was determined in wildtype and *Kras*^{LA2} mutant mouse lungs by immunohistochemistry. Nuclei were counterstained with hematoxylin (blue). IgG served as negative control (not shown). Staining was performed by T. Meul, master student at the CPC 2016.

7.2.6.3 Tumor cells but not tumor stroma and necrotic areas express PA200

Expression of PA200 was also analyzed in tumor tissue sections of lung cancer patients, which were kindly provided by the Asklepios Klinik in Gauting, Germany. Distinct PA200 overexpressing areas were identified by immunohistochemistry (Figure 7.40). Analysis of different subtypes of non-small cell lung cancer unambiguously showed that PA200 was strongly induced in cancer cells, whereas surrounding tumor stroma and necrotic areas indicate expression of the activator.

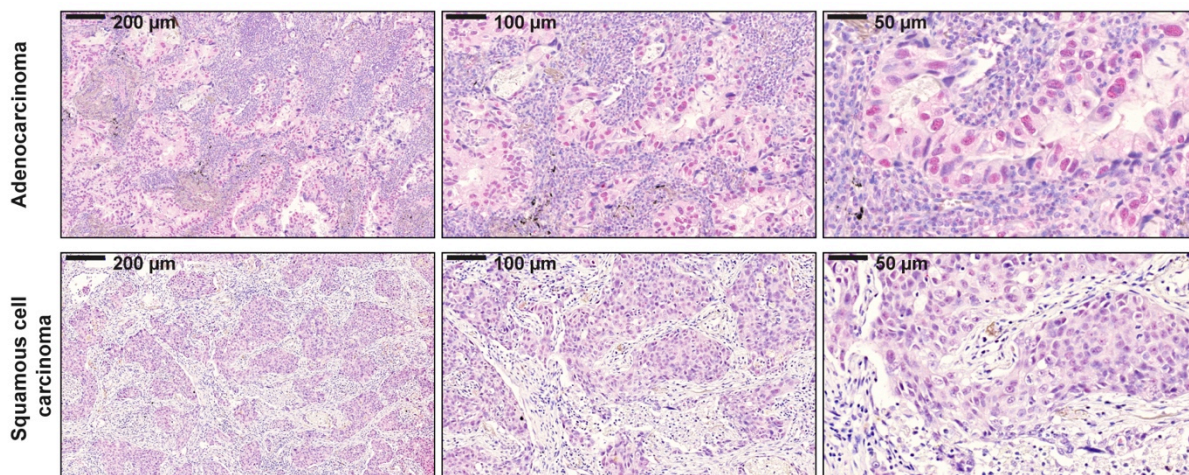


Figure 7.40: Immunohistochemistry of human lung tumor biopsies identifies PA200-positive cancer cells. Paraffin tissue sections of different human lung carcinomas were analyzed for expression of PA200 (pink) using immunohistochemistry. Figure indicates representative staining of biopsies in different magnifications. Nuclei were counterstained with hematoxylin (blue). IgG served as negative control (not shown). Staining was performed by T. Meul and C. Lukas.

Concluding, analysis of PA200 expression showed a remarkably strong induction in lung cancer tissues. PA200 was highly expressed in tumor cells but not in tumor stroma or necrotic areas. Therefore, these findings show that upregulation of PA200 protein level might be a common feature of lung tumor cells.

7.3 Discussion

Although PA200 has been first described as a proteasomal activator already in 2002, little is known about its exact cellular function as well as its regulation in disease (Ustrell et al., 2002). Using validated antibodies, the present study reveals a so far unknown upregulation of PA200 protein levels in hyperproliferative chronic lung diseases, namely idiopathic pulmonary fibrosis and lung cancer. Moreover, not only the expression of PA200 but also its association with the proteasome and its interactome were regulated according to cellular activation and growth in primary human fibroblasts of the lung. Functional analyses involving transcriptomic and proteomic screens of PA200 silencing in pHLF predicted an activation of growth and survival pathways in these cells and *in vitro* experiments in pHLF confirmed PA200 as a novel regulator of cellular growth and survival.

7.3.1 Induction of PA200 in hyperproliferative tissues is a new aspect of proteasome regulation in diseased tissues

Being the main protein degradation machinery within the cell, the proteasome regulates many different cellular processes including cell differentiation, proliferation, apoptosis, signal transduction, gene transcription, and MHC I antigen presentation (Bowerman, 2006; Collins and Tansey, 2006; Naujokat and Hoffmann, 2002; Strehl et al., 2005; Taylor and Jobin, 2005). Proper control of proteasome function is essential for maintenance of protein homeostasis and cell function. For this reason, dysregulation of proteasome system in diseases is obvious and has been described for several disorders such as neurodegenerative and autoimmune disorders, viral infections and cancer (Dahlmann, 2007). However - besides an induction of PA28 γ in cancer tissues - the role of alternative proteasome activators in diseases is still largely unknown and requires detailed investigation (Mao et al., 2008). Therefore, the upregulation of PA200 upon fibrotic tissue remodeling and in lung tumors provides a novel aspect of regulation of alternative proteasome complexes in diseased tissues.

7.3.1.1 Induction of PA200 is a novel aspect of proteasome deregulation in fibrotic tissue remodeling of the lung

Beside the discovery of proteasomal degradation of TGF- β pathway components, studies analyzing the proteasome in fibrotic lung remodeling have been very limited (Imamura et al., 2013; Soond and Chantry, 2011). Mutlu *et al.* reported anti-fibrotic effects of proteasome inhibitor treatment in bleomycin-induced lung fibrosis in mice and claimed that the anti-fibrotic effects of bortezomib treatment were mediated by decreased expression of TGF- β target genes (Mutlu et al., 2012). The regulation of the proteasome itself in lung fibrosis was first analyzed in a previous study of our group. Here, we observed that 26S proteasome activity is induced upon fibrotic remodeling of the lung and proteasome function is required for TGF- β 1-driven differentiation of myofibroblasts (Semren et al., 2015). However, the regulation of alternative proteasome activators – and especially of PA200 – was not analyzed in this context.

A strong induction of PA200 protein expression was observed in fibrotic lungs of both IPF patients and bleomycin-instilled mice. Enhanced PA200 protein levels are more likely to be caused by protein stabilization than by increased expression, as mRNA levels were not significantly altered. Analyzing the cell types with increased expression of PA200 identified pronounced expression of the activator in hyperplastic bronchial basal cells and myofibroblasts of fibroblast foci, which are a classical histological feature of the disease (Jones et al., 2016). Activation of fibroblasts and differentiation into myofibroblasts, which produce excess of extracellular matrix leading to scar formation, is a major pathological hallmark of the disease (Wynn, 2011). Here, the pro-fibrotic cytokine TGF- β 1 is considered as one of the main drivers of myofibroblast differentiation (Fernandez and Eickelberg, 2012b; Noble et al., 2012). In addition, accumulation of KRT5-positive basal cells was recently described as another characteristic feature of IPF tissues and dysregulation of basal cell proliferation or differentiation leading to hyperplasia has been identified in several diseases such as chronic obstructive pulmonary disease (COPD) and cystic fibrosis (Rock et al., 2010; Smirnova et al., 2016).

Indeed, *in vitro* analysis of PA200 regulation during differentiation of primary human bronchial basal cells as well as primary human lung fibroblast into myofibroblasts accorded well with expression analysis in donor and IPF tissue. Upon differentiation of phBECs, PA200 mRNA and protein levels were significantly decreased, implying a generally higher

expression in undifferentiated basal cells of the bronchial epithelium. IHC analysis of healthy lung sections also showed a more pronounced expression of PA200 in undifferentiated KRT5-positive basal cells when compared to differentiated bronchial epithelial cells. Moreover, analysis of PA200 in TGF- β 1-activated myofibroblasts revealed a significant increase in expression and formation of PA200-containing alternative proteasome complexes, which also confirms IHC analysis of IPF tissue sections.

7.3.1.2 PA200^{-/-} mice better cope with bleomycin challenge of the lung

In order to investigate the role of PA200 in the development of lung fibrosis, fibrotic lung remodeling in response to bleomycin instillation was analyzed in PA200^{-/-} compared to wildtype mice. Although the survival of bleomycin-instilled PA200^{-/-} was significantly enhanced compared to wildtype animals, the development of fibrosis at day 14 was comparable in all animals.

The applied bleomycin mouse model has several limitations, although it is widely used to mimic the development of fibrosis in an experimental setting. First, instillation of bleomycin into the lungs induces an initial inflammatory response and therefore rather resembles an acute lung injury before the actual fibrotic remodeling is initiated (Matute-Bello et al., 2008). Second, this model does not involve the formation of so-called myofibroblast foci and induction of alveolar epithelial cell hyperplasia, which are both a hallmark of the human disease (Degryse and Lawson, 2011; Moeller et al., 2008; Moore et al., 2013). Lastly, fibrotic lung remodeling is restored within approximately 56 days after instillation of bleomycin, which is in large contrast to the human chronic and progressive disease. For these reasons, the bleomycin mouse model does not exactly resemble the human disease. The similar development of fibrosis in wildtype and PA200^{-/-} mice might occur due to a different pathogenesis of fibrotic wound healing in the mouse model. In this study, PA200 was mainly identified in myofibroblasts of myofibroblast foci in human IPF tissues. Moreover, functional analysis discovered it as a regulator of fibroblast activation, proliferation, and survival. Nevertheless, the improved survival of PA200^{-/-} upon bleomycin challenge of the lung accords well with increased survival of pHLF in response to PA200 silencing *in vitro*. In line with this study, Khor *et al.* reported no significant differences in survival of wildtype and PA200^{-/-} mice suggesting that an additional challenge is required to observe a differential

effect (Khor et al., 2006). Blm10, the yeast homologue of PA200, was discovered due to its responsiveness to bleomycin-induced DNA damage. However, this was not confirmed for the murine PA200 protein, because murine wildtype and PA200^{-/-} embryonic stem cells showed a similar response to bleomycin treatment with no defects in the repair of DNA double strand breaks (Khor et al., 2006). Therefore, the enhanced survival of PA200^{-/-} mice upon bleomycin challenge is presumably caused by a differential response in lung remodeling upon lung injury and not by a differential response to DNA damage caused by bleomycin.

7.3.1.3 Regulation of PA200 is not only restricted to fibrotic remodeling of the lung

Fibrotic remodeling of tissues from different organs shares common pathological characteristics, such as activation of myofibroblasts causing excess deposition of extracellular matrix components, which leads to scarring of the tissue and finally loss of proper organ function (Bataller and Brenner, 2005; Gabbiani, 2003; Wynn, 2011). Small molecule proteasome inhibitors have also been successfully applied for interference with fibrotic remodeling of experimentally induced fibrosis from other organs such as kidney, liver, heart or dermis (Anan et al., 2006; Koca et al., 2012; Meiners et al., 2004; Tashiro et al., 2003). However, regulation of the proteasome has not been investigated in other fibrotic organs except from the lung. Therefore, the present study shows for the first time that adaption of proteasome function is not only restricted to fibrosis of the lung, but can also be found in experimentally induced fibrotic kidney remodeling. Beside increased proteasome activity and induced expression of rate-limiting 19S regulatory subunits RPN6 (data of increased RPN6 expression not shown), expression of PA200 and the formation of PA200 alternative proteasome complexes was significantly enhanced in homogenates of fibrotic kidneys. Hence, these findings suggest that induction of proteasome activity and PA200 alternative proteasomes is a general feature of fibrotic tissue remodeling from different organs and not only restricted to the lung.

Lung cancer is another devastating lung disease characterized by aberrant and massive cell growth within the lung. Several hallmarks of cancer are also true for myofibroblasts in the fibrotic lung: resistance to cell death, evasion of growth suppressors, increased proliferation and invasion (Horowitz et al., 2016). *In vitro* experiments of this study analyzing the functional consequence of PA200 silencing in pHLF indicated a strong upregulation of

cellular proliferation and survival involving induction of AKT signaling and suppression of apoptosis. These observations suggest that pHLF acquired a cancer cell-like phenotype upon loss of PA200 function. Of note, PA200 protein levels were significantly upregulated in lung tumor tissues when compared to non-tumorous lung tissue of the same patient. Moreover, induction of PA200 expression was also observed in lung tumors of *Kras*^{LA2} mutant mice. However, only the tumor cells but not the tumor stroma or necrotic areas of human lung cancer biopsies expressed PA200. Tumor stroma consists of non-malignant tumor cells, such as carcinoma-associated fibroblasts (CAFs), mesenchymal cells, immune cells, endothelial cells and pericytes, and extracellular matrix (Bremnes et al., 2011). Therefore, the expression of PA200 in different cell types in IPF and lung cancer tissues suggests that its regulation is rather related to cellular phenotypes, such as increased proliferation and survival, and not to the cellular identity.

Several studies observed an activation of the ubiquitin-proteasome system in tumor cells, which strongly depend on proteasomal protein degradation due to their high proliferation capacity, but the knowledge on the regulation of the proteasome and its activators in lung cancer is very limited ((Arlt et al., 2009; Chen and Madura, 2005; Shen et al., 2013). Therefore, the here observed increased PA200 expression in tumor cells of the lung is a so far unknown aspect of proteasome regulation in lung cancer and suggests that PA200 upregulation is a common feature of (hyper-)proliferative cells and tissues.

7.3.2 Characterization of PA200 in the cell

7.3.2.1 PA200 localizes to both cytosolic and nuclear compartments of the cell

So far PA200 has been considered as a nuclear protein because a nuclear localization signal was discovered within the sequence of the human gene (Ustrell et al., 2002). Interestingly, homologs of the activator in *Saccharomyces cerevisiae*, *Arabidopsis thaliana* and *Caenorhabditis elegans* do not contain such a nuclear targeting sequence, but their sequence homology of 17-29 % with the human protein is also very low (Ustrell et al., 2002).

Cellular localization of PA200 has only been analyzed by immunofluorescence staining in two studies by Ustrell *et al.* and Qian *et al.* (Qian et al., 2013; Ustrell et al., 2002). However, as discussed in section 5.3.2, both studies used non-specific antibodies and thus obtained results are not reliable. Indeed, immunocytochemistry (ICC) is the most reliable method for

cellular localization of proteins, but it requires the use of specific antibodies compatible with the applied staining conditions, especially with the fixation of cells. Testing a variety of antibodies and conditions for ICC of PA200 in the present study did not produce reliable results in PA200-silenced cells and controls (data not shown); Thus, PA200 can only be trustworthily detected by IHC and immunofluorescence staining of tissues. Here, staining of human and mouse tissue sections with two validated PA200 antibodies provided first reliable evidence for localization of the activator indicating that PA200 localizes mainly to the nucleus but is also present in the cytosol of cells in healthy and diseased lung tissue. In this context, the interactome analysis also revealed that many cytosolic proteins, such as ribosomal proteins, co-immunoprecipitated with PA200. Therefore, this study provides very exciting and new insights into the localization of the activator and contradicts the general notion that PA200 is an exclusively nuclear protein.

Blickwedehl *et al.* analyzed the solubility profile of PA200 in response to digitonin extraction or crosslinking of cellular proteins with PFA and proposed that the 200 kDa protein is, although partially soluble, also associated with cellular components because PA200 was only detected in the pellets of lysates from PFA-fixed cells (Blickwedehl *et al.*, 2007). In contrast, in the present study PA200 was efficiently extracted by cell lysis under detergent-free and non-denaturing conditions when compared to extraction of the remaining pellet in RIPA buffer (data not shown). Moreover, using the histone extraction protocol PA200 was only detected in the soluble fraction and not found in association with chromatin (data not shown), which is also contradictory to the previously reported detection of PA200 in chromatin fractions of HeLa cells (Blickwedehl *et al.*, 2007). Concluding, these observations suggest that PA200 is not tightly associated with cellular components in pHLF, especially not of the nuclear compartment. The here discovered discrepancy regarding the solubility of PA200 might have two reasons: First, analysis of protein association with cellular compartments by PFA fixation of cells or cell lysis with buffers of varying degrees of stringency as performed by Blickwedehl *et al.* is a very artificial setting and can lead to misinterpretation of results. Or second, PA200 is differentially associated with cellular components in different cell types.

7.3.2.2 PA200 mainly associates with the constitutive 20S proteasome in pHLF

Several studies observed the association of PA200 with the proteasome forming 20S singly- and doubly-capped as well as 26S hybrid alternative proteasome complexes using qualitative approaches involving co-IP of the 20S core particle (Blickwedehl et al., 2007; Fabre et al., 2013, 2014, 2015; Ustrell et al., 2002). Ortega and colleagues analyzed PA200-20S proteasomes isolated by anion exchange chromatography and gradient gel centrifugation with electron microscopy and observed that PA200 interacts with all subunits of the α -ring except $\alpha 7$ thereby forming an opening into the particle and that PA200 binding to the 20S proteasome induces opening of its axial channel (Ortega et al., 2005). The determination of the interaction stoichiometry between PA200 and other proteasomal subunits by proteomic analysis of PA200 co-immunoprecipitating proteins is a novel approach because it allows for a quantitative assessment of all PA200 alternative proteasome complexes in cell extracts.

Although the PA200 interactome was strongly adapting to cellular growth conditions, association of the activator with the proteasome was observed under all applied settings. Here, PA200 was preferentially associated with subunits of the constitutive 20S proteasome as it was only poorly interacting with immunoproteasome subunits that are, however, generally low expressed in non-immune cells. Nevertheless, this observation accords well with a previous study by Fabre *et al.* analyzing protein abundance correlation of affinity purified 20S complexes and interacting proteins in nine different human cell lines (Fabre et al., 2015). In the same context, Blickwedehl *et al.* reported that PA200 is not regulated by INF γ and interacted with 20S proteasomes in LMP2- and LMP7-deficient HeLa cells (Blickwedehl et al., 2007).

In pHLF, PA200 is associated with the constitutive proteasome subunits at an interaction stoichiometry ratio of approximately 1. The interaction with 19S regulatory subunits forming PA200-26S hybrid complexes was substantially lower, which accords well with native gel analysis of PA200 alternative proteasomes in pHLF extracts. Using electron microscopy analysis of 20S proteasomes isolated from bovine testis, Ortega *et al.* proposed that 50 % of isolated 20S was uncapped, 40 % of 20S was PA200 singly capped and 10 % of 20S proteasomes were PA200 doubly capped (Ortega et al., 2005). In contrast, results of the present study suggest that 20S particles are mainly singly capped in pHLF under the applied conditions. However, composition of PA200 alternative proteasome complexes may vary among different cellular conditions and cell types, as the activator also shows a differential

expression pattern in different organs including a much higher expression in testis when compared to the lung (Ustrell et al., 2002). Moreover, isolation of proteasome complexes and electron microscopy as performed by Ortega et al. is a rather time consuming and harsh process, which in the end might not totally reflect the cellular situation.

Interestingly, LC-MS/MS analysis revealed that PA28 α , PA28 β and PA28 γ interact with PA200. This provides first evidence for the formation of mixed alternative proteasome complexes composed of two different activators associated with the 20S core particle. It requires further analysis to determine whether those particles have distinct functions or if they are bi-functional and exert activator-specific functions simultaneously at both sides of the 20S core particle.

7.3.2.3 PA200 is regulated according to cellular growth and activation

PA200 expression and association with proteasome was significantly enhanced in pHLF cultured under growth conditions in cell culture medium containing 10 % FBS compared to 1 % FBS, which accorded well with increased levels of proliferation markers. Moreover, the present study also observed induction of PA200 alternative proteasome complexes in TGF- β 1-induced myofibroblasts, which are characterized by an activated phenotype involving induction of SMAD and AKT signaling, increased invasion capacity, survival and secretion of ECM components (Clark et al., 1997; Hinz et al., 2007; Horowitz et al., 2004). Of note, analysis of the PA200 interactome upon these different cellular stimuli indicated that not only the expression of the activator but also its interaction with other proteins strongly adapts to growth and activation of pHLF.

Expression of PA200 was also significantly induced in non-differentiated basal cells when compared to differentiated pHBEs. Basal cells are self-renewing, multi-potent progenitor cells of the lung airway epithelium which can differentiate into Club cells, goblet cells and ciliated cells and thus play an important role in regeneration of the lung epithelium (Hong et al., 2006; Rock et al., 2009). PA200 expression mainly declined between day 0 and 7 of their differentiation, when expression of proliferation and basal cell markers is also largely decreasing (unpublished data of Dr. A. Schamberger, postdoctoral scientist at the CPC). Therefore, PA200 expression levels accord well with the self-renewing state of these cells.

Although ubiquitin-dependent protein degradation has been observed in a variety of different settings to be co-regulated with cellular proliferation and increased proteasome activity was recently reported to be essential for maintenance of pluripotency in human embryonic stem cells, the regulation of alternative proteasome activators in these processes has not been investigated so far (Ichihara and Tanaka, 1995; Vilchez et al., 2012). Therefore, this study provides first evidence for the regulation of PA200 alternative proteasome complexes depending on cellular proliferation and activation and thereby describes a new aspect of regulation of proteasome function according to cellular stimuli.

7.3.2.4 PA200 regulates activation, proliferation and survival of pHLF

PA200 is not essential for cellular function, as PA200^{-/-} mice do not show any distinct phenotype except from defects in spermatogenesis (Khor et al., 2006). Moreover, pHLF coped well with silencing of the activator. Although PA200 is ubiquitously expressed in different organs and cell types, its expression - except from testis - is rather low (Ustrell et al., 2002). Analyzing the interaction of the 20S proteasome with different activators in 9 human cell lines, Fabre *et al.* discovered a very low abundance of PA200 alternative proteasomes comprising less than 5 % of all proteasome complexes (Fabre et al., 2014). The present study also observed that expression in the healthy lung is very low and that the amount of PA200 alternative complexes is tightly regulated according to cellular growth or activation. However, loss of the small cellular pool of PA200 alternative proteasomes induced a remarkably strong cellular phenotype suggesting that these complexes have an important function and are tightly regulated to ensure proper cell function.

Gene expression profiling in response to PA200 silencing in pHLF using transcriptomic and proteomic screens revealed a so far unrecognized induction of cellular proliferation and survival, which was validated by *in vitro* experiments in these cells.

Protein kinase AKT was significantly activated in response to PA200 silencing. This observation corresponds well to activation of proliferation and survival predicted by molecular function analysis of regulated genes and proteins upon PA200 silencing. AKT is a central signaling pathway of the cell regulating survival and also proliferation of cells via a plethora of mechanisms (Manning and Cantley, 2007). PA200 silencing also strongly induced proliferation of pHLF, which accorded well with increased mRNA and protein expression of

the proliferation marker and cell cycle regulator cyclin D1. Moreover, enhanced expression of the myofibroblast marker α SMA and the cytokine TGF- β 1 point towards an activated, myofibroblast-like phenotype upon PA200 silencing. In this context, molecular function analysis of regulated genes upon PA200 silencing also indicates the activation of processes that are characteristic for a myofibroblast-like phenotype, such as activation of cell spreading, microtubule dynamics as well as organization of cytoplasm and cytoskeleton. These data are partly in line with a study in HeLa cells by Blickwedehl *et al.*, who observed that PA200 silencing enhances proliferation and activates the mTOR target ribosomal S6 kinase in serum-starved cells and that this effect depends on glutamine supplementation (Blickwedehl *et al.*, 2012). In the present study, induction of mTOR signaling was not observed (data not shown), although AKT serves as a major upstream regulator of the mTOR pathway (Laplane and Sabatini, 2012). These differences might result from the fact that both studies used different cell types – immortalized cancer cells versus primary cells – and differential serum conditions.

PA200 silencing also induced proteasome activity and formation of standard 20S, 26S and 30S proteasome complexes in phLF suggesting a general adaption of proteasome activity according to cellular proliferation and activation. Regulation of protein degradation according to cellular growth and activity has been suspected for a long time, as cell cycle progression for example is largely depending on proteasomal degradation, and proteasome function is important for amino acid recycling (Hershko, 1997; Suraweera *et al.*, 2012; Vabulas and Hartl, 2005). However, analysis of the exact mechanism in a complex cellular environment is challenging and results presumably largely depend on the applied experimental setup. Recently, regulation of the proteasome according to cellular growth was controversially discussed in the context of mTOR signaling but the exact mechanism and differential findings of these studies require further investigation (Zhang *et al.*, 2014; Zhao *et al.*, 2015).

Beside the induction of proliferation, transcriptomic and proteomic analyses also revealed downregulation of CASP3 and FAS, which are both important components of the apoptotic cascade. This is a completely new and exciting finding, as PA200 has not been described as a regulator of apoptosis so far. Downregulation of CASP3 protein levels was validated by Western blotting showing a strong decrease over time. Moreover, the activation of the apoptotic cascade was significantly impaired in PA200-deficient phLF upon treatment with

the apoptosis-inducer staurosporine, which inhibits protein kinases by binding to their ATP binding sites (Karaman et al., 2008). Concluding from these observations, downregulation of apoptotic proteins by PA200 silencing decreases the ability of pHLF to undergo apoptosis, which accords well with activation of AKT signaling in these cells. The AKT pathway is a prominent regulator of cellular survival by increasing cellular growth and proliferation and decreasing apoptosis at the same time *via* a plethora of downstream targets (Manning and Toker, 2017; Zhang et al., 2011). AKT activation for example decreases apoptotic signaling by phosphorylation and inactivation of pro-apoptotic signals, such as the Bcl-2-associated death promoter (BAD) and different forkhead box (FoxO) transcription factors driving transcription of apoptosis-inducing genes.

The regulation of cellular apoptosis by PA200 is a completely new finding, as so far survival of cells upon PA200 silencing has only been analyzed in response to radiation treatment in HeLa cells, but neither the basal difference in survival between PA200-expressing and -deficient cells nor effects on cellular apoptosis have been investigated (Blickwedehl et al., 2008).

Resistance to apoptosis is a widely discussed phenotype of both normal lung fibroblasts as well as myofibroblast of the fibrotic lung (Thannickal and Horowitz, 2006). Upon normal tissue injury, the physiological function of activated myofibroblasts is to secrete ECM components providing a scaffold for migration of epithelial cells and to facilitate wound closure due to their contractile function thereby allowing for re-epithelialization (Martin, 1997; Singer and Clark, 1999). Proper restoration of the tissue also requires resolution of the ECM scaffold and apoptosis of myofibroblasts (Desmoulière et al., 1995). Fibrotic tissue remodeling is described as dysregulated wound healing process leading to excess deposition of ECM and persistence of myofibroblasts (Thannickal et al., 2004). Low levels of apoptosis have been observed in myofibroblasts of human IPF tissues, and fibroblasts isolated from normal and IPF lungs were described to be resistant to apoptosis (Frankel et al., 2006; Plataki et al., 2005; Tanaka et al., 2002; Uhal et al., 1998). However, so far there has been no conclusive evidence that the persistence of myofibroblasts in the fibrotic lung is caused by resistance to apoptotic signaling. Although several mediators of apoptosis resistance in fibroblasts have been proposed, the exact mechanism still needs to be clarified (Ajayi et al., 2013; Bühling et al., 2005; Im et al., 2016). Therefore, the discovery of PA200 as a regulator of

apoptosis in pHLF is a novel and exciting finding describing a so far unrecognized function of this proteasome activator.

Taken together, this study provides novel insights into the function of PA200 in pHLF. The observation that inactivation of PA200 function drives activation, proliferation and survival of pHLF suggests that it functions as a negative regulator of these processes in pHLF. The underlying mechanism, however, will be the subject of future studies.

Of note, enhanced AKT signaling, proliferation, metabolic activity, and apoptosis resistance point towards induction of a myofibroblast-like phenotype upon loss of PA200 function. This observation is in striking contrast to increased PA200 protein levels in TGF- β 1-differentiated myofibroblasts, myofibroblasts of IPF tissues and tumor cells of lung cancer biopsies, as both of these cell types are characterized by increased proliferation and survival (Figure 7.41). Therefore, upregulation of PA200 might represent the frustrated cellular attempt to limit cellular growth and survival in diseased tissues. The exact molecular mechanism describing how PA200 silencing induces activation, proliferation and survival in pHLF needs to be investigated in future studies. Taking into account that PA200 is a proteasome activator mediating the degradation of certain proteins, the potential substrate could be a driver of cellular proliferation and survival that is strongly induced in myofibroblast and also cancer cells. However, this is rather speculative as the function of PA200 with regard to degradation of specific substrates is unclear, as discussed in the following section. Moreover, as PA200 silencing increased proteasome activity in pHLF, PA200 could also be a regulator of 26S proteasome function by competing with the 19S regulator for binding to the 20S proteasome core complex. Lastly, PA200 might function as an adaptor protein thereby not being directly involved in protein degradation but rather targeting proteasome complexes to defined subcellular localizations.

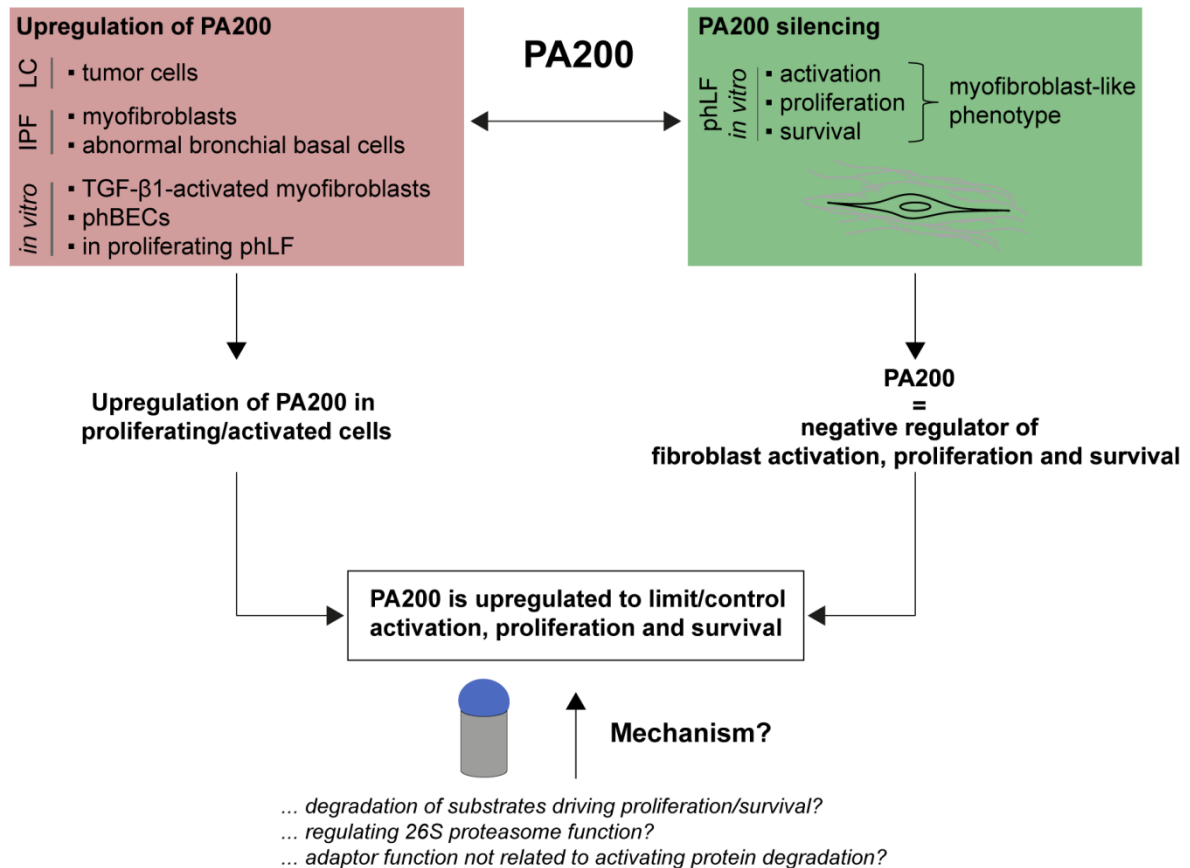


Figure 7.41: Scheme of PA200 function in the lung. Upregulation of PA200 was observed in myofibroblasts and abnormal bronchial basal cells of IPF tissues, which accords well with increased PA200 expression in these cells *in vitro* at conditions of TGF- β 1- or serum-induced cell growth. This suggests a general induction of PA200 alternative proteasomes in activated or proliferating cells. In contrast to these observations, silencing of PA200 in phLF induced activation, proliferation and survival constituting a myofibroblast-like phenotype. This suggests that PA200 is a negative regulator of fibroblast activation, proliferation and survival and is therefore induced in diseased tissues to limit these processes. Elucidating the exact underlying mechanism will be subject of future studies but could involve the following: PA200 mediates degradation of specific substrates driving proliferation or survival of fibroblasts; PA200 regulates activity of 26S proteasomes; PA200 serves as an adaptor molecule localizing proteasomes to certain cellular compartments and is not directly involved in the degradation of proteins.

7.3.2.5 Defining the exact molecular mechanism of PA200 function remains challenging

Since the first description of PA200 as a proteasomal activator, a variety of different hypotheses regarding its exact mechanism of action have been proposed. The first study in 2002 investigating the function of human PA200 claimed that the activator preferentially stimulates C-L activity of the 20S proteasome and only facilitates the degradation of peptides but not of intact proteins (Ustrell et al., 2002). In contrast, in the present study silencing of PA200 led to an increase of proteasome activity and formation of proteasome complexes in phLF. Moreover, the amount of PA200 bound to the proteasome in the cell is

rather low with only 5 % of 20S complexes being associated with the activator, which hinders detection of changes in proteasome activity mediated through activation of 20S complexes by PA200 (Fabre et al., 2014). Ustrell and colleagues also hypothesized that PA200 could antagonize protein degradation by competing with a 19S regulator for binding to the 20S core particle. In a later study Ortega *et al.* showed that binding of PA200 to the 20S core complexes triggers opening of its axial channel supporting its function as a proteasome activator (Ortega et al., 2005). Reviewing PA200 literature, Savulescu *et al.* proposed that by forming hybrid complexes with the 26S proteasome PA200 could also function as a peptide flusher accelerating the exit of cleaved peptides (Savulescu and Glickman, 2011). Moreover, they also hypothesized that PA200 might mediate degradation of damaged or misfolded proteins or even unfolded and defective proteins sequestered by ribosomes in an ubiquitin-independent fashion. Indeed, Qian *et al.* have been the first and only ones so far claiming that PA200 mediates degradation of certain substrates (Qian et al., 2013). They proposed that PA200 facilitates ubiquitin-independent proteasomal degradation of acetylated core histones during spermatogenesis and DNA damage. Moreover, they concluded that acetylated histones are specifically recognized via the bromodomain-like region of PA200. However, this study has major deficits questioning the specific degradation of histones, although the observations accord well with the early finding that PA200 is essential for normal spermatogenesis (Khor et al., 2006; Qian et al., 2013). For example, the applied PA200^{-/-} mouse model encompasses only deletion of exons 25 and 26 out of in total 45 coding exons of the PA200 gene and is thus not a full knockout (Qian et al., 2013). Moreover, Western blot analysis and immunostaining of tissues and cells suggest that the applied PA200 antibody is not specific for recognition of the protein and proper controls are missing. Finally, this study claims to observe the same function for human PA200 and its yeast analogue Blm10, which are only poorly conserved and most probably have different functions. In the present study, the effect of PA200 silencing and overexpression on the regulation of total and acetylated histones was analyzed and did not confirm that PA200 mediates degradation of acetylated histones in pHLF.

Identification of potential substrates of PA200 is a very challenging approach for several reasons. First, PA200 was observed to tightly interact with the 20S proteasome, which impedes the detection of direct interactors of the activator. Here in this study, the interactome analysis discovered a variety of proteins binding to the activator, and many of

them were also detected in a pulldown of the 20S proteasome followed by proteomic analysis (data not shown). Therefore, it is difficult to judge whether a protein directly interacts with PA200 or whether it interacts with PA200 via the 20S proteasome. THBS1, which was identified in the PA200 interactome, was still associated with the 20S proteasome in PA200-deficient cells. These data suggest that THBS1 - and potentially also other proteins identified in the co-IP of PA200 - interact with the activator via the 20S proteasome. And second, the degradation of a potential substrate is a very fast process and therefore the interaction of this substrate with PA200 might occur within a very limited amount of time, which hinders proper detection of substrates *via* mass spectrometry (Peth et al., 2013).

Crosslinking mass spectrometry (XL-MS) is a promising approach for future studies to detect proteins that are directly interacting with PA200 ((Liu et al., 2015). This method involves linkage of amino acids in close proximity within a protein extract with an MS-cleavable linker and subsequent analysis of linked peptides by LC-MS/MS. Thus, this method provides not only information on the interaction but also on the structure of proteins and protein complexes. Although at the moment XL-MS requires further optimization because resolution for detection of cross-linked fragments and their exact annotation are limited, it is a very promising method for detection of direct protein-protein interacts in the future.

However, observations from this and other studies suggest that PA200 might function as an adaptor protein and is therefore only indirectly regulating protein degradation. Adaptor proteins interact with protein binding partners *via* specific protein binding modules and can thereby organize large protein complexes in a spatial and temporal manner (Flynn, 2001; Pawson, 1997). Bringing specific proteins together, they are important mediators of signaling cascades as they transfer signals to specific protein complexes or subcellular compartments, for example during signal transduction *via* receptor tyrosine kinases from the cell surface into the cytosol. Another proteasome interacting protein, ECM29, has been suggested to act as an adaptor protein coupling proteasomes to the microtubules, the centrosome, the endocytic vesicles and the endoplasmic reticulum in mammalian cells (Gorbea et al., 2004, 2010). Similar to PA200, ECM29 is a 200 kDa monomer composed of HEAT repeats that binds to the 26S proteasome and localizes to distinct cellular compartments supporting its role as an adaptor protein (Gorbea et al., 2010; Kajava et al., 2004).

For several reasons, it is tempting to speculate that PA200 also functions as an adaptor: First, as several other adaptor molecules, PA200 is a monomeric protein composed of HEAT

repeats (Andrade et al., 2001; Kajava et al., 2004; Kobe et al., 1999). Second, it strongly interacts with the 20S proteasome. However, recent studies on human PA200 or its yeast homologue Blm10 concluded that its pore is too small to facilitate entry of intact proteins to the catalytic core and could therefore only mediate uptake of unstructured peptides, which points towards a function not directly related to protein degradation (Ortega et al., 2005; Sadre-Bazzaz et al., 2010). Third, in the present study PA200 alternative proteasome complexes interacted mainly with ribosomal proteins and hnRNPs suggesting that PA200 alternative proteasomes might preferentially localize to these cellular compartments, which accords well with its cytosolic and nuclear expression. And fourth, beside the regulation of PA200 expression according to cellular proliferation and activation, silencing of PA200 strongly induced cellular survival, which both points towards a regulation of major cellular signaling pathways as it is the case for many adaptor proteins (Flynn, 2001). And lastly, analysis of gene expression in pHLF upon PA200 silencing by transcriptomic and proteomic screens revealed a similar regulation on mRNA and protein level. Here, genes that were strongly induced on their protein level were mostly regulated *via* mRNA expression. Assuming that PA200 targets specific substrates for degradation and that these proteins accumulate upon silencing of the activator, genes only regulated on protein level were of particular interest for this analysis. However, proteins that were exclusively altered on the protein level showed a similar extent of up- and downregulation and were mainly found to be only induced. Therefore, the analysis did not clearly display potential substrates of PA200. All these aspects suggest that PA200 might function as an adaptor protein to localize proteasomes to ribosomes and hnRNPs thereby adjusting previously described proteasomal protein degradation during ribosome biogenesis or protein synthesis (Stavreva et al., 2006; Turner and Varshavsky, 2000). Moreover, having an NLS and localizing to both the cytosol and nucleus, PA200 could theoretically also shuttle proteasome complexes between these compartments, as recently described for its yeast homologue Blm10 (Chowdhury and Enekel, 2015; Weberruss et al., 2013).

Concluding, evidence for a function of PA200 in mediating the degradation of specific substrates has been very limited so far. Although degradation of one or more proteins driving cell growth and survival would provide a logical explanation for the cellular phenotype observed in PA200-deficient pHLF, other modes of action have to be considered.

8 Concluding remarks

In the present thesis, the role of alternative activators was dissected in lung biology and disease with a particular focus on the fast adaption of alternative activator complexes according to cellular stimuli and the regulation and function of the proteasome activator PA200 in hyperproliferative lung diseases.

In the first part of the study, specificity testing of a widely used PA200 antibody revealed that this antibody is not specific for detection of the activator but also recognizes a protein species, which - in contrast to the statement of an early publication by Ustrell and colleagues - is not related to PA200 (Ustrell et al., 2002). This is an important finding, as many observations on the function and regulation of PA200 are based on experiments using this antibody and thus need to be considered with caution. Therefore, the findings of the initial study of the present thesis illustrate the importance of careful validation of antibody specificity using siRNAs or knockout mice.

In the second part of the study, the regulation of alternative proteasome complexes was investigated in response to proteotoxic stress caused by proteasome inhibition. Here, a strong and fast recruitment of the alternative activators PA28 γ and PA200 to the proteasome was observed. This is a very exciting finding, as it provides first evidence for the previously proposed building block concept predicting that recruitment of proteasome activators to the proteasome represents one possibility to quickly adapt proteasome function to cellular needs.

The third part of this study provided first evidence for a regulation of PA200 in diseased tissues and discovered novel aspects on its function in pHLF which largely extends the until now limited knowledge on the activator. Here, the upregulation of PA200 in fibrotic tissue remodeling as well as tumor cells of different lung cancer subtypes accorded well with the observation that PA200 is regulated according to cellular growth and activity. PA200 was discovered to be controlled on different levels, including its expression, its recruitment to the proteasome and its interactome. Moreover, the functional analysis of PA200 in pHLF discovered the activator as a novel regulator of cellular activation, proliferation and survival.

In conclusion, the here obtained results support the idea that proteasome function is regulated according to cellular needs on the level of activator recruitment to the 20S

proteasome complex, as proposed by the building block concept (Figure 8.1). Moreover, the here performed studies largely extend the so far limited knowledge on PA200 by identifying it as a novel regulator of cellular activation and survival and observing its induction in hyperproliferative lung disease, such as IPF and lung cancer. The results thereby further validate the building block concept and provide novel aspects for the pathogeneses of both diseases.

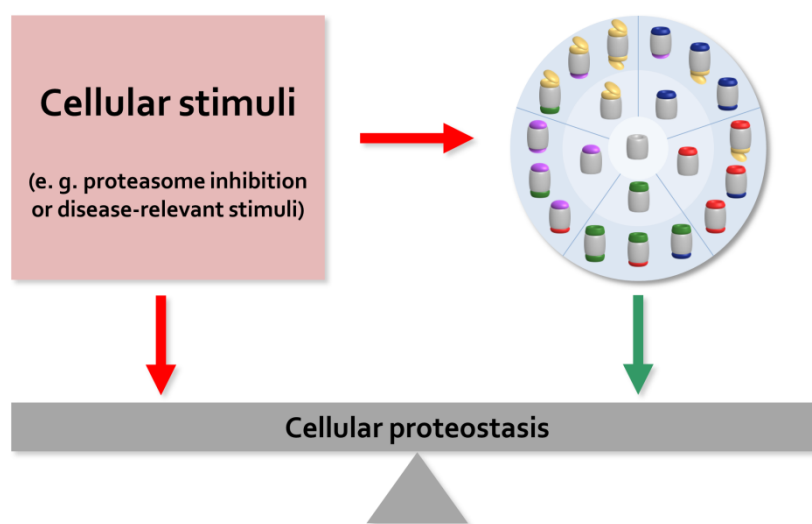


Figure 8.1: The building block concept. In order to maintain cellular proteostasis, proteasome function can be quickly adapted according to cellular stimuli, such as inhibition of proteasome function or disease-relevant stimuli, *via* formation of the different proteasome complexes upon recruitment of proteasome activators to the 20S core complex.

Although the present and recent studies have contributed to a better understanding of alternative proteasome activators, further studies are required to dissect their exact function in more detail. One controversially discussed and fundamental question is whether these alternative activators are actually able to facilitate the degradation of intact proteins. Several studies reported that the pore of these activators is actually too small to allow for the entry of intact proteins and therefore can only facilitate the entry of small, unfolded peptides, which challenges the general concept that these activators mediate the degradation of specific proteins. Especially for PA200 several different mechanisms explaining how the activator regulates cellular survival and proliferation are plausible beyond a function in promoting degradation of specific substrates: first, PA200 may function as a placeholder by binding to 20S proteasomes and thereby controlling the association of the 20S core with the 19S regulator; second, it may function as shuttle protein bringing specific proteins in close

proximity to the proteasome; and third, PA200 may function as an adaptor bringing proteasomes to distinct cellular compartments. In this regard, the development of inhibitors for the specific interaction of an alternative proteasome activator with the 20S proteasome will allow for more detailed characterization of their mechanism of action and may also provide a new therapeutic tool for diseases that are related to increased formation of PA200 alternative proteasome complexes.

9 References

- Acosta-Alvear, D., Cho, M.Y., Wild, T., Buchholz, T.J., Lerner, A.G., Simakova, O., Hahn, J., Korde, N., Landgren, O., Maric, I., Choudhary, C., Walter, P., Weissman, J.S., and Kampmann, M. (2015). Paradoxical resistance of multiple myeloma to proteasome inhibitors by decreased levels of 19S proteasomal subunits. *Elife* 4, e08153.
- Ajayi, I.O., Sisson, T.H., Higgins, P.D.R., Booth, A.J., Sagana, R.L., Huang, S.K., White, E.S., King, J.E., Moore, B.B., and Horowitz, J.C. (2013). X-linked inhibitor of apoptosis regulates lung fibroblast resistance to fas-mediated apoptosis. *Am. J. Respir. Cell Mol. Biol.* 49, 86–95.
- Anan, A., Baskin-Bey, E.S., Bronk, S.F., Werneburg, N.W., Shah, V.H., and Gores, G.J. (2006). Proteasome inhibition induces hepatic stellate cell apoptosis. *Hepatology* 43, 335–344.
- Andrade, M.A., Perez-Iratxeta, C., and Ponting, C.P. (2001). Protein Repeats: Structures, Functions, and Evolution. *J. Struct. Biol.* 134, 117–131.
- Araya, J., Kojima, J., Takasaka, N., Ito, S., Fujii, S., Hara, H., Yanagisawa, H., Kobayashi, K., Tsurushige, C., Kawaishi, M., Kamiya, N., Hirano, J., Odaka, M., Morikawa, T., Nishimura, S.L., Kawabata, Y., Hano, H., Nakayama, K., et al. (2013). Insufficient autophagy in idiopathic pulmonary fibrosis. *AJP Lung Cell. Mol. Physiol.* 304, L56–L69.
- Arciniega, M., Beck, P., Lange, O.F., Groll, M., and Huber, R. (2014). Differential global structural changes in the core particle of yeast and mouse proteasome induced by ligand binding. *Proc. Natl. Acad. Sci. U. S. A.* 111, 9479–9484.
- Arlt, A., Bauer, I., Schafmayer, C., Tepel, J., Mürköster, S.S., Brosch, M., Röder, C., Kalthoff, H., Hampe, J., Moyer, M.P., Fölsch, U.R., and Schäfer, H. (2009). Increased proteasome subunit protein expression and proteasome activity in colon cancer relate to an enhanced activation of nuclear factor E2-related factor 2 (Nrf2). *Oncogene* 28, 3983–3996.
- Armanios, M.Y., Chen, J.J.-L., Cogan, J.D., Alder, J.K., Ingersoll, R.G., Markin, C., Lawson, W.E., Xie, M., Vulto, I., Phillips, J.A., Lansdorp, P.M., Greider, C.W., and Loyd, J.E. (2007). Telomerase Mutations in Families with Idiopathic Pulmonary Fibrosis. *N. Engl. J. Med.* 356, 1317–1326.
- Arrigo, A.P., Tanaka, K., Goldberg, A.L., and Welch, W.J. (1988). Identity of the 19S “prosome” particle with the large multifunctional protease complex of mammalian cells (the proteasome). *Nature* 331, 192–194.
- Bader, M., Benjamin, S., Wapinski, O.L., Smith, D.M., Goldberg, A.L., and Steller, H. (2011). A conserved F box regulatory complex controls proteasome activity in *Drosophila*. *Cell* 145, 371–382.
- Baker, M. (2015). Reproducibility crisis: Blame it on the antibodies. *Nature* 521, 274–276.
- Balch, W.E., Morimoto, R.I., Dillin, A., and Kelly, J.W. (2008). Adapting Proteostasis for Disease Intervention. *Science* 319, 916–919.
- Balch, W.E., Sznajder, J.I., Budinger, S., Finley, D., Laposky, A.D., Cuervo, A.M., Benjamin, I.J., Barreiro, E., Morimoto, R.I., Postow, L., Weissman, A.M., Gail, D., Banks-Schlegel, S., Croxton, T., and Gan, W. (2014). Malfolded protein structure and proteostasis in lung diseases. *Am. J. Respir. Crit. Care Med.* 189, 96–103.
- Bataller, R., and Brenner, D. (2005). Liver fibrosis. *J. Clin. Invest.* 115, 209–218.

- Baugh, J., Viktorova, E., and Pilipenko, E. (2009). Proteasomes can degrade a significant proportion of cellular proteins independent of ubiquitination. *J. Mol. Biol.* *386*, 814–827.
- Baumgartner, K.B., Samet, J.M., Coultas, D.B., Stidley, C.A., Hunt, W.C., Colby, T. V, and Waldron, J.A. (2000). Occupational and environmental risk factors for idiopathic pulmonary fibrosis: a multicenter case-control study. Collaborating Centers. *Am. J. Epidemiol.* *152*, 307–315.
- Beck, P., Dubiella, C., and Groll, M. (2012). Covalent and non-covalent reversible proteasome inhibition. *Biol. Chem.* *393*, 1101–1120.
- Ben-Nissan, G., and Sharon, M. (2014). Regulating the 20S proteasome ubiquitin-independent degradation pathway. *Biomolecules* *4*, 862–884.
- Berglund, L., Björling, E., Oksvold, P., Fagerberg, L., Asplund, A., Al-Khalili Szigartyo, C., Persson, A., Ottosson, J., Wernérus, H., Nilsson, P., Lundberg, E., Sivertsson, Å., Navani, S., Wester, K., Kampf, C., Hober, S., Pontén, F., and Uhlén, M. (2008). A Genecentric Human Protein Atlas for Expression Profiles Based on Antibodies. *Mol. Cell. Proteomics* *7*, 2019–2027.
- Bieler, S., Meiners, S., Stangl, V., Pohl, T., and Stangl, K. (2009). Comprehensive proteomic and transcriptomic analysis reveals early induction of a protective anti-oxidative stress response by low-dose proteasome inhibition. *Proteomics* *9*, 3257–3267.
- Blickwedehl, J., McEvoy, S., Wong, I., Kousis, P., Clements, J., Elliott, R., Cresswell, P., Liang, P., and Bangia, N. (2007). Proteasomes and proteasome activator 200 kDa (PA200) accumulate on chromatin in response to ionizing radiation. *Radiat. Res.* *167*, 663–674.
- Blickwedehl, J., Agarwal, M., Seong, C., Pandita, R.K., Melendy, T., Sung, P., Pandita, T.K., and Bangia, N. (2008). Role for proteasome activator PA200 and postglutamyl proteasome activity in genomic stability. *Proc. Natl. Acad. Sci. U. S. A.* *105*, 16165–16170.
- Blickwedehl, J., Olejniczak, S., Cummings, R., Sarvaiya, N., Mantilla, A., Chanan-Khan, A., Pandita, T.K., Schmidt, M., Thompson, C.B., and Bangia, N. (2012). The proteasome activator PA200 regulates tumor cell responsiveness to glutamine and resistance to ionizing radiation. *Mol. Cancer Res.* *10*, 937–944.
- Book, A.J., Gladman, N.P., Lee, S.S., Scalf, M., Smith, L.M., and Vierstra, R.D. (2010). Affinity purification of the Arabidopsis 26 S proteasome reveals a diverse array of plant proteolytic complexes. *J. Biol. Chem.* *285*, 25554–25569.
- Bordeaux, J., Welsh, A.W., Agarwal, S., Killiam, E., Baquero, M.T., Hanna, J.A., Anagnostou, V.K., and Rimm, D.L. (2010). Antibody validation. *Biotechniques* *48*, 197–209.
- Bowerman, B. (2006). Degrade to create: developmental requirements for ubiquitin-mediated proteolysis during early *C. elegans* embryogenesis. *Development* *133*, 773–784.
- Bradbury, A., and Plückthun, A. (2015). Reproducibility: Standardize antibodies used in research. *Nature* *518*, 27–29.
- Brannigan, J.A., Dodson, G., Duggleby, H.J., Moody, P.C.E., Smith, J.L., Tomchick, D.R., and Murzin, A.G. (1995). A protein catalytic framework with an N-terminal nucleophile is capable of self-activation. *Nature* *378*, 416–419.

- Bremnes, R.M., Dønnem, T., Al-Saad, S., Al-Shibli, K., Andersen, S., Sirera, R., Camps, C., Marinez, I., and Busund, L.-T. (2011). The Role of Tumor Stroma in Cancer Progression and Prognosis: Emphasis on Carcinoma-Associated Fibroblasts and Non-small Cell Lung Cancer. *J. Thorac. Oncol.* 6, 209–217.
- Brosch, M., Yu, L., Hubbard, T., and Choudhary, J. (2009). Accurate and sensitive peptide identification with mascot percolator. *J. Proteome Res.* 8, 3176–3181.
- Bühling, F., Wille, A., Röcken, C., Wiesner, O., Baier, A., Meinecke, I., Welte, T., and Pap, T. (2005). Altered expression of membrane-bound and soluble CD95/Fas contributes to the resistance of fibrotic lung fibroblasts to FasL induced apoptosis. *Respir. Res.* 6, 37.
- Cabrera, S., Maciel, M., Herrera, I., Nava, T., Vergara, F., Gaxiola, M., Lopez-Otín, C., Selman, M., and Pardo, A. (2015). Essential role for the ATG4b protease and autophagy in bleomycin-induced pulmonary fibrosis. *Autophagy* 11, 670–684.
- Cavazza, A., Rossi, G., Carbonelli, C., Spaggiari, L., Paci, M., and Roggeri, A. (2010). The role of histology in idiopathic pulmonary fibrosis: An update. *Respir. Med.* 104, S11–S22.
- Chai, F., Liang, Y., Bi, J., Chen, L., Zhang, F., Cui, Y., Bian, X., and Jiang, J. (2014). High expression of REGγ is associated with metastasis and poor prognosis of patients with breast cancer. *Int J Clin Exp Pathol* 7, 7834–7843.
- Chen, L., and Madura, K. (2005). Increased proteasome activity, ubiquitin-conjugating enzymes, and eEF1A translation factor detected in breast cancer tissue. *Cancer Res.* 65, 5599–5606.
- Chen, X., Barton, L.F., Chi, Y., Clurman, B.E., and Roberts, J.M. (2007). Ubiquitin-independent degradation of cell-cycle inhibitors by the REGγ proteasome. *Mol. Cell* 26, 843–852.
- Chowdhury, M., and Enenkel, C. (2015). Intracellular Dynamics of the Ubiquitin-Proteasome-System. *F1000Research* 367, 1–17.
- Ciechanover, A., and Schwartz, A.L. (1998). The ubiquitin-proteasome pathway: the complexity and myriad functions of proteins death. *Proc. Natl. Acad. Sci. U. S. A.* 95, 2727–2730.
- Ciechanover, A., Hod, Y., and Hershko, A. (1978). A heat-stable polypeptide component of an ATP-dependent proteolytic system from reticulocytes. *Biochem. Biophys. Res. Commun.* 81, 1100–1105.
- Clark, R.A.F., McCoy, G.A., Folkvord, J.M., and McPherson, J.M. (1997). TGF-β1 stimulates cultured human fibroblasts to proliferate and produce tissue-like fibroplasia: A fibronectin matrix-dependent event. *J. Cell. Physiol.* 170, 69–80.
- Collins, G.A., and Goldberg, A.L. (2017). The Logic of the 26S Proteasome. *Cell* 169, 792–806.
- Collins, G.A., and Tansey, W.P. (2006). The proteasome: A utility tool for transcription? *Curr. Opin. Genet. Dev.* 16, 197–202.
- Dahlmann, B. (2007). Role of proteasomes in disease. *BMC Biochem.* 8, S3.
- Dahlmann, B. (2016). Mammalian proteasome subtypes: Their diversity in structure and function. *Arch. Biochem. Biophys.* 591, 132–140.
- Degryse, A.L., and Lawson, W.E. (2011). Progress Toward Improving Animal Models for Idiopathic Pulmonary Fibrosis. *Am. J. Med. Sci.* 341, 444–449.

- Desmoulière, A., Redard, M., Darby, I., and Gabbiani, G. (1995). Apoptosis mediates the decrease in cellularity during the transition between granulation tissue and scar. *Am. J. Pathol.* *146*, 56–66.
- Dick, L.R., and Fleming, P.E. (2010). Building on bortezomib: second-generation proteasome inhibitors as anti-cancer therapy. *Drug Discov. Today* *15*, 243–249.
- Dick, T.P., Ruppert, T., Groettrup, M., Kloetzel, P.M., Kuehn, L., Koszinowski, U.H., Stevanović, S., Schild, H., and Rammensee, H.G. (1996). Coordinated dual cleavages induced by the proteasome regulator PA28 lead to dominant MHC ligands. *Cell* *86*, 253–262.
- Doherty, K.M., Pride, L.D., Lukose, J., Snydsman, B.E., Charles, R., Pramanik, A., Muller, E.G., Botstein, D., and Moore, C.W. (2012). Loss of a 20S Proteasome Activator in *Saccharomyces cerevisiae* Downregulates Genes Important for Genomic Integrity, Increases DNA Damage, and Selectively Sensitizes Cells to Agents With Diverse Mechanisms of Action. *G3 Genes|Genomes|Genetics* *2*, 943–959.
- Dong, S., Jia, C., Zhang, S., Fan, G., Li, Y., Shan, P., Sun, L., Xiao, W., Li, L., Zheng, Y., Liu, J., Wei, H., Hu, C., Zhang, W., Chin, Y.E., Zhai, Q., Li, Q., Liu, J., et al. (2013). The REGy proteasome regulates hepatic lipid metabolism through inhibition of autophagy. *Cell Metab.* *18*, 380–391.
- Erales, J., and Coffino, P. (2014). Ubiquitin-independent proteasomal degradation. *Biochim. Biophys. Acta* *1843*, 216–221.
- Etlinger, J.D., and Goldberg, A.L. (1977). A soluble ATP-dependent proteolytic system responsible for the degradation of abnormal proteins in reticulocytes. *Proc. Natl. Acad. Sci. U. S. A.* *74*, 54–58.
- Fabre, B., Lambour, T., Delobel, J., Amalric, F., Monsarrat, B., Burlet-Schiltz, O., and Bousquet-Dubouch, M.-P. (2013). Subcellular distribution and dynamics of active proteasome complexes unraveled by a workflow combining in vivo complex cross-linking and quantitative proteomics. *Mol. Cell. Proteomics* *12*, 687–699.
- Fabre, B., Lambour, T., Garrigues, L., Ducoux-Petit, M., Amalric, F., Monsarrat, B., Burlet-Schiltz, O., and Bousquet-Dubouch, M.-P. (2014). Label-Free Quantitative Proteomics Reveals the Dynamics of Proteasome Complexes Composition and Stoichiometry in a Wide Range of Human Cell Lines. *J. Proteome Res.* *13*, 3027–3037.
- Fabre, B., Lambour, T., Garrigues, L., Amalric, F., Vigneron, N., Menneteau, T., Stella, A., Monsarrat, B., Van den Eynde, B., Burlet-Schiltz, O., and Bousquet-Dubouch, M.-P. (2015). Deciphering preferential interactions within supramolecular protein complexes: the proteasome case. *Mol. Syst. Biol.* *11*, 771.
- Fehlker, M., Wendler, P., Lehmann, A., and Enenkel, C. (2003). Bim3 is part of nascent proteasomes and is involved in a late stage of nuclear proteasome assembly. *EMBO Rep.* *4*, 959–963.
- Fernandez, I.E., and Eickelberg, O. (2012a). New cellular and molecular mechanisms of lung injury and fibrosis in idiopathic pulmonary fibrosis. *Lancet* *380*, 680–688.
- Fernandez, I.E., and Eickelberg, O. (2012b). The Impact of TGF- β on Lung Fibrosis. *Proc. Am. Thorac. Soc.* *9*, 111–116.
- Finley, D. (2009). Recognition and processing of ubiquitin-protein conjugates by the proteasome. *Annu. Rev. Biochem.* *78*, 477–513.

- Flynn, D.C. (2001). Adaptor proteins. *Oncogene* 20, 6270–6272.
- Förster, A., Masters, E.I., Whitby, F.G., Robinson, H., and Hill, C.P. (2005). The 1.9 Å structure of a proteasome-11S activator complex and implications for proteasome-PAN/PA700 interactions. *Mol. Cell* 18, 589–599.
- Fort, P., Kajava, A. V., Delsuc, F., and Coux, O. (2015). Evolution of proteasome regulators in eukaryotes. *Genome Biol. Evol.* 7, 1363–1379.
- Frankel, S.K., Cosgrove, G.P., Cha, S.I., Cool, C.D., Wynes, M.W., Edelman, B.L., Brown, K.K., and Riches, D.W.H. (2006). TNF- α sensitizes normal and fibrotic human lung fibroblasts to Fas-induced apoptosis. *Am. J. Respir. Cell Mol. Biol.* 34, 293–304.
- Gabbiani, G. (2003). The myofibroblast in wound healing and fibrocontractive diseases. *J. Pathol.* 200, 500–503.
- Gaczynska, M., and Osmulski, P.A. (2015). Targeting Protein-Protein Interactions in the Proteasome Super-Assemblies. *Curr. Top. Med. Chem.* 15, 2056–2067.
- Gorbea, C., Goellner, G.M., Teter, K., Holmes, R.K., and Rechsteiner, M. (2004). Characterization of mammalian Ecm29, a 26 S proteasome-associated protein that localizes to the nucleus and membrane vesicles. *J. Biol. Chem.* 279, 54849–54861.
- Gorbea, C., Pratt, G., Ustrell, V., Bell, R., Sahasrabudhe, S., Hughes, R.E., and Rechsteiner, M. (2010). A protein interaction network for Ecm29 links the 26 S proteasome to molecular motors and endosomal components. *J. Biol. Chem.* 285, 31616–31633.
- Groettrup, M., Soza, A., Eggers, M., Kuehn, L., Dick, T.P., Schild, H., Rammensee, H.G., Koszinowski, U.H., and Kloetzel, P.M. (1996). A role for the proteasome regulator PA28 α in antigen presentation. *Nature* 381, 166–168.
- Groettrup, M., Khan, S., Schwarz, K., and Schmidtke, G. (2001). Interferon- γ inducible exchanges of 20S proteasome active site subunits: Why? In *Biochimie*, pp. 367–372.
- Groettrup, M., Kirk, C.J., and Basler, M. (2010). Proteasomes in immune cells: more than peptide producers? *Nat. Rev. Immunol.* 10, 73–78.
- Groll, M., and Huber, R. (2003). Substrate access and processing by the 20S proteasome core particle. *Int. J. Biochem. Cell Biol.* 35, 606–616.
- Groll, M., Ditzel, L., Löwe, J., Stock, D., Bochtler, M., Bartunik, H.D., and Huber, R. (1997). Structure of 20S proteasome from yeast at 2.4Å resolution. *Nature* 386, 463–471.
- Groll, M., Bajorek, M., Köhler, A., Moroder, L., Rubin, D.M., Huber, R., Glickman, M.H., and Finley, D. (2000). A gated channel into the proteasome core particle. *Nat. Struct. Biol.* 7, 1062–1067.
- Grosche, A., Hauser, A., Lepper, M.F., Mayo, R., von Toerne, C., Merl-Pham, J., and Hauck, S.M. (2016). The Proteome of Native Adult Müller Glial Cells From Murine Retina. *Mol. Cell. Proteomics* 15, 462–480.
- Guo, X., Wang, X., Wang, Z., Banerjee, S., Yang, J., Huang, L., and Dixon, J.E. (2015). Site-specific proteasome phosphorylation controls cell proliferation and tumorigenesis. *Nat. Cell Biol.* 18, 202–212.
- Guo, X., Huang, X., and Chen, M.J. (2017). Reversible phosphorylation of the 26S proteasome. *Protein Cell* 8, 255–272.

- Hanahan, D., and Weinberg, R.A. (2011). Hallmarks of cancer: The next generation. *Cell* 144, 646–674.
- Hartl, F.U., Bracher, A., and Hayer-Hartl, M. (2011). Molecular chaperones in protein folding and proteostasis. *Nature* 475, 324–332.
- Haselbach, D., Schrader, J., Lambrecht, F., Henneberg, F., Chari, A., and Stark, H. (2017). Long-range allosteric regulation of the human 26S proteasome by 20S proteasome-targeting cancer drugs. *Nat. Commun.* 8, 15578.
- Hauck, S.M., Dietter, J., Kramer, R.L., Hofmaier, F., Zipplies, J.K., Amann, B., Feuchtinger, A., Deeg, C.A., and Ueffing, M. (2010). Deciphering Membrane-Associated Molecular Processes in Target Tissue of Autoimmune Uveitis by Label-Free Quantitative Mass Spectrometry. *Mol. Cell. Proteomics* 9, 2292–2305.
- Herndon, T.M., Deisseroth, A., Kaminskas, E., Kane, R.C., Koti, K.M., Rothmann, M.D., Habtemariam, B., Bullock, J., Bray, J.D., Hawes, J., Palmbly, T.R., Jee, J., Adams, W., Mahayni, H., Brown, J., Dorantes, A., Sridhara, R., Farrell, A.T., et al. (2013). U.S. Food and Drug Administration approval: carfilzomib for the treatment of multiple myeloma. *Clin. Cancer Res.* 19, 4559–4563.
- Hershko, A. (1997). Roles of ubiquitin-mediated proteolysis in cell cycle control. *Curr. Opin. Cell Biol.* 9, 788–799.
- Hershko, A., and Ciechanover, A. (1998). The ubiquitin system. *Annu. Rev. Biochem.* 67, 425–479.
- Hershko, A., Ciechanover, A., Heller, H., Haas, A.L., and Rose, I.A. (1980). Proposed role of ATP in protein breakdown: conjugation of protein with multiple chains of the polypeptide of ATP-dependent proteolysis. *Proc. Natl. Acad. Sci.* 77, 1783–1786.
- Hinz, B., Phan, S.H., Thannickal, V.J., Galli, A., Bochaton-Piallat, M.-L., and Gabbiani, G. (2007). The Myofibroblast. *Am. J. Pathol.* 170, 1807–1816.
- Hong, K.U., Reynolds, S.D., Watkins, S., Fuchs, E., R, B., and Stripp, B.R. (2006). In vivo differentiation potential of tracheal basal cells: evidence for multipotent and unipotent subpopulations. *Am. J. Physiol.* 15260, 643–649.
- Horowitz, J.C., Lee, D.Y., Waghray, M., Keshamouni, V.G., Thomas, P.E., Zhang, H., Cui, Z., and Thannickal, V.J. (2004). Activation of the pro-survival phosphatidylinositol 3-kinase/AKT pathway by transforming growth factor-beta1 in mesenchymal cells is mediated by p38 MAPK-dependent induction of an autocrine growth factor. *J. Biol. Chem.* 279, 1359–1367.
- Horowitz, J.C., Osterholzer, J.J., Marazioti, A., and Stathopoulos, G.T. (2016). “Scar-cinoma”: Viewing the fibrotic lung mesenchymal cell in the context of cancer biology. *Eur. Respir. J.* 47, 1842–1854.
- Hough, R., Pratt, G., and Rechsteiner, M. (1987). Purification of two high molecular weight proteases from rabbit reticulocyte lysate. *J. Biol. Chem.* 262, 8303–8313.
- Huber, E.M., and Groll, M. (2017). The Mammalian Proteasome Activator PA28 Forms an Asymmetric $\alpha\beta\beta\beta$ Complex. *Structure* 25, 1473–1480.e3.
- Hutchinson, J., Fogarty, A., Hubbard, R., and McKeever, T. (2015). Global incidence and mortality of idiopathic pulmonary fibrosis: A systematic review. *Eur. Respir. J.* 46, 795–806.

- Ichihara, A., and Tanaka, K. (1995). Roles of proteasomes in cell growth. *Mol. Biol. Rep.* *21*, 49–52.
- Im, J., Kim, K., Hergert, P., and Nho, R.S. (2016). Idiopathic pulmonary fibrosis fibroblasts become resistant to Fas ligand-dependent apoptosis via the alteration of decoy receptor 3. *J. Pathol.* *240*, 25–37.
- Imamura, T., Oshima, Y., and Hikita, A. (2013). Regulation of TGF- β family signalling by ubiquitination and deubiquitination. *J. Biochem.* *154*, 481–489.
- Iwanczyk, J., Sadre-Bazzaz, K., Ferrell, K., Kondrashkina, E., Formosa, T., Hill, C.P., and Ortega, J. (2006). Structure of the Blm10-20 S Proteasome Complex by Cryo-electron Microscopy. Insights into the Mechanism of Activation of Mature Yeast Proteasomes. *J. Mol. Biol.* *363*, 648–659.
- Jagannathan, S., Vad, N., Vallabhapurapu, S., Anderson, K.C., and Driscoll, J.J. (2015). MiR-29b replacement inhibits proteasomes and disrupts aggresome+autophagosome formation to enhance the antimyeloma benefit of bortezomib. *Leukemia* *29*, 727–738.
- Johnson, L., Mercer, K., Greenbaum, D., Bronson, R.T., Crowley, D., Tuveson, D.A., and Jacks, T. (2001). Somatic activation of the K-ras oncogene causes early onset lung cancer in mice. *Nature* *410*, 1111–1116.
- Jones, M.G., Fabre, A., Schneider, P., Cinetto, F., Sgalla, G., Mavrogordato, M., Jogai, S., Alzetani, A., Marshall, B.G., O'Reilly, K.M.A., Warner, J.A., Lackie, P.M., Davies, D.E., Hansell, D.M., Nicholson, A.G., Sinclair, I., Brown, K.K., and Richeldi, L. (2016). Three-dimensional characterization of fibroblast foci in idiopathic pulmonary fibrosis. *JCI Insight* *1*, 1–11.
- Jordana, M., Newhouse, M.T., and Gauldie, J. (1987). Alveolar macrophage/peripheral blood monocyte-derived factors modulate proliferation of primary lines of human lung fibroblasts. *J. Leukoc. Biol.* *42*, 51–60.
- Jordana, M., Befus, A.D., Newhouse, M.T., Bienenstock, J., and Gauldie, J. (1988). Effect of histamine on proliferation of normal human adult lung fibroblasts. *Thorax* *43*, 552–558.
- Kajava, A. V., Gorbea, C., Ortega, J., Rechsteiner, M., and Steven, A.C. (2004). New HEAT-like repeat motifs in proteins regulating proteasome structure and function. *J. Struct. Biol.* *146*, 425–430.
- Kammerl, I.E., Dann, A., Mossina, A., Brech, D., Lukas, C., Vosityka, O., Nathan, P., Conlon, T.M., Wagner, D.E., Overkleeft, H.S., Prasse, A., Rosas, I.O., Straub, T., Krauss-Etschmann, S., Konigshoff, M., Preissler, G., Winter, H., Lindner, M., et al. (2016). Impairment of immunoproteasome function by cigarette smoke and in chronic obstructive pulmonary disease. *Am. J. Respir. Crit. Care Med.* *193*, 1230–1241.
- Kane, R.C., Bross, P.F., Farrell, A.T., and Pazdur, R. (2003). Velcade: U.S. FDA approval for the treatment of multiple myeloma progressing on prior therapy. *Oncologist* *8*, 508–513.
- Kane, R.C., Farrell, A.T., Sridhara, R., and Pazdur, R. (2006). United States Food and Drug Administration approval summary: Bortezomib for the treatment of progressive multiple myeloma after one prior therapy. *Clin. Cancer Res.* *12*, 2955–2960.
- Kane, R.C., Dagher, R., Farrell, A., Ko, C.W., Sridhara, R., Justice, R., and Pazdur, R. (2007). Bortezomib for the treatment of mantle cell lymphoma. *Clin. Cancer Res.* *13*, 5291–5294.

- Karaman, M.W., Herrgard, S., Treiber, D.K., Gallant, P., Atteridge, C.E., Campbell, B.T., Chan, K.W., Ciceri, P., Davis, M.I., Edeen, P.T., Faraoni, R., Floyd, M., Hunt, J.P., Lockhart, D.J., Milanov, Z. V., Morrison, M.J., Pallares, G., Patel, H.K., et al. (2008). A quantitative analysis of kinase inhibitor selectivity. *Nat. Biotechnol.* *26*, 127–132.
- Khor, B., Bredemeyer, A.L., Huang, C., Turnbull, I.R., Evans, R., Maggi, L.B., White, J.M., Walker, L.M., Carnes, K., Hess, R.A., and Sleckman, B.P. (2006). Proteasome activator PA200 is required for normal spermatogenesis. *Mol. Cell. Biol.* *26*, 2999–3007.
- Kikis, E.A., Gidalevitz, T., and Morimoto, R.I. (2010). Protein homeostasis in models of aging and age-related conformational disease. *Adv. Exp. Med. Biol.* *694*, 138–159.
- King, T.E., Pardo, A., and Selman, M. (2011). Idiopathic pulmonary fibrosis. *Lancet* *378*, 1949–1961.
- Kirk, R., Laman, H., Knowles, P.P., Murray-Rust, J., Lomonosov, M., Meziane, E.K., and McDonald, N.Q. (2008). Structure of a conserved dimerization domain within the F-box protein Fbxo7 and the PI31 proteasome inhibitor. *J. Biol. Chem.* *283*, 22325–22335.
- Kish-Trier, E., and Hill, C.P. (2013). Structural Biology of the Proteasome. *Annu. Rev. Biophys.* *42*, 29–49.
- Kisselev, A.F., Akopian, T.N., Woo, K.M., and Goldberg, A.L. (1999). The sizes of peptides generated from protein by mammalian 26 and 20 S proteasomes. Implications for understanding the degradative mechanism and antigen presentation. *J. Biol. Chem.* *274*, 3363–3371.
- Kisselev, A.F., Van Der Linden, W.A., and Overkleeft, H.S. (2012). Proteasome inhibitors: An expanding army attacking a unique target. *Chem. Biol.* *19*, 99–115.
- Kleijnen, M.F., Roelofs, J., Park, S., Hathaway, N.A., Glickman, M., King, R.W., and Finley, D. (2007). Stability of the proteasome can be regulated allosterically through engagement of its proteolytic active sites. *Nat. Struct. Mol. Biol.* *14*, 1180–1188.
- Kobe, B., Gleichmann, T., Horne, J., Jennings, I.G., Scotney, P.D., and Teh, T. (1999). Turn up the HEAT. *Structure* *7*.
- Koca, S.S., Ozgen, M., Dagli, F., Tuzcu, M., Ozercan, I.H., Sahin, K., and Isik, A. (2012). Proteasome inhibition prevents development of experimental dermal fibrosis. *Inflammation* *35*, 810–817.
- Korfei, M., Ruppert, C., Mahavadi, P., Henneke, I., Markart, P., Koch, M., Lang, G., Fink, L., Bohle, R.M., Seeger, W., Weaver, T.E., and Guenther, A. (2008). Epithelial endoplasmic reticulum stress and apoptosis in sporadic idiopathic pulmonary fibrosis. *Am. J. Respir. Crit. Care Med.* *178*, 838–846.
- Korfei, M., Ruppert, C., Loeh, B., Mahavadi, P., and Guenther, A. (2016). The role of Endoplasmic Reticulum (ER) stress in pulmonary fibrosis. *Endoplasmic Reticulum Stress Dis.* *3*, 16–49.
- Lander, G.C., Estrin, E., Matyskiela, M.E., Bashore, C., Nogales, E., and Martin, A. (2012). Complete subunit architecture of the proteasome regulatory particle. *Nature*.
- Lander, G.C., Martin, A., and Nogales, E. (2013). The proteasome under the microscope: The regulatory particle in focus. *Curr. Opin. Struct. Biol.* *23*, 243–251.

- Laplante, M., and Sabatini, D.M. (2012). mTOR Signaling in Growth Control and Disease. *Cell* 149, 274–293.
- Lawson, W.E., Crossno, P.F., Polosukhin, V. V., Roldan, J., Cheng, D.-S., Lane, K.B., Blackwell, T.R., Xu, C., Markin, C., Ware, L.B., Miller, G.G., Loyd, J.E., and Blackwell, T.S. (2008). Endoplasmic reticulum stress in alveolar epithelial cells is prominent in IPF: association with altered surfactant protein processing and herpesvirus infection. *AJP Lung Cell. Mol. Physiol.* 294, L1119–L1126.
- Lehmann, M., Korfei, M., Mutze, K., Klee, S., Skronska-Wasek, W., Alsafadi, H.N., Ota, C., Costa, R., Schiller, H.B., Lindner, M., Wagner, D.E., Günther, A., and Königshoff, M. (2017). Senolytic drugs target alveolar epithelial cell function and attenuate experimental lung fibrosis *ex vivo*. *Eur. Respir. J.* 50, 1602367.
- Li, N., Kuo, C.-L., Paniagua, G., van den Elst, H., Verdoes, M., Willems, L.I., van der Linden, W.A., Ruben, M., van Genderen, E., Gubbens, J., van Wezel, G.P., Overkleeft, H.S., and Florea, B.I. (2013). Relative quantification of proteasome activity by activity-based protein profiling and LC-MS/MS. *Nat. Protoc.* 8, 1155–1168.
- Li, X., Lonard, D.M., Jung, S.Y., Malovannaya, A., Feng, Q., Qin, J., Tsai, S.Y., Tsai, M.-J., and O'Malley, B.W. (2006). The SRC-3/AIB1 coactivator is degraded in a ubiquitin- and ATP-independent manner by the REGgamma proteasome. *Cell* 124, 381–392.
- Li, X., Amazit, L., Long, W., Lonard, D.M., Monaco, J.J., and O'Malley, B.W. (2007a). Ubiquitin- and ATP-independent proteolytic turnover of p21 by the REGgamma-proteasome pathway. *Mol. Cell* 26, 831–842.
- Li, X., Kusmierczyk, A.R., Wong, P., Emili, A., and Hochstrasser, M. (2007b). beta-Subunit appendages promote 20S proteasome assembly by overcoming an Ump1-dependent checkpoint. *EMBO J.* 26, 2339–2349.
- Li, X., Thompson, D., Kumar, B., and DeMartino, G.N. (2014). Molecular and cellular roles of PI31 (PSMF1) protein in regulation of proteasome function. *J. Biol. Chem.* 289, 17392–17405.
- Liu, C.-W., Li, X., Thompson, D., Wooding, K., Chang, T., Tang, Z., Yu, H., Thomas, P.J., and DeMartino, G.N. (2006). ATP binding and ATP hydrolysis play distinct roles in the function of 26S proteasome. *Mol. Cell* 24, 39–50.
- Liu, F., Rijkers, D.T.S., Post, H., and Heck, A.J.R. (2015). Proteome-wide profiling of protein assemblies by cross-linking mass spectrometry. *Nat. Methods* 12, 1179–1184.
- Livnat-Levanon, N., Kevei, E., Kleifeld, O., Krutauz, D., Segref, A., Rinaldi, T., Erpapazoglou, Z., Cohen, M., Reis, N., Hoppe, T., and Glickman, M. (2014). Reversible 26S proteasome disassembly upon mitochondrial stress. *Cell Rep.* 7, 1371–1380.
- Livneh, I., Cohen-Kaplan, V., Cohen-Rosenzweig, C., Avni, N., and Ciechanover, A. (2016). The life cycle of the 26S proteasome: from birth, through regulation and function, and onto its death. *Cell Res.* 26, 869–885.
- Lokireddy, S., Kukushkin, N.V., and Goldberg, A.L. (2015). cAMP-induced phosphorylation of 26S proteasomes on Rpn6/PSMD11 enhances their activity and the degradation of misfolded proteins. *Proc. Natl. Acad. Sci.* 112, E7176–E7185.

- Lopez, A.D., Tar, K., Krügel, U., Dange, T., Ros, I.G., Schmidt, M., Krugel, U., Dange, T., Ros, I.G., and Schmidt, M. (2011). Proteasomal degradation of Sfp1 contributes to the repression of ribosome biogenesis during starvation and is mediated by the proteasome activator Blm10. *Mol. Biol. Cell* 22, 528–540.
- Manning, B., and Cantley, L. (2007). AKTPKB Signaling: Navigating Downstream. *Cell* 129, 1261–1274.
- Manning, B.D., and Toker, A. (2017). AKT/PKB Signaling: Navigating the Network. *Cell* 169, 381–405.
- Mao, I., Liu, J., Li, X., and Luo, H. (2008). REGy, a proteasome activator and beyond? *Cell. Mol. Life Sci.* 65, 3971–3980.
- Marques, A.J., Glanemann, C., Ramos, P.C., and Dohmen, R.J. (2007). The C-terminal extension of the $\beta 7$ subunit and activator complexes stabilize nascent 20 S proteasomes and promote their maturation. *J. Biol. Chem.* 282, 34869–34876.
- Martin, P. (1997). Wound Healing--Aiming for Perfect Skin Regeneration. *Science* 276, 75–81.
- Martinez, F.J., Collard, H.R., Pardo, A., Raghu, G., Richeldi, L., Selman, M., Swigris, J.J., Taniguchi, H., and Wells, A.U. (2017). Idiopathic pulmonary fibrosis. *Nat. Rev. Dis. Prim.* 3, 17074.
- Matute-Bello, G., Frevert, C.W., and Martin, T.R. (2008). Animal models of acute lung injury. *Am. J. Physiol. Lung Cell. Mol. Physiol.* 295, L379-99.
- Meiners, S., and Ballweg, K. (2014). Proteostasis in pediatric pulmonary pathology. *Mol. Cell. Pediatr.* 7, 11.
- Meiners, S., Heyken, D., Weller, A., Ludwig, A., Stangl, K., Kloetzel, P.-M., and Krüger, E. (2003). Inhibition of proteasome activity induces concerted expression of proteasome genes and de novo formation of Mammalian proteasomes. *J. Biol. Chem.* 278, 21517–21525.
- Meiners, S., Hocher, B., Weller, A., Laule, M., Stangl, V., Guenther, C., Godes, M., Mrozikiewicz, A., Baumann, G., and Stangl, K. (2004). Downregulation of matrix metalloproteinases and collagens and suppression of cardiac fibrosis by inhibition of the proteasome. *Hypertension* 44, 471–477.
- Meiners, S., Ludwig, A., Lorenz, M., Dreger, H., Baumann, G., Stangl, V., and Stangl, K. (2006). Nontoxic proteasome inhibition activates a protective antioxidant defense response in endothelial cells. *Free Radic. Biol. Med.* 40, 2232–2241.
- Meiners, S., Ludwig, A., Stangl, V., and Stangl, K. (2007). Proteasome Inhibitors: Poisons and Remedies. *Med. Res. Rev.* 28, 309–327.
- Meiners, S., Keller, I.E., Semren, N., and Caniard, A. (2014). Regulation of the proteasome: evaluating the lung proteasome as a new therapeutic target. *Antioxid. Redox Signal.* 21, 2364–2382.
- Merl, J., Ueffing, M., Hauck, S.M., and von Toerne, C. (2012). Direct comparison of MS-based label-free and SILAC quantitative proteome profiling strategies in primary retinal Müller cells. *Proteomics* 12, 1902–1911.

- Mitsiades, N., Mitsiades, C.S., Poulaki, V., Chauhan, D., Fanourakis, G., Gu, X., Bailey, C., Joseph, M., Libermann, T.A., Treon, S.P., Munshi, N.C., Richardson, P.G., Hideshima, T., and Anderson, K.C. (2002). Molecular sequelae of proteasome inhibition in human multiple myeloma cells. *Proc. Natl. Acad. Sci. U. S. A.* 99, 14374–14379.
- Moeller, A., Ask, K., Warburton, D., Gauldie, J., and Kolb, M. (2008). The bleomycin animal model: A useful tool to investigate treatment options for idiopathic pulmonary fibrosis? *Int. J. Biochem. Cell Biol.* 40, 362–382.
- Moore, B.B., Lawson, W.E., Oury, T.D., Sisson, T.H., Raghavendran, K., and Hogaboam, C.M. (2013). Animal models of fibrotic lung disease. *Am. J. Respir. Cell Mol. Biol.* 49, 167–179.
- Mora, A.L., Bueno, M., and Rojas, M. (2017). Mitochondria in the spotlight of aging and idiopathic pulmonary fibrosis. *J. Clin. Invest.* 127, 405–414.
- Mosmann, T. (1983). Rapid colorimetric assay for cellular growth and survival: Application to proliferation and cytotoxicity assays. *J. Immunol. Methods* 65, 55–63.
- Muchamuel, T., Basler, M., Aujay, M.A., Suzuki, E., Kalim, K.W., Lauer, C., Sylvain, C., Ring, E.R., Shields, J., Jiang, J., Shwonek, P., Parlati, F., Demo, S.D., Bennett, M.K., Kirk, C.J., and Groettrup, M. (2009). A selective inhibitor of the immunoproteasome subunit LMP7 blocks cytokine production and attenuates progression of experimental arthritis. *Nat. Med.* 15, 781–787.
- Mulay, S.R., Eberhard, J.N., Pfann, V., Marschner, J.A., Darisipudi, M.N., Daniel, C., Romoli, S., Desai, J., Grigorescu, M., Kumar, S. V, Rathkolb, B., Wolf, E., Hrabě de Angelis, M., Bäuerle, T., Dietel, B., Wagner, C.A., Amann, K., Eckardt, K.-U., et al. (2016). Oxalate-induced chronic kidney disease with its uremic and cardiovascular complications in C57BL/6 mice. *Am. J. Physiol. Renal Physiol.* 310, F785–F795.
- Mulugeta, S., Nureki, S.-I., and Beers, M.F. (2015). Lost after translation: insights from pulmonary surfactant for understanding the role of alveolar epithelial dysfunction and cellular quality control in fibrotic lung disease. *Am. J. Physiol. - Lung Cell. Mol. Physiol.* 309, L507–L525.
- Murata, S., Kawahara, H., Tohma, S., Yamamoto, K., Kasahara, M., Nabeshima, Y.-I., Tanaka, K., and Chiba, T. (1999). Growth Retardation in Mice Lacking the Proteasome Activator PA28. *J. Biol. Chem.* 274, 38211–38215.
- Murata, S., Sasaki, K., Kishimoto, T., Niwa, S.-I., Hayashi, H., Takahama, Y., and Tanaka, K. (2007). Regulation of CD8+ T Cell Development by Thymus-Specific Proteasomes. *Science* 316, 1349–1353.
- Mutlu, G.M., Budinger, G.R.S., Wu, M., Lam, A.P., Zirk, A., Rivera, S., Urich, D., Chiarella, S.E., Go, L.H.T., Ghosh, A.K., Selman, M., Pardo, A., Varga, J., Kamp, D.W., Chandel, N.S., Sznajder, J.I., and Jain, M. (2012). Proteasomal inhibition after injury prevents fibrosis by modulating TGF-1 signalling. *Thorax* 67, 139–146.
- Myeku, N., Clelland, C.L., Emrani, S., Kukushkin, N. V, Yu, W.H., Goldberg, A.L., and Duff, K.E. (2015). Tau-driven 26S proteasome impairment and cognitive dysfunction can be prevented early in disease by activating cAMP-PKA signaling. *Nat. Med.* 22, 46–53.
- Nalysnyk, L., Cid-Ruzafa, J., Rotella, P., and Esser, D. (2012). Incidence and prevalence of idiopathic pulmonary fibrosis: Review of the literature. *Eur. Respir. Rev.* 21, 355–361.

- Naujokat, C., and Hoffmann, S. (2002). Role and Function of the 26S Proteasome in Proliferation and Apoptosis. *Lab. Investig.* 82, 965–980.
- Noble, P.W., Barkauskas, C.E., and Jiang, D. (2012). Review series pulmonary fibrosis: patterns and perpetrators. *Am J Physiol Lung Cell Mol Physiol* 122, 4–10.
- Okamura, T., Taniguchi, S.-I., Ohkura, T., Yoshida, A., Shimizu, H., Sakai, M., Maeta, H., Fukui, H., Ueta, Y., Hisatome, I., and Shigemasa, C. (2003). Abnormally high expression of proteasome activator-gamma in thyroid neoplasm. *J. Clin. Endocrinol. Metab.* 88, 1374–1383.
- Ortega, J., Heymann, J.B., Kajava, A. V, Ustrell, V., Rechsteiner, M., and Steven, A.C. (2005). The axial channel of the 20S proteasome opens upon binding of the PA200 activator. *J. Mol. Biol.* 346, 1221–1227.
- Osmulski, P.A., and Gaczynska, M. (2000). Atomic Force Microscopy Reveals Two Conformations of the 20 S Proteasome from Fission Yeast. *J. Biol. Chem.* 275, 13171–13174.
- Osmulski, P.A., Hochstrasser, M., and Gaczynska, M. (2009). A Tetrahedral Transition State at the Active Sites of the 20S Proteasome Is Coupled to Opening of the α -Ring Channel. *Structure* 17, 1137–1147.
- Pardo, A., and Selman, M. (2016). Lung fibroblasts, aging, and idiopathic pulmonary fibrosis. *Ann. Am. Thorac. Soc.* 13, S417–S421.
- Patel, A.S., Lin, L., Geyer, A., Haspel, J.A., An, C.H., Cao, J., Rosas, I.O., and Morse, D. (2012). Autophagy in Idiopathic Pulmonary Fibrosis. *PLoS One* 7, e41394.
- Pathare, G.R., Nagy, I., Bohn, S., Unverdorben, P., Hubert, A., Korner, R., Nickell, S., Lasker, K., Sali, A., Tamura, T., Nishioka, T., Forster, F., Baumeister, W., and Bracher, A. (2012). The proteasomal subunit Rpn6 is a molecular clamp holding the core and regulatory subcomplexes together. *Proc. Natl. Acad. Sci.* 109, 149–154.
- Pawson, T. (1997). Signaling Through Scaffold, Anchoring, and Adaptor Proteins. *Science* 278, 2075–2080.
- Peth, A., Nathan, J.A., and Goldberg, A.L. (2013). The ATP costs and time required to degrade ubiquitinated proteins by the 26 S proteasome. *J. Biol. Chem.* 288, 29215–29222.
- Pickering, A.M., and Davies, K.J.A. (2013). Differential Roles of Proteasome and Immunoproteasome Regulators Pa28 $\alpha\beta$, Pa28 γ and Pa200 in the Degradation of Oxidized Proteins. *Arch Biochem Biophys* 523, 181–190.
- Plataki, M., Koutsopoulos, A. V., Darivianaki, K., Delides, G., Siafakas, N.M., and Bouros, D. (2005). Expression of apoptotic and antiapoptotic markers in epithelial cells in idiopathic pulmonary fibrosis. *Chest* 127, 266–274.
- Preckel, T., Fung-Leung, W.-P., Cai, Z., Vitiello, A., Salter-Cid, L., Winqvist, O., Wolfe, T.G., Herrath v., M., Angulo, A., Ghazal, P., Lee, J.-D., Fourie, A.M., Wu, Y., Pang, J., Ngo, K., Peterson, P.A., Früh, K., and Yang, Y. (1999). Impaired Immunoproteasome Assembly and Immune Responses in PA28 $^{-/-}$ Mice. *Science* 286, 2162–2165.
- Qian, M.X., Pang, Y., Liu, C.H., Haratake, K., Du, B.Y., Ji, D.Y., Wang, G.F., Zhu, Q.Q., Song, W., Yu, Y., Zhang, X.X., Huang, H.T., Miao, S., Chen, L. Bin, Zhang, Z.H., Liang, Y.N., Liu, S., Cha, H., et al. (2013). Acetylation-mediated proteasomal degradation of core histones during DNA repair and spermatogenesis. *Cell* 153.

- Radhakrishnan, S.K., Lee, C.S., Young, P., Beskow, A., Chan, J.Y., and Deshaies, R.J. (2010). Transcription factor Nrf1 mediates the proteasome recovery pathway after proteasome inhibition in mammalian cells. *Mol. Cell* 38, 17–28.
- Rafii, R., Juarez, M.M., Albertson, T.E., and Chan, A.L. (2013). A review of current and novel therapies for idiopathic pulmonary fibrosis. *J. Thorac. Dis.* 5, 48–73.
- Raghu, G., and Meyer, K.C. (2012). Silent gastro-oesophageal reflux and microaspiration in IPF: Mounting evidence for anti-reflux therapy? *Eur. Respir. J.* 39, 242–245.
- Raghu, G., Collard, H.R., Egan, J.J., Martinez, F.J., Behr, J., Brown, K.K., Colby, T. V., Cordier, J.F., Flaherty, K.R., Lasky, J.A., Lynch, D.A., Ryu, J.H., Swigris, J.J., Wells, A.U., Ancochea, J., Bouros, D., Carvalho, C., Costabel, U., et al. (2011). An Official ATS/ERS/JRS/ALAT Statement: Idiopathic pulmonary fibrosis: Evidence-based guidelines for diagnosis and management. *Am. J. Respir. Crit. Care Med.* 183, 788–824.
- Realini, C., Jensen, C.C., Zhang, Z. -g., Johnston, S.C., Knowlton, J.R., Hill, C.P., and Rechsteiner, M. (1997). Characterization of recombinant REGalpha, REGbeta, and REGgamma proteasome activators. *J. Biol. Chem.* 272, 25483–25492.
- Rechsteiner, M., and Hill, C.P. (2005). Mobilizing the proteolytic machine: cell biological roles of proteasome activators and inhibitors. *Trends Cell Biol.* 15, 27–33.
- Rechsteiner, M., Realini, C., and Ustrell, V. (2000). The proteasome activator 11 S REG (PA28) and Class I antigen presentation. *Biochem. J.* 345, 1–15.
- Rock, J.R., Onaitis, M.W., Rawlins, E.L., Lu, Y., Clark, C.P., Xue, Y., Randell, S.H., and Hogan, B.L.M. (2009). Basal cells as stem cells of the mouse trachea and human airway epithelium. *Proc. Natl. Acad. Sci. U. S. A.* 106, 12771–12775.
- Rock, J.R., Randell, S.H., and Hogan, B.L.M. (2010). Airway basal stem cells: a perspective on their roles in epithelial homeostasis and remodeling. *Dis. Model. Mech.* 3, 545–556.
- Rock, K.L., Gramm, C., Rothstein, L., Clark, K., Stein, R., Dick, L., Hwang, D., and Goldberg, A.L. (1994). Inhibitors of the proteasome block the degradation of most cell proteins and the generation of peptides presented on MHC class I molecules. *Cell* 78, 761–771.
- Rockey, D.C., Bell, P.D., and Hill, J.A. (2015). Fibrosis — A Common Pathway to Organ Injury and Failure. *N. Engl. J. Med.* 372, 1138–1149.
- Ruschak, A.M., and Kay, L.E. (2012). Proteasome allostery as a population shift between interchanging conformers. *Proc Natl Acad Sci U S A* 109, E3454-62.
- Sadre-Bazzaz, K., Whitby, F.G., Robinson, H., Formosa, T., and Hill, C.P. (2010). Structure of a Blm10 Complex Reveals Common Mechanisms for Proteasome Binding and Gate Opening. *Mol. Cell* 37, 728–735.
- Santamaria, P.G., Finley, D., Ballesta, J.P.G., and Remacha, M. (2003). Rpn6p, a proteasome subunit from *Saccharomyces cerevisiae*, is essential for the assembly and activity of the 26 S proteasome. *J. Biol. Chem.* 278, 6687–6695.
- Savulescu, A.F., and Glickman, M.H. (2011). Proteasome Activator 200: The HEAT is on.... *Mol. Cell. Proteomics* 10, R110.006890.

- Schamberger, A.C., Staab-Weijnitz, C.A., Mise-Racek, N., and Eickelberg, O. (2015). Cigarette smoke alters primary human bronchial epithelial cell differentiation at the air-liquid interface. *Sci. Rep.* *5*, 8163.
- Schmidt, M., and Finley, D. (2014). Regulation of proteasome activity in health and disease. *Biochim. Biophys. Acta* *1843*, 13–25.
- Schmidt, M., Haas, W., Crosas, B., Santamaria, P.G., Gygi, S.P., Walz, T., and Finley, D. (2005). The HEAT repeat protein Bim10 regulates the yeast proteasome by capping the core particle. *Nat. Struct. Mol. Biol.* *12*, 294–303.
- Schmidtke, G., Kraft, R., Kostka, S., Henklein, P., Frömmel, C., Löwe, J., Huber, R., Kloetzel, P.M., and Schmidt, M. (1996). Analysis of mammalian 20S proteasome biogenesis: the maturation of beta-subunits is an ordered two-step mechanism involving autocatalysis. *EMBO J.* *15*, 6887–6898.
- Seibold, M.A., Wise, A.L., Speer, M.C., Steel, M.P., Brown, K.K., Loyd, J.E., Fingerlin, T.E., Zhang, W., Gudmundsson, G., Groshong, S.D., Evans, C.M., Garantziotis, S., Adler, K.B., Dickey, B.F., Bois, R.M., Yang, I. V., Herron, A., Kervitsky, D., et al. (2012). A Common MUC5B Promoter Polymorphism and Pulmonary Fibrosis. *N Engl J Med* *364*, 1503–1512.
- Selman, M., and Pardo, A. (2014). Revealing the pathogenic and aging-related mechanisms of the enigmatic idiopathic pulmonary fibrosis: An integral model. *Am. J. Respir. Crit. Care Med.* *189*, 1161–1172.
- Semren, N., Welk, V., Korfei, M., Keller, I.E., Fernandez, I.E., Adler, H., Günther, A., Eickelberg, O., and Meiners, S. (2015). Regulation of 26S Proteasome Activity in Pulmonary Fibrosis. *Am. J. Respir. Crit. Care Med.* *192*, 1089–1101.
- Sha, Z., and Goldberg, A.L. (2014). Proteasome-mediated processing of Nrf1 is essential for coordinate induction of all proteasome subunits and p97. *Curr. Biol.* *24*, 1573–1583.
- Sharon, M., Taverner, T., Ambroggio, X.I., Deshaies, R.J., and Robinson, C. V. (2006). Structural organization of the 19S proteasome lid: Insights from MS of intact complexes. *PLoS Biol.* *4*, 1314–1323.
- Shechter, D., Dormann, H.L., Allis, C.D., and Hake, S.B. (2007). Extraction, purification and analysis of histones. *Nat. Protoc.* *2*, 1445–1457.
- Shen, M., Schmitt, S., Buac, D., and Ping Dou, Q. (2013). Targeting the ubiquitin - proteasome system for cancer therapy. *Expert. Opin. Ther. Targets* *17*, 1091–1108.
- Shibatani, T., Carlson, E.J., Larabee, F., McCormack, A.L., Früh, K., and Skach, W.R. (2006). Global organization and function of mammalian cytosolic proteasome pools: Implications for PA28 and 19S regulatory complexes. *Mol. Biol. Cell* *17*, 4962–4971.
- Silva, G.M., Netto, L.E.S., Simões, V., Santos, L.F.A., Gozzo, F.C., Demasi, M.A.A., Oliveira, C.L.P., Bicev, R.N., Klitzke, C.F., Sogayar, M.C., and Demasi, M. (2012). Redox Control of 20S Proteasome Gating. *Antioxid. Redox Signal.* *16*, 1183–1194.
- Singer, A.J., and Clark, R.A. (1999). Cutaneous wound healing. *N. Engl. J. Med.* *341*, 738–746.
- Smirnova, N.F., Chamberger, A.C., Nayakanti, S., Hatz, R., Behr, J., and Eickelberg, O. (2016). Detection and quantification of epithelial progenitor cell populations in human healthy and IPF lungs. *Respir. Res.* *17*, 83.

- Soond, S.M., and Chantry, A. (2011). How ubiquitination regulates the TGF- β signalling pathway: New insights and new players: New isoforms of ubiquitin-activating enzymes in the E1-E3 families join the game. *BioEssays* 33, 749–758.
- Stadtmueller, B.M., and Hill, C.P. (2011). Proteasome Activators. *Mol. Cancer Res.* 41, 8–19.
- Stavreva, D.A., Kawasaki, M., Dundr, M., Koberna, K., Muller, W.G., Tsujimura-Takahashi, T., Komatsu, W., Hayano, T., Isobe, T., Raska, I., Misteli, T., Takahashi, N., and McNally, J.G. (2006). Potential Roles for Ubiquitin and the Proteasome during Ribosome Biogenesis. *Mol. Cell. Biol.* 26, 5131–5145.
- Steffen, J., Seeger, M., Koch, A., and Krüger, E. (2010). Proteasomal degradation is transcriptionally controlled by TCF11 via an ERAD-dependent feedback loop. *Mol. Cell* 40, 147–158.
- Strehl, B., Seifert, U., Kruger, E., Heink, S., Kuckelkorn, U., and Kloetzel, P.-M. (2005). Interferon-gamma, the functional plasticity of the ubiquitin-proteasome system, and MHC class I antigen processing. *Immunol. Rev.* 207, 19–30.
- Suraweera, A., Münch, C., Hanssum, A., and Bertolotti, A. (2012). Failure of amino acid homeostasis causes cell death following proteasome inhibition. *Mol. Cell* 48, 242–253.
- Tanahashi, N., Tamura, T., Tsurumi, C., and Tanaka, K. (1993). Molecular Structures of 20S and 26S Proteasomes. *Enzym. Protein* 47, 241–251.
- Tanaka, T., Yoshimi, M., Maeyama, T., Hagimoto, N., Kuwano, K., and Hara, N. (2002). Resistance to Fas-mediated apoptosis in human lung fibroblast. *Eur. Respir. J.* 20, 359–368.
- Tar, K., Dange, T., Yang, C., Yao, Y., Bulteau, A.L., Salcedo, E.F., Braigen, S., Bouillaud, F., Finley, D., and Schmidt, M. (2014). Proteasomes associated with the blm10 activator protein antagonize mitochondrial fission through degradation of the fission protein dnm1. *J. Biol. Chem.* 289, 12145–12156.
- Tashiro, K., Tamada, S., Kuwabara, N., Komiya, T., Takekida, K., Asai, T., Iwao, H., Sugimura, K., Matsumura, Y., Takaoka, M., Nakatani, T., and Miura, K. (2003). Attenuation of renal fibrosis by proteasome inhibition in rat obstructive nephropathy: possible role of nuclear factor kappaB. *Int J Mol Med* 12, 587–592.
- Taylor, C., and Jobin, C. (2005). Ubiquitin protein modification and signal transduction: implications for inflammatory bowel diseases. *Inflamm. Bowel Dis.* 11, 1097–1107.
- Thannickal, V.J., and Horowitz, J.C. (2006). Evolving concepts of apoptosis in idiopathic pulmonary fibrosis. *Proc. Am. Thorac. Soc.* 3, 350–356.
- Thannickal, V.J., Toews, G.B., White, E.S., Lynch III, J.P., and Martinez, F.J. (2004). Mechanisms of Pulmonary Fibrosis. *Annu. Rev. Med.* 55, 395–417.
- Thrower, J.S., Hoffman, L., Rechensteiner, M., and Pickart, C.M. (2000). Recognition of the polyubiquitin proteolytic signal. *EMBO J.* 19, 94–102.
- Tonoki, A., Kuranaga, E., Tomioka, T., Hamazaki, J., Murata, S., Tanaka, K., and Miura, M. (2009). Genetic evidence linking age-dependent attenuation of the 26S proteasome with the aging process. *Mol. Cell. Biol.* 29, 1095–1106.

- Tsvetkov, P., Mendillo, M.L., Zhao, J., Carette, J.E., Merrill, P.H., Cikes, D., Varadarajan, M., van Diemen, F.R., Penninger, J.M., Goldberg, A.L., Brummelkamp, T.R., Santagata, S., and Lindquist, S. (2015). Compromising the 19S proteasome complex protects cells from reduced flux through the proteasome. *Elife* 4, 1–22.
- Tsvetkov, P., Sokol, E., Jin, D., Brune, Z., Thiru, P., Ghandi, M., Garraway, L.A., Gupta, P.B., Santagata, S., Whitesell, L., and Lindquist, S. (2017). Suppression of 19S proteasome subunits marks emergence of an altered cell state in diverse cancers. *Proc. Natl. Acad. Sci.* 114, 382–387.
- Turner, G.C., and Varshavsky (2000). Detecting and Measuring Cotranslational Protein Degradation in Vivo. *Science* 289, 2117–2120.
- Uhal, B.D., Joshi, I., Hughes, W.F., Ramos, C., Pardo, A., and Selman, M. (1998). Alveolar epithelial cell death adjacent to underlying myofibroblasts in advanced fibrotic human lung. *Am. J. Physiol.* 275, L1192-9.
- Uhlen, M., Bandrowski, A., Carr, S., Edwards, A., Ellenberg, J., Lundberg, E., Rimm, D.L., Rodriguez, H., Hiltke, T., Snyder, M., and Yamamoto, T. (2016). A proposal for validation of antibodies. *Nat. Methods*.
- Ustrell, V., Hoffman, L., Pratt, G., and Rechsteiner, M. (2002). Pa200, a nuclear proteasome activator involved in DNA repair. *EMBO J.* 21, 3516–3525.
- Vabulas, R.M., and Hartl, F.U. (2005). Protein Synthesis upon Acute Nutrient Restriction Relies on Proteasome Function. *Science* 310, 1960–1963.
- Verdoes, M., Florea, B.I., Menendez-Benito, V., Maynard, C.J., Witte, M.D., van der Linden, W.A., van den Nieuwendijk, A.M.C.H., Hofmann, T., Berkers, C.R., van Leeuwen, F.W.B., Groothuis, T.A., Leeuwenburgh, M.A., Ovaa, H., Neefjes, J.J., Filippov, D. V., van der Marel, G.A., Dantuma, N.P., and Overkleeft, H.S. (2006). A Fluorescent Broad-Spectrum Proteasome Inhibitor for Labeling Proteasomes In Vitro and In Vivo. *Chem. Biol.* 13, 1217–1226.
- Verdoes, M., Willems, L.I., van der Linden, W.A., Duivenvoorden, B.A., van der Marel, G.A., Florea, B.I., Kisselev, A.F., and Overkleeft, H.S. (2010). A panel of subunit-selective activity-based proteasome probes. *Org. Biomol. Chem.* 8, 2719.
- Vernace, V.A., Arnaud, L., Schmidt-Glenewinkel, T., and Figueiredo-Pereira, M.E. (2007). Aging perturbs 26S proteasome assembly in *Drosophila melanogaster*. *FASEB J.* 21, 2672–2682.
- VerPlank, J.J.S., and Goldberg, A.L. (2017). Regulating protein breakdown through proteasome phosphorylation. *Biochem. J.* 474, 3355–3371.
- Vilchez, D., Boyer, L., Morantte, I., Lutz, M., Merkwirth, C., Joyce, D., Spencer, B., Page, L., Masliah, E., Berggren, W.T., Gage, F.H., and Dillin, A. (2012). Increased proteasome activity in human embryonic stem cells is regulated by PSMD11. *Nature* 489, 304–308.
- Wang, D., Fang, C., Zong, N.C., Liem, D.A., Cadeiras, M., Scruggs, S.B., Yu, H., Kim, A.K., Yang, P., Deng, M., Lu, H., and Ping, P. (2013). Regulation of Acetylation Restores Proteolytic Function of Diseased Myocardium in Mouse and Human. *Mol. Cell. Proteomics* 12, 3793–3802.

- Wang, F., Ma, H., Liang, W.-J., Yang, J.-J., Wang, X.-Q., Shan, M.-R., Chen, Y., Jia, M., Yin, Y.-L., Sun, X.-Y., Zhang, J.-N., Peng, Q.-S., Chen, Y.-G., Liu, L.-Y., Li, P., Guo, T., and Wang, S.-X. (2017). Lovastatin upregulates microRNA-29b to reduce oxidative stress in rats with multiple cardiovascular risk factors. *Oncotarget* 8, 9021–9034.
- Weberruss, M.H., Savulescu, A.F., Jando, J., Bissinger, T., Harel, A., Glickman, M.H., and Enenkel, C. (2013). Blm10 facilitates nuclear import of proteasome core particles. *EMBO J.* 32, 2697–2707.
- Weiss, C.H., Budinger, G.R.S., Mutlu, G.M., and Jain, M. (2010). Proteasomal Regulation of Pulmonary Fibrosis. *Proc. Am. Thorac. Soc.* 7, 77–83.
- Welk, V., Coux, O., Kleene, V., Abeza, C., Trümbach, D., Eickelberg, O., and Meiners, S. (2016). Inhibition of Proteasome Activity Induces Formation of Alternative Proteasome Complexes. *J. Biol. Chem.* 291, 13147–13159.
- Whitby, F.G., Masters, E.I., Kramer, L., Knowlton, J.R., Yao, Y., Wang, C.C., and Hill, C.P. (2000). Structural basis for the activation of 20S proteasomes by 11S regulators. *Nature* 408, 115–120.
- Wilkins, O.M., Downey, S.L., Weyburne, E.S., Williams, D.A., Mirabella, A.C., Overkleeft, H.S., and Kisselev, A.F. (2014). Cell-line-specific high background in the Proteasome-Glo assay of proteasome trypsin-like activity. *Anal. Biochem.* 451, 1–3.
- Wiśniewski, J.R., Zougman, A., Nagaraj, N., and Mann, M. (2009). Universal sample preparation method for proteome analysis. *Nat. Methods* 6, 359–362.
- Wójcik, C., and DeMartino, G.N. (2002). Analysis of Drosophila 26 S proteasome using RNA interference. *J. Biol. Chem.* 277, 6188–6197.
- Wolters, P.J., Collard, H.R., and Jones, K.D. (2014). Pathogenesis of idiopathic pulmonary fibrosis. *Annu. Rev. Pathol.* 9, 157–179.
- Wynn, T.A. (2011). Integrating mechanisms of pulmonary fibrosis. *J. Exp. Med.* 208, 1339–1350.
- Xiong, S., Zheng, Y., Jiang, P., Liu, R., Liu, X., Qian, J., Gu, J., Chang, L., Ge, D., and Chu, Y. (2014). PA28gamma emerges as a novel functional target of tumour suppressor microRNA-7 in non-small-cell lung cancer. *Br. J. Cancer* 110, 353–362.
- Zhang, F., Su, K., Yang, X., Bowe, D.B., Paterson, A.J., and Kudlow, J.E. (2003). O-GlcNAc modification is an endogenous inhibitor of the proteasome. *Cell* 115, 715–725.
- Zhang, X., Tang, N., Hadden, T.J., and Rishi, A.K. (2011). Akt, FoxO and regulation of apoptosis. *Biochim. Biophys. Acta - Mol. Cell Res.* 1813, 1978–1986.
- Zhang, Y., Nicholatos, J., Dreier, J.R., Ricoult, S.J.H., Widenmaier, S.B., Hotamisligil, G.S., Kwiatkowski, D.J., and Manning, B.D. (2014). Coordinated regulation of protein synthesis and degradation by mTORC1. *Nature* 513, 440–443.
- Zhao, J., Zhai, B., Gygi, S.P., and Goldberg, A.L. (2015). mTOR inhibition activates overall protein degradation by the ubiquitin proteasome system as well as by autophagy. *Proc. Natl. Acad. Sci.* 112, 15790–15797.

List of abbreviations

A

aa	amino acids
ABP	activity-based probe
ADP	adenosine diphosphate
AEC1	type 1 alveolar epithelial cell
AEC2	type 2 alveolar epithelial cell
α SMA	alpha smooth muscle actin
ATCC	American Type Culture Collection
ATP	adenosine triphosphate
AV	AnnexinV

B

BAD	Bcl-2-associated death promoter
BAL	bronchoalveolar lavage
BCA	bicinchoninic acid
bp	base pair
BrdU	bromodeoxyuridine
BSA	bovine serum albumin
BZ	bortezomib

C

$^{\circ}$ C	degree Celsius
C-L	caspase-like
<i>C. elegans</i>	<i>Caenorhabditis elegans</i>
CAF	cancer-associated fibroblast
CASP3	caspase 3
CCND1	cyclin D1
CD	cluster of differentiation
cDNA	complementary DNA
CKD	chronic kidney disease
cm	centimeter
CO ₂	carbon dioxide
CPC	Comprehensive Pneumology Center
CT-L	chymotrypsin-like
ctrl	control

D

Da	dalton
DMEM	Dulbecco's modified Eagle's medium
DMSO	dimethyl sulfoxide
DNA	deoxyribonucleic acid
DTT	dithiothreitol

E

ECM	extracellular matrix
EDTA	ethylenediaminetetraacetate
EGTA	ethyleneglycoltetraacetate
EM	electron microscopy
EMT	epithelial-mesenchymal transition
ER	endoplasmic reticulum

F

FACS	fluorescence-activated cell sorting
FBS	fetal bovine serum

FDA Food and Drug Administration
 FDR false discovery rate
 FN fibronectin
 FoxO forkhead box class O

G

g gram

H

h hour(s)
 H&E hematoxylin & eosin
 HEAT repeat huntingtin, elongation factor 3, protein phosphatase 2A and the yeast kinase TOR1 repeat
 HMGU Helmholtz Zentrum München - Deutsches Forschungszentrum für Gesundheit und Umwelt
 hnRNPS heterogeneous nuclear ribonucleoproteins
 HRP horseradish peroxidase
 HPRT hypoxanthine-guanine phosphoribosyltransferase

I

ICC immunocytochemistry
 IFN γ interferon gamma
 IHC immunohistochemistry
 ILBD Institute for Lung Biology and Disease
 ILD interstitial lung disease
 IPA Ingenuity pathway analysis
 IPF idiopathic pulmonary fibrosis

K

K48 lysine 48
 kDa kilodalton
 kg kilogram
 KO knockout
 KRT5 keratin 5

L

LB lysogeny broth
 LC-MS/MS liquid chromatography tandem mass spectrometry
 LMP low molecular mass protein
 LPS lipopolysaccharide

M

M molar
 mA milliampere
 MECL-1 multicatalytic endopeptidase complex-like 1
 MEFs mouse embryonic fibroblasts
 MHC major histocompatibility complex
 μ g mikrogram
 μ L mikroliter
 μ m micrometer
 min minute
 mL milliliter
 MMF medetomidine, midazolam and fentanyl
 mRNA messenger ribonucleic acid
 ms milliseconds
 mTOR mammalian target of rapamycin
 MTT 3-(4,5-dimethylthiazol-2-yl)-2,5 diphenyltetrazolium bromide

N

nL	nanoliter
nm	nanometer
NRF-1	nuclear factor erythroid 2-related factor 1

O

OZ	oprozomib
----	-----------

P

%	percent
p16	cyclin-dependent kinase inhibitor 2A, multiple tumor suppressor 1
p21	cyclin-dependent kinase inhibitor 1
PA200	proteasome activator 200 kDa
PA28	proteasome activator 28 kDa
PAGE	polyacrylamide gel electrophoresis
PARP	poly (ADP-ribose) polymerase
PBS	phosphate buffered saline
PFA	paraformaldehyde
phBEC	primary human bronchial epithelial cell
phLF	primary human lung fibroblasts
PI	propidium iodide
PI31	proteasome inhibitor 31 kDa
PSMA	proteasome subunit alpha type
PSMB	proteasome subunit alpha type
PSMC	26S proteasome ATPase regulatory subunit
PSMD	26S proteasome non-ATPase regulatory subunit
PTM	post-translational modification
PVDF	polyvinylidenedifluoride

Q

qPCR	quantitative polymerase chain reaction
------	--

R

RNAi	ribonucleic acid interference
RP	regulatory particle
RPL19	ribosomal protein 19
rpm	revolutions per minute
RPN	regulatory particle non-ATPase
RPT	regulatory particle ATPase
RT	room temperature

S

SCR-3	steroid receptor co-activator 3
SDS	sodium dodecyl sulfate
SEM	standard error of the mean
siRNA	small interfering ribonucleic acid
SIRT1	NAD-dependent deacetylase sirtuin-1
SMAP	small animal platform
STS	staurosporine

T

T-L	trypsin-like
TFA	trifluoroacetic acid
TFBS	transcription factor binding site
TGF- β 1	transforming growth factor beta 1
Thr1	threonine 1

TNC tenascin c
TNF α tumor necrosis factor alpha
TSS transcription start site

U

U unit
UBIK48 proteins ubiquitinated at lysine 48
UGMLC Universities of Giessen & Marburg Lung Center
UIP usual interstitial pneumonia
UPR unfolded protein response
UPS ubiquitin-proteasome system
UTR untranslated region

V

V Volt

W

WB Western blot
WT wildtype

X

x g times gravity
XL-MS crosslinking mass spectrometry

Y

Z

Acknowledgements

I want to express my sincere gratitude to my supervisor Prof. Dr. Silke Meiners for her great guidance and constant support; with her help I learned a lot about science and the proteasome. I especially would like to thank her for giving me the opportunity to work on this challenging but also really fascinating project, for long discussions, for her always open door, for prompt feedbacks, for allowing me to develop and follow my own ideas as well as for giving me the possibility to present my data at numerous conferences.

Moreover, I would like to acknowledge the Comprehensive Pneumology Center and the Helmholtz Zentrum München for providing me an outstanding environment to pursue my PhD. I also thank the members of my thesis committee, Prof. Dr. Burkhard Dahlmann and Prof. Dr. Oliver Eickelberg, for fruitful discussions and very helpful advices.

Furthermore, I am very thankful for all the support I received from collaboration partners from the CPC & ILBD (Dr. Tobias Stöger, David Kutschke, Dr. Andrea Schamberger and Dr. Isis E. Fernandez), from the Helmholtz Zentrum München (Dr. Juliane Merl-Pham and Dr. Stefanie Hauck, Dr. Martin Irmeler, and Dr. Dietrich Trümbach) and external institutions (Dr. Martina Korfei and Prof. Dr. Andreas Günther, Dr. Olivier Coux, Dr. Shrikant Mulay and Prof. Dr. Hans-Joachim Anders).

The members of CPC & ILBD family constantly supported me whenever I needed help and advice, wherefore I am very thankful.

I am also very grateful for the training and support I received from the Research School „Lung Biology and Disease“ and Dr. Doreen Franke.

It has been my good fortune to work with the best colleagues one can ever imagine. Due to the superb team spirit, helping hands and advice whenever needed, fruitful discussions and the high enthusiasm for our research I always very much enjoyed working in the Meiner's Lab. I'm extremely grateful for all the mental and practical support I received from the current and past members of our lab, and the very fun times we had together beyond proteasome research.

I would like to address my special thanks to Dr. Ilona Kammerl and Dr. Korbinian Berschneider for their support since my very first steps as a PhD student and I am sincerely grateful for the help of Dr. Ilona Kammerl with Paul & Willi.

Moreover, I thank Thomas Meul and Vera Kleene for allowing me to practice my teaching skills and for their contributions to my research projects.

And of course, I would like to thank the people who spent a lot of time with proofreading of this thesis.

I am extremely thankful for the support I received from my parents throughout my studies and beyond as well as for providing a welcome change to the daily life by all the journeys we made together.

Finally, I would like to thank Patrick for being the perfect regulator of work life balance during the past years.